Theoretical investigation of some inorganic complexes and electron correlation in atomic systems

Msugh Targema

Supervisor: Prof. Hazel Cox

Submitted towards fulfilment of the requirements for the degree of Doctor of Philosophy

Department of Chemistry
School of Life Sciences
University of Sussex
United Kingdom

April 2021

Declaration

I hereby declare that except for reference made to the work of others, the contents of this thesis are original and have not and will not be, submitted in whole or in part to another University or School in this University for consideration for the award of any other degree or qualification.

Msugh Targema

April 2021

Dedication

To the blessed memory of my mother, **Mnguzamber Elisabeth Iorvaa**

Acknowledgements

I would like to express my profound gratitude to my supervisor, Prof. Hazel Cox for her kind and unwavering guidance, support, patience and understanding in the course of my PhD studies. There are no words to express my heartfelt appreciation for her friendly disposition, advice and kind assistance during trying times in the course of my PhD studies. All I can say is, THANK YOU!!!

I would also like to thank my co-supervisor, Dr John F.C. Turner for his contributions towards the direction of this thesis and helpful discussions. In the same vein, I would like to thank my experimental collaborator, Prof. John Spencer for his helpful discussions in the course of my PhD and during the preparation of our manuscript for publication. In addition, I would like to thank Prof. Anthony McCaffery for his encouragement and comments.

To the Cox group members, past and present; Dr Gavin W. Roffe, Dr Sarote Boonseng, Dr Adam L. Baskerville, Dr Rob Ziolek, Kylie Okoro, Ryan Hinton, Abigail Guy, Jamie Murray and Charlotte Clarke, many thanks for making the office a fun and supportive study environment. I wish you the best in your present and future endeavours.

My gratitude also goes to the Tertiary Education Trust Fund (TETFund) of Nigeria for sponsorship through the Benue State University, Makurdi. You have indeed, invested into the future! I would also like to thank Prof. Simon T. Ubwa for finding me employable, you are indeed a visionary.

My special appreciation to my family, the family of Prof. and Mrs Targema Iorvaa, for being part of my journey up to PhD! You have been incredible. I would also like to thank Barr. George O.N. Ayia for his support and kind words of encouragement.

To my friend, Dr Andrew T.T. Tyowua, thank you for your encouragement, support and being an excellent motivator. You will always be appreciated for your words and kind support. Many thanks also to Mumandim Tenpo Billion for his immeasurable support over the years this PhD study lasted.

My deepest gratitude goes to Ter-Nguveren (as I love to call her) for her patience, love, prayers, encouragement and assistance, especially in the last year of my PhD studies.

Lastly and most importantly, thank God!!! This thesis has been possible by Your Spirit.

Abstract

This thesis presents theoretical investigations that elucidate experimental observations and test theory.

Firstly, density functional theory (DFT) is used to determine the mechanism for Pd(0) formation from the pincer palladacycle, PdSCN, with and without solvent effects. The elucidated mechanism involves two key steps, transmetallation and reductive elimination. Transmetallation is computed as the rate-determining step and the energy barriers to increase with increasing solvent dielectric constant.

The thermal Claus process is an industrially important method of liquid sulfur production from H_2S, yet there remain questions of why liquid sulfur is paramagnetic and why H_2S persists in recovered sulfur. To answer these questions, a suitable computational methodology is established and used to investigate the structure and stabilities of cyclic and open chain S_n ($n \leq 5$ and 8) on the singlet and triplet potential energy surfaces (PESs). All stable cyclic structures are found to have singlet states whereas open chain structures, S, S_2, S_5 and S_8 have triplet ground states. These results provide a possible explanation for the observed paramagnetism of liquid sulfur. The mechanism for formation of hydrogen polysulfanes ($HS_{n+1}H$) from open chain S_n and singlet H_2S is thereafter investigated. In all cases the most stable $HS_{n+1}H$ is formed exergonically on the singlet PES. However, in the case of S_n clusters with a triplet ground state, the singlet product arises from curve crossing and the triplet product is formed endergonically. The instability of the triplet product provides a mechanism for the persistence of H_2S.

The DFT correlation functional, LYP, is based on a correlation energy formula derived from the Hartree-Fock (HF) second order reduced density matrix and an exponential correlation factor obtained by fitting to helium data. In this thesis, the formula is re-parametrised using accurate HF densities for helium and hydride and the correlation energy calculated for several atomic systems.

Contents

List of Figures

List of Schemes

List of Tables

1 Introduction

Conventional quantum chemistry methods involve using increasingly sophisticated methods to accurately model and/or treat electron-electron correlation interactions, which are essential for interpreting chemical processes or predicting the structure of challenging chemical species. As such, compounds or processes that are dangerous, difficult or even too expensive to be investigated experimentally are conveniently studied using computational quantum chemistry approaches. Several studies of the structure, spectroscopy and reactivity of inorganic compounds exist in literature.[1–10] Nevertheless, more investigations are still necessary to complement the existing ones or add new information in the literature for a better understanding and application of inorganic species. This is because the indispensability of inorganic compounds in applications or processes ranging from devices, industry, agriculture to biology and the atmosphere cannot be overemphasised. For example, inorganic compounds are involved in catalytic applications or processes leading to the formation of useful chemical species (e.g., in pharmaceutical industries and organic synthesis).[11] In such applications or processes, the active catalytic species is often not known.[11] Inorganic clusters are also implicated in sulfur recovery in the modern thermal Claus process for desired end uses.[12] This process is known to suffer a daunting hydrogen sulfide elimination problem that limits the transportation and application of the sulfur recovered from it.[12–15] Some of the species and their accompanying spin behaviours that are usually implicated in these processes are often elusive to experimental observation. As a result, computational approaches are required in the investigation of their structure, stability, spectroscopy, reactivity and to accurately model methods which include electron-electron correlation which is critical to understanding chemical phenomena.[16–18]

This computational/theoretical thesis using quantum chemistry methodologies involves the elucidation of experimental observations involving some inorganic complexes and modelling of methods that include electron-electron correlation. The research will primarily focus on the structure, stability and reactivity of transition metal and main group complexes. The outcome of this

will contribute towards understanding the structure, stabilities and reactivity of these species for better production and applications. The research will then be extended to re-parameterising a correlation functional methodology, based on Hartree-Fock theory, to determine high-accuracy electron correlation data for atomic systems. The outcome of this will contribute to future quantum chemistry methodological developments or improvements. This is because conventional computational techniques are often only as good as their underlying approximations, mathematics or computational implementations and hence, require continuous review and developments or improvements for better performance.

1.1 Computational chemistry

Computational chemistry deals with a set of techniques that allow the calculation or investigation of chemical problems (e.g., molecular geometries, reactivity, spectra and other properties of chemical systems) on a computer using a mathematical description of chemistry generally referred to as theoretical chemistry.[19,20] As such, the term "computational chemistry" is often used when a mathematical method or approximation is sufficiently developed to the point that it is implemented in a computer software program for use by practitioners. Such software programs are now often used by many with little or no knowledge of its underlying mathematical or theoretical principles.[20] In addition, the advent of powerful computers that reduce computation time to facilitate simple to higher-level accurate calculations has given computational chemistry an overwhelming attraction in recent years for a good description and reproducibility or even prediction of experimental findings.[21–23] This has augmented the understanding of chemical phenomena and is continuing to help in predicting the results of future experiments.

Generally, the tools available for use in computational chemistry for the investigation of chemical problems are present in two broad classes viz:[19,20]

1. Molecular mechanics and/or dynamics: based on models of systems (molecules) as a collection of balls (atoms) held together by springs (bonds) and is useful for investigating fairly large systems like proteins, cholesterol etc. This class depends solely on application of the laws of classical mechanics.
2. Quantum mechanics: based on the Schrödinger equation and provides, in principle, an almost exact description of how the electrons in a system (atom or molecule) behave or are distributed. The methods in this class may either be wavefunction or density functional based. This class is particularly suited for calculation of small (e.g., atoms and small molecules) to medium sised systems (e.g., inorganic compounds or clusters).

Herein, we will adopt the quantum mechanics approach to perform our calculations as the systems under consideration are of small or medium sises. Nevertheless, it should be noted that the Schrödinger equation cannot be solved exactly for any system with more than one electron. As a result, approximate methods (e.g., *ab initio* and density functional theory (DFT) methods) and key approximations relevant to the work covered in this thesis will be employed. The basic ideas and concepts of these methods and approximations will be provided in the theoretical background chapter. Some of the approximations common in most computational programs (e.g., Gaussian[24]) are the Born-Oppenheimer or fixed nucleus approximation and the Hartree-Fock (HF) theory which form the foundation of computational chemistry[16] codes amongst various other approximations on electron-electron interactions.

To test some of these theories and approximations especially with regards to electron correlation require small or few particle systems. This is because three-body or few-particle systems are the smallest systems in which the electron-electron correlation can be calculated to a high degree of accuracy. Three-body systems here refer to any system constituted from three particles, which may be a two-electron atom (e.g., helium) or ion (e.g., hydride ion). These two-electron systems and the hydrogen molecule have been the laboratory for accurate determination of electron-electron correlation data for quantum method developments for decades.[17,25] In this thesis, accurate HF wavefunctions of the helium atom and hydride ion are computed and used to re-parameterise a correlation energy formula used in DFT. Results obtained from these kinds of calculations will go a long way in contributing to or facilitating quantum method developments or improvements.

1.2 Thesis overview

This thesis presents the computational/theoretical investigation of the structure, stability and reactivity of inorganic complexes (pincer palladacycles, sulfur clusters (S_n) and hydrogen polysulfanes ($HS_{n+1}H$)). This is hoped to facilitate an understanding of pincer palladacycles for application in catalysis and augment clean sulfur recovery in modern thermal Claus plants as well as its transportation and application after recovery. The thesis also presents the re-parametrisation of the Colle and Salvetti (CS) correlation formula[26] using accurate HF densities for helium and hydride and the computation of correlation energies for several atomic systems using a form of the Lee-Yang-Parr (LYP) density correlation functional.[27]

The theoretical background and the mathematical basis (i.e., the computational and/or chemical physics methodologies and approximations) for the description of the chemistry presented in this thesis is presented in Chapter 2. Chapter 3 presents the theoretical investigation of the structure and reaction mechanisms of the unsymmetrical SCN pincer palladacycle for the formation of Pd(0),

using already validated[28] methodology. The Gibbs free energy profiles and energy barriers of Pd(0) generation from the species are compared to investigate the reactivity of the pincer palladacycles in the absence and presence of a base and in the absence and presence of a solvent. The results are used to rationalise the catalytic activity observed experimentally[29] for Suzuki-Miyaura carbon-carbon (C-C) cross-coupling reactions. The findings of this chapter have been published in the Journal of Organometallic Chemistry.[11] The determination of a suitable and/or reliable computational methodology for the calculation of the geometry, vibrational frequencies and energies of sulfur clusters (S_n) and hydrogen polysulfanes ($HS_{n+1}H$) is presented in Chapter 4. The determined methodology is used to investigate the electronic structure and stability of sulfur clusters, presented in Chapter 5 and the reactivity of stable open chains of sulfur clusters with hydrogen sulfide, presented in Chapter 6. A manuscript describing the results in Chapter 5 and 6 is in preparation. Chapter 7 describes the re-parametrisation of the CS formula using accurate HF densities for helium and hydride and the computation of correlation energies for several atomic systems using a form of the LYP formula in an in-house code. A manuscript describing the results in Chapter 7 has been submitted. Chapter 8 presents the summary and concluding remarks of this thesis.

2 Theoretical Background

This chapter provides the theoretical background and mathematical basis for the description of the chemistry and quantum data that will be presented in this thesis.

2.1 The Schrödinger Equation

The non-relativistic, time-independent Schrödinger equation is an eigenvalue equation for the Hamiltonian operator,[19,20,30,31] the operator for the total energy of a system.[32] The eigenvalue of this operator, E, is the value of the energy of a system and is often called the energy eigenvalue. This is the principal piece of information extracted from the Schrödinger equation of a system. When atomic or molecular systems are considered, the non-relativistic, time-independent Schrödinger equation is generally summarised to the simple-looking form:

$$\hat{H}\psi = E\psi \tag{2.1}$$

where $\hat{H}$ is the Hamiltonian operator, ψ is the normalised wavefunction of the system. The wavefunction, ψ contains all the dynamical information that defines a quantum system[30,33] or state of the system.[32–34] The Hamiltonian operator is defined as the sum of the kinetic and potential energy operators:[20,32,33,35]

$$\hat{H} = \hat{T} + \hat{V} \tag{2.2}$$

In general, for an N-particle system, the Hamiltonian operator is written in atomic units ($m_e = e = (4\pi\epsilon_0)^{-1} = \hbar = a_0 = 1$) as:[20]

$$\hat{H} = -\frac{1}{2}\sum_{i=1}^{N}\frac{1}{m_i}\nabla_i^2 + \sum_{i=1}^{N}\sum_{i<j}^{N}\frac{Z_i Z_j}{r_{ij}} \tag{2.3}$$

indicating that:

$$\hat{T} = -\frac{1}{2}\sum_{i=1}^{N}\frac{1}{m_i}\nabla_i^2 \tag{2.4}$$

and

$$\hat{V} = \sum_{i=1}^{N}\sum_{i<j}^{N}\frac{Z_i Z_j}{r_{ij}} \tag{2.5}$$

where m_i is the mass of the ith particle; N is the total number of particles in the system; Z_i and Z_j is the charge on the ith and jth particle, respectively; r_{ij} is the distance between particle i and j while the Laplacian for the ith particle in Cartesian coordinates (∇_i^2)[20,30–35] is expressed as:

$$\nabla_i^2 = \frac{\partial^2}{\partial x_i^2} + \frac{\partial^2}{\partial y_i^2} + \frac{\partial^2}{\partial z_i^2} \tag{2.6}$$

The Hamiltonian operator for a system with N-electrons and M-nuclei is usually expressed in atomic units as:[31]

$$\hat{H} = -\frac{1}{2}\sum_{i=1}^{N}\frac{1}{m_i}\nabla_i^2 - \frac{1}{2}\sum_{i=\mathrm{A}}^{M}\frac{1}{m_\mathrm{A}}\nabla_\mathrm{A}^2 - \sum_{i=1}^{N}\sum_{\mathrm{A}=1}^{M}\frac{Z_\mathrm{A}}{r_{i\mathrm{A}}} + \sum_{i=1}^{N}\sum_{i<j}^{N}\frac{1}{r_{ij}} + \sum_{\mathrm{A}=1}^{M}\sum_{\mathrm{A}<\mathrm{B}}^{M}\frac{Z_\mathrm{A}Z_\mathrm{B}}{r_{\mathrm{AB}}} \tag{2.7}$$

with A and B running over the M-nuclei in the system, i and j denote the N-electrons in the system while the terms are colour coded for clarity. The red and cyan terms represent the electronic and nuclear kinetic energies, respectively. The brown term represents the electron-nucleus potential energy; the green term is the electron-electron interaction potential energy while the **black** term represents the nuclear-nuclear interaction potential energy of the system. m_i is the mass of an electron, m_A is the mass of the nucleus A in multiples of the electron mass, r_{ij} is the electron-electron separation between electron i and j, r_{AB} represents the nuclear-nuclear separation while Z_A and Z_B is the charge on the A and B nucleus, respectively in the system. The Hamiltonian operator as given in eq. (2.7) is scarcely ever used in this form in current computational chemistry software codes, it is instead simplified to obtain an approximate solution to the Schrödinger equation using the Born-Oppenheimer Approximation.[20,35]

2.2 The Born-Oppenheimer Approximation

The Schrödinger equation cannot be solved exactly analytically for systems with more than one electron.[19,20,32,33,35] For many-electron systems, solutions of the Schrödinger equation can be

obtained within the Born-Oppenheimer (BO) approximation.[19,32,33,35] This approximation assumes that the nuclei are fixed relative to the electrons moving around them in a system.[19,20,31] This suggests that the nuclear and electronic motions are treated separately.[20,35] In this regard, the Hamiltonian operator in eq. (2.7) reduces, for a system with N-electrons and M-nuclei where the nuclei are assumed to be stationary, to the electronic Hamiltonian operator:

$$\hat{H}_e = -\frac{1}{2}\sum_{i=1}^{N}\frac{1}{m_i}\nabla_i^2 - \sum_{i=1}^{N}\sum_{\mathrm{A}=1}^{M}\frac{Z_{\mathrm{A}}}{r_{i\mathrm{A}}} + \sum_{i=1}^{N}\sum_{i<j}^{N}\frac{1}{r_{ij}} \tag{2.8}$$

with the colour coded terms and parameters retaining their meanings as in eq. (2.7). Substituting eq. (2.8) into eq. (2.1) yields the electronic energy of the system (E_e) since $\hat{H}_e$ will then operate on the electronic wavefunction (ψ_e). As a consequence, the total energy of the system may then be obtained by adding the constant nuclear-nuclear repulsion term (E_{nuc}, colour coded **black** in eq. (2.7)) at the end of the calculation,[19,20,35] i.e.,

$$E_{tot} = E_e + E_{nuc} \tag{2.9}$$

This suggests that the goal of approximating the solution of the Schrödinger equation in the BO approximation is to obtain the electronic energy of a system as a function of the fixed positions of the nuclei. From here, only the electronic Schrödinger equation will be considered and the subscripts to $\hat{H}_e$, ψ_e and E_e can be dropped.[31] Because electron-electron interactions are critical in the understanding and prediction of chemical behaviour,[17,32,35] it is important to include these interactions in electronic structure treatment[32] and method developments.[17,35] These interactions are included in increasingly sophisticated electronic structure methods in an attempt to recover the energies that systems possess as a result of electron-electron correlation beginning with an average treatment at the Hartree-Fock (HF) level.[17,32] The motion of the nuclei in a system (described by the cyan term in eq. (2.7)) can be accounted for by considering this entire formulation to be a potential energy surface (PES) on which the nuclei move.[20] As such, concepts such as potential energy surfaces (PESs)[19,20] and the Hartree-Fock theory (HF)[16,32,35] which form the foundation of computational chemistry codes such as Gaussian[24] arise.

The PES is a plot of a number of different nuclear geometries for a given system as a function of energy. As a consequence, fixed nuclear coordinates represent molecular geometry with electrons acting as a cloud of negative charge distributed around the positions of nuclei (stationary points). In this regard, a minimum energy point on the PES corresponds to a stable structure for a given system in that region of configuration space while a maximum energy point corresponds to a first-order or higher-order saddle point.[19,20,33,35] To distinguish the types of stationary points on the PES, the

second derivatives of the energy with respect to the nuclear coordinates (q) are considered with the aid of Hessian matrices.[19,32,35] Mathematically, minima and saddle points differ in that although both are stationary points (have zero first derivatives),[19,32,35]

$$\frac{\partial^2 E}{\partial q^2} > 0 \tag{2.10}$$

for a minimum for all q and

$$\frac{\partial^2 E}{\partial q^2} < 0 \tag{2.11}$$

for a transition state. For a transition state, eq. (2.10) is obeyed for all q along one or more directions except along the reaction coordinate where eq. (2.11) holds.[19] Some points on the PES have a negative second derivative of the energy with respect to more than one coordinate. These are called higher-order saddle points.[19] In practice, once a stationary point has been found in a calculation (e.g., geometry optimisation), the nature of that geometry is usually determined by calculating the vibrational frequencies of the geometry.[19,35] A minimum energy point on the PES has all positive force constants (vibrational frequencies) while a transition state has one negative force constant (imaginary frequency)[19,35] and higher-order saddle points on the PES possess more than one imaginary frequency.[19,31,35]

Once the nature of a stationary point for a system has been determined, it is then also possible to characterise its equilibrium structure in terms of bond lengths and angles.[32] It is noteworthy that a quantum system is never completely at rest,[19,30,32,33] i.e., even in the minimum stationary state, it possesses some kinetic energy as it still vibrates. This energy is always positive valued and irremovable and is called the zero-point energy (ZPE).[30,32,33] As such, for accurate computational energies, thermal corrections and ZPE's are calculated during frequency calculations at 298.15 K and 1 atm and added to the frozen-nuclei energy obtained at the stationary points on the PES.[19,36,37]

2.3 The Variation Principle

In order to compute the electronic energy of any system, the Hamiltonian operator ($\hat{H}$) for such a system is set up[31] and a trial wavefunction (ψ_{trial}) is used to generate the expectation value of the Hamiltonian to give its energy, E.[31,32] The system is then subjected to an energy optimising procedure that minimises its energy[19,31,32,35] to systematically approach the wavefunction of the ground state (ψ_0) of the system.[31] It should be noted that ψ_0 of the system will give the lowest

energy (ground state eigenvalue, E_{exact}) of the system.[31,32] The expectation value of the un-normalised trial wavefunction,[19,33,35] is given by the Rayleigh ratio:[32]

$$\langle \hat{H} \rangle = \frac{\langle \psi_{trial} | \hat{H} | \psi_{trial} \rangle}{\langle \psi_{trial} | \psi_{trial} \rangle} \tag{2.12}$$

Nevertheless, when ψ_{trial} is normalised, $\langle \psi_{trial} | \psi_{trial} \rangle = 1$. The variation principle therefore states that:[19,30–32,35]

$$\langle \hat{H} \rangle \geq E_{exact} \tag{2.13}$$

where E_{exact} (or E_0 in some texts) is the true or exact energy of the ground state[19,30–32,35] of the system. This indicates that $\langle \hat{H} \rangle$ is an upper bound to E_{exact} and that the equality in eq. (2.13) holds if and only if $\psi_{trial} = \psi_0$.[19,30–32] The significance of this principle is that ψ_{trial} giving the lowest $\langle \hat{H} \rangle$ is the optimum function of the system[32] and gives the best estimate of the ground state energy of the system. The variation principle therefore suggests that the average value of every measurable property of a system (e.g., energy) can be calculated, at least in principle, by calculating the expectation value of the operator.[19]

2.4 Hartree-Fock Theory

The impossibility of analytic solutions to the electronic Schrödinger equation for poly-electronic systems due to the electron-electron interaction term in eq. (2.8) gave rise to the HF approximation to enable calculation of many electron wavefunctions and energies.[19] In HF theory, each electron in a system of N-electrons is considered to be moving in the electrostatic field of the nuclei and the average field of the other $N-1$ electrons present in the system.[16,32] The approximation is often referred to as the central field approximation.[20,32] The starting point of this theory is to write the Hartree wavefunction for an N-electron system as a product of N one electron wavefunctions:[19,32,33]

$$\Psi_N = \psi_1(1)\psi_2(2)\psi_3(3) \ldots \psi_N(N) \tag{2.14}$$

where Ψ_N is the approximated total wavefunction in which ψ_1 is a function of the coordinates of electron 1, ψ_2 is a function of the coordinates of electron 2 and so on and the functions are called the orbitals of the system. Ψ_N however, does not satisfy the anti-symmetry principle. It is therefore required that this wavefunction (Ψ_N) must satisfy the Pauli principle, i.e., it must be anti-symmetric (change sign under the permutation of any pair of electrons).[19,32,33] For this requirement to be satisfied, the Slater wavefunction, composed of both spatial and spin coordinates of the

electrons,[19,32] is employed. Using a Slater wavefunction implies that all electrons are indistinguishable and each electron is associated with every orbital. The Slater wavefunction uses the Slater determinant which for a closed-shell system of electrons is:[19,32,33]

$$\Psi_N = \frac{1}{\sqrt{N!}}\begin{vmatrix} \psi_1(1)\alpha(1) & \psi_1(1)\beta(1) & \cdots & \psi_N(1)\alpha(1) & \psi_N(1)\beta(1) \\ \psi_1(2)\alpha(2) & \psi_1(2)\beta(2) & \cdots & \psi_N(2)\alpha(2) & \psi_N(2)\beta(2) \\ \vdots & \vdots & \ddots & \vdots & \vdots \\ \psi_1(N)\alpha(N) & \psi_1(N)\beta(N) & \cdots & \psi_N(N)\alpha(N) & \psi_N(N)\beta(N) \end{vmatrix} \tag{2.15}$$

where $\psi_1(1)\alpha(1)$ refers to electron 1 with α-spin (spin up) occupies orbital ψ_1 and $\psi_1(2)\beta(2)$ indicates the occupation of orbital ψ_1 by electron 2 with a β-spin (spin down) etc. while the initial factor on the right hand side of eq. (2.15) ensures that the wavefunction is normalised. Here, a mean field approximation will then suggest that the electrons in the system move independently of each other and that a Coulomb repulsion will be experienced due to the average field of all other electrons in the system. As such, one can then assume that they can be described by a Slater determinant and can be minimised using eq. (2.12). Therefore if ψ_{trial} in eq. (2.12) is replaced by the total wavefunction (Ψ_N) in eq. (2.15), the optimum wavefunction of a system in the sense of corresponding to the lowest total energy of the system must satisfy the HF equation:[19,31–33]

$$\hat{F}\psi_i(1) = \varepsilon_i\psi_i(1) \tag{2.16}$$

where ε_i is the eigenvalue and $\hat{F}$ is the one-electron Fock-operator:

$$\hat{F} = \hat{H}^{core}(1) + \sum_{j=1}^{N}\left(2\hat{J}_j(1) - \hat{K}_j(1)\right) \tag{2.17}$$

where the one-electron core Hamiltonian operator ($\hat{H}^{core}$), the Coulomb operator ($\hat{J}$, representing the Coulombic interaction between electron 1 in orbital i and electron 2 in orbital j) and the exchange operator ($\hat{K}$, which represents a correction to the electrostatic repulsion between the electrons in orbital j) are defined as:

$$\hat{H}^{core}(i) = -\frac{1}{2}\nabla_i^2 - \sum_{\mathrm{A}=1}^{M}\frac{Z_{\mathrm{A}}}{r_{i\mathrm{A}}} \tag{2.18}$$

$$\hat{J}_j(1)\psi_i(1) = \left\{\int \psi_j^*(2)\frac{1}{r_{12}}\psi_j(2)d\tau_2\right\}\psi_i(1) \tag{2.19}$$

$$\hat{K}_j(1)\psi_i(1) = \left\{\int \psi_j^*(2)\frac{1}{r_{12}}\psi_i(2)d\tau_2\right\}\psi_j(1) \tag{2.20}$$

This minimisation procedure is continued for N cycles in an iterative manner, guessing the form of the initial wavefunction at the beginning while each cycle adopts the wavefunction of the previous one. This goes on until the eigenvalue of $\hat{F}$ and ψ_i remain unchanged within a chosen convergence criterion (i.e., when the solution is self-consistent).[19,31–33] Hence the name, self-consistent field (SCF) given to the procedure.[32,33] However, because the Fock operator calculates the energy of each spatial orbital, ε_i has the physical meaning of the energy levels of a system.[31,32] To obtain the total energy of a system using this procedure, the idea of linear combination of atomic orbitals (LCAO) or basis functions is employed.[19,31–33] In this regard, expanding the wavefunction is a set of functions:

$$\psi_i = \sum_{j=1}^{M} c_{ji}\phi_j \tag{2.21}$$

where M represents the total number of basis functions, c_{ji}'s are the expansion coefficients of the ϕ_j (basis functions) of the ψ_i (molecular orbital). Eq. (2.21) is then applied to the HF equation (eq. (2.16)) to give the Roothaan equation:[19,32,33]

$$\hat{F}\sum_{j=1}^{M} c_{ji}\phi_j\,(1) = \varepsilon_i \sum_{j=1}^{M} c_{ji}\phi_j\,(1) \tag{2.22}$$

It can be written from eq. (2.22) that:[19]

$$\varepsilon_i = \sum_{j=1}^{M} c_{ji} \int \phi_j(1)\hat{F}\phi_j(1)d\tau \tag{2.23}$$

which follows from simply multiplying both sides of the HF equation by $\psi_i(1)$ and integrating over all space and spin coordinates ($d\tau$) while noting that ψ_i is normalised. By applying the Fock operator, eq. (2.22) becomes:

$$\varepsilon_i = \int \psi_i^*(1)\hat{H}^{core}(1)\psi_i(1)d\tau + \sum_{j=1}^{N}\big(2J_{ij}(1) - K_{ij}(1)\big) \tag{2.24}$$

where J_{ij} and K_{ij} are the Coulomb and exchange integrals defined as:

$$J_{ij} = \int \psi_i^*(1)\psi_i(1)\left(\frac{1}{r_{12}}\right)\psi_j^*(2)\psi_j(2)d\tau_1 d\tau_2 \tag{2.25}$$

$$K_{ij} = \int \psi_i^*(1)\psi_j^*(2)\left(\frac{1}{r_{12}}\right)\psi_i(2)\psi_j(1)d\tau_1 d\tau_2 \tag{2.26}$$

It can be written from eq. (2.24) that:

$$H_{ii} = \int \psi_i^*(1)\hat{H}^{core}(1)\psi_i(1)d\tau \tag{2.27}$$

So that eq. (2.24) transforms to:

$$\varepsilon_i = H_{ii} + \sum_{j=1}^{N}\left(2J_{ij}(1) - K_{ij}(1)\right) \tag{2.28}$$

The total energy of the systems in terms of the MO's can therefore be obtained as;[19]

$$E = 2\sum_{i=1}^{N} H_{ii} + \sum_{i=1}^{N}\sum_{j=1}^{N}\left(2J_{ij}(1) - K_{ij}(1)\right) \tag{2.29}$$

Supposing that the repulsion energies of electron 1 and electron 2 are added, i.e., the repulsion energy of electron 1 on the remaining $N-1$ (2, 3, 4, …, N) electrons and the repulsion energy of electron 2 on the remaining $N-1$ (1, 3, 4, … N) electrons, each repulsion is counted twice.[19] Therefore, eq. (2.29) over counts the electron-electron repulsion potential;[19] i.e.,

$$E_{overestimate} = 2\sum_{i=1}^{N} \varepsilon_i \tag{2.30}$$

As such, to eliminate the double counting of the repulsion or the superfluous interactions, the sum over N of the repulsion energy ($\sum\sum\left(2J_{ij}(1) - K_{ij}(1)\right)$) is subtracted from the right hand side of eq. (2.30). Much algebraic manipulations are then performed to eliminate the J and K over the MO's so as to obtain E_{HF} in terms of the c's and/or ψ_i's (MO's) as:[19,32]

$$E_{HF} = 2\sum_{i=1}^{N} \varepsilon_i - \sum_{i=1}^{N}\sum_{j=1}^{N}\left(2J_{ij}(1) - K_{ij}(1)\right) = \sum_{i=1}^{N}\left(\varepsilon_i + \left\langle\psi_i(1)\middle|\hat{H}^{core}(1)\middle|\psi_i(1)\right\rangle\right) \tag{2.31}$$

Alternatively, by multiplying both sides of eq. (2.22) by $\phi_i^*(1)$ and integrating over $d\tau$ results in:[32]

$$\sum_{j=1}^{M} c_{ji}\int \phi_i^*(1)\hat{F}\phi_j(1)d\tau = \varepsilon_i\sum_{j=1}^{M} c_{ji}\int \phi_i^*(1)\phi_j(1)d\tau \tag{2.32}$$

where:[19,32,33]

$$F_{ij} = \int \phi_i^*(1)\hat{F}\phi_j(1)d\tau \tag{2.33}$$

and

$$S_{ij} = \int \phi_i^*(1)\phi_j(1)d\tau \tag{2.34}$$

are the Fock and overlap matrices, respectively. Putting eq. (2.33) and eq. (2.34) into eq. (2.32) gives the Roothaan-Hall equations:[19,32,33]

$$\sum_{j=1}^{M} F_{ij}c_{ji} = \varepsilon_i \sum_{j=1}^{M} S_{ij}c_{ji} \tag{2.35}$$

which is one in a set of M simultaneous equations (one for each value of i).[32] The entire set of the equations in eq. (2.35) which are primarily aimed at computing the c_{ji}'s of the basis functions of the ψ_i's (MO's) can be written as the general single matrix equation:[19,32,33]

$$\mathbf{FC} = \boldsymbol{\varepsilon}\mathbf{SC} \tag{2.36}$$

where $\mathbf{C}$ is an $M \times M$ matrix composed of elements c_{ji} and $\boldsymbol{\varepsilon}$ is an $M \times M$ diagonal matrix of the orbital energies, ε_i.[19,32] The unknown electronic energy levels of the system in eq. (2.35) or eq. (2.36) may therefore be found by solving the secular equation:[32]

$$\det|F - \varepsilon_i S| = 0 \tag{2.37}$$

But eq. (2.37) cannot be solved trivially as F_{ij} involves integrals over $\hat{J}$ and $\hat{K}$, which are also dependent on spatial wavefunctions. Therefore the SCF procedure is adopted instead to obtain the c_{ji}'s and/or ε_i's with each iteration (cycle) giving a better value until the convergence criterion is achieved.[32] When this is achieved, eq. (2.22) to eq. (2.31) is employed to obtain the total electronic energy of the system as an upper bound to its exact energy.

The above formalism considers only systems in which there are an even number of electrons thereby supposing that the spatial components of the spin orbitals are identical for each member of a pair of electrons (closed-shell).[31,32] As such, the wavefunction as in eq. (2.15) is called the restricted Hartree-Fock (RHF) wavefunction[32] and the overall approximation, the restricted Hartree-Fock approximation.[31] This procedure is basically used to describe closed-shell organic or inorganic compounds.[31] The wavefunction involved in this approximation is an eigenfunction and the HF equations (eq. (2.16) to eq. (2.20)) can be converted to spatial eigenvalue problems by integrating over the spin functions and using the orthonormality of the spins.[32] The RHF formalism is however, inadequate for describing systems with an odd number of electrons or systems with an even number of electrons which are open-shell systems.[31] For such systems, two procedures are commonly adopted in their treatment in the HF approximation.[31,32] The first procedure is called the

restricted open-shell HF (ROHF) procedure. Here, all the α and β electrons except those occupying open-shell orbitals are forced to occupy the spatial orbitals in pairs. This method is not used in this thesis. The second approach is the unrestricted Hartree-Fock (UHF) method in which the α and β electrons in a system are not constrained to have the same spatial wavefunction. By relaxing the constraint of pair-wise occupation of orbitals, the UHF formalism yields a lower variational energy in comparison with the ROHF formalism. However, the disadvantage of the UHF formalism is that the UHF wavefunction is not an eigenfunction of the spin operator, $\langle \hat{S}^2 \rangle$, like that of the RHF.[31,32] This implies that the total spin angular momentum is not well-defined for the UHF wavefunction.[32] Usually, the more the $\langle \hat{S}^2 \rangle$ of the Slater determinant deviates from the $S(S+1)$ value, its true value in a system for a state,[31,32] the more the UHF determinant is contaminated by functions from states of higher spin multiplicity and the less physically meaningful it gets.[31,35] S stands for the spin quantum number representing the total spin of the system.

The HF approach only accounts for about 99 % of the total energy of a system but the 1 % unaccounted for[17,35] due to the electron-electron repulsion term is usually very important for describing chemical processes.[17,19,35] As a result, great efforts are made to recover the electron-electron correlation energy of systems computed at this level. This has given rise to many different sophisticated electron correlation approaches to solving the Schrödinger equation for many-electron systems with the HF approximation usually adopted as the starting point.[17,32,35] The RHF and UHF methods are used in this thesis to generate the canonical orbitals of species employed in post HF methodologies discussed in **2.5**. Also, the RHF method used to generate accurate densities for the helium atom and the hydride ion that are then employed in re-parameterising the CS correlation formula in **Chapter 7**.

2.5 Post-Hartree-Fock Methods

As mentioned in **2.4**, the HF ground-state wavefunction is not the 'exact' wavefunction of such systems notwithstanding how good it may be as the method does not take account of electron correlation.[32,38] Nevertheless, it is worth noting that the HF theory accounts for the correlated motion of electrons of the same spin (Fermi correlation) but ignores the spin independent correlated motion of electrons (Coulomb correlation).[16–18] Consequently, it does not consider the instantaneous Coulombic interactions between electrons nor account for the quantum mechanical effects on electron distributions since the effect of the $N-1$ electrons on the electron in question is treated as an average. It can therefore be summarised that the HF approximation ignores electron correlation - the correlated motion of electrons.[19,32,38] This suggests that even though the HF

calculations are adequate for many purposes, there are cases where a better treatment of electron correlation is needed. In this regard, the post-Hartree-Fock methods are attempts to treat such correlated motion better than they are in the HF procedure, i.e., they are correlated calculations.[19] Löwdin defined the energy of the ignored correlated motion of the electrons, E_c, as:[39,40]

$$E_c = E_{exact} - E_{HF} \tag{2.38}$$

where E_c is the correlation energy while E_{exact} and E_{HF} is the exact non-relativistic and HF energy of a system, respectively. Three basic approaches exist for treating electron correlation namely:[19]

1. Explicit use of inter-electronic distances as variables in the Schrödinger equation: this is reserved for treatment of atoms and small molecules as it quickly leads to mathematically intractable problems;
2. Treatment of real systems (molecules) as perturbed HF systems and
3. Explicit inclusion of electronic configurations other than that of the ground state in the wavefunction.

The approaches in 2 and 3 are general but very important as they form the basis of the many-body perturbation, coupled-cluster and the configuration interaction procedures.[19] Also, approach 3 introduces the concept of configuration state functions (CSF's), which are determinants, for equivalent symmetry adapted electronic states that differ only by an electron occupation upon promotion from the ground state.[19,31,32] CSF's are crucial in the formulation of the post-HF procedures as will be discussed below.

2.5.1 The Configuration Interaction Method

The HF method produces a finite set of $2M$ spin orbitals which can be ordered energetically from the lowest (occupied) to the highest (unoccupied), when a finite basis set expansion is used.[32] Assuming the lowest to be occupied by N ground state electrons, its HF wavefunction ψ_{HF} can be formed leaving a $2M - N$ set of virtual (unoccupied) orbitals. Consequently, many Slater determinants can be formed from the set with ψ_{HF} as one of them for a given system especially when electron excitement is involved. As such, it can be written that:[32]

$$\psi_{HF} = \frac{1}{\sqrt{N!}} det|\psi_1\psi_2 \dots \psi_a\psi_b \dots \psi_N| = \|\psi_1\psi_2 \dots \psi_a\psi_b \dots \psi_N\| \tag{2.39}$$

where ψ_a and ψ_b are among the occupied spin orbitals of the ψ_{HF} ground state; normalisation and determinant are further simplified and implied by $\|\dots\|$. A singly excited determinant, say ψ_a^p,

corresponding to one for which a single electron in the occupied orbital ψ_a has been promoted to the virtual spin orbital, ψ_p will be:

$$\psi_a^p = \|\psi_1\psi_2 \dots \psi_p\psi_b \dots \psi_N\| \tag{2.40}$$

And a determinant representing doubly excited electrons from spin orbitals ψ_a and ψ_b to spin orbitals ψ_p and ψ_q, ψ_{ab}^{pq} will be:

$$\psi_{ab}^{pq} = \|\psi_1\psi_2 \dots \psi_p\psi_q \dots \psi_N\| \tag{2.41}$$

These determinants can also be formed for multiple excitation of electrons, each of which is called a configuration state function (CSF).[32] Eq. (2.39) to eq. (2.41) can be presented diagrammatically as in **Figure 2.1**.

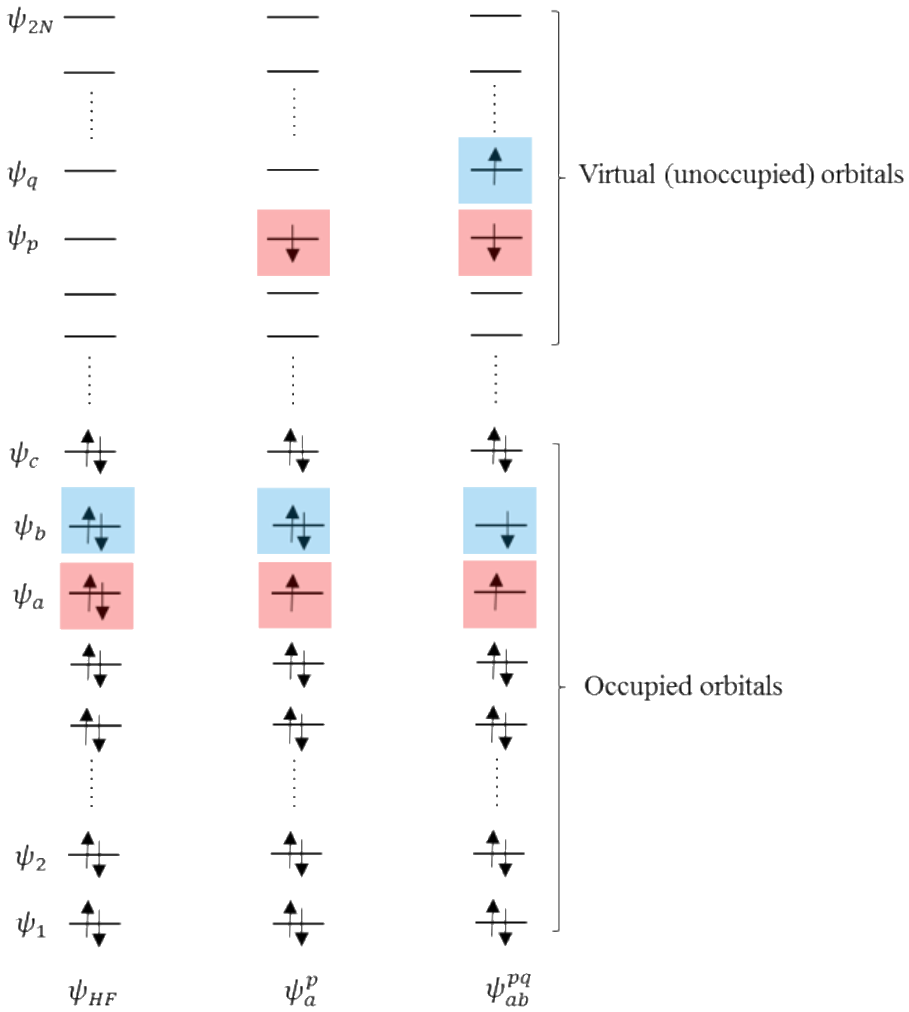

Figure 2.1. Notation for ground and excited state determinants showing promotion of electrons whose spin can be α or β.

The excited CSF's are used to approximate excited state wavefunctions or used in a linear combination with ψ_{HF} to improve the representation of the ground state or any excited state wavefunction.[32]

In the configuration interaction (CI) procedure, the HF determinant (ψ_{HF}) is considered as the ground state while the excited determinants are approximated as promotion of electrons from the ground state to unoccupied/virtual orbitals for treating electron correlation.[19] The exact ground or excited state wavefunction for this formalism can therefore be written as a linear combination of all possible N-electron Slater determinants arising from a complete set of spin orbitals in the form:[19,32,35]

$$\psi_{CI} = c_0\psi_{HF} + \sum_{a,p} c_a^p \psi_a^p + \sum_{\substack{a<b \\ p<q}} c_{ab}^{pq} \psi_{ab}^{pq} + \sum_{\substack{a<b<c \\ p<q<r}} c_{abc}^{pqr} \psi_{abc}^{pqr} + \cdots = \sum_{J=0}^{L} c_J \psi_J \tag{2.42}$$

where c_a^p, c_{ab}^{pq}, … and/or c_J are the expansion coefficients, the limits in the summation $\binom{a<b}{p<q}$,...) are to ensure that the sum is over all the unique pairs, unique triplets etc. of spin orbitals in doubly, triply etc. excited determinants.[32] When the procedure exhausts all the possible electron excitations for a finite basis set, the calculation is considered a full CI calculation.[19,32] Full CI is however, not always possible except for very small systems.[35] The c_a^p, c_{ab}^{pq}, … and/or c_J in eq. (2.42) and hence the energy of a system can either be computed by variational minimisation using eq. (2.12) and ψ_{CI} as the trial wavefunction or solving the matrix equations:[32]

$$\mathbf{HC} = \boldsymbol{\varepsilon}\mathbf{SC} \tag{2.43}$$

like in eq. (2.36). Here,

$$H_{ij} = \langle \psi_i | \hat{H} | \psi_j \rangle \tag{2.44}$$

and

$$S_{ij} = \langle \psi_i | \psi_j \rangle \tag{2.46}$$

Some of the common computationally tractable variants of this procedure include; CIS where the CI approach involves only single excitations, CID which involves only double excitations, CISD in which the CI procedure involves single and double excitations and CISD(T) in which the CI scheme involves single, double and perturbative triple excitations etc.[19,31,32,35] The disadvantage of this method is that it lacks sise consistency.[19,32,35] Nevertheless, this can be corrected by using the Davidson correction:[32,35,41]

$$\Delta E_Q = (1 - c_0^2)(E_{CISD} - E_{SCF}) \tag{2.46}$$

which can correct the error significantly.[32] ΔE_Q is the estimation of the contribution of the quadruply excited determinant (usually denoted by attaching $+Q$ to the methodology,[35] e.g., $\mathrm{CISD}+Q$) to the correlation energy, E_{CISD} is the ground state energy computed using CISD and E_{SCF} is the ground state energy associated with ψ_{HF} while c_0 is the ψ_{HF} expansion coefficient computed with the CISD procedure.[32,35] Corrections of sise-consistency due to more complicated contributions from higher excited determinants have also been proposed in the literature.[42] This method gives the basic background to the multi-configurational SCF (MCSCF) methods, e.g., the complete active space SCF (CASSCF) discussed in the next section.

2.5.2 The Complete Active Space Self-Consistent Field Method

The CASSCF approach[38] to recovering the correlation energy ignored by the HF method is a variant of MCSCF method, pioneered by Björn Roos.[19,32,35,43] In the MCSCF formalism, both the c_{ji}'s of eq. (2.21) and c_J's of eq. (2.42) are iteratively optimised together with the MO's making up the determinants using eq. (2.12).[19,32,35] In addition, the optimal values of the c_{ji}'s in eq. (2.21) are predetermined by a HF-SCF calculation and used in the formation of excited Slater determinants in subsequent CI calculations.[32,35,38] In the CASSCF method, the MO's are divided into three sets viz:[19,32,35,38,43]

1. Inactive orbitals: lowest energy orbitals that are doubly occupied in all determinants and correspond to core orbitals;
2. Virtual orbitals: very high in energy and are unoccupied in all determinants and
3. Active orbitals: these orbitals fall in between the virtual and inactive orbitals energetically; i.e., they are often some of the highest occupied and lowest unoccupied orbitals. Within these MO's, full CI is performed and the proper symmetry-adapted CSF's are included in the optimisation.

The active orbitals and electrons are usually chosen manually based on chemistry of the system investigated with this approach. These then give rise to all the possible ways of distributing the active electrons over the active orbitals to give CSF's that are included in the CASSCF procedure.[19,32,35] The CI wavefunction is then used as the trial wavefunction and iteratively solved over the included CSF's until self-consistency is achieved, i.e., when the determined c_J's remain constant within a chosen convergence criterion. This method will be used in this thesis.

The post-HF methodologies described so far involve CSF's arising from electron excitation from the ψ_{HF} determinant. Nevertheless, MCSCF wavefunction(s) may also be chosen as reference from

which a set of excited CSF's can be formed for use in a CI calculation.[32,35] When this is the case, the methodology is termed multi-reference configuration interaction (MRCI).[35]

2.5.3 Møller-Plesset Many-Body Perturbation Theory

The post-HF methods described above are non-perturbative approaches[44] to treating the electron correlation problem using the HF determinant as the reference wavefunction. The Møller-Plesset perturbation theory (MPPT)[45] is one of the commonly employed perturbative approaches to the electron correlation problem and is usually carried out from second to fourth-order.[44,46] In this theory, the zero-order Hamiltonian of a system ($\hat{H}^{(0)} \equiv \hat{H}_{HF}$) composed of N-interacting electrons is selected to be the sum of one-electron Fock operators as:[32,35]

$$\hat{H}^{(0)} = \sum_{i=1}^{N} \hat{F}_i \tag{2.47}$$

with its corresponding eigenvalue, $E_0^{(0)}$ given by the sum of the orbital energies of all the occupied MO's. The Hamiltonian for the perturbation of the system ($\hat{H}^{(1)}$) which represents the extent to which the true Hamiltonian differs from the model one is defined as:[32,33,35,47]

$$\hat{H}^{(1)} = \hat{H} - \sum_{i=1}^{N} \hat{F}_i \tag{2.48}$$

where $\hat{H}$ is the true electronic Hamiltonian of the system. But the HF ground state energy (E_{HF}) associated with the normalised ground state wavefunction (ψ_{HF}) is:

$$E_{HF} = \langle \psi_{HF} | \hat{H} | \psi_{HF} \rangle \tag{2.49}$$

Putting eq. (2.48) into eq. (2.49) yields:

$$E_{HF} = \langle \psi_{HF} | \hat{H}^{(0)} + \hat{H}^{(1)} | \psi_{HF} \rangle \tag{2.50}$$

It can therefore be shown from eq. (2.50) that:[32]

$$E_0^{(0)} = \langle \psi_{HF} | \hat{H}^{(0)} | \psi_{HF} \rangle \tag{2.51}$$

$$E^{(1)} = \langle \psi_{HF} | \hat{H}^{(1)} | \psi_{HF} \rangle = \lambda^0 E_0^{(0)} + \lambda E_0^{(1)} + \lambda^2 E_0^{(2)} + \lambda^3 E_0^{(3)} + \cdots \tag{2.52}$$

where λ^i represents the order of perturbation while $E_0^{(i)}$ stands for correction to the unperturbed energy ($E_0^{(0)}$) of a system corresponding to the level of perturbation.

But[32]

$$E_{HF} = \lambda^0 E_0^{(0)} + \lambda E_0^{(1)} \tag{2.53}$$

$\Rightarrow$ therefore that eq. (2.53) is the first-order correction to the energy of the system and is essentially the HF energy of the ground state. Consequently, correction for electron correlation energy will therefore begin at the second-order with the choice of $\hat{H}^{(0)}$ as discussed. This energy correction, which is the first contribution to the correlation energy, will only involve a sum over doubly excited determinants resulting from promotion of electrons which makes it easier for the electrons to avoid one another.[19,32,35] This is the essence of the MPPT.[19] In this regard, the second-order correction to the energy of the system will be:[32,35,45]

$$E_0^{(2)} = \frac{1}{4}\sum_{a<b}^{occ}\sum_{p<q}^{virt}\frac{(ab\|pq)(pq\|ab)}{\varepsilon_a + \varepsilon_b - \varepsilon_p - \varepsilon_q} \tag{2.54}$$

where the sum is restricted so that the excited determinant is only counted once.[35] In addition,[32,35]

$$(ab\|pq)(pq\|ab) = \langle\psi_a\psi_b|\psi_p\psi_q\rangle - \langle\psi_a\psi_b|\psi_q\psi_p\rangle \tag{2.55}$$

and[19,32]

$$(ab\|pq) = \int \psi_a^*(1)\psi_b^*(2)\frac{1}{r_{12}}\psi_p(1)\psi_q(2)d\tau_1 d\tau_2 - \int \psi_a^*(1)\psi_b^*(2)\frac{1}{r_{12}}\psi_q(1)\psi_p(2)d\tau_1 d\tau_2 \tag{2.56}$$

with ψ_a and ψ_b as the occupied MO's and ψ_p and ψ_q as the virtual (unoccupied) MO's. The MPPT with inclusion of the second-order corrections to the energy of the system is designated MP2[19,32,35] for short; this level and higher-order corrections[44,46] can be written for short as MP*n* where *n* = 2, 3, 4, 5, … .[32,35] Whereas the MPPT calculations are sise consistent, they are not variational[19,32,35] like the full CI method as they do not, in general, give energies that are upper bounds to the exact energy.[32] The MPPT (MP*n*) method is not used in this thesis but is incorporated in the method discussed in the next section which is employed in this thesis.

2.5.4 The Coupled Cluster Method

The coupled cluster (CC) method[48–51] for solving the Schrödinger equation for many electron systems in electronic structure incorporates the mathematical features of the many-body perturbation theory (MBPT) and higher-electronic state CI methods.[32,35] The CC method is also used in this thesis. The basic idea of this theory is to express the correlated wavefunction with an exponential ansatz assuming normalisation[19,32,35,48,52] as:

$$\psi_{CC} = \left(1 + \hat{T} + \frac{\hat{T}^2}{2!} + \frac{\hat{T}^3}{3!} + \cdots\right)\psi_{HF} = \left(\sum_{i=1}^{N} \frac{1}{k!}\hat{T}_i^k\right)\psi_{HF} = e^{\hat{T}}\psi_{HF} \tag{2.57}$$

where

$$\hat{T} = \sum_{i=1}^{N} \hat{T}_i \tag{2.58}$$

also, $i = 1, 2, 3, \ldots, N$ and $k = 0, 1, 2, 3, \ldots$, $\hat{T}$ and/or $\hat{T}_i$ are called the cluster or excitation operator(s) and are defined for singly, doubly, triply, etc. excitations[32,35,52] as:

$$\hat{T}_1\psi_{HF} = \sum_{a}^{occ}\sum_{p}^{virt} t_a^p \psi_a^p \tag{2.59}$$

$$\hat{T}_2\psi_{HF} = \sum_{a<b}^{occ}\sum_{p<q}^{virt} t_{ab}^{pq} \psi_{ab}^{pq} \tag{2.60}$$

$$\hat{T}_3\psi_{HF} = \sum_{a<b<c}^{occ}\sum_{p<q<r}^{virt} t_{abc}^{pqr} \psi_{abc}^{pqr} \tag{2.61}$$

$\Rightarrow$ the $\hat{T}_i$ operator acting on ψ_{HF} (the reference wavefunction) generates all the ith excited Slater determinants involved in the system. The t_a^p, t_{ab}^{pq}, t_{abc}^{pqr} etc. are called the excitation amplitudes accordingly.[32,35] The effect of $e^{\hat{T}}$ on ψ_{HF} is that it leads to eq. (2.59) to eq. (2.61) and the products of the $\hat{T}_i$ operators, e.g., $\hat{T}_1\hat{T}_1$, $\hat{T}_1\hat{T}_2$, $\hat{T}_1\hat{T}_3$, $\hat{T}_2\hat{T}_3$, $\hat{T}_1^2$, $\hat{T}_2^2$, $\hat{T}_1^3$ etc.[32,35,52] Here, for instance, when the excitation involves $\hat{T}_2\psi_{HF}$, the double-excitation amplitudes (t_{ab}^{pq}) appear whereas the product of single-excitation amplitudes, $t_a^p t_b^q$ results when the excitation involves $\hat{T}_1\hat{T}_1\psi_{HF}$ or $\hat{T}_1^2\psi_{HF}$.[32] One can then say that $\hat{T}_2\psi_{HF}$ represents a connected double-excitation contribution while $\hat{T}_1\hat{T}_1\psi_{HF}$ or $\hat{T}_1^2\psi_{HF}$ represents a disconnected double-excitation contribution[32,35] to the total wavefunction of the system. Physically, a connected excitation such as $\hat{T}_2\psi_{HF}$ corresponds to two interacting electrons undergoing simultaneous excitation while a disconnected excitation such as $\hat{T}_1\hat{T}_1\psi_{HF}$ or $\hat{T}_1^2\psi_{HF}$ corresponds to two non-interacting electrons undergoing simultaneous excitation.[35] Therefore for a double-excitation contribution to the total wavefunction of a system, when $\hat{T}_1$ is small, $\hat{T}_1^2$ will (must) also be small and the most important contribution therefore comes from $\hat{T}_2$. Arising from eq. (2.57), the Schrödinger equation (eq. (2.1)) may be transformed[32,35] as:

$$\hat{H}e^{\hat{T}}\psi_{HF} = Ee^{\hat{T}}\psi_{HF} \tag{2.62}$$

and the energy of the system obtained as:[35]

$$E_{CC} = \langle \psi_{HF} | \hat{H} e^{\hat{T}} | \psi_{HF} \rangle \tag{2.63}$$

by multiplying eq. (2.62) from the left by ψ_{HF}^{*} and integrating over all space and spin coordinates. The amplitudes can be obtained by projecting eq. (2.62) onto the space of the singly, doubly, triply etc. excited determinants in a similar manner as in eq. (2.63).[35] This must proceed on the premise of expanding the exponential in eq. (2.57) and using the fact that the Hamiltonian operator contains only one- and two-electron operators.[35] If all the excitation operators up to $\hat{T}_N$ are included in eq. (2.63), all possible excited determinants will be generated and E_{CC} will be equivalent to that of a full CI. This is however impossible for all but the smallest systems.[19,32,35] The cluster operator must therefore be truncated (reduced) at some level of excitation. When this is done, the calculated energy will also be approximate and can include some perturbative contributions to reduce computational cost.[19,35] As such, based on the number of terms included in eq. (2.58), the coupled cluster doubles (CCD), coupled cluster singles and doubles (CCSD) or coupled cluster singles, doubles and triples (CCSDT) procedure may be formed with the following excitation operators:[19]

$$\hat{T}_{CCD} = e^{\hat{T}_2} \psi_{HF} \tag{2.64}$$

$$\hat{T}_{CCSD} = e^{(\hat{T}_1 + \hat{T}_2)} \psi_{HF} \tag{2.65}$$

$$\hat{T}_{CCSDT} = e^{(\hat{T}_1 + \hat{T}_2 + \hat{T}_3)} \psi_{HF} \tag{2.66}$$

CCSDT calculations are computationally very demanding except for the smallest systems and so its variant, CCSD(T) including the triples contribution in a perturbative fashion is more often employed.[19,35] This CC variant (CCSD(T)) is currently, generally speaking, the benchmark for calculations on systems of up to moderate sise[19] and is used in this thesis. The CC procedure like the MP*n* approach, is sise consistent but not variational.[19,32,35] Since the singly excited determinants in the CC wavefunction (ψ_{CC}) allow the MO's to relax in order to describe its multi-reference character, the magnitude of the singles amplitude is an indication of how good the ψ_{HF} is as a reference function.[35] As such, the $\mathcal{T}_1$ Diagnostic of Lee and Taylor[53,54] is often used to evaluate the quality (extent of the multi-configurational and/or multi-reference character) of the ψ_{CC} in CCSD or CCSD(T) for a given system.[3,53,54] In essence, this Diagnostic is used to determine the reliability of single-reference-based techniques for computing, in addition to the HF energy, the electron correlation energies of chemical systems. Consequently, this Diagnostic will be used in this thesis to determine the reliability of single-reference methodologies for investigation of sulfur species.

The $\mathcal{T}_1$ Diagnostic is the Euclidian norm of the vector t_1 amplitudes (for single excitations) divided by the square root of the number of correlated electrons in a system, N:[54]

$$\mathcal{T}_1 = \frac{\|t_1\|}{\sqrt{N}} \tag{2.67}$$

Eq. (2.67) was formulated for closed-shell systems[53–55] and is the equation implemented in the Gaussian code for the determination of the reliability of single-reference methods for both open and closed-shell systems.[56] It is asserted that using this formalism, the threshold for a system that does not possess significant multi-reference character is 0.02.[53,54] However, an alternative equation for calculating the values of the Diagnostic for open-shell systems that is consistent with the closed-shell formalism has since been derived.[55] The open-shell formalism was employed to clarify the use of the Diagnostic by Schaefer and co-workers.[57] The authors asserted that the threshold for open-shell systems should be 0.045 and not 0.02. It has also been argued that the $\mathcal{T}_1$ Diagnostic for open-shell reactions (or systems) computed using the closed-shell formalism is likely to be higher than the threshold[56] of the formalism developed for the open-shell systems. Furthermore, when using the Gaussian code to compute an open-shell species, the $\mathcal{T}_1$ Diagnostic can have values in excess of the threshold without significant multi-configurational or multi-reference character.[56]

2.6 Density Functional Theory

This is an alternative computational technique to the HF or post-HF wavefunction-based methods.[19,33,58] Unlike the HF-based approaches, the density functional approach is based on the electron probability density instead of the wavefunction of a system. The main advantages of this technique over the post-HF methods discussed above are that:[19,32,33]

1. It is less demanding in terms of computational efforts (computation time and computer memory) especially when computations require big basis sets for accurate results and
2. Its results can agree better with experiments in many instances.

The density functional theory (DFT) procedure for computing the electronic energy of systems was initiated by the work of Hohenberg and Kohn in 1964[59] and that of Kohn and Sham in 1965.[60] In this technique, the basic idea is that the energy and all other properties of systems in their ground electronic state are determined in terms of their ground state electron probability density, $\rho(\boldsymbol{r})$.[19,32,34] This is because unlike the wavefunction which is not a physical observable, the electron density of a system is a physical observable.[19,31] For a system of N-electrons, $\rho(\boldsymbol{r})$

represents the total electron density of the system at point $\boldsymbol{r}$ in space[32] and is related to the wavefunction (one-electron spatial orbitals) of the system as:[60]

$$\rho(\boldsymbol{r}) = \sum_{i=1}^{N} \left|\psi_i^{KS}(\boldsymbol{r})\right|^2 \tag{2.68}$$

where the sum is over all occupied Kohn-Sham (KS) orbitals, ψ_i^{KS} and $\rho(\boldsymbol{r})$ is known once the KS-orbitals are computed. Also for the system whose $\rho(\boldsymbol{r})$ is expressed as eq. (2.68), its ground state energy is expressed as:[19,31,34,35,59,60]

$$E_0 \leq E[\rho] = T[\rho] + V_{ne}[\rho] + V_{ee}[\rho] \tag{2.69}$$

since $V_{nn}[\rho]$ (the nuclear-nuclear repulsion functional) will be constant within the BO approximation. E_0 is the exact total electronic energy of the system, $E[\rho]$ is the total electronic energy functional, $T[\rho]$ is the kinetic energy functional, $V_{ne}[\rho]$ is the nuclear-electron interaction functional and $V_{ee}[\rho]$ is the electron-electron repulsion functional of the system. The $V_{ee}[\rho]$ term of eq. (2.69) comprises of the Coulomb functional ($J[\rho]$) and exchange-correlation energy functional ($E_{XC}[\rho]$) parts[31,32,35] and so eq. (2.69) can be re-written as:

$$E_0 \leq E[\rho] = T[\rho] + V_{ne}[\rho] + J[\rho] + E_{XC}[\rho] \tag{2.70}$$

where

$$V_{ne}[\rho] = -\sum_{i=1}^{N}\sum_{\mathrm{A}=1}^{M} \frac{Z_{\mathrm{A}}}{r_{i\mathrm{A}}}\rho(\boldsymbol{r}_1)d\boldsymbol{r}_1 \tag{2.71}$$

and

$$J[\rho] = \frac{1}{2}\int\int \frac{\rho(\boldsymbol{r}_1)\rho(\boldsymbol{r}_2)}{r_{12}}\, d\boldsymbol{r}_1 d\boldsymbol{r}_2 \tag{2.72}$$

Nevertheless, treatment of $T[\rho]$ in eq. (2.69) is complicated and is replaced instead by $T_S[\rho]$ which was proposed by Kohn and Sham and includes the KS one-electron orbitals[60] with the subscript *S* implying that $T_S[\rho]$ is calculated from a Slater determinant,[19,31,35] i.e.,

$$E_0 \leq E[\rho] = T_S[\rho] + V_{ne}[\rho] + J[\rho] + E_{XC}[\rho] \tag{2.73}$$

The kinetic energy functional in eq. (2.73), $T_S[\rho]$ for an N-electron system is exactly defined as:[19,31,32,35]

$$T_S[\rho] = -\frac{1}{2}\sum_{i=1}^{N}\left\langle \psi_i^{KS}(\boldsymbol{r}_1)\middle|\nabla_1^2\middle|\psi_i^{KS}(\boldsymbol{r}_1)\right\rangle \tag{2.74}$$

Putting eq. (2.71), eq. (2.72) and eq. (2.74) into eq. (2.73) gives:

$$E[\rho] = -\frac{1}{2}\sum_{i=1}^{N}\left\langle \psi_i^{KS}(\boldsymbol{r}_1)\middle|\nabla_1^2\middle|\psi_i^{KS}(\boldsymbol{r}_1)\right\rangle - \sum_{i=1}^{N}\sum_{\mathrm{A}=1}^{M}\frac{Z_{\mathrm{A}}}{r_{i\mathrm{A}}}\rho(\boldsymbol{r}_1)d\boldsymbol{r}_1 + \frac{1}{2}\int\int\frac{\rho(\boldsymbol{r}_1)\rho(\boldsymbol{r}_2)}{r_{12}}d\boldsymbol{r}_1 d\boldsymbol{r}_2 + E_{XC}[\rho] \tag{2.75}$$

As a consequence, the only unknown term is the $E_{XC}[\rho]$ which takes into account all the effects of non-classical interactions and consists of the exact correlation energy term, $E_C[\rho]$ and the exchange energy term, $E_X[\rho]$ and may be written as:[35]

$$E_{XC}[\rho] = (T[\rho] - T_S[\rho]) + (V_{ee}[\rho] - J[\rho]) = E_X[\rho] + E_C[\rho] \tag{2.76}$$

This is where approximate density functional developments take root as it is the main source of error when using DFT.[19,31,32] It should be noted nevertheless, that the contribution of $E_X[\rho]$ to $E_{XC}[\rho]$ is always bigger than that of $E_C[\rho]$.[19] Substitution of eq. (2.68) into eq. (2.75) for the electron density and differentiating to vary $E[\rho]$ in terms of ψ_i^{KS} (provided they remain orthonormal) led to the derivation of the Kohn-Sham equations for one-electron orbitals:[31,60]

$$\left\{-\frac{1}{2}\nabla_1^2 - \sum_{\mathrm{A}=1}^{M}\frac{Z_{\mathrm{A}}}{r_{\mathrm{A}1}} + \int\frac{\rho(\boldsymbol{r}_2)}{r_{12}}d\boldsymbol{r}_2 + V_{XC}(\boldsymbol{r}_1)\right\}\psi_i^{KS}(\boldsymbol{r}_1) = \varepsilon_i^{KS}\psi_i^{KS}(\boldsymbol{r}_1) \tag{277}$$

where ε_i^{KS} are the Kohn-Sham orbital energies and $V_{XC}(\boldsymbol{r}_1)$ is the exchange-correlation potential which is a functional derivative of $E_{XC}[\rho]$ defined as:[19,32,33]

$$V_{XC}(\boldsymbol{r}_1) = \frac{\delta E_{XC}[\rho(\boldsymbol{r})]}{\delta\rho(\boldsymbol{r})} \tag{2.78}$$

The ψ_i^{KS} are found by applying the Hohenberg-Kohn variational principle with an initial set of trial KS-orbitals[32,34] in an iterative and self-consistent manner[32,33] as in eq. (2.12). The choice of density functional technique adopted (which determines how $E_{XC}[\rho]$ and hence $V_{XC}(\boldsymbol{r}_1)$ is dealt with[32,33]) for a given computation is therefore important in determining the accuracy of the result so obtained.[35] As a consequence, a systematic method determination by comparison of DFT results with experimental findings is critical to the accuracy of computations when DFT methodologies are employed for a given investigation. As a consequence, a systematic method determination will be performed to obtain suitable DFT functionals to model systems investigated in this thesis.

2.6.1 Exchange-Correlation Functionals

The DFT methodologies that will be employed in this thesis will now be discussed. Numerous exchange-correlation functionals for use in DFT are being developed in order to obtain approximate forms of the exchange-correlation energy.[32,61–63] The choice of a density functional technique adopted for a given computation therefore specifies how the $E_{XC}[\rho]$ and hence $V_{XC}(\boldsymbol{r}_1)$ is dealt with[32,33] for accurate computational results.[35]

2.6.1.1 The Local Density Approximation

The simplest of these approximations is the local density approximation (LDA) which is derived from a uniform homogeneous electron gas without accounting for electron spin.[31–33,35,61] This suggests that the electron density is distributed all over space of infinite volume for a given system.[19,32,64] In this formalism, the $E_X[\rho]$ component of $E_{XC}[\rho]$ is the Slater exchange[31] and is approximated as:[35,58,64]

$$E_X^{LDA}[\rho] = -C_X \int \rho^{4/3}(\boldsymbol{r})\, d\boldsymbol{r} \tag{2.79}$$

where C_X is:

$$C_X = \frac{3}{4}\left(\frac{3}{\pi}\right)^{1/3} \tag{2.80}$$

There is however no known explicit expression for the correlation part of this formalism.[31] Nevertheless, the purely dynamical analytical form of the correlation component in this approximation was derived in the low density[65] and high density[66] regions using perturbation expansions. Furthermore, the correlation term in this approximation for intermediate densities may be determined using quantum Monte Carlo methods when run long enough. This was demonstrated by Ceperley and Alder in 1980.[67] The work of Ceperley and Alder have now given rise to various analytical expressions that are now widely used, e.g., the Vosko, Wilk and Nusair (VWN)[68] correlation functional. This formalism forms the bedrock of almost all approximations currently used in DFT[61] with authors continuously presenting improvements in the form of analytical expressions of $E_C[\rho]$ based on sophisticated interpolation schemes.[31,58] The LDA uses spatial orbitals in $\rho(\boldsymbol{r})$ (eq. (2.75)) that are spin-paired to ensure electro-neutrality and so behaves fairly well for closed-shell systems but not for open-shell systems.[31,32] Generally, this procedure underestimates $E_X[\rho]$ by roughly 10 %.[61,64] It also underestimates ionisation and ground state energies but overestimates binding energies and $E_C[\rho]$.[32,58]

2.6.1.2 The Local Spin Density Approximation

When the LDA is extended to open-shell systems to allow for occupation of different spatial orbitals by different spins, the local spin density approximation (LSDA) is obtained.[19,31] This then allows for inclusion of electron density functions for the different spins ($\rho_\alpha(\boldsymbol{r})$ and $\rho_\beta(\boldsymbol{r})$).[19,58] For closed-shell systems, the LSDA is equal to the LDA.[19,35,58] Molecular geometries, frequencies and electron distribution properties computed using LSDA are fairly reasonable, but it produces rather poor dissociation energies.[19] A popular LSDA method is the SVWN (Slater exchange plus VWN[68] correlation functional) method.[19,35] Here, $E_X[\rho]$ is expressed as:[35,58]

$$E_X^{LSDA}[\rho] = -2^{1/3} C_X \int \left(\rho_\alpha^{4/3}(\boldsymbol{r}) + \rho_\beta^{4/3}(\boldsymbol{r})\right) d\boldsymbol{r} \tag{2.81}$$

while $E_C[\rho]$ is expressed as:[69,70]

$$E_C^{LSDA}[\rho] = \int \rho(\boldsymbol{r})\, \epsilon_C \left(\rho_\alpha(\boldsymbol{r}), \rho_\beta(\boldsymbol{r})\right) d\boldsymbol{r} \tag{2.82}$$

This procedure also underestimates $E_X[\rho]$ by roughly 10 %[35,71] but overestimates $E_C[\rho]$.[69] In molecular systems, electron density is inhomogeneous[32] and so the LDA and LSDA approaches become grossly inadequate in treating such systems.[64,69]

2.6.1.3 The Generalised Gradient Approximation

To correct these functionals for the inhomogeneity of the electron density in real systems, the gradient of the electron density ($\nabla\rho(\boldsymbol{r})$) is often added to $E_X[\rho]$ in eq. (2.81) and $E_C[\rho]$ in eq. (2.82).[31,32,35,70] This leads to the popular generalised gradient approximation (GGA) procedures. Here, $E_{XC}[\rho]$ is expressed as:[31,61]

$$E_{XC}^{GGA}[\rho_\alpha, \rho_\beta] = \int f\left(\rho_\alpha(\boldsymbol{r}), \rho_\beta(\boldsymbol{r}), \nabla\rho_\alpha(\boldsymbol{r}), \nabla\rho_\beta(\boldsymbol{r})\right) d\boldsymbol{r} \tag{2.83}$$

where f is a function of the densities and their gradients. The $E_X[\rho]$ component of $E_{XC}[\rho]$ in this approximation is written as:[31]

$$E_X^{GGA}[\rho_\alpha, \rho_\beta] = E_X^{LSDA}[\rho_\alpha, \rho_\beta] - \sum_\sigma \int f\big(s_\sigma(\boldsymbol{r})\big)\rho_\sigma^{4/3}(\boldsymbol{r})\, d\boldsymbol{r} \tag{2.84}$$

where $\sigma = \alpha$ or β and $s_\sigma(\boldsymbol{r})$ is a local inhomogeneity parameter expressed as:

$$s_\sigma(\boldsymbol{r}) = \frac{|\nabla\rho_\sigma(\boldsymbol{r})|}{\rho_\sigma^{4/3}(\boldsymbol{r})} \tag{2.85}$$

The $E_C[\rho]$ component of $E_{XC}[\rho]$ in the GGA technique is expressed as:[69]

$$E_C^{GGA}[\rho_\alpha, \rho_\beta] = E_C^{LSDA}[\rho_\alpha, \rho_\beta] + \int \frac{d^{-1}e^{-\Phi}C(\rho)|\nabla\rho|^2}{\rho^{4/3}}\, d\boldsymbol{r} \tag{2.86}$$

where

$$d = 2^{1/3}\left[\left(\frac{1+\zeta}{2}\right)^{5/3} + \left(\frac{1-\zeta}{2}\right)^{5/3}\right]^{1/2} \text{ with } \zeta = \rho_\alpha + \rho_\beta \tag{2.87}$$

and

$$\Phi = 1.745\tilde{f}\frac{[C(\infty)/C(\rho)]|\nabla\rho|}{\rho^{7/6}} \tag{2.88}$$

and the cut-off parameter, $\tilde{f} = 0.11$. A range of GGA methods or calculations can be performed by combining the exchange and correlation portions of the $E_{XC}[\rho]$.[19] An example of such functionals that is used in this thesis is the Perdew-Burke-Ernzerhof functional[72] whose $E_{XC}[\rho]$ may be expressed as:

$$E_{XC}^{PBE}[\rho_\alpha, \rho_\beta] = E_X^{PBE}[\rho_\alpha, \rho_\beta] + E_C^{PBE}[\rho_\alpha, \rho_\beta] \tag{2.89}$$

where[35,72]

$$E_X^{PBE}[\rho_\alpha, \rho_\beta] = E_X^{LSDA}[\rho_\alpha, \rho_\beta] \cdot F\big(s(\boldsymbol{r})\big) \tag{2.90}$$

with

$$s(\boldsymbol{r}) = \frac{|\nabla\rho(\boldsymbol{r})|}{2k_F\rho(\boldsymbol{r})} \tag{2.91}$$

$$F\big(s(\boldsymbol{r})\big) = 1 + \kappa - \frac{\kappa}{1 + \frac{\mu s^2}{\kappa}};\ \kappa = 0.804 \tag{2.92}$$

$$\mu = \beta\left(\frac{\pi^2}{3}\right) \simeq 0.21951 \tag{2.93}$$

and

$$E_C^{PBE}[\rho_\alpha, \rho_\beta] = E_C^{LSDA}[\rho_\alpha, \rho_\beta] + H(r_s, \zeta, t) \tag{2.94}$$

where r_s is the local Seitz radius, ζ is the relative spin polarisation,

$$H = \left(\frac{e^2}{a_0}\right)\gamma\phi^3 \times \ln\left\{1 + \frac{\beta}{\gamma}t^2\left[\frac{1+At^2}{1+At^2+A^2t^4}\right]\right\} \tag{2.95}$$

$$A = \frac{\beta}{\gamma}\left[e^{-\left\{\epsilon_C^{LSDA}/\gamma\phi^3 e^2/a_0\right\}} - 1\right]^{-1}$$

$$t = \frac{|\nabla\rho(\boldsymbol{r})|}{2\phi k_s \rho(\boldsymbol{r})}$$

$$k_s = \sqrt{\frac{4k_F}{\pi a_0}}$$

$$a_0 = \frac{\hbar^2}{me^2}$$

$$\gamma = \frac{1 - \ln 2}{\pi^2} \simeq 0.031091$$

ϕ is a spin scaling factor, k_s is the Thomas-Fermi screening wavenumber, $\beta \simeq 0.066725$.

2.6.1.4 The Meta-Generalised Gradient Approximation

Moving on from GGA's, improvements that allow the exchange and correlation functionals to depend on the second derivatives of the electron densities of the spins ($\nabla^2\rho$) are formed.[19,35] These functionals are called the meta (beyond)-generalised gradient approximation (m-GGA) functionals. Here,

$$E_{XC}^{m-GGA}[\rho_\alpha, \rho_\beta] = \int f\left(\rho_\alpha(\boldsymbol{r}), \rho_\beta(\boldsymbol{r}), \nabla\rho_\alpha(\boldsymbol{r}), \nabla\rho_\beta(\boldsymbol{r}), \nabla^2\rho_\alpha(\boldsymbol{r}), \nabla^2\rho_\beta(\boldsymbol{r})\right) d\boldsymbol{r} \tag{2.96}$$

Nevertheless, functionals that depend on $\nabla^2\rho$ present some computational difficulties.[19] This is often overcome by making such functionals to depend instead on the kinetic energy density, $\tau(\boldsymbol{r})$ which varies with $\rho(\boldsymbol{r})$ in the same manner as ∇^2,[19,73] but is numerically more stable.[35] $\tau(\boldsymbol{r})$ has the form:[19,35,73,74]

$$\tau(\boldsymbol{r}) = \frac{1}{2}\sum_{i=1}^{occ}\left|\nabla\psi_i^{KS}(\boldsymbol{r})\right|^2 \tag{2.97}$$

and for a single orbital, $\tau(\boldsymbol{r})$ is identical to the Weizsäcker kinetic energy, $\tau_W(\boldsymbol{r})$ expressed as:[35,63]

$$\tau_W(\boldsymbol{r}) = \frac{|\nabla\rho(\boldsymbol{r})|^2}{8\rho(\boldsymbol{r})} \tag{2.98}$$

For such functionals,[63,75]

$$E_{XC}^{m-GGA}[\rho_\alpha, \rho_\beta] = \int \rho(\boldsymbol{r})\, \epsilon_{XC}^{m-GGA} \times \left(\rho_\alpha(\boldsymbol{r}), \rho_\beta(\boldsymbol{r}), \nabla\rho_\alpha(\boldsymbol{r}), \nabla\rho_\beta(\boldsymbol{r}), \tau_\alpha(\boldsymbol{r}), \tau_\beta(\boldsymbol{r})\right) d\boldsymbol{r} \quad (2.99)$$

Furthermore, for other m-GGA approximations, the $E_{XC}[\rho]$ is dependent on semi-local Laplacians of the spin densities and kinetic energy density and may be written as:[74]

$$E_{XC}^{m-GGA}[\rho_\alpha, \rho_\beta] = \int \rho(\boldsymbol{r})\, \epsilon_{XC}^{m-GGA} \times \left(\rho_\alpha, \rho_\beta, \nabla\rho_\alpha, \nabla\rho_\beta, \nabla^2\rho_\alpha, \nabla^2\rho_\beta, \tau_\alpha, \tau_\beta\right) d\boldsymbol{r} \quad (2.100)$$

Examples of the m-GGA functionals include the TPSS[75] and the MO6-L.[76] The TPSS is used in this thesis. The mathematics and theory behind $E_X[\rho]$ and $E_C[\rho]$ in the m-GGA's exists in the literature.[74–76]

2.6.1.5 The Hybrid-Generalised Gradient Approximation

An alternative approach to improving the performance of the GGA's is by adding a percentage of the Hartree-Fock exchange energy to their $E_{XC}[\rho]$;[19,35,58] i.e., such functionals combine KS-DFT and wavefunction theory.[77] The theory that makes this feasible is the adiabatic connection model (ACM):[19,31,35]

$$E_{XC} = \int_0^1 \langle\psi_\lambda|V_{XC}(\lambda)|\psi_\lambda\rangle d\lambda \quad (2.101)$$

where λ is the degree of electron-electron interactions. When $\lambda = 0$, only the HF exchange energy contributes to E_{XC} as the electrons do not interact.[31,35] As $\lambda \to 1$, the degree of correlation increases and at $\lambda = 1$ the electrons in the system are fully correlated. When $\lambda = 0$ the exact exchange, K term in the HF approximation can be computed if the KS-orbitals are available.[31,35] This is then added to a choice GGA E_{XC}^{GGA} to form a new functional. Such functionals that incorporate exact exchange are referred to as hybrid functionals (h-GGA's).[19,31,35,77] Often times, these functionals also comprise of a range-separation or range-correction[77,78] and a dispersion correction term to treat non-covalent interactions (e.g., π-π stacking[79]) and give accurate thermochemical and kinetic results.[77,80,81] An example of such functionals used in the present thesis is the ωB97XD.[80] The E_{XC}^{h-GGA} for this functional is expressed as:[77,80]

$$E_{XC}^{\omega B97XD} = E_X^{LR-HF} + c_X E_X^{SR-HF} + E_X^{B97} + E_C^{B97} + E_{disp} \quad (2.102)$$

where LR-HF and SR-HF imply long- and short-range HF exchange, respectively. E_X^{B97} and E_C^{B97} are the exchange and correlation energies proposed by Becke in 1997.[82] c_X is the fractional number of the short-range operator determined by fitting to accurate experimental or theoretical data and is a small constant. ω is the parameter that controls the partitioning of the inter-electronic distances

and is also obtained by fitting to accurate experimental or theoretical data. The X in ωB97XD denotes the fraction of the HF exchange in the functional. The D in ωB97XD is the last term in eq. (2.102) and represent the dispersion correction included in the functional and is given by:[80]

$$E_{disp} = -\sum_{i=1}^{N_{atom}-1}\sum_{j=i+1}^{N_{atom}} \frac{C_6^{ij}}{R_{ij}^6}\left(\frac{1}{1+a\left({R_{ij}}/{R_r}\right)^{-12}}\right) = -\sum_{i=1}^{N_{atom}-1}\sum_{j=i+1}^{N_{atom}} \frac{C_6^{ij}}{R_{ij}^6}\cdot f_{damp}(R_{ij}) \quad (2.103)$$

where N_{atom} is the number of atoms in a system, C_6^{ij} is the dispersion coefficient for atom pair ij, R_{ij} is the interatomic distance, R_r is the sum of the van der Waals (vdW) radii of atomic pair ij. The $f_{damp}(R_{ij})$ reduces at large R_{ij} and vanishes quickly at small R_{ij} to prevent divergence of the undamped vdW potentials. ωB97XD employs 100 % HF exchange for long-range interactions but only a small fraction of the exchange for short-range electron-electron interactions. Another example of the h-GGA's used in this thesis is the Coulomb-attenuating method B3LYP (CAM-B3LYP) functional.[83] This functional comprises of 19 % HF exchange in addition to 81 % B88 exchange at short-range but 65 % HF exchange and 35 % B88 exchange at long-range. The B88 exchange was proposed by Becke in 1988.[64]

2.6.1.6 The Hybrid Meta-Generalised Gradient Approximation

Analogous functionals to the h-GGA's having the fraction of the HF exchange added to the m-GGA's rather than the GGA's whilst also depending on $\nabla\rho_\sigma(\boldsymbol{r})$ and $\nabla^2\rho_\sigma(\boldsymbol{r})$ and/or $\tau_\sigma(\boldsymbol{r})$ are termed the hybrid m-GGA's.[19] These are high level functionals in common routine use.[19] An example of this class of functionals used in this thesis is the M11 functional.[78] The E_{XC} of this functional is expressed as:

$$E_{XC}^{M11} = \left(\frac{X}{100}\right)E_X^{HF} + \left(1-\frac{X}{100}\right)\left(E_X^{LR-HF} + E_X^{SR-M11}\right) + E_C^{M11} \quad (2.104)$$

where E_X^{HF} is the full-range non-local HF exchange with both E_X^{SR-M11} and E_C^{M11} depending on ρ_σ, τ_σ and s_σ where:

$$s_\sigma(\boldsymbol{r}) = \frac{|\nabla\rho_\sigma(\boldsymbol{r})|}{2(3\pi^2)^{1/3}\rho_\sigma^{4/3}(\boldsymbol{r})} \quad (2.105)$$

This functional is especially good in producing atomisation energies, proton affinities, bond dissociation energies, barrier heights, non-covalent interactions and charge-transfer electronic excitation.[78] It comprises of 100 % HF exchange at long-range (large) electronic separations and 42.8 % HF exchange at short-range.

All these classes of exchange-correlation functional approximations are proposed to form the rungs of the Jacob's ladder with LDA or LSDA forming the lowest rung of the ladder while more sophisticated approximations form higher rungs accordingly.[58,63] In this regard, users of DFT make their choice as suits their requirements by either going up or down the ladder in search of computational precision and efficiency.[58,63] It should be noted however that each higher level of sophistication may bring along additional computational costs but may not be complemented by higher chemical accuracy.[58,63]

2.7 Accounting for the Effects of Solvation

The effects of solvents can be accounted for in a computational calculation by employing a solvation model.[35,84–89] This can be done in two ways: the explicit and implicit approaches.[19] In the explicit approach, actual solvent moieties are placed around the system under consideration whereas the implicit approach models the system in the cavity of a continuous medium (a continuum) which serves as a uniform polarisable medium with a dielectric constant, ε.[89–91] The implicit continuum approaches are so far, the most used and easiest ways of treating solvent effects.[19,87,91] The most common class of the implicit approaches often found in computational packages in recent years is the polarisable continuum model (PCM)[87,88,90,92] whose formulation began in 1981.[84] This model is used to investigate the effects of solvents on reaction energies in this thesis. The principal idea behind this class of implicit models is that the solute (system under consideration) is placed in a cavity of a solvent medium formed by interlocking vdW sphere radii scaled by an empirical factor and the interaction between the solute and the solvent cavity is calculated.[90] The solute in these models is usually placed in a solvent cavity that matches their shape where the shapes and sises of the cavities define the surface area of the solvent accessible to the solute.[19,90] Once in the cavity, the interaction of the solute and the solvent is treated as electrostatic polarisation of the solute's charge distribution by the continuous dielectric field that represents the solvent.[90,92] For computational packages like Gaussian,[24] the implemented versions of the PCM for computation are the integral equation formalism of PCM (IEF-PCM) of Cancès et al.,[93–95] the conductor-like PCM (C-PCM) of Cossi and co-workers[88,96] and the continuous surface charge PCM (CSC-PCM) of Scalmani and Frisch.[87] The interaction energies of the solvent-solute interactions are usually computed iteratively in the context of the SCF procedure thereby resulting in the self-consistent reaction field (SCRF) calculations.[19,35] These formalisms have been implemented in computational packages for electronic structure calculations.[19,35,91] In this regard, accurate approximations of the solvation Gibbs free energies of systems in comparison with experiments[88,96–98] describing the effects of solvents can be obtained from calculations.

2.8 Basis Sets

A common but key factor in obtaining accurate and reliable results in computational quantum chemistry calculations is the quality, type and sise of basis set combined with a chosen computational method.[19,20,35,99–104] A basis set is a set of atomic or molecular orbitals or mathematical functions (basis functions) such as presented in eq. (2.21) expanded in a set of known functions which are usually, but not invariably, centred on atomic nuclei for use in a computational calculation.[19,32,34,35] There are two broad types of basis functions commonly used in computational chemistry calculations:[103]

1. The Slater-type orbitals (STO's) and
2. The Gaussian-type orbitals (GTO's)

These are especially employed in Chapter 3 to Chapter 6 of this thesis. Nevertheless, other types of basis sets are also possible, e.g., the Laguerre basis sets[17,105,106] used in Chapter 7 of this thesis and plane waves.[21] The STO's[107] have the functional form in terms of polar coordinates as:[35,103]

$$\chi_{\xi,n,l,m}(r,\theta,\varphi) = NY_{l,m}(\theta,\varphi)r^{n-1}e^{-\xi r} \tag{2.106}$$

The GTO's[108] on the other hand can be written in terms of polar coordinates as:[35,103]

$$\chi_{\xi,n,l,m}(r,\theta,\varphi) = NY_{l,m}(\theta,\varphi)r^{2n-2-l}e^{-\alpha r^2} \tag{2.107}$$

where N is a normalisation constant and $Y_{l,m}(\theta,\varphi)$ are spherical harmonic functions, ξ and α are the positive-valued orbital exponent occurring in the radial part ($e^{-\xi r}$ or $e^{-\alpha r^2}$) of eq. (2.106) and eq. (2.107), respectively while r is the distance of an electron from an atomic nucleus.

The GTO's are inferior to the STO's due to the dependence on r^2 in the radial part of eq. (2.107) in two ways.[103] The first is that an $n = 1$ STO has a cusp (discontinuous derivative) at the nucleus just like a $1s$ hydrogenic atomic orbital whereas the GTO does not.[31,32,103] This causes the GTO's serious problems in representing proper behaviour near or at atomic nuclei.[32,35,103] The second problem is that the GTO's fall off too rapidly as $r \to \infty$ from the nucleus.[19,31,103] As a consequence, one requires more GTO's to achieve certain accuracy comparable to that obtained with STO's.[31,32,103] Nevertheless, the GTO's are mathematically more tractable and efficient than the STO's as they require less computer time to compute many-centre two-electron integrals, such as described by Coulomb and exchange integrals for many electron systems that are notoriously difficult to compute with STO's.[19,31,32,103] As a result, GTO's are usually used to approximate the physically more realistic STO's, hence making Gaussian functions the most common basis functions in electronic structure calculations.[19,31,35] Another major advantage of the GTO's is that

the product of two Gaussian functions at different centres is equivalent to a single Gaussian function centred at a point between the two centres.[32]

2.8.1 Gaussian Basis Sets

As mentioned above, a single Gaussian (GTO) is usually a poor approximation to provide the description of an orbital. To circumvent this, several Gaussian functions are combined to form contracted Gaussian functions that approximate an STO.[19,32,103] For instance, when three Gaussians are combined to approximate the Slater function, the resulting function may be written as STO-3G implying that the STO is approximated by 3 GTO's. Each contracted Gaussian, χ_r consists of several primitive Gaussians, g_{nr}, centered on the same atomic nucleus in a system and can be expressed for an STO-3G contracted Gaussian as:[19,32,35]

$$\chi_r = \sum_{n=1}^{k} d_{nr}\mathrm{g}_{nr} = \sum_{n=1}^{3} d_{nr}\mathrm{g}_{nr} = d_{1r}\mathrm{g}_{1r} + d_{2r}\mathrm{g}_{2r} + d_{3r}\mathrm{g}_{3r} \tag{2.108}$$

where d_{nr} are the contraction coefficients and k is the degree of contraction, typically ranging from 1 to 10. d_{nr} and the parameters characterising g_{nr} are kept constant (fixed) during a calculation. The spatial orbitals are therefore expressed as a linear combination of the contracted Gaussians:[32,109]

$$\psi_i(\boldsymbol{r}) = \sum_{r=i=1}^{k} c_{ir}\chi_r(\boldsymbol{r}) \tag{2.109}$$

where c_{ir} are the unknown coefficients. As such the number of the c_{ir} that will be computed in eq. (2.109) is greatly reduced leading to reduction in computational time with little loss of accuracy when the χ_r's are carefully chosen.

There is a host of contracted basis sets implemented in computational packages from which users usually select the one that suits a given calculation.[19,35] A short description of the basis sets used in this thesis is given below.

2.8.1.1 Minimal Basis Set

This is the simplest but least accurate type of contracted Gaussian basis set in which one function is employed to represent each atomic orbital in elementary valence theory.[31,32] This type of basis set contains the smallest (minimum) number of basis functions required for the description of an atom.[31,109] An example of this type of basis set is the STO-3G[32,35,110] used in this thesis in combination with the HF method to generate and select the canonical orbitals of species for use in

CASSCF calculations. This type of basis set is not recommended for consistent and accurate calculations of molecular energies but their structure gives room for visualising qualitative aspects of chemical bonds.[32,109,110]

2.8.1.2 Split-Valence Basis Set

The accurate treatment of electronic structure of chemical systems requires extensive basis sets. Such extensive basis sets are found in the form of double-, triple-, quadruple-etc. zeta basis sets, which are improvements over minimal basis sets. In the double- and triple-zeta (DZ and TZ) basis set for instance, each basis function in the minimal basis set is replaced by two or three sets of each basis function to describe an atom, respectively.[32,35] These latter basis sets however double or triple the number of the c_{ir}'s in eq. (2.109) for each computation thereby increasing the computational demands of the calculations.[19,32]

The split-valence basis sets were introduced by Pople and co-workers,[111–114] and are also called the Pople-type basis sets.[19,35] They present a compromise between the computational inaccuracy of the minimal basis sets and the computational demands of the DZ, TZ, etc.[32] Generally, the split valence basis set employs one function for core orbitals and two or three functions for valence orbitals.[32,35,110] As such, it is generally denoted as the *k-nlm*G basis sets where *k* represents the number of the pGTO's used for in the cGTO that describes the core orbitals while the *nl* or *nlm* before G (Gaussian) stand for basis functions of a double and triple split valence basis set, respectively.[35] The double split valence basis set e.g., 3-21G basis set, for instance, uses one cGTO consisting of three pGTO's to treat the core orbitals while using two cGTO's, one consisting of pGTO's to describe the outer-valence orbitals and the other comprising two pGTO's for the inner-valence orbitals of the system.[19,32,35,110] An example of the *k-nlm*G basis set is the 6-311G basis set which is of TZ quality for the valence electrons with three cGTO's defined by three, one and one pGTO's. The purpose of splitting the valence shell is to increase the flexibility of basis functions to provide a realistic description of orbitals or electron distribution and by so doing lead to consistent and accurate computational predictions at less computational effort.[19,32,110]

2.8.1.3 Polarisation and Diffuse Functions

Polarisation (basis functions of higher angular momentum other than the occupied atomic orbitals) and diffuse functions can be added to the *k-nlm*G basis sets to improve their flexibility and hence performance for better description of orbitals and/or electronic charge or density distribution in a system.[35,109,110] The polarisation functions are denoted by either asterisk(s); * (for non-hydrogen and helium) and ** (for all atoms) or *p*-, *d*- and/or *f*-functions after the G in the *k-nlm*G basis sets e.g., 6-31G* (or 6-31G(d)), 6-31G** (or 6-31G(d,p)), 6-311G(2df,2pd)) etc. They allow the orbitals

to change shape readily to accommodate any anisotropic electronic charge or density distribution in a system.[19,20,32] Polarisation functions also bring additional lowering in the total variational energy of a system as much as adding another cGTO and leads to more accurate geometries and vibrational frequencies.[20] The diffusion functions on the other hand are denoted by + (for non-hydrogen atoms) or ++ (for all atoms in the system) before the G in the *k-nlm*G basis sets, e.g., 6-31+G, 6-31++G, etc. Basis sets comprising these functions are useful for better description of anions, excited systems and hetero-atomic systems with lone-pair electrons.[19,20,109] Basis sets containing diffuse functions are known as augmented basis sets and are often also used to treat long-range interactions such as vdW interactions[20] in combination with suitable methods. All these functions can be combined in one basis set e.g., 6-31+G(d), 6-311++G(2df,2p), 6-311++G(3df,3pd), etc.[35] Split-valence basis sets incorporating polarisation and diffuse functions are especially used in the present thesis for accurate results.

2.8.1.4 Correlation-Consistent Basis Sets

The above schemes can be further improved upon by increasing the number of polarisation and/or diffuse functions.[19,20,31] In this regard, the correlation-consistent (cc) type of basis sets developed by Dunning and co-workers[100,101,115–118] represent another type of such schemes in terms of contracted Gaussian functions. These basis sets are designated for example as the cc-pV*x*Z, aug-cc-pV*x*Z, cc-pV(*x*+*d*)Z or aug-cc-pV(*x*+*d*)Z where aug-cc includes diffuse functions. The p stands for polarised and valence (V) *x* (doubly (D), triply (T), quadruply (Q), quintuply (5) or sextuply (6) split) zeta (Z) basis sets. *d* in cc-pV(*x*+*d*)Z and aug-cc-pV(*x*+*d*)Z stands for tight higher exponent *d*-function useful for recovering core-core and core-valence electron correlation energy.[35,117] This type of split-valence basis sets is especially useful when electron correlation energy is to be recovered in a calculation and hence are particularly useful for high-accuracy post-HF calculations.[19,20,35,117] As such, high-accuracy post-HF calculations performed in this thesis also employ the cc-pV*x*Z or aug-cc-pV*x*Z basis sets.

2.8.1.5 Effective Core Potentials (*Pseudo*-potentials)

Even with the large non-relativistic split-valence and cc basis sets discussed above, the treatment of heavy elements with a large number of core electrons e.g., potassium to krypton or higher atomic numbered elements (19 or more electrons) is difficult.[19,20,31,35] This is because when the number of core electrons is large, relativistic effects arising from the dependence of the masses of the particles on their velocities and spin coupling terms become significant.[19,20,35] To deal with the situation, the effective core potential (ECP) or *pseudo*-potential basis sets which include relativistic effects, initially proposed by Hellmann[119] and improved upon by other researchers[120–123] are usually

employed.[19,20,31,35] This is done by replacing the core electrons of the heavy systems and their basis functions in a calculation with the ECP's while treating the valence non-relativistic electrons and every other light atom in the system with Gaussian functions developed to accompany the ECP's and one of the already discussed basis sets, respectively.[19,20,35,103] Examples of ECP's in current use with computational methodologies are the Los Alamos National Laboratory Double Zeta (LanL2DZ)[120,121] and the Stuttgart/Dresden (SDD)[122,123] basis set.[19,103] The ECP's can either be of the minimal or split-valence type.[19,103] In this thesis, the relativistic Stuttgart/Dresden (SDD)[122,123] basis set is used to describe palladium with 46 electrons.

2.9 Theory of Atoms in Molecules

The theory of atoms in molecules was developed by Bader and co-workers.[124–133] This theory derives from the mathematical partitioning of systems into regions (basins) relying on the system's electron density ($\rho(\boldsymbol{r})$) that correspond to atoms.[19,35,129,131,134] The theory deals with analysing the variation of the electron density function of a system with position (i.e., its topology, a scatterplot of ρ *vs* $\boldsymbol{r}$ yielding minima, maxima or saddle points) with $\rho(\boldsymbol{r}) = \rho(x, y, z)$.[19,35] This property ($\rho(\boldsymbol{r})$) can be derived/computed from the wavefunction of a system.[19,129,133] The basic idea in the topology of the electron density function is that local maxima in a system occurs at the nuclear positions in the system.[129,134] Elsewhere in a system with defined nuclear configurations, the topological properties of ρ are fully mapped out in an associated density gradient vector field, $\nabla\rho(\boldsymbol{r})$ which exhibits trajectories in real space called gradient paths.[127,129] This leads to the concepts of critical points (cp's) in real space; where $\nabla\rho(\boldsymbol{r}) = 0$.[126,127,129] Consequently, the definition of an isolated atom, that in a molecule, a chemical bond and hence molecular structure can be derived from the properties of the critical points of charge density in a system.[127] In this regard, an interatomic surface $S(\boldsymbol{r_s})$ separating the basins of two interacting atoms is defined by a two-dimensional manifold spanned by an infinite set of the trajectories of $\nabla\rho(\boldsymbol{r})$ terminating at a cp while their interaction line is defined by a unique set of trajectories originating at the cp and terminating at the nucleus of a neighbouring atom.[127,130,133] In a state of stable electrostatic equilibrium where the atoms are involved in a bond in the usual chemical sense, the atomic interaction line is referred to as a bond path and the associated cp, a bond critical point.[129,133] As such, molecular structure is defined as the network of bond paths that link neighbouring nuclei in a system.[126–130,133] Nevertheless, bond paths do not necessarily imply chemical bonds between interacting species but their interaction[135] as in hydrogen bonds[11,136] and π-π interactions[137] in molecular systems. The preceding discussion above suggests therefore, that information about the bonding and group of atoms in a system can be derived from an analysis of the topology of its electron density.

2.9.1 Critical Points

The topology of $\rho(\boldsymbol{r})$ as mentioned in **2.9** results in minima, maxima or saddle points in space that can be observed as the first derivatives of electron density, $\nabla\rho(\boldsymbol{r})$, the gradient field. All points at which $\nabla\rho(\boldsymbol{r})$ vanishes are called critical points, i.e.,[127,134]

$$\nabla\rho(\boldsymbol{r}) = \boldsymbol{i}\frac{\partial\rho}{\partial x} + \boldsymbol{j}\frac{\partial\rho}{\partial y} + \boldsymbol{k}\frac{\partial\rho}{\partial z} \rightarrow \begin{cases} = \vec{0} & (\text{at cp's and } \infty) \\ \neq \vec{0} & (\text{at other points}) \end{cases} \tag{2.110}$$

$\Rightarrow$ the local maximum is a type of cp, a nuclear critical point.[19,134] In order to characterise the type of cp as a local minimum, maximum or saddle point, requires the second derivatives of $\rho(\boldsymbol{r})$ which constitutes a Hessian matrix, **A** of the $\rho(\boldsymbol{r})$ at each critical point.[127,134] In the neighbourhood of a critical point ($\boldsymbol{r_c}$) defined as:[127]

$$\nabla\rho(\boldsymbol{r}, \mathbf{X})|_{\boldsymbol{r}=\boldsymbol{r_c}} = 0 \tag{2.111}$$

where **X** is a point in space, the gradient path is defined as:[127]

$$\frac{d\boldsymbol{r}(s)}{ds} = \mathbf{A}(\boldsymbol{r} - \boldsymbol{r_c}) \tag{2.112}$$

where[127,134]

$$\mathbf{A}(\boldsymbol{r_c}) = A_{ij}(\boldsymbol{r_c}) = \left(\frac{\partial^2\rho}{\partial x_i \partial x_j}\right)_{\boldsymbol{r}=\boldsymbol{r_c}} \tag{2.113}$$

Eq. (2.113) consists of nine second derivatives of $\rho(\boldsymbol{r})$ at $\boldsymbol{r_c}$. The general solution to eq. (2.112) is:[127]

$$\boldsymbol{r}(s) = \alpha\mathbf{v}_1 e^{\lambda_1 s} + \beta\mathbf{v}_2 e^{\lambda_2 s} + \gamma\mathbf{v}_3 e^{\lambda_3 s} \tag{2.114}$$

where λ_i's are the eigenvalues of the eigenvectors, $\mathbf{v}_i$'s. These eigenvalues are the diagonal elements of $\mathbf{A}(\boldsymbol{r_c})$:[134] Diagonalisation of $\mathbf{A}(\boldsymbol{r_c})$ is equivalent to the rotation:[134] $\boldsymbol{r}(x, y, z) \rightarrow \boldsymbol{r}(x', y', z')$ via a unitary transformation constructed from the eigenvalues in eq. (2.114); λ_1, λ_2 and λ_3, superimposing a new set of axes (x', y', z') on the principal curvature axes of the cp.[134] As such, a trace of $\mathbf{A}(\boldsymbol{r_c})$ can therefore be expressed as:[134]

$$\nabla^2\rho(\boldsymbol{r}) = \begin{pmatrix} \frac{\partial^2\rho}{\partial x'^2} & 0 & 0 \\ 0 & \frac{\partial^2\rho}{\partial y'^2} & 0 \\ 0 & 0 & \frac{\partial^2\rho}{\partial z'^2} \end{pmatrix}_{\boldsymbol{r}=\boldsymbol{r_c}} = \begin{pmatrix} \lambda_1 & 0 & 0 \\ 0 & \lambda_2 & 0 \\ 0 & 0 & \lambda_3 \end{pmatrix} = \lambda_1 + \lambda_2 + \lambda_3 \tag{2.115}$$

where $\nabla^2\rho(\boldsymbol{r})$ is called the Laplacian of the density and the sign of the λ_i's defines the curvatures (nature of cp's) of the density with respect to the principal axes; x, y and z, when $x = x'$, $y = y'$ and $z = z'$.[127,134] Also, the magnitude of the curvatures at a cp gives an indication of the magnitude of $\rho(\boldsymbol{r})$ at such cp compared to that in the atomic basins. The cp's are therefore classified by their rank (ω) and signature (σ), with a cp labelled by giving values of the rank and signature as (ω, σ) to represent a particular element of molecular structure. [127,134,138] A cp with $\omega = 3$ is generally stable energetically while cp's with $\omega < 3$ are degenerate and unstable and so the appearance of the latter denotes the onset of a change in structure.[127,134,138] As such, the nature and definition of a chemical bond and/or molecular structure derives from the properties of a cp with $\omega = 3$.[127] The rank of a cp is the number of non-zero curvatures of $\rho(\boldsymbol{r})$ while the signature is the algebraic sum of the signs of the curvatures at a cp.[127,134,138] There are basically four significant stable cp's ($\omega = 3$) with each labelled as (ω, σ), namely:[127,134,138]

1. The (3, -3) cp: this is called the nuclear cp (ncp). This cp has three negative curvatures. $\rho(\boldsymbol{r})$ is a local maximum at $\boldsymbol{r_c}$;
2. The (3, -1) cp: this is referred to as the bond cp (bcp) and has two negative curvatures. Here, $\rho(\boldsymbol{r})$ is a maximum at $\boldsymbol{r_c}$ in the plane defined by two axes (λ_1 and λ_2) but a minimum at $\boldsymbol{r_c}$ along the third associated axis (λ_3) that is perpendicular to the plane defined by the first two axes. This cp represents saddle points on a molecular graph;
3. The (3, +1) cp: this is known as the ring cp (rcp) and possesses two positive curvatures and $\rho(\boldsymbol{r})$ is a minimum at $\boldsymbol{r_c}$ in the plane defined by two axes (λ_1 and λ_2) but a maximum at $\boldsymbol{r_c}$ along the third associated axis (λ_3) that is perpendicular to the plane defined by the first two axes.
4. The (3, +3) cp: called the cage cp (ccp) comprises of three positive curvatures and $\rho(\boldsymbol{r})$ is a minimum at $\boldsymbol{r_c}$.

The number and type of these cp's that can coexist in a structure is governed by the Poincaré-Hopf relationship for isolated molecular structures[127,134,138] expressed as:

$$n_{ncp} - n_{bcp} + n_{rcp} - n_{ccp} = 1 \tag{2.116}$$

where n is the number of the subscripted type of cp and $\{n_{ncp}, n_{bcp}, n_{rcp}, n_{ccp}\}$ is the characteristic set of the structure in question. When eq. (2.116) is satisfied, it is taken as a confirmation of consistency and completeness of the characteristic set of a given system, i.e., confirms that all cp's have been found.

2.9.2 Nature and Strength of Chemical Bonds

There is always one bcp between every two interacting atoms linked by a bond path and information about the nature of the interaction is conveyed in the value of $\nabla^2\rho(\boldsymbol{r})$ at the bcp, while its strength is indicated by the magnitude of $\rho(\boldsymbol{r})$ at the bcp.[28,35] These indices define the energetic stability of a given structure[138] and hence the characterisation and classification of a chemical bond is based on the magnitude of $\rho(\boldsymbol{r})$, $\nabla^2\rho(\boldsymbol{r})$ or λ_1, λ_2 and/or λ_3 at the bcp between two interacting atoms.[28,134] The extent of concentration or depletion of charge density at a bcp is provided by $\nabla^2\rho(\boldsymbol{r})$, given in eq. (2.115), where $|\lambda_1| > |\lambda_2|$ by convention and indicates the nature of a bond.[28,134,138] When $\nabla^2\rho(\boldsymbol{r}) < 0$ at a bcp, the value of $\rho(\boldsymbol{r})$ is greater than its average in the immediate neighbourhood of $\boldsymbol{r}$ signifying that it is concentrated at the bcp and defines a covalent bond. When $\nabla^2\rho(\boldsymbol{r}) > 0$ at a bcp, the value of $\rho(\boldsymbol{r})$ is less than its average in the immediate neighbourhood of $\boldsymbol{r}$ and suggests that it is depleted at the bcp and indicates ionic, hydrogen bonding or vdW (i.e., closed-shell) interactions.

Bond ellipticity (ε) defined as:[134,138]

$$\varepsilon = \frac{\lambda_1}{\lambda_2} - 1 \quad (|\lambda_1| \geq |\lambda_2|) \tag{2.117}$$

provides a measure of the extent to which the density is preferentially concentrated at a bcp and can be used to determine whether a bond is of a sigma (σ) or pi (π) character. When $\varepsilon = 0$, the bond is cylindrically symmetrical and is thus a single σ-bond or a triple bond whereas $\varepsilon > 0$ signifies a π-bond. The strength of a chemical bond is reflected in the magnitude of $\rho(\boldsymbol{r})$ at a bcp. Generally, $\rho(\boldsymbol{r}) > 0.20$ a.u. for covalently bonded atoms and $\rho(\boldsymbol{r}) < 0.10$ a.u. for closed-shell interactions.[134]

An alternative means to characterise the nature and strength of a chemical bond is to compute the gradient kinetic ($G(\boldsymbol{r})$) and potential energy ($V(\boldsymbol{r})$) densities at the bcp between a pair of bonded atoms which are related by the virial relationship expressed as:[128,130,134,138]

$$\left(\frac{\hbar^2}{4m}\right)\nabla^2\rho(\boldsymbol{r}) = 2G(\boldsymbol{r}) + V(\boldsymbol{r}) \tag{2.118}$$

But the point-wise sum of $G(\boldsymbol{r})$ and $V(\boldsymbol{r})$ yields the total electron density energy ($H(\boldsymbol{r})$):[139]

$$H(\boldsymbol{r}) = G(\boldsymbol{r}) + V(\boldsymbol{r}) \tag{2.119}$$

$G(\boldsymbol{r})$ is always positive while $V(\boldsymbol{r})$ is always negative therefore the sign of $H(\boldsymbol{r})$ and hence $\nabla^2\rho(\boldsymbol{r})$ is always determined by their balance. As such, the value of $H(\boldsymbol{r})$, $\nabla^2\rho(\boldsymbol{r})$, $\rho(\boldsymbol{r})$ and the delocalisation index ($\delta(\mathrm{A},\mathrm{B})$)[28,134] or a combination of two of these parameters facilitates the determination of the nature and strength of a bond. In this regard, when $H(\boldsymbol{r}) > 0$, the bond is of a

closed-shell type and when $H(\boldsymbol{r}) < 0$, the bond is of a covalent type; covalency is also indicated by the value of $\delta(\mathrm{A},\mathrm{B})$ which is an independent measure of bond covalency.[28,140] Furthermore, the ratio $\left|\frac{H(\boldsymbol{r})}{\rho(\boldsymbol{r})}\right|$ called the bond degree parameter provides information about the strength of a bond.[28,136] $H(\boldsymbol{r}) < 0$ signifies that $V(\boldsymbol{r})$ dominates and electron density is concentrated at a bcp and while $H(\boldsymbol{r}) > 0$ indicates that $G(\boldsymbol{r})$ dominates and the charge density is depleted at the bcp.[140] In addition, $H(\boldsymbol{r})$ has a positive sign when $G(\boldsymbol{r})$ dominates but a negative sign when $V(\boldsymbol{r})$ dominates. These parameters are employed to elucidate the nature of the bonding in the complexes considered.

3 Rationalisation of *base-free* formation of Pd(0) from a novel SCN unsymmetrical pincer palladacycle

*This chapter describes the elucidation of the model mechanism of **in-situ**, **base-free** Pd(0) formation from a novel SCN pincer palladacycle in the gas-phase using density functional theory (DFT). Two hypothetical mechanisms of Pd(0) formation have been elucidated to proceed through four main steps namely; transmetallation (TM), first de-coordination, reductive elimination (RE) and second de-coordination in that order. TM for the **base-free** mechanisms is the rate-determining step, though the process is both energetically and kinetically unfavourable. The two functionals employed in the study yield similar energetic profiles and follow the same general patterns in the gas and solvent phase even though they differ with respect to the first de-coordination step and the product of reductive elimination. The results suggest that the novel pincer complex employed in the Pd(0) formation possesses relatively good stability for use as a pre-catalyst in cross-coupling reactions. Comparison of the **base-free** mechanism and the elucidated mechanism **with base** shows that the role of the base in the formation of Pd(0) from the pincer complex (pre-catalyst) is to significantly lower the activation energy barrier of TM for the reaction to be initiated.*

3.1 Introduction

Any palladium compound that incorporates at least one palladium-carbon bond that is intra-molecularly stabilised by one or two neutral donor atoms, mainly phosphorous (P), sulphur (S), oxygen (O) or nitrogen (N), is known as a palladacycle.[28,141–145] A special subclass of this group of compounds is the pincer type of palladacycles where two fused rings are incorporated in one compound[142] with side arms bearing the same donor atoms/groups e.g., PdNCN, PdSCS, PdPCP; symmetrical pincers[28,142,144,146,147] or the less common, different donor atoms/groups e.g., PdSCN, PdPCN; unsymmetrical pincers.[28,142,147–152] Some bimetallic palladacycles are also known.[163-167] Knowledge of this class of compounds dates back to the 1960's.[141,143] They are known to possess

therapeutic activity against cancer cells,[141,158,159] photo-physical and catalytic properties.[28,141–143,145,152,160] They have been studied, tested and applied as such over the years.[28,141,158–160]

The catalytic application of palladacycles has recorded an overwhelming attention from researchers in the last few decades since their discovery as catalytically active species in the Heck and Suzuki cross-coupling reactions by Herrmann and Beller *et al*.,[161,162] with a plethora of scholarly articles and reviews (Refs. cited herein and more) now available. This is because aromatic carbon-carbon (C-C) bond coupling reactions have emerged in recent years as an exceedingly important and facile way of preparing complex pharmaceuticals, natural products, optical devices and industrially important starting materials.[144,145]

3.1.1 Literature Review

In 1995, Catellani *et al*.,[163] in an invited review reported that the use of palladacycles derived from norbornene insertion into aryl-palladium bonds followed by cyclisation allowed the selective functionalisation of either end of the metallacycle and formation of condensed rings. They went on to state that a catalytic process involving Pd(II)/Pd(IV) metallacycle intermediates had been achieved. Later in that year, Herrmann and Beller *et al*.,[161,162] reported for the first time the use of palladacycles (furnished from treating Pd(II) acetate with tris(*o*-tolyl)phosphane in toluene) in the Heck and Suzuki C-C coupling reactions as catalysts that were an order of magnitude more active and thermally more stable than conventional catalysts. They however, noted that neither the cleavage of phosphorous-carbon bond nor deposition of palladium occurred in the catalytic process. This led them to suggest the possibility of a Pd(II)/Pd(IV) catalytic process. Ohff *et al*., 1997[164] explored the possibility of catalysis using new, X-ray characterised Pd(II) pincer PCP palladacycles (obtained from the reaction of $Pd(OCOCF_3)_2$ and corresponding diphosphines in tetrahydrofuran (THF) at 80 °C) in the Heck reaction and reported that the complexes exhibited exceptionally high catalytic activity. They further observed that the new complexes were extraordinarily thermally stable and did not decompose under catalytic conditions to give Pd(0) nor its complex species. They then concluded that the studied catalytic process may not have included the Pd(0)/Pd(II) cycle. Lagunas *et al*., 1998[154] described a novel synthetic route and characterised a dimeric PdNCN pincer by single-crystal X-ray diffraction for use as a precursor to conducting organometallic molecular wires (oligomers and polymers). Also in the same year, Shaw *et al*.,[165] reported a new and very efficient method of separating products of reaction from the catalyst when they used NMR characterised palladacycles derived from tri(1-naphthyl)phosphine in the Heck reaction. They asserted that the complexes were very active catalysts that followed the Pd(II)/Pd(IV) mechanism in the catalytic process. Weissman and Milstein in 1999[166] reported that a thermally stable phosphine-

free imine palladacycle, an excellent catalyst for the Suzuki cross-coupling, lead to more than 100000 turnovers with non-activated aryl bromides. Akira Suzuki acknowledged these new advances to the coupling reaction of organoboron compounds with organic halides or triflates in 1999.[167]

In 2000, Zim *et al*.,[168] stated that cyclopalladated compounds derived from the ortho-metallation of benzylic *tert*-butylthioethers were excellent catalyst precursors for the Suzuki cross-coupling reaction of aryl bromides and chlorides with phenylboronic acid under mild reaction conditions. They concluded that a broad range of substrates and functional groups were tolerated in the protocol with high catalytic activity attained. Bedford and Cazin in 2001[169] presented simple tricyclohexylphosphine adducts of palladium complexes with ortho-metallated N-donor ligands that showed the highest catalytic activity yet reported in the Suzuki coupling of aryl chlorides even under aerobic conditions. They concluded that the active catalyst (a low-coordinate Pd(0) species) that gave this high activity was generated *in situ* from the adducts in the course of reaction. Also in 2001, Bedford and Welch[170] reported some phosphinite based palladacycles obtained at reflux temperatures in toluene and THF that showed extremely high catalytic activity in the Suzuki coupling of both sterically hindered and electronically deactivated aryl bromides especially in the presence of one equivalent free ligand. They went on to suggest therefore, that the active catalyst in the studied reactions may be a low-coordinate Pd(0) species. Dupont *et al*., in a microreview stated that N, P and S containing palladacycles were emerging as new catalyst precursors and that the complexes exhibited thermal and air stability.[143] They went on to assert that the complexes were now being successfully exploited in catalytic reactions ranging from classical hydrogenations to enantioselective aldol-type condensations. Whitcombe *et al*., in a review on the advances in the Heck chemistry of aryl bromides and chlorides using cyclopalladated complexes as catalysts (including pincer type palladacycles) suggested that more mechanistic studies on the reactions be performed to reveal the true nature/form of the active catalyst as it was not yet clear whether the complexes were engaged in the Pd(0)/Pd(II) or Pd(II)/Pd(IV) catalytic cycle in the reaction process.[171] Bedford *et al*., 2002[172] reported simple mixed palladium complexes which acted as catalyst precursors for the Suzuki coupling of aryl chlorides stating that they displayed extremely high catalytic activity. Herrmann *et al*., 2003[153] presented a summary of the applications of palladium complexes with phosphorous ligands containing a metallated sp^3-carbon centre or with *N*-heterocyclic carbene ligands in C-C and carbon-nitrogen (C-N) coupling reactions of aryl halides including results of mechanistic discussions about their role in the catalytic cycle. They concluded that although the complexes were efficient pre-catalysts, neither of the phospha-palladacycles

underwent cleavage nor did the NHC ligands dissociate from the metal centre in the course of the reaction hence, avoiding the generation of Pd(0) particles or palladium black.

Consorti *et al*., in 2004 reported low fluorescence emissions from a newly synthesised and characterised palladacycle in both solution and solid state ascribing the emissions to excimeric emissions due to the rigid and totally flat structure of the complex in solid state confirmed by X-ray diffraction.[146] Consorti *et al*., established new catalysts based on unsymmetrical NCP pincer palladacycles for the Heck reaction in 2004.[147] They averred that these new catalytic systems acted as a reservoir of the catalytically active Pd(0) species and hence, proposed that the reaction followed the Pd(0)/Pd(II) catalytic mechanism. Following this development, Yu *et al*., 2004[173] ruled out the possibility of a Pd(II)/Pd(IV) catalytic mechanism under their reaction conditions while using silica-polynorbornene immobilised palladium (II) SCS pincer complex in the Mizoroki-Heck coupling of iodobenzene and *n*-butyl acrylate. They asserted that the pincer complexes decomposed under reaction conditions by rupture of ligand bonds to generate active Pd(0) homogeneous species with no evidence of catalysis by the Pd(II) complexes, thus supporting the Pd(0)/Pd(II) catalytic mechanism. Bedford *et al*., while reviewing the design and application of new homogeneous palladium catalysts for the formation of C-C and C-heteroatom bonds stated that palladacycles (catalyst precursors) played a significant role as alternative sources that improved activity when used in association with bulky electron-rich phosphines and carbenes which increased the electron density on the palladium centre(s).[174] Nevertheless, they concluded that very many interesting problems and taxing issues in the use of this class of substrates in coupling chemistry still needed to be addressed. Yu *et al*., reiterated that pincer complexes were only pre-catalysts in the Heck coupling reactions and that there was no evidence of catalysis by Pd(II)-SCS complex when they performed kinetic experiments and poisoning studies with the complex immobilised on porous silica and soluble polynorbornene supports in 2005.[175] Later that same year, Sommer *et al*.,[176] reported a similar study with PdPCP complexes that was in complete agreement with the findings of Yu *et al*.[173,175] Also in 2005, Dupont *et al*., asserted that palladacycles possessed a plethora of interesting and useful properties accounting for their increasing applications.[141] The authors went on to state that the vast majority of the applications of palladacycles involved an intact Pd-C bond. Furthermore, they concluded that in their use as catalytic systems, the Pd(II)/Pd(IV) mechanism of catalysis was highly unlikely as solid based catalysts designed for reusability probably generate Pd(0) in the course of the reaction, and as such, only act as pre-catalysts. d'Orlye and Jutand then reported the *in situ* formation of a Pd(0) complex from a palladacycle in dimethylformamide (DMF) at 80 °C in the absence of reducing agents in an endergonic equilibrium and proposed it to have occurred via reductive elimination.[155]

de Vries in 2006[156] stated that in all Heck reactions at high temperatures, (irrespective of the nature of precursor) palladium catalysts reduced rapidly to Pd(0) with the tendency of forming soluble colloids in solution. In addition, he stated that after the completion of the Heck cycle in solution, the palladium could either fall back to form colloidal particles or re-enter the catalytic cycle by engaging in another oxidative addition. Cardenas *et al*., performed a computational study at the B3LYP/6-31G(d)[LANL2DZ] level of theory to determine the mechanism of the key steps of Pd-catalysed domino reactions in which a $C(sp^2)$-$C(sp^2)$ bond is formed from aryl and alkenyl halides.[177] They explored the oxidative addition of these halides to palladacycles to give the Pd(IV) intermediates and the transmetallation of the halides between two Pd(II) centres to assert that a palladacycle and a Pd(II) complex formed by oxidative addition of the halides to Pd(0). The authors then concluded that the oxidative addition of iodoethylene to Pd(0) precursors was much more favourable than oxidative addition of the halide to Pd(II) palladacycles while the transmetallation between Pd(II) complexes was facile. Phan *et al*., in that same year noted in a review that research had begun shedding light on the transformations that palladium pre-catalysts undergo prior to and during catalytic transformations, thereby narrowing the scope of the types of palladium complexes that might be regarded as 'true catalysts' in the Heck and Suzuki coupling reactions.[144] The authors went on to state that there was a likelihood of the decomposition of many pre-formed metal-ligand complexes or a mixture of palladium sources and ligands at high temperatures to liberate Pd(0) nano-particles. In addition, they stated that the liberated nano-particles would in turn act as precursors to dimeric palladium species that would be the true catalysts in an anionic catalytic cycle. They then concluded that a Pd(II)/Pd(IV) catalytic cycle was yet to be proven while palladacycles have all been shown to operate by a Pd(0)/Pd(II) mechanism over the years.[144] Weck and Jones, 2007[178] observed that minimising the costs associated with the Mizoroki-Heck reaction by developing high turnover number catalysts or facilitating catalyst recovery and elucidation of the true nature of the active catalytic species in the reaction when using various pre-catalysts were the two main challenges faced by practitioners of the Heck or other Pd-catalysed coupling reactions. They then asserted from their study that all pre-catalysts decomposed at high temperature (120 °C) to generate the active Pd(0) species that were the true catalysts. They also enumerated the techniques for elucidating the nature of the true active Pd species which included; mercury, Hg(0), poisoning, kinetic tests, three-phase tests, filtration or split tests and use of soluble and insoluble catalyst poisons. da Costa *et al*., synthesised novel fluorous palladacycles in 2008 and found that they were effective catalyst precursors for the Heck reaction of iodobenzene and methyl acrylate in DMF.[179] They observed that the catalyst could not be recycled in fluorous solvents and that low valent palladium nano-particle species believed to be the true catalysts were present in the reaction

medium via transmission electron microscopy (TEM). Thereafter, Kozlov *et al*., 2008[149] synthesised and characterised two pincer SCS palladacycles by X-ray diffraction and reported the complexes to show high catalytic activity for the Suzuki cross-coupling of aryl bromides with phenylboronic acid. They also stated that the complexes exhibited luminescence at 77 and 300 K. Zhang *et al*., 2009[180] reported the synthesis and characterisation (using spectroscopic techniques and single-crystal X-ray diffraction) of five unsymmetrical PCN pincer palladacycles and found them to be effective catalysts for the Suzuki and copper-free Sonogashira cross-coupling reactions. The authors observed that the complexes were insensitive to air and moisture thereby allowing for ease of handling. That same year, Muniz presented evidence of the Pd(II)/Pd(IV) catalytic mechanism for the first time in the developing field of Pd catalysis in a mini-review stating that the frequently encountered Pd(0)/Pd(II) cycle was characterised by the presence of strong oxidants that prevented further oxidation of Pd(II) at a given point in the cycle.[157] He however, observed that the stability of Pd(IV) complexes was too low to allow for structure isolation and advanced mechanistic studies of the catalysis. Hao *et al*., 2010[148] reported the synthesis, characterisation (using spectroscopic and single-crystal X-ray diffraction techniques) and testing of some symmetrical and unsymmetrical pincer palladacycles for the Suzuki coupling of aryl bromides and activated aryl chlorides with phenylboronic acid in different media and at different temperatures. The researchers suggested from their study that the unsymmetrical pincers showed greater catalytic activity when compared with the symmetrical pincer complexes. They also noted that because palladium black (agglomerated Pd nano-particles[156]) was generated in the catalytic process, the reactions proceeded via the Pd(0)/Pd(II) catalytic cycle and that the pincers were only precursors in the process. Kozlov *et al*., 2011[150] reported synthetic approaches to novel symmetrical and unsymmetrical hybrid pincer Pd(II) complexes of the type PdSCE (E = S, N, O) that displayed high to excellent catalytic activities in the Suzuki cross-coupling reactions of aryl bromides with phenylboronic acid. They observed that the asymmetry of pincer complexes was a factor in its catalytic activity; the higher the asymmetry, the greater the activity. This is because the authors found pincer complexes with two fused 5,6-membered SCS' and SCN metallacycles to show higher catalytic activity over their 5,5-membered analogues.[150] Later that year, Selander and Szabo[142] in a review asserted that the reduction of Pd(II) to Pd(0) during catalysis in the presence of strong bases at high temperatures imposed a limitation on the direct application of pincer palladacycles as catalysts for coupling reactions. They went on to suggest that these limitations could be avoided by performing these reactions without the redox conditions or diverting the redox to a Pd(II)/Pd(IV) catalytic cycle in lieu of the Pd(II)/Pd(0) cycle. These assertions agreed with those held by Muniz[157] in proposing his Pd(II)/Pd(IV) catalytic mechanism. They further argued that because of the decomposition of the

complexes under catalytic conditions, the advantageous effects of the pincer ligands would not be employed in catalytic reactions. Kozlov *et al*., reported yet another set of PdNCS pincer complexes which proved to be excellent pre-catalysts for the Suzuki cross-coupling of electronically varied bromoarenes and chloroacetophenone with phenylboronic acid that same year.[151] The researchers affirmed that the generation of Pd(0) in the catalytic process was in agreement with previous views that the Pd(0)/Pd(II) mechanism of catalysis was the most appropriate cycle for the couplings with Pd(0) as the true catalysts in the process. Also in 2011, Fortman and Nolan discussed cross-coupling reactions that utilised NHC palladacycles as catalysts[145] stating that the catalysts were becoming increasingly applicable industrially and in academia. They observed that the development of economically viable and efficient catalysts was on going, with excellent catalytic species derived by mimicking the Pd-NHC architecture.

Aleksanyan *et al*., 2012 reported the synthesis, isolation and characterisation of novel hybrid pincer palladacycles with molecular structures:

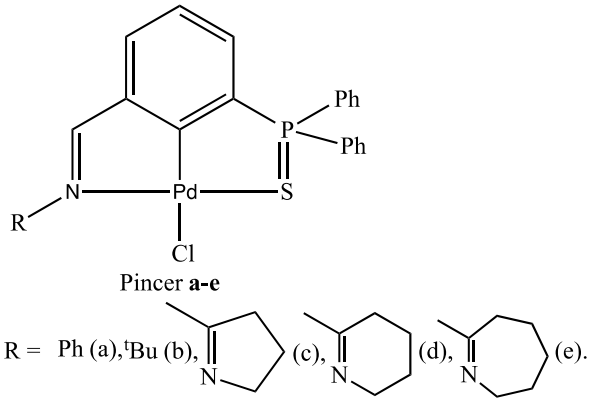

Pincer **a-e**

R = Ph (a), ^{t}Bu (b), (c), (d), (e).

that demonstrated high activity as pre-catalysts for the Suzuki cross-coupling of phenylboronic acid with aryl bromides.[152] The authors found that the release of Pd(0), the catalytically active species, and hence catalysis was controlled by steric effects; the greater the steric hindrances, the more facile the generation of Pd(0) and so, the lesser the catalytic action. Jin and Lei later that same year provided insights into the elementary steps in the Negishi coupling reactions employing palladacycles as pre-catalysts, stating that kinetic investigations were one of the most important strategies of understanding oxidative addition, transmetallation and reductive elimination in mechanistic studies of such reactions.[181] Karami *et al*., 2012[158] performed synthesis, structural characterisation and *in-vitro* cytotoxicity assays of dinuclear and mononuclear cyclopalladated complexes against human cervix carcinoma, colon cancer, leukaemia cancer cell line and human breast carcinoma. The authors compared the activity of these complexes against these conditions with the activity of cisplatin against same conditions to conclude that they performed better than

cisplatin. Kapdi *et al*., 2013[182] developed an efficient and practical synthetic route to Pd-(palladacycle)-catalysed intra-molecular C-H bond functionalisation of coumaryl esters affording benzofurocoumarins. The authors noted that the palladacycles proved to be efficient catalysts in the reaction. Kapdi and Fairlamb, 2014[159] in a review stated that palladacycles or cyclopalladated complexes showed promising activity as anti-cancer agents with Pd nano-particle species (resulting from these complexes) imparting interesting effects on cancer cell lines. They however, noted that this area is only emerging and needs to be explored for more insights into the correlation of the water solubility of palladacycles and cytotoxicity as the complexes exhibited better solubility in water compared to cisplatin. They asserted that such studies could provide a lead way to the discovery of an important and attractive way of treating cancer. Ratti 2014[183] in a review highlighted the application of palladacycles as catalysts/catalyst precursors for the Mizoroki-Heck, Sonogashira, Suzuki, Stille and Negishi cross-coupling reactions. The author observed that the use of magnetic nano-particles as supports for active palladacycles in the catalytic process could be a fruitful area of research. Later that year, Font *et al*.,[184] studied the cyclometallation reactions of dinuclear acetato bridged palladacycles from a kinetico-mechanistic perspective to assert that they were excellent starting materials in the facile activation of C-H bonds. Kapdi *et al*., also in 2014 reported the direct transmetallation between palladacycles and arylboronic acid to afford isolable transmetallation products stating that the reaction occurred in less than 30 minutes in THF.[185] The authors noted that prolonged reaction times lead to the generation of dinuclear complexes with hydroxo and acetoxy bridging ligands. They then concluded that insight into pre-catalyst activation for the Suzuki-Miyaura cross-coupling using palladacycles had been gained with the acetate and *N*-imidate anions activating the neutral arylboronic acid.

Chapman *et al*., 2015[186] described the unusual cyclometallation reaction at palladium that proceeded through the functionalisation of vinylic C(sp^2)-H bond tethered to an NHC ligand concluding that the energetic balance between palladacycle formation and bis-NHC complexation was found to be subtle. Roy *et al*., 2015[160] reported the formation of some palladacycles from 2-(phenylazo)azobenzene stating that planar complexes were furnished using crystallographic analysis. The researchers then computationally studied the obtained complexes for photo-physical properties using the time dependent density functional theory at the B3LYP/6-311+G(d,p)[LANL2DZ] level of theory and natural transition orbital (NTO) analyses to observe that the complexes exhibited luminescence in solution at ambient temperature. In addition, they concluded that the palladacycles were potential candidates for use as pre-catalysts in the Suzuki-Miyaura and Heck-type reactions. Rosa *et al*.,[187] investigated the optimisation of a novel PdNCP pincer palladacycle as a catalyst for the Sonogashira coupling reaction using an experimental

technique to assess the effects of bases, solvents and reaction temperature on the second step of the reaction via the two-factor design. They concluded from the study that temperature was statistically significant in relation to the yield of the reaction. Boonseng *et al*., also in 2015, evaluated the accuracy of DFT optimised geometries of symmetrical (PdNCN and PdSCS) pincer palladacycles by investigating the performance of eight commonly used density functionals with four different combinations of basis sets to reproduce the crystal structures of the complexes.[28] They noted that the ωB97XD functional performed best overall but that the PBE and TPSS functionals also performed very well and had the advantage of being computationally faster and hence, less expensive. The authors, using the Bader's "Atoms In Molecules (AIM)"[124–133] method to elucidate the nature of bonding in the complexes concluded that the distinct differences in bond strength and nature of interaction between Pd and the donor atoms in the palladacycles supported their thermodynamic stabilities.

3.1.2 Justification of Study

Some reports[148,150,180,188,189] suggest that unsymmetrical pincer palladacycles possess greater catalytic activity than their symmetrical pincer analogues. Dr G.W. Roffe synthesised a range of unsymmetrical pincer palladacycles for testing their catalytic activity in the Suzuki-Miyaura reactions in the experimental group of Prof. John Spencer at Sussex.[29,190] The X-ray structure of one of his novel PdSCN complex, investigated in this chapter, is presented in **Figure 3.1**.

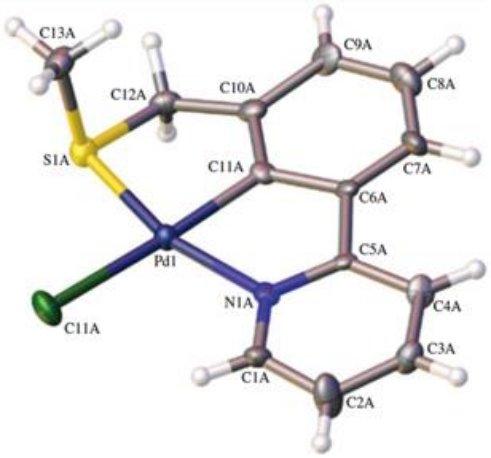

Figure 3.1. X-ray crystal structure of the novel PdSCN unsymmetrical pincer palladacycle (**1**) investigated in this Chapter. Adapted from Roffe et al., *R. Soc. Open Sci.* **2016**, *3*, 150656.[190]

The focus of this chapter is to rationalise the formation of Pd(0), the active catalyst[141–143] in the Suzuki-Miyaura cross-coupling reactions from **1** to complement the work of Dr G.W. Roffe.[29] It was found from the experimental work of Dr G.W. Roffe[29] that both unsymmetrical and

symmetrical pincer palladacycles were good pre-catalysts in the Suzuki-Miyaura carbon-carbon cross-coupling reactions.

3.1.3 Aim of Study

The aim of this Chapter is to elucidate the stepwise mechanism of Pd(0) formation without base and/or redox agents for catalysis. The effects of non-polar and polar solvents on the elucidated mechanism are also determined. This investigation was performed in parallel with the computational investigation of the mechanism of Pd(0) formation with base by Dr G.W. Roffe in the Cox group. The solvents were chosen to complement his experimental work in the Spencer group. This work has now been published in the Journal of Organometallic Chemistry.[11]

3.2 Computational Details

All computations were performed using DFT methods as implemented in the Gaussian 09 package[24] to locate minima and/or transition states[19,36,191,192] of the neutral singlet spin systems investigated. The GGA functional, PBE[72,193,194] and the h-GGA functional, ωB97XD[77,80] previously validated in the Cox group[28] were employed. The Pd atom was described by the ECP, SDD[122,123] which includes a set of *f*-polarisation functions.[195] Standard basis sets,[99,111–113,196,197] 6-31+G(d,p) and 6-31++G(d,p), that provide great flexibility without substantial increase in computational time[28] were used for C, B, N, O, Cl, S and H for computations at the PBE and ωB97XD levels of theory, respectively. All the ground state and transition state structures involved in the reaction of PdSCN (**1**) with phenylboronic acid *without base* were fully optimised at the PBE/6-31+G(d,p)[SDD] and ωB97XD/6-31++G(d,p)[SDD] levels of theory without any symmetry restrictions.[192,198] These calculations locate the most stable local equilibrium structure of a chemical species (atom, ion, molecule or compound) on the PES of the system by changing its geometry and electronic structure to obtain a stationary point that corresponds to an energy minimum or transition state structure.[19,36,191,192,198–200] Frequency calculations were performed on stationary points obtained from the optimisations at 298.15 K and 1 atm to confirm and ascertain their nature. The absence of an imaginary frequency indicated a minima and the presence of a single imaginary frequency indicated a first-order saddle point (transition state) on the PES.[19,36,191,201,202] The connectivity of the transition states to their adjacent minima was confirmed by intrinsic reaction coordinate (IRC) calculations.[19,191,201,202] To obtain accurate energy and activation barrier height values, single-point energy (SPE) calculations were performed on the optimised geometries at the ωB97XD with a larger standard basis set, 6-311++G(2df,2p) and the ECP in the gas phase.[28]

ZPE corrections to the electronic energies and thermal corrections to the Gibbs free energies of all the species were obtained from the frequency calculations.[19,30,32,36,37] The implicit solvation model based on the polarisable continuum model (PCM) of Tomasi and co-workers,[84,90] more specifically, the continuous surface charge PCM (CSC-PCM) of Scalmani and Frisch[87] as implemented in the Gaussian09 package[24] was employed to obtain the solvent corrected energies. Solvent effects on the gas-phase optimised geometries were performed using ωB97XD. The solvents used to compute solvent corrected energies of the stationary points obtained at the PBE level of theory are toluene (To, $\varepsilon = 2.4$), tetrahydrofuran (THF, $\varepsilon = 7.4$) and acetonitrile (AN, $\varepsilon = 35.7$). Those used for the calculation of solvent corrected energies of the stationary points obtained at the ωB97XD level of theory are o-xylene (o-X, $\varepsilon = 2.5$) and AN. The DFT methods employed can be summarised as ωB97XD/6-311++G(2df,2p)[SDD]//PBE/6-31+G(d,p)[SDD] and ωB97XD/6-311++G(2df,2p)[SDD]//ωB97XD/6-31++G(d,p)[SDD]. A topological analysis of the electron density of the species was performed using Bader's Quantum Theory of Atoms in Molecules (QTAIM)[124–133] as implemented in the Multiwfn package.[203] In doing this, the ωB97XD/6-311++G(2df,2p)[DGDZVP] level of theory was employed in which the all electron basis set, DGDZVP[204] was used instead of the SDD[122,123] for the Pd atom to generate the wavefunctions of the investigated species.

3.3 Results and Discussion

3.3.1 Molecular Structure

The reaction of PdSCN (**1**, **Figure 3.1**) with phenylboronic acid to form Pd(0), **Scheme 3.1**, was investigated and the optimised structures are provided in **Figure 3.2**. For each conformer, a frequency calculation was performed at the optimised geometry to confirm that it was minimum and their ZPE corrected electronic energies and thermal corrected Gibbs free energies are reported in **Table 3.1**.

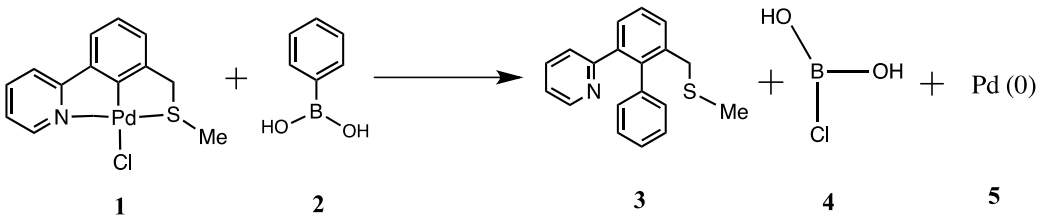

Scheme 3.1. Formation of biphenyl product, boric chloride and Pd(0) using a novel unsymmetrical pincer palladacycle, **1**[29] and phenylboronic acid.

The frequency checks in **Table 3.1** indicate that all the geometries of the species obtained at the PBE/6-31+G(d,p)[SDD] level of theory except **2b** (**Figure 3.2**) correspond to a minimum stationary point on the PES. This structure however, optimised upon frequency displacement to the same structure as **2a**. The energy difference between **2** and **2a** and **4** and **4a** is ~10 to 16 kJ mol^{-1}. In both cases, the most stable conformer, **2** and **4** corresponds to a structure in which the hydrogen-hydrogen distances are maximised and the ∠OBO angle is closer to the trigonal angle of 120 °[205] (**Table 3.2**). As a consequence, **2** and **4** possess the minimum energies on the PES.

Table 3.1. Zero point corrected electronic energies (E_{ZPC}), thermal corrected Gibbs free energies (G_{TC}) and frequency checks for negative eigenvector of the gas-phase optimised structures of the species of **Scheme 3.1**.

Species	E_{ZPC} / kJ mol^{-1}		G_{TC} / kJ mol^{-1}		Frequency Check‡
	PBE	ωB97XD	PBE	ωB97XD	
1	-4052586.131	-4052575.854	-4052702.507	-4052691.478	+
2	-1071595.060	-1071589.926	-1071682.851	-1071679.174	+
2a	-1071586.601	*	-1071673.255	*	+
2b	-1071564.337	*	-1071648.132	*	-
3	-3116158.398	-3116144.681	-3116288.195	-3116271.556	+
4	-1672043.792	-1672042.423	-1672115.807	-1672114.259	+
4a	-1672026.679	*	-1672098.860	*	+
5	-335735.8212	-335735.8212	-335779.3835	-335779.3835	+

‡: - Indicates that the structure is not a minimum due to presence of an imaginary frequency mode; + indicates that the obtained structure is in a minimum stationary point on the PES as no imaginary frequency mode is present. * means the energies are not computed

Table 3.2. Selected bond angles / ° of the conformational isomers of boronic species (**2** and **4**).

Structure	OBO / °	BOH / °	CBO/ClBO / °
2	117.0	111.2, 113.8	118.4, 124.6
2a	124.0	115.5, 115.5	118.0, 118.0
4	120.9	111.3, 113.4	117.7, 121.4
4a	127.0	115.2, 115.2	116.5, 116.5

Two conformational isomers of the palladacycle, **1** were found at the same energy on the PES, either with the methyl group below or above the plane of the molecule. This finding agrees with experimental result of the synthesis of two enantiomeric pincers.[29] Three conformers of the biphenyl product were also found basically at the same energy (energy difference between the conformers is less than 1.0 kJ mol^{-1}) on the PES depending on the orientation of the pyridyl group. Following the findings at this level of theory, only the most stable structures of the species in **Scheme 3.1** were re-optimised at the ωB97XD/6-31++G(d,p)[SDD] level of theory for the purpose of comparison (**Table 3.1**). As shown in **Figure 3.1** and **Figure 3.2**, the ligand coordinates to the

Pd(II) centre of the pincer complex, **1**, through the pyridyl nitrogen atom, the carbon atom of the central aryl ring and the sulphur atom of the group, -SMe in a tridentate manner. This is also confirmed by the molecular graph of the moiety generated from QTAIM analysis of the structure presented in **Figure 3.3**.

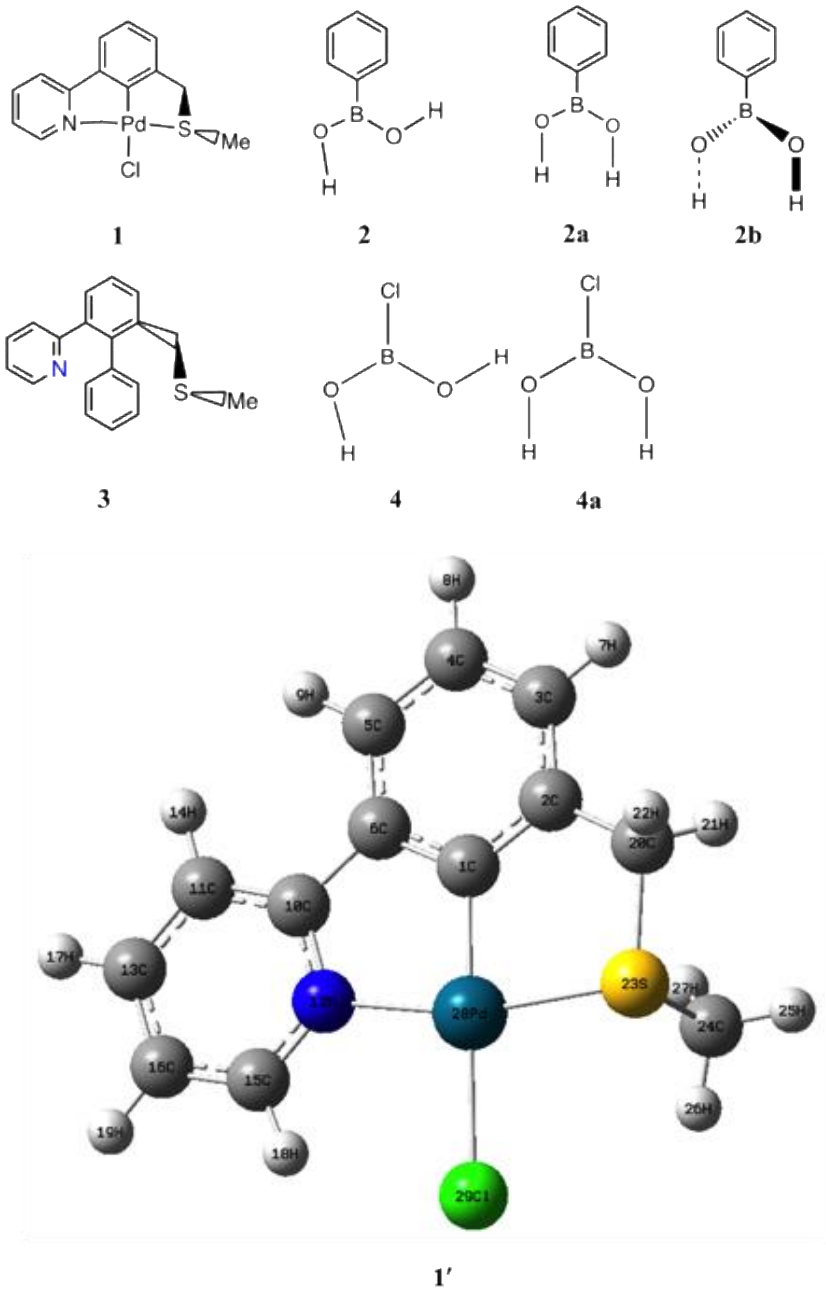

Figure 3.2. The optimised conformational structures of the species in **Scheme 3.1**; **1′** is the 3-D view of **1**.

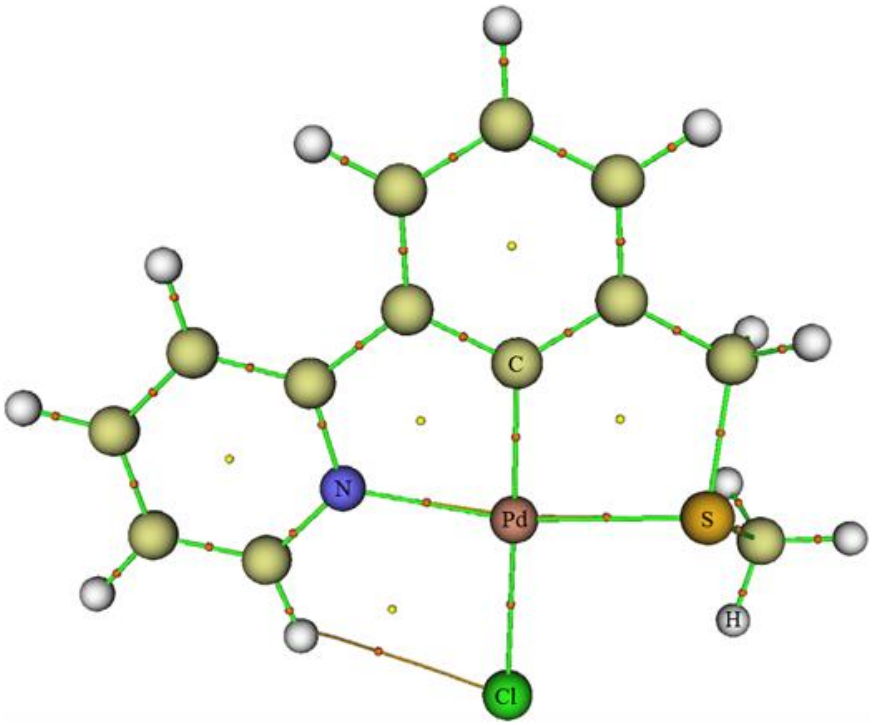

Figure 3.3. The molecular graph of **1** showing the connectivity of the atoms in its structure via bond paths (green solid links), the bcp's (orange dots) between bonded atoms and rcp's (yellow dots).

The Pd(II) centre adopts a slightly distorted square-planar geometry having the chloride in the fourth coordination site to produce a PdSCN pincer complex with two five-membered metallacycles. This geometry is as expected for unsymmetrical pincers that generate Pd(0) *in-situ* during catalysis[148,151,152,180] and is buttressed by the results summarised in **Table 3.3** and **Table A.1.1** (see **Appendix A.1**). **Table 3.3** and **Table A.1.1** present a summary of key structural (geometric) parameters in the palladium-ligand (Pd-L) environment of **1** obtained from experiment (X-ray crystallography),[29] and computation in the present work.

Table 3.3. Some experimental[29] and optimised (calculated) bond lengths and angles of **1**.

Bond length	Value / Å			Bond Angle	Value / °		
	Expt.	PBE	ωB97XD		Expt.	PBE	ωB97XD
Pd28-N12	2.09(3)	2.07	2.08	C1-Pd28-N12	80.6(14)	80.6	80.5
Pd28-S23	2.291(8)	2.29	2.31	C1-Pd28-S23	84.9(10)	85.0	85.2
Pd28-C1	1.95(3)	1.96	1.95	C1-Pd28-Cl29	174.0(11)	177.0	175.8
Pd28-Cl29	2.423(8)	2.40	2.40	N12-Pd28-S23	165.3(10)	164.3	165.7
				N12-Pd28-Cl29	98.0(3)	98.3	98.3
				S23-Pd28-Cl29	96.3(3)	96.4	95.8

The pincer complex, **1**, displays a nearly linear co-ordination at the Pd(II) centre. The bond angles; C1-Pd28-Cl29 measuring 174.0 (11) °,[29] is overestimated to the extent of 3.0 ° at the PBE method and 1.8 ° at the *ω*B97XD level of theory while N12-Pd28-S23 measuring 165.3 (10) °[29] is underestimated to the extent of 1.0 ° at the PBE but overestimated by 0.4 ° at the *ω*B97XD level of theory. This is an additional confirmation of the slight distortion of the square-planar geometry of the complex around its Pd(II) centre. Furthermore, the dihedral angles (**Table A.1.1**, in **Appendix A.1**) involving the -SMe group in the Pd-L environment together with the bond lengths and angles mentioned above suggest that the geometry of **1** obtained via calculation at the *ω*B97XD/6-31++G(d,p)[SDD] level of theory agrees slightly better in comparison with the experimental geometry[29] than that obtained at the PBE/6-31+G(d,p)[SDD] level of theory. This is evident in **Table A.1.1** where PBE either fails to predict the correct sign of the dihedral angle or gives greater over or underestimates of the parameter compared to *ω*B97XD on the overall. Nevertheless, both methods performed well in reproducing the geometry of **1** with emphasis on its Pd-L environment in good computational time. Both approaches give values of the key structural parameters comparable to their experimentally[29] determined values. This finding is in perfect accord with the findings of Boonseng *et al*.[28] The result also, agrees with the reports of Minenkov *et al*.,[10,206] and Waller *et al*.,[79] that the GGA (e.g., PBE) and h-GGA (e.g., *ω*B97XD) functionals are better at reproducing the geometries of transition metal complexes (with respect to the metal-ligand, M-L, environment) especially the hybrids accounting for dispersions such as *ω*B97XD.

3.3.2 Mechanism of Pd(0) Formation - Reaction Pathway for Scheme 3.1

Two model mechanisms of *in situ* Pd(0) formation for the Suzuki C-C cross-coupling reactions have been elucidated. These mechanisms are presented in **Scheme 3.2** and **Scheme 3.3**, respectively. The main difference between these schemes is that the first de-coordination step leading to the formation of **Int4** is different depending on the de-coordinating side-arm (-N or -S).

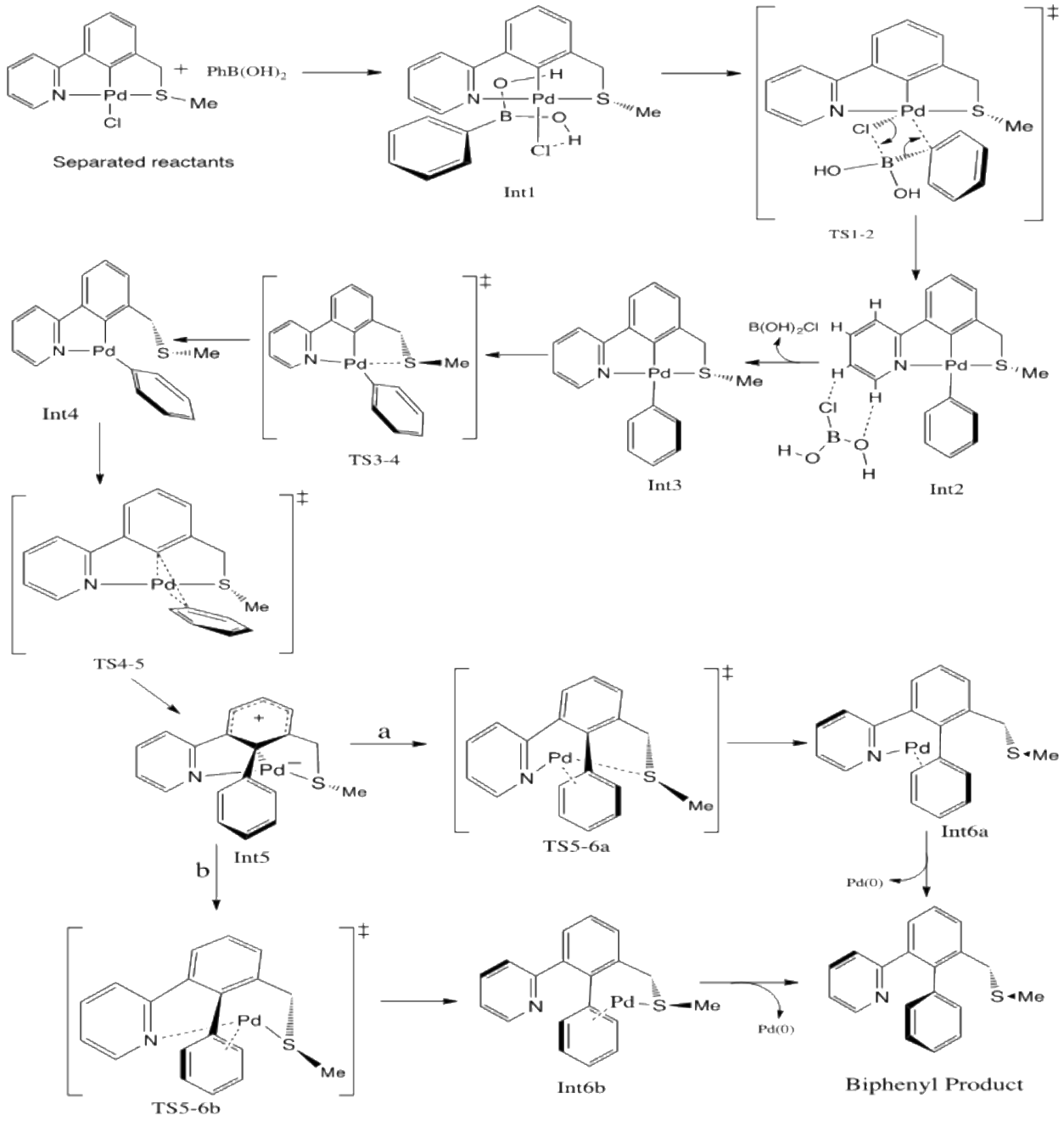

Scheme 3.2. Base free, gas-phase mechanism of Pd(0) formation from novel unsymmetrical pincer palladacycle (**1**)[29] computed at the PBE/6-31+G(d, p)[SDD] level of theory.

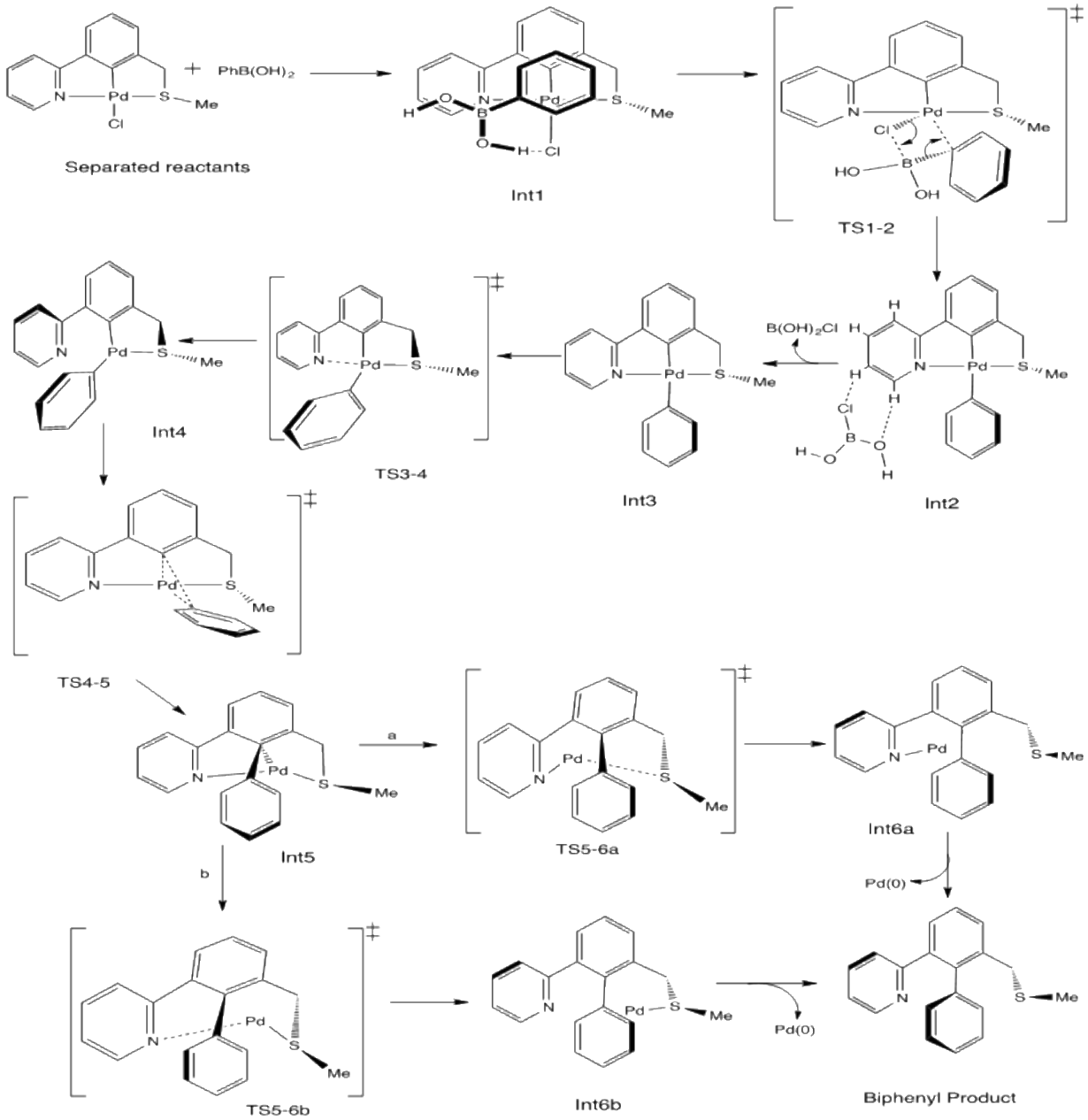

Scheme 3.3. Base free, gas-phase mechanism of Pd(0) formation formation from novel unsymmetrical pincer palladacycle (**1**)[29] computed with *ω*B97XD/6-31++G(d,p)[SDD].

The *in situ* formation of Pd(0) has been thought to presumably occur before catalysis begins in a reaction.[151,152,185] Each of the mechanisms as presented is found to involve four main steps namely: the transmetallation (TM; **TS1-2**), the first de-coordination (Dc<u>n</u>-1; **TS3-4**), reductive elimination (RE; **TS4-5**) and a second de-coordination (Dc<u>n</u>-2; **TS5-6**) in that order, respectively. From the presented schemes, it is observed that the pre-catalyst activation begins with the non-covalent attractive interaction[207] of the reacting species via the weak inter-molecular dispersive forces[152]

e.g., hydrogen bonding[208] and π-π interaction.[207] The molecular graphs of **Int1** showing these weak interactions are presented in **Figure 3.4**.

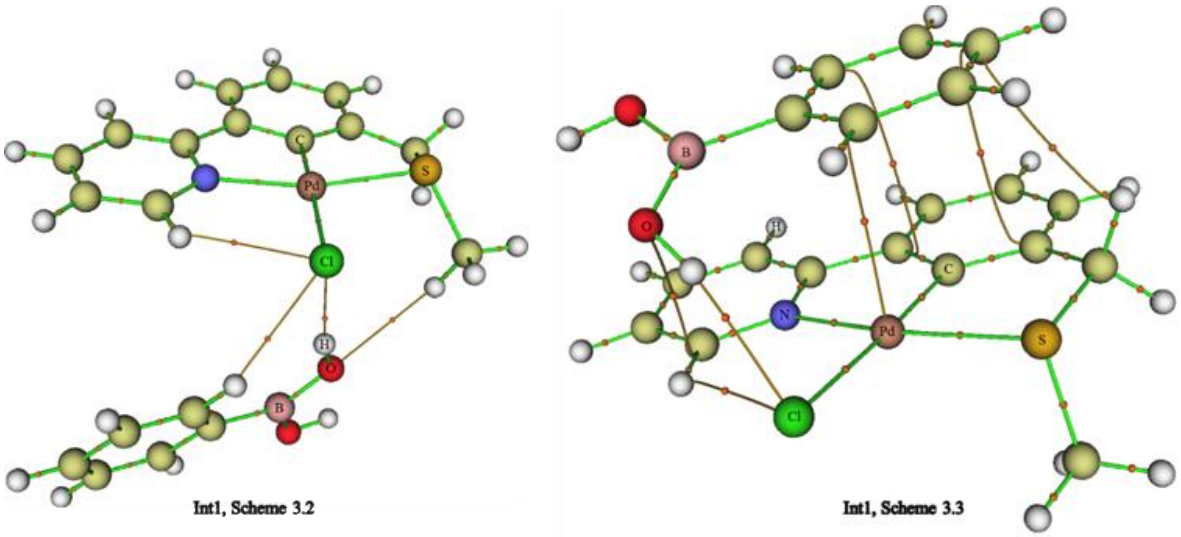

Figure 3.4. The molecular graphs of **Int1** for **Scheme 3.2** and **Scheme 3.3** showing the hydrogen bonding and π-π interaction (brown linkages) between the reacting species.

Hydrogen bonding occurs between the chloride of **1** and one of the hydrogen of the hydroxyl groups of the phenylboronic acid (for both schemes) while π-π interaction occurs between the aryl ring of the acid and the central aryl ring of **1** (**Scheme 3.3**). The Gibbs free energy profiles of **Scheme 3.2** and **Scheme 3.3** are presented in **Figure 3.5** and **Figure 3.6**, respectively. It is found from **Figure 3.5** and **Figure 3.6**, that the weak interactions in **Figure 3.4** lead to the stabilisation and orientation[207,209,210] of **Int1** (intermediate one). The process then proceeds to **Int2** (intermediate two) through a concerted,[210] four-centred transition state, [198,211] (**TS1-2**). In this transition state, the Pd(II) coordination sphere becomes trigonal bi-pyramidal by incorporation of the phenylboronic acid as the chloride assumes an apical position. This is the TM step in which the chloride is cleaved from the Pd(II) centre as the organic moiety (aryl ring) of phenylboronic acid is transferred to the Pd(II) centre from boron.[209,210] The cleaved Cl^- then binds to the formed electron deficient boron species to stabilise the system. **Figure 3.7** presents the molecular graph of the TM product showing the nature of interactions in the TM product. The TM products are initially held together by weak, inter-molecular hydrogen bonding[209,210] (**Figure 3.7**). This occurs between one of the oxygen of the boronic chloride and one of the hydrogen atoms of the pyridyl group of the pincer and between the chlorine atom of the boric chloride and another hydrogen atom of the pyridyl group of the pincer. These hydrogen bonds are soon separated as the reaction proceeds to form **Int3** as $ClB(OH)_2$ is eliminated.

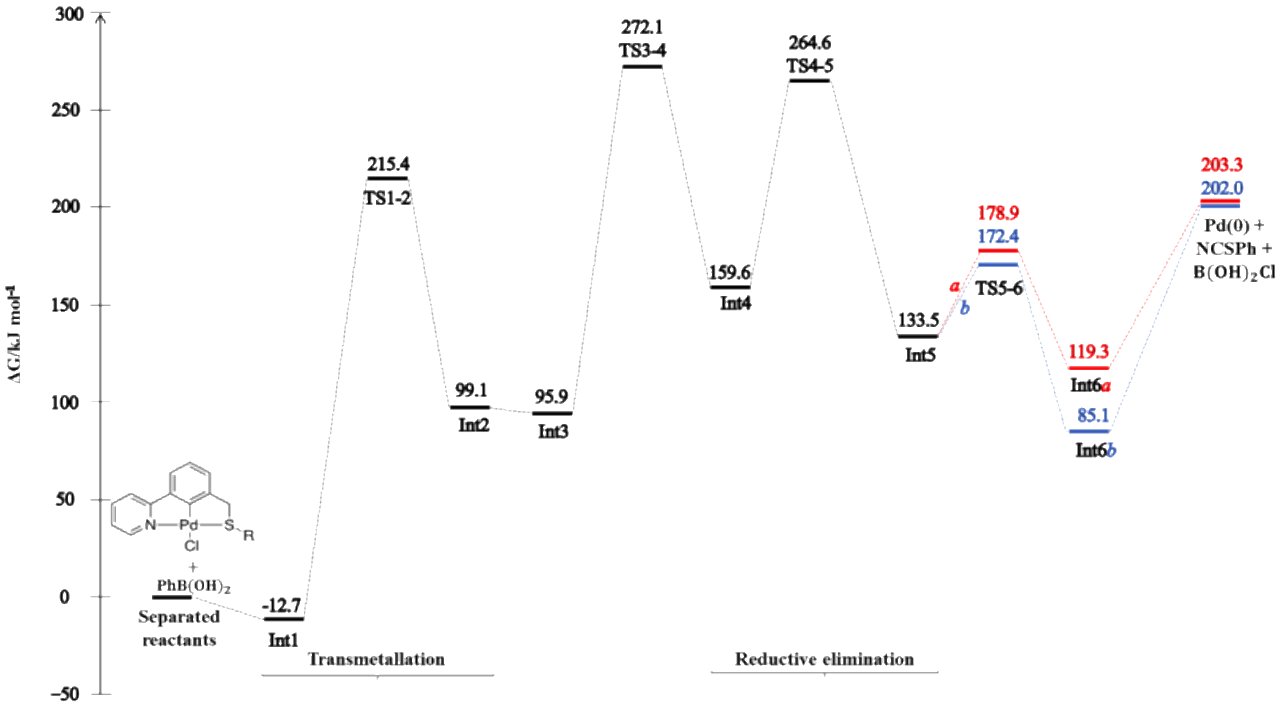

Figure 3.5. The lowest Gibbs free energy profile of the base-free, gas-phase mechanism of Pd(0) formation presented in **Scheme 3.2**; R = Me.

Thus, TM introduces the σ-bonded carbon atom into the coordination sphere[181] of the Pd(II) centre of **1**. In order to achieve a mutual disposition of the two leaving aryl groups[151,152,185] needed for facile formation of a low energy barrier three-centred dissociative transition state (**TS4-5**),[192,200] the RE step, one of the ancillary arms of the ligand de-coordinates in the Dcn-1 step via **TS3-4**. This is the essential step for C-C bond formation.[181] It is observed that the Dcn-1 and RE steps are different for the two DFT methods employed in the investigation as can be seen in the schemes arising from them respectively. In **Scheme 3.2** (arising from the PBE method), it is found that the Dcn-1 step (**TS3-4**) involves the de-coordination of the S atom of the ancillary -SMe group from the central Pd(II) of the complex (**Int3**). For **Scheme 3.3**, the nitrogen, N atom of the ancillary pyridyl group is observed to de-coordinate from the Pd(II) centre of **Int3**. PBE does not achieve N de-coordination from **Int3** while ωB97XD achieves S de-coordination from **Int3** but because the generated intermediate does not connect to the RE (**TS4-5**) at this level, it is omitted from the mechanism (**Scheme 3.3**). This occurrence may be attributed to the peculiarities of the two DFT functionals involved. PBE, a GGA comprising of total electron density ($\rho_\sigma(\boldsymbol{r})$) and electron density gradient ($\nabla_{\rho_\sigma}(\boldsymbol{r})$) tends to possess a better capacity to correctly account for the r_{Pd-N} coordinate (dative) bond but finds it difficult accounting for non-covalent and dispersion-type interactions when compared to ωB97XD.[10,212]

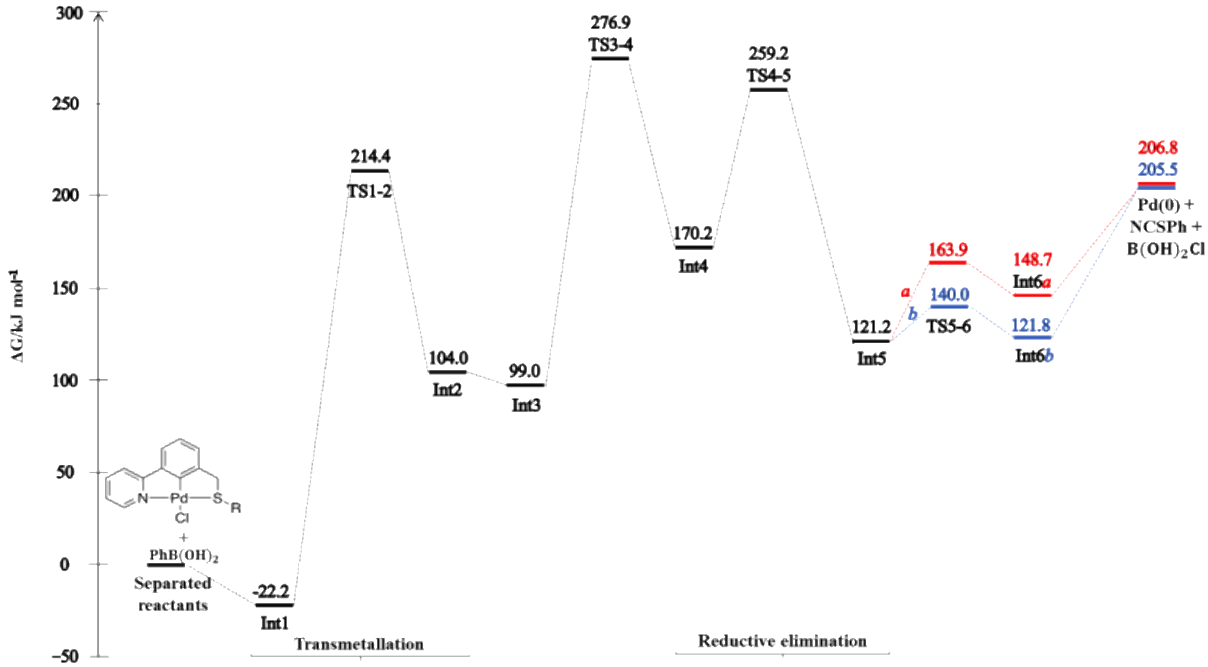

Figure 3.6. The lowest Gibbs free energy profile of the base-free, gas-phase mechanism of Pd(0) formation presented in **Scheme 3.3**; R = Me.

ωB97XD includes Hartree-Fock (X) exchange[77] and an empirical damping dispersion (D)[80,212] to account better for oxygen-metal (and by extension, sulphur-metal e.g., r_{Pd-S}, since they are group members with sulphur also forming softer Lewis bases than nitrogen[205]) coordinate (dative) bond, non-covalent and dispersion-type interactions when compared to PBE.[10,212]

Furthermore, the de-coordination of ancillary pyridyl arm at the ωB97XD level of theory could also be rationalised on the grounds of the trans-influence of the much better σ-donating ability[200,213,214] of the -SMe group on the arm. The de-coordination of ancillary -SMe arm at the PBE level of theory could be rationalised on the basis of dπ-pπ (Pd-pyridyl) back-bonding with a concomitant strengthening[192,215–217] of the r_{Pd-N} bond unlike the -SMe arm. Hence, the different nature and structure of both **Int4** and **Int5** (intermediate four and five) obtained at the two levels of theory. The nature and structure of the stable arenium complex (**Int5**) having an sp^3 (almost tetrahedral) instead of an sp^2 *ipso*-carbon obtained at the PBE level of theory from the present study is supported by reports of similar stable and isolable intermediates obtained from the experimental studies of van Koten and co-workers.[218–220] Thermodynamically stable intermediates of this nature that can undergo re-aromatisation (just as **Int5** in **Scheme 3.2**) are crucial either in the formation or cleavage of C-C bonds.[219,220] The *ipso*-carbon of **Int5** in **Scheme 3.3** is also observed to exhibit a slight distortion from the sp^2 hybridisation but still retains it probably because of the ability of the ωB97XD functional to effectively account for non-covalent and dispersion-type interactions.[10,212]

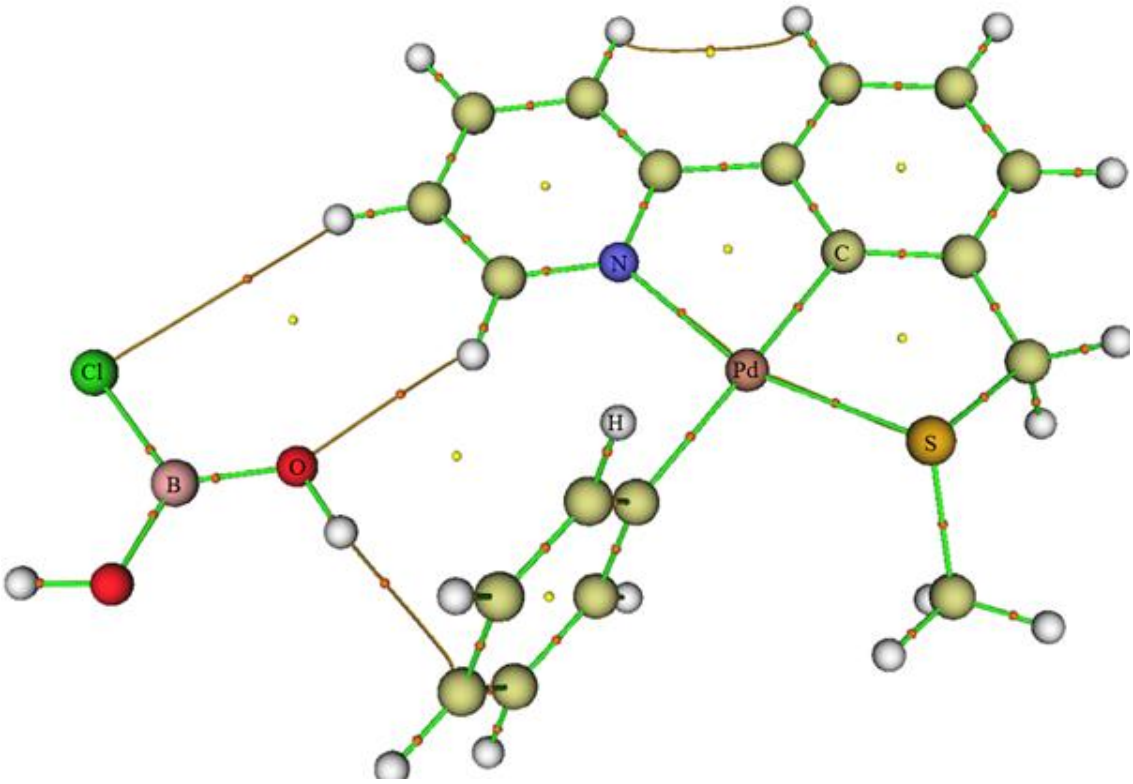

Figure 3.7. The molecular graph of **Int2** for **Scheme 3.2** and **Scheme 3.3** showing the hydrogen bonding (brown linkages) in the product of transmetallation.

This slight out-of-plane distortion of the *ipso*-carbon of **Int5** in both schemes due to the incipient formation of a Pd-$C_{(of\ central\ aryl\ moiety)}$ bond in the presence of the new C_{aryl}-C_{aryl} bond may be attributed to the re-organisation of the complex (**Int5**) to reduce the repulsive steric crowding[198] introduced by the in-coming aryl moiety from the phenylboronic acid. The mechanisms (**Scheme 3.2** and **Scheme 3.3**) again agree at the Dcn-2 step that splits into two: **a** (when the -SMe arm de-coordinates from the Pd(0)) and **b** (when the pyridyl arm de-coordinates from the Pd(0)), both leading to the formation of Pd(0), the active catalyst[141–143] and the biaryl (biphenyl) product.

3.3.3 Energetics and Concomitant Kinetics of the Pd(0) Formation Pathways

The Gibbs free energy profiles of **Scheme 3.2** and **Scheme 3.3** are presented in **Figure 3.5** and **Figure 3.5**, respectively. It is worthy of note that these energies are relative to the energy of the separated reactants. As can be seen in **Scheme 3.2** and **Scheme 3.3**, (or **Figure 3.5** and **Figure 3.6**) respectively, the TM occurs in two steps.[209,210] The first of which is the stabilisation and orientation of the reactants by non-covalent and weak dispersive attractive interactions[149,151,152,209,210] that result in the formation of **Int1** which lies 12.7 and 22.2 kJ mol^{-1} below the separated reactants, respectively. This corresponds to a Cl···H hydrogen bond distance of 2.23 Å and 2.29 Å,

respectively and an additional aryl-aryl π-π interaction distance of approximately 3.50 Å for **Scheme 3.3**. The second step is the TM itself via a trigonal bi-pyramidal, four-centred transition state, (**TS1-2**)[209–211] in an uphill, endergonic process[33,209,210] with the transition state structure located 215.4 and 214.4 kJ mol^{-1} above the separated reactants, respectively for **Scheme 3.2** and **Scheme 3.3**. This corresponds to the computed incipient r_{Pd-C} (2.22 and 2.24 Å, respectively) and r_{Cl-B} (1.87 and 1.86 Å, respectively) formation, r_{Pd-Cl} (3.13 and 3.12 Å, respectively) and r_{B-C} (2.21 and 2.20 Å, respectively) breakage. The r_{Pd-C} formed in the process is computed as 2.09 and 2.08 Å while the r_{Cl-B} is computed as 1.80 and 1.80 Å, respectively.

The energy barriers for the key steps of the mechanism presented in **Scheme 3.2** and **Scheme 3.3** in vacuum and solvent phase are summarised in **Table 3.4** and **Table 3.5**, respectively. The concomitant energy barrier for the TM step is 228.1 and 236.6 kJ mol^{-1}, respectively (**Table 3.4** and **Table 3.5**, respectively) with attendant rate constants of 6.8×10^{-28} and 2.2×10^{-29} s^{-1}.

Table 3.4. Gibbs free energy barriers ($\Delta G^{\ddagger}$) and Gibbs free energy of reaction (ΔG_r) computed with ωB97XD/6-311++G(2df,2p)[SDD]//PBE/6-31+G(d,p)[SDD] in the absence and presence of solvent effects.

Reaction step	$\Delta G^{\ddagger}$ / kJ mol^{-1}			
	Gas	To	THF	AN
TM ($(\Delta G_{r,TS1-2}) - (\Delta G_{r,Int1})$)	228.1	231.1	232.7	233.2
Dc<u>n</u>-1 ($(\Delta G_{r,TS3-4}) - (\Delta G_{r,Int3})$)	176.2	170.2	165.1	162.1
RE ($(\Delta G_{r,TS4-5}) - (\Delta G_{r,Int4})$)	105.0	111.5	118.0	122.0
Dc<u>n</u>-2 ($(\Delta G_{r,TS5-6}) - (\Delta G_{r,Int5})$)	45.5(38.9)	43.7(37.8)	42.2(36.8)	41.5(36.3)
ΔG_r (Products) / kJ mol^{-1}	203.2(202.0)	214.7(213.3)	223.1(222.0)	226.7(225.8)

TM stands for Transmetallation; Dc<u>n</u>-1 for First de-coordination; RE for Reductive elimination and Dc<u>n</u>-2 for Second de-coordination. To stands for Toluene ($\varepsilon = 2.4$); THF for Tetrahydrofuran ($\varepsilon = 7.4$) and AN for Acetonitrile ($\varepsilon = 35.7$). The values in brackets are for the nitrogen de-coordination path of Dc<u>n</u>-2 step.

The rate constants are calculated from the simplified or conventional Eyring's activated complex (transition state) theory:[89,221–223]

$$k_r = \left(\frac{k_B T}{h}\right) e^{-\left(\frac{\Delta G^{\ddagger}}{RT}\right)} \tag{3.1}$$

where k_r = rate constant, k_B = Boltzmann's constant (1.381×10^{-23} J K^{-1}), h = Planck's constant (6.626×10^{-34} J s), R = gas constant (8.314 J mol^{-1} K^{-1}), T = operational temperature (298.15 K) and $\Delta G^{\ddagger}$ = Gibbs free energy barrier of the process. It is observed from the barriers and rate constants of this step that the difference between the two pathways is not significantly large, both energetically (8.5 kJ mol^{-1}) and kinetically (6.6×10^{-28} s^{-1}), thereby giving confidence in the results. It is found that **Int3** is formed from **Int2** in a barrierless process by the elimination of $ClB(OH)_2$ in which the

formed r_{Pd-C} shorten from 2.09 and 2.08 Å in **Int2** (of **Scheme 3.2** and **Scheme 3.3**, respectively) to 2.09 and 2.08 Å in **Int3** (of **Scheme 3.2** and **Scheme 3.3**, respectively).

Table 3.5. Gibbs free energy barriers ($\Delta G^{\ddagger}$) and Gibbs free energy change of reaction (ΔG_r) computed with ωB97XD/6-311++G(2df,2p)[SDD]//ωB97XD/6-31++G(d,p)[SDD] without base in the absence and presence of solvent effects.

Reaction step	$\Delta G^{\ddagger}$ / kJ mol^{-1}		
	Gas	o-X	AN
TM ($(\Delta G_{r,TS1-2}) - (\Delta G_{r,Int1})$)	236.6	241.2	244.5
Dc$\underline{n}$-1 ($(\Delta G_{r,TS3-4}) - (\Delta G_{r,Int3})$)	177.9	169.2	158.7
RE ($(\Delta G_{r,TS4-5}) - (\Delta G_{r,Int4})$)	89.0	95.5	103.3
Dc$\underline{n}$-2 ($(\Delta G_{r,TS5-6}) - (\Delta G_{r,Int5})$)	42.7(18.8)	40.6(16.2)	37.9(14.3)
ΔG_r (Products) / kJ mol^{-1}	205.5(206.8)	219.2(220.7)	232.0(234.1)

TM stands for Transmetallation; Dc$\underline{n}$-1 for First de-coordination; RE for Reductive elimination and Dc$\underline{n}$-2 for Second de-coordination. o-X stands for o-xylene ($\varepsilon = 2.5$) and AN for Acetonitrile ($\varepsilon = 35.7$). The values in brackets are for the nitrogen de-coordination path of Dc$\underline{n}$-2 step.

Int3 is located at 95.9 and 99.0 kJ mol^{-1} above the separated reactants, respectively for **Scheme 3.2** and **Scheme 3.3** (or **Figure 3.2** and **Figure 3.3**). The de-coordination of one of its ancillary (-SMe or pyridyl in **Int3**) arms via **TS3-4**, located at 272.1 kJ mol^{-1} or 276.9 kJ mol^{-1} above the separated reactants is found to involve an energy barrier of 176.2 or 177.9 kJ mol^{-1}, respectively. It is observed that the energy barrier ($\Delta G^{\ddagger}$) for the process is similar for both types of ancillary arms (differing only by 1.7 kJ mol^{-1}) and hence, DFT methods. The concomitant k_r for this step is 8.4×10^{-19} (**Scheme 3.2**) and 4.2×10^{-19} s^{-1} (**Scheme 3.3**). The bonds broken in the process, r_{Pd-S} (**Scheme 3.2**) and r_{Pd-N} (**Scheme 3.3**), are computed as 2.28 and 2.10 Å, respectively in **Int3** and 2.58 and 2.40 Å, respectively in the transition structure. After formation, **Int4** located 159.6 and 170.2 kJ mol^{-1} above the separated reactants proceeds to generate **Int5** via a low RE energy barrier of 105.0 and 89.0 kJ mol^{-1} with k_r of 2.5×10^{-6} and 1.6×10^{-3} s^{-1}, respectively. During this process, the two r_{Pd-C} bonds are broken in order to form the r_{C-C} bond. First, the r_{Pd-C} bonds being broken are computed as 2.00 Å with the central aryl ring, 1.98 Å with incorporated aryl ring (**Int4**, **Scheme 3.2**). For **Scheme 3.3**, the first broken bonds are computed as 1.99 Å with the central aryl ring, 1.98 Å with incorporated aryl ring (**Int4**). These bonds in the transition structures are computed as 1.98 Å with the central aryl ring, 2.13 Å with incorporated aryl ring (**TS4-5**, **Scheme 3.2**) and 1.99 Å with the central aryl ring, 2.11 Å with incorporated aryl ring (**TS4-5**, **Scheme 3.3**). On the other hand, the r_{C-C} distance and bond between the aryl moieties in the mentioned species are computed as; 3.17 Å in **Int4**, 2.16 Å in **TS4-5** and 1.52 Å in **Int5** (**Scheme 3.2**) and 2.87 Å in **Int4**, 2.08 Å in **TS4-5** and 1.50 Å in **Int5** (**Scheme 3.3**). It can therefore be reckoned that the r_{Pd-C} bonds are lengthened in the process while the r_{C-C} distance is shortened until the r_{Pd-C} bonds are broken as

the r_{C-C} bond is formed. **Int5** undergoes either an N- or S- de-coordinating step to generate the active catalyst, Pd(0) and the biphenyl product for both methods. Of the two final de-coordination steps, the most energetically and kinetically favourable step is the N- de-coordination step as it has the lowest energy barrier (38.9 and 18.8 kJ mol^{-1}, **TS5-6b** of the respective schemes) and highest k_r (9.5×10^5 and 3.2×10^9 s^{-1} for the respective schemes) compared to the S- de-coordination step with concomitant energy barrier of 45.5 and 42.7 kJ mol^{-1} (**TS5-6a**) for the respective schemes with k_r of 6.6×10^4 and 2.0×10^5 s^{-1}, respectively.

The overall reaction leading to the formation of Pd(0), the active catalyst[141–143] is found to be uphill, endergonic process. These results indicate that the overall energy, ΔG_r of the process is 202.6 and 206.2 kJ mol^{-1} between the separated reactants and the products of the respective pathways (**Figure 3.2** and **Figure 3.3**). From the preceding, it is found that the transmetallation step is the rate determining (slowest) step[28,33,181,224] on the basis of its highest Gibbs free activation energy barrier and smallest rate constant[28,89,181,224] for both mechanisms. The results therefore indicate that the TM step is energetically extremely demanding and kinetically less favourable such that the reacting species would scarcely react on their own.[199,200]

This situation is even worsened when a solvent field is incorporated to obtain the solvent corrected energies for the obtained mechanisms (**Table 3.4** and **Table 3.5**). The pattern of the elucidated pathways however, remains the same as in the gas phase.[217] The energy barrier of TM, RE and the Gibbs free energy of reaction (ΔG_r) increase with increasing solvent static dielectric constant (polarity) while the energy barrier for the Dc**n**-1 and Dc**n**-2 steps decrease with increasing solvent static dielectric constant. These trends may be explained by contributions of Lewis acid-base or electrostatic and non-electrostatic (e.g., cavitation energy and solute-solvent dispersion) interactions between the solvent and solute fields to the free energy of the systems.[89,91,221–223] In this regards, the field of the solvents move in to stabilise the electron deficient palladium centres in the Dc**n**-1 and Dc**n**-2 steps via electron density (charge) transfer to the centre (and molecules in general) and hence, decreasing their energy barrier from To to o-X to AN. This effect becomes more pronounced as the static dielectric constants of the solvents increase.[222] The energy barriers for the TM, RE and ΔG_r on the other hand increase with solvent static dielectric constant due to their cavitation energies.[89,91] Cavitation here refers to the repulsive interaction between solute and solvent fields (charges) due to some solute charges lying outside the solute cavity.[19,20,89–91] The cavitation energy is therefore, the energy required for producing a cavity in the solvent to contain a solute.[19,20,90,225]

The result summarised in **Table 3.4** and **3.5** also suggests that irrespective of the method used, the Gibbs free activation energy barriers of the steps of the elucidated mechanisms and the overall Gibbs free energy of reaction are similar and follow the same trends in the gas and solvent phase. In

addition, the results reveal that the process will not be spontaneous since it is uphill on the overall.[33] This result is a good indication of the stability of the pincer palladacycle[142] used in the reaction and may be attributed to the relatively strong tridentate co-ordination mode of the pincer complex that renders it relatively stable to high thermal energy.[142] As a consequence of this stability, the decomposition of the complex is controlled for optimum catalysis, which ensures a broad scope of reaction. This is required because, if the pincer decomposes too fast, catalysis will be hindered due to the formation of catalytically inactive palladium black.[148,152,226] It is observed that this energy increases with solvent static dielectric constant (solvent polarity).

3.3.4 Comparison with Mechanism Elucidated with Base

The results presented in **3.3.3** are compared with the mechanism of Pd(0) formation from **1** involving bases determined in parallel in the Cox group by Dr G.W. Roffe.[29] **Table 3.6** summarises energy barriers of the key steps involved in the two mechanisms.

Table 3.6. Gibbs free energy barriers ($\Delta G^{\ddagger}$) and Gibbs free energy of reaction (ΔG_r) computed at the ωB97XD/6-311++G(2df,2p)[SDD]//ωB97XD/6-31++G(d,p)[SDD] level of theory in the absence and presence[29] of a base.

Reaction step	$\Delta G^{\ddagger}$ / kJ mol^{-1} without base			$\Delta G^{\ddagger}$ / kJ mol^{-1} with base		
	Gas	o-X	AN	Gas	o-X	AN
TM ($(\Delta G_{r,TS1-2}) - (\Delta G_{r,Int1})$)	236.6	241.2	244.5	97.8	99.7	102.4
Dc<u>n</u>-1 ($(\Delta G_{r,TS3-4}) - (\Delta G_{r,Int3})$)	177.9	169.2	158.7	174.7	172.2	161.7
RE ($(\Delta G_{r,TS4-5}) - (\Delta G_{r,Int4})$)	89.0	95.5	103.3	88.9	95.4	103.3
Dc<u>n</u>-2 ($(\Delta G_{r,TS5-6}) - (\Delta G_{r,Int5})$)	18.8	16.2	14.3	17.5	14.3	11.8
ΔG_r (Products) / kJ mol^{-1}	206.8	220.7	234.1	120.0	72.4	54.7

TM stands for Transmetallation; Dc<u>n</u>-1 for First de-coordination; RE for Reductive elimination and Dc<u>n</u>-2 for Second de-coordination. o-X stands for o-xylene ($\varepsilon = 2.5$) and AN for Acetonitrile ($\varepsilon = 35.7$). The numbering of the steps are taken from Scheme 3.3 but the steps are the same/similar with those in Scheme 3.4 from TM.

The mechanism with base that was computed by Dr G.W. Roffe in parallel with the present work is presented in **Scheme 3.4**. It is observed that the mechanism in **Scheme 3.4** has more steps and intermediates prior to transmetallation compared to the base-free mechanism presented in **Scheme 3.3**. **Scheme 3.4** suggests that the base initially attacks the acid to form the boronate species which in turn interacts with the pincer complex to from **Int1** in agreement with literature[209–211,217] reports. It is observed from **Scheme 3.4** that **Int1** proceeds to an oxidative addition step (**TS1-2**), the product of which enters the TM step (**TS3-4**). This is also in agreement with literature[217] reports. In these literature reports,[209–211,217] only one or two of oxidative addition, TM and RE are usually studied, the complete Pd(0) mechanism has not been elucidated before now. Comparatively, it is found that from the TM step to Pd(0) formation, the mechanism in **Scheme 3.4** is similar to the

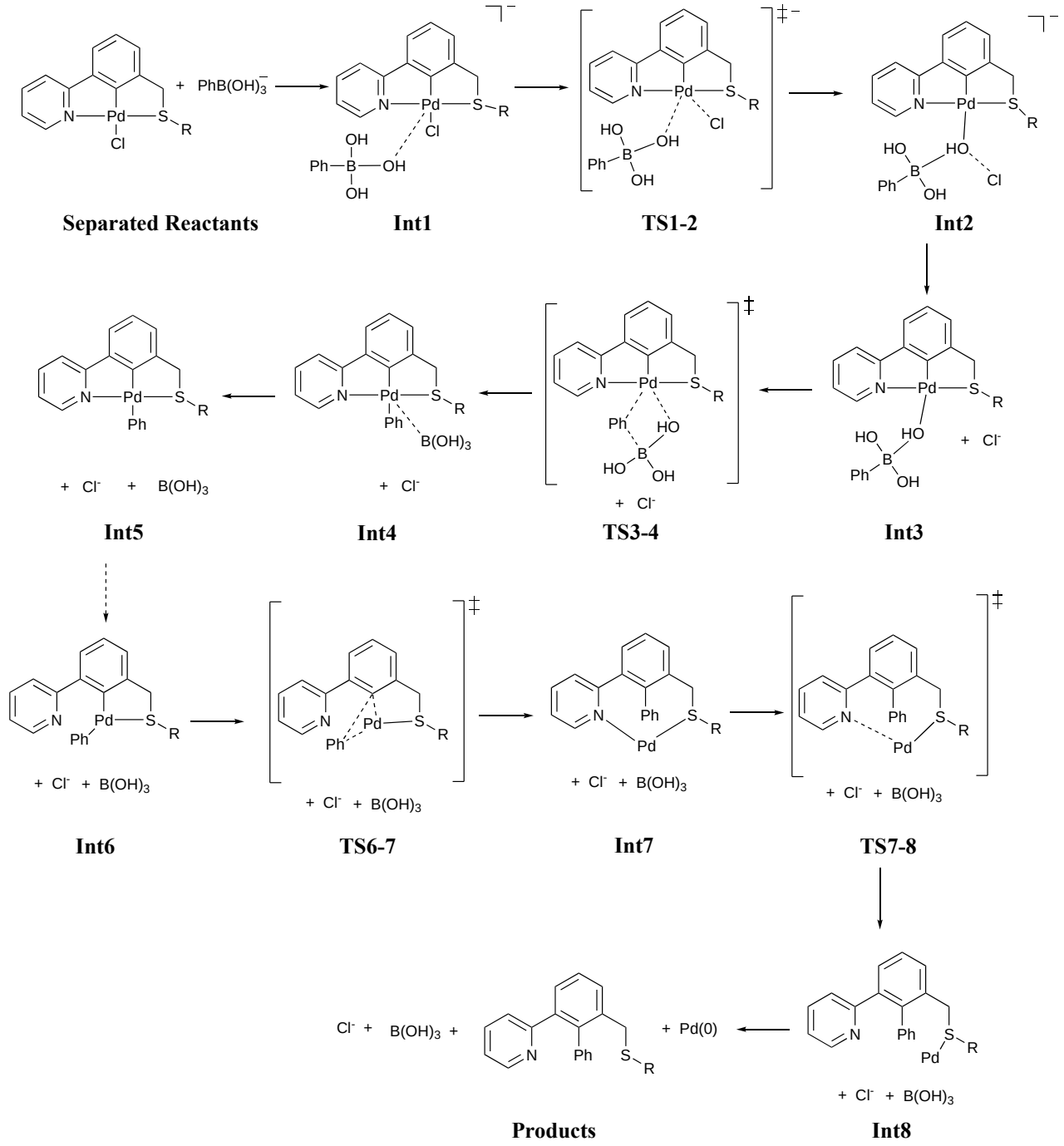

Scheme 3.4. Base mechanism of Pd(0) formation formation from novel unsymmetrical pincer palladacycle (**1**)[29,190] computed with ωB97XD/6-31++G(d,p)[SDD] by Roffe[29] in the gas phase.

mechanism presented in **Scheme 3.3** with respect to number of steps, intermediates and transition states.[11] Comparison between the energetics of **Scheme 3.3** and **Scheme 3.4** is therefore made on the basis of the energy barriers for the TM, Dc<u>n</u>-1, RE and Dc<u>n</u>-2 steps for the respective schemes.

The result presented in **Table 3.6** is for the most energetically and kinetically favoured mechanism. It is observed that the primary role of the base in the elucidated mechanism is to significantly lower the activation energy barrier of the TM step[209,210,217] and overall energy of reaction, attributable to the presence of Cl^-, to facilitate Pd(0) formation for catalysis. This was especially confirmed by the catalytic activity of **1** (**Figure 3.1**) in the Suzuki-Miyaura cross-coupling reaction experiments in the presence of a base.[11] It is also observed from **Table 3.6** that when the base is present in the reaction, the Dc<u>n</u>-1 step becomes the rate determining (slowest) step in the reaction in comparison with the TM, RE and Dc<u>n</u>-2 steps. This is because the energy barrier of the Dc<u>n</u>-1 step calculated as 174.7 kJ mol^{-1} has an attendant k_r of about 1.5×10^{-18} s^{-1}. The energy barriers of the TM, RE and the Dc<u>n</u>-2 steps are 97.8, 88.9 and 17.5 kJ mol^{-1}, respectively while their rate constants are 4.6×10^{-5}, 1.7×10^{-3} and 5.3×10^{9} s^{-1}, respectively. Furthermore, the energy barriers of the TM, Dc<u>n</u>-1, RE and Dc<u>n</u>-2 steps are observed to maintain the trend as discussed above for the mechanism elucidated without base (**Scheme 3.3** and **Figure 3.6**) with increasing solvent dielectric constants. The overall energy change of the reaction in the presence of a base is noted to decrease with increasing solvent polarity (dielectric constants). This is also attributable to the presence of the halide ion.[217]

3.3.5 Comparison with Model Unsymmetrical PdSCN

To determine electronic and steric effects on the formation of Pd(0) from pincer complexes, the results presented in **Table 3.5** for the mechanism in **Scheme 3.2** is compared with the mechanism computed in parallel with the present work in the Cox group using a simple PdSCN by Dr S. Boonseng.[227] His results for the key steps of the Pd(0) formation reaction are summarised in **Table 3.7**. The PdSCN complex investigated by Dr S. Boonseng is presented in **Figure 3.8**. Both pathways were computed at the same level of theory.

Table 3.7. Gibbs free energy barriers ($\Delta G^{\ddagger}$) and Gibbs free energy change of reaction (ΔG_r) computed at the ωB97XD/6-311++G(2df,2p)[SDD]//PBE/6-31+G(d,p)[SDD] level of theory without base[227]

Reaction step	$\Delta G^{\ddagger}$ / kJ mol^{-1}			
	Gas	To	THF	AN
TM ($(\Delta G_{r,TS1-2}) - (\Delta G_{r,Int1})$)	204.0	210.1	214.5	216.3
RE ($(\Delta G_{r,TS4-5}) - (\Delta G_{r,Int4})$)	114.7	123.0	131.1	135.8
Dc<u>n</u>-2 ($(\Delta G_{r,TS5-6}) - (\Delta G_{r,Int5})$)	43.4(17.9)	41.8(17.4)	40.7(16.7)	40.2(16.3)
ΔG_r (Products) / kJ mol^{-1}	181.0	194.2	204.9	210.0

TM stands for Transmetallation; RE for Reductive elimination and Dc<u>n</u>-2 for Second de-coordination. To stands for Toluene ($\varepsilon = 2.4$); THF for Tetrahydrofuran ($\varepsilon = 7.4$) and AN for Acetonitrile ($\varepsilon = 35.7$). The values in brackets are for the nitrogen de-coordination path of Dc<u>n</u>-2 step.

It is observed that the Dc<u>n</u>-1 step is absent in the mechanism[227] summarised in **Table 3.7** and that transmetallation yields an intermediate with a de-coordinated side-arm directly and so does not need the Dc<u>n</u>-1 step. It is also noted that for the system in **Figure 3.8**, (**6**) there are two pathways leading to Pd(0) formation from the TM step:

1. when TM yields an -NMe_2 de-coordinated intermediate and
2. when it generates an -SMe de-coordinated intermediate.

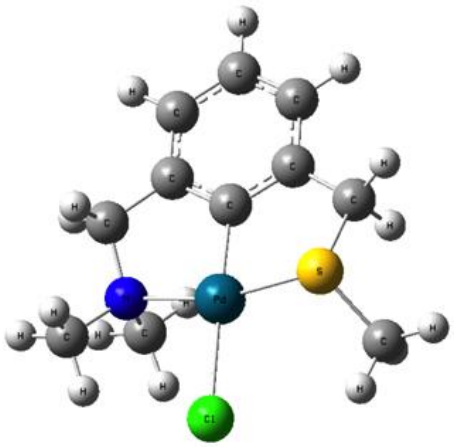

6

Figure 3. 8. The The optimised minimum energy structure of the model PdSCN investigated by Dr S. Boonseng[227] for Pd(0) formation.

The unsymmetrical pincer complex, **1** investigated in this thesis gives only one pathway as presented in **Scheme 3.2**. This is likely due to a difference in the electronic and steric effects in the complexes investigated. With respect to the electronic effects, **1** is a push-pull system[104,228] while the PdSCN (**6**) in **Figure 3.8** is not. In terms of steric effects, **6** is less sterically hindered while **1** much more sterically hindered.[152]

In terms of the energetic and concomitant kinetics of the two similar pathways emanating from pincer **1** and **6**, it is observed that the energy barrier for TM in the mechanism involving pincer **1** (**Figure 3.1** and **Figure 3.2**) is greater than that of pincer **6** by 24.1 kJ mol^{-1}. The energy barrier for RE in the mechanism involving pincer **1** (**Figure 3.1** and **Figure 3.2**) is less than that of pincer **6** by 9.7 kJ mol^{-1}. This result is expected because as steric effects increase, facile formation of Pd(0) for catalysis is less favoured.[152] In addition, complexes possessing electron withdrawing group(s) are much more labile to the RE of C-C bonds than those bearing electron donating groups.[229–231] It should be noted also that TM is favoured by less sterically hindered electron donating groups in cross-coupling reactions.[232,233] More so, Ariafard and Yates showed that RE is more favourable for

systems with sterically demanding, weakly basic, π-accepting ligands[234] such as the pyridyl group. This is because they reduce electron density at the metal centre thereby rendering them electron poor.[192] The preceding therefore suggests that the TM involving the pincer **1** (**Figure 3.1** and **Figure 3.2**) is less kinetically favoured compared to TM involving pincer **6** (**Figure 3.8**). Furthermore, the RE involving pincer **1** (**Figure 3.1** and **Figure 3.2**) is more kinetically favoured in comparison with RE involving pincer **6**. The mechanisms of Pd(0) emanating from pincer **1** and **6** show similar energetic and kinetic behaviours at the Dc**n**-2 step when the -SMe group de-coordinates but vary significantly when the -NMe_2 or pyridyl group de-coordinates. It is observed that the energy barrier when the pyridyl group de-coordinates is greater than that arising from the de-coordination of the -NMe_2 group by ca. 21 kJ mol^{-1}. This may be accounted for by the fact that increasing bulkiness and concomitant non-covalent (long-range) interactions contribute additively to the binding energy of transition metal systems.[235] Based also on this reasoning, the overall Gibbs free energy of the reaction employing pincer **1** (**Figure 3.1** and **Figure 3.2**) is greater than that of pincer **6** not minding which arm de-coordinates in the Dc**n**-2 step by ca. 22 kJ mol^{-1}. The trend of these energies in solvent field is the same for both pathways as discussed earlier for **Scheme 3.2** above.

On the overall, the mechanism employing the less sterically hindered pincer **6** with electron donating (-NMe_2) group would be favoured over that employing pincer **1** (**Figure 3.2**) with a sterically hindered electron withdrawing side-arm.

3.4 Conclusions

A rational model *base-free* mechanism of the active catalyst, Pd(0) formation for the Suzuki cross-coupling reactions have been elucidated using two DFT methodologies. The elucidated mechanisms involve four main steps namely; transmetallation, two de-coordination steps and a reductive elimination step. The reductive elimination step lies between the de-coordination steps after the transmetallation step, with the transmetallation step as the rate-determining step. The result of the calculations indicates that the reaction of interest is an uphill, endergonic (non-spontaneous) process that will in fact, scarcely occur without a base. Nevertheless, the results suggest good thermal stability of the studied novel pincer palladacycle. This stability is a good index for its use in catalysis. This is because, if it decomposes too readily, catalysis will be hindered by the formation of the catalytically inactive palladium black.[142,148,152,226] Furthermore, the two functionals used and hence elucidated pathways have similar energetic profiles and follow the same general patterns in gas and solvent phase even though they differ with respect to the first de-coordination step and

product of RE. Comparison of the elucidated *base-free* mechanism of Pd(0) formation with the mechanism of Pd(0) formation elucidated with base shows that:

1. More steps are involved prior to transmetallation when the base is employed in the reaction of pincers with phenylboronic acid,
2. The primary role of the base in the process is to significantly lower the activation energy barrier of transmetallation[209,210] and overall reaction energy in order to facilitate[217] the formation of Pd(0), the active catalyst and
3. The first de-coordination step rather than TM or RE becomes the rate determining step.

Comparison of the elucidated *base-free* mechanisms of Pd(0) formation at the PBE/6-31+G(d,p)[SDD] level of theory employing two different PdSCN pincers; one with a pyridyl and the other with -NMe_2 side arm bearing the N donor atom beside -SMe with S donor atom, indicates that:

1. The pincer with the -NMe_2 side-arm is energetically and kinetically favoured over the pincer with the pyridyl side-arm in the formation of Pd(0) and
2. Sterically less demanding, electron donating ligands favour transmetallation while sterically demanding, weakly basic, π-accepting ligands favour reductive elimination.

4 Method determination for calculation of sulfur clusters and their reactivity with hydrogen sulfide

This chapter describes the determination of an appropriate computational methodology for the calculation of the geometry, vibrational frequencies and energies of sulfur clusters (S_n) and the species involved in their reaction with hydrogen sulfide (H_2S). The optimum method for computing the geometry and vibrational frequencies of the species is ωB97XD/6-311++G(2df,2p) while the suitable method for calculating the energies of the species of interest is CCSD(T)/aug-cc-pVTZ. These methods are determined by comparison of computed geometries (HS_2H, S_2), bond dissociation energies (HS_2H) and vibrational frequencies (S_2) and singlet-triplet energy splitting for S and S_2 using different computational methods with experiment. The reliability of these single-reference methods is tested by the $\mathcal{T}_1$ Diagnostic of singlet, doublet and triplet state sulfur species.

4.1 Introduction

Obtaining accurate, cost effective and computationally applicable method(s) for electronic structure calculations has been the primary objective of computational chemistry for decades.[236,237] Some computational method combinations are known to reproduce experimental geometries or bond dissociation energies, but often not both.[236,238,239] Also, the singlet-triplet energy splitting for chemical species has remained a challenging property to calculate accurately for many computational methods.[19,240] Nevertheless, the combination of the augmented correlation-consistent type of basis sets (aug-cc-pV*x*Z, *x* = D, T, Q, 5 or 6) with the coupled cluster singles, doubles and perturbative triples method (CCSD(T)) is usually adopted as the gold standard of quantum chemistry for the computation of the thermochemical properties of chemical species.[236,241–243] This is because it often gives results within 1 kcal mol^{-1} of the exact energy (the chemical accuracy) of a system whereas the accuracy of most computational methods, especially DFT methods, is limited to at best 2 to 3 kcal mol^{-1}.[244–246] However, other theoretical studies in the

literature[243,247–250] assert that the standard Pople-type of basis set in combination with DFT methods often reproduce experimentally determined geometries and energies at cheaper computational costs. It is worthy of note that every chemical species has its peculiarities hence no practical universal computational method exists for electronic structure calculations. One general factor that is key in obtaining accurate results from a computational study is the quality of basis set combined with a chosen method for calculation.[19,20,35,99–102] In this regard, it is believed that *higher-order* polarisation (angular momentum) functions are required for a better description of molecular geometries and properties.[20,35,99–101,251] Furthermore, it is asserted that diffuse functions are also required in basis sets of choice in a computational calculation for a more accurate and balanced description of long-range interactions, relative energies between structures and vertical transition energies associated with a chemical species.[20,35,99–101,252]

The electronic structure and properties of sulfur and sulfur containing species has been widely studied using different computational methodologies for many different reasons over the years. However, little or no information exists in the literature for a deliberate basis set validation and method evaluation in reproducing the molecular geometries and properties of sulfur clusters. Nevertheless, a significant number of existing literature reports on other chemical species provide useful benchmarking studies, comparing different computational chemistry methods with experiment.

In 1995, Rossi and Truhlar investigated the scaling-all-correlation (SAC) method:

$$E_{\mathrm{SAC}} = E_{HF} + \frac{E_c - E_{HF}}{\mathcal{F}} \tag{4.1}$$

with different *ab initio* methods in combination with correlation-consistent and Pople-type of basis sets.[247] This method estimates the internuclear distance dependence of the full correlation energy of a system on the basis of *ab initio* calculations. The authors described the numerator of the fraction in eq. (4.1) as an estimate of the correlation energy of a system by a single-reference method and $\mathcal{F}$ as an assumed factor that is independent of the geometry of the system. The authors found that the Pople-type basis set, 6-31G** outperformed the correlation-consistent type (cc-pVDZ) of basis sets in computing the scale factors that gave a quantitative estimate of how well a particular level of theory was correlation balanced. Later the same year, Bauschlicher and Partridge compared the accuracy of the correlation-consistent type of basis sets with the Pople-type of basis sets for the calculation of the atomisation energies of many different chemical species using the G2(B3LYP/MP2/CC) level of theory.[248] The authors asserted that the correlation-consistent type of basis sets do not have the same type of balance where a simple additive *higher-order* correction can be used to dramatically reduce the error in the atomisation energy of a variety of molecules.

Goddard and co-workers investigated the dependencies of basis sets and functionals in DFT to establish an optimal method combination for the computation of atomisation energies and reaction enthalpies for a set of 44 molecules using gradient-corrected DFT methods in 1997.[253] The authors asserted that a similar behaviour was shown by 6-31G(d,p), 6-311G(d,p), cc-pVDZ and cc-pVTZ in calculating the atomisation energies and reaction enthalpies of the molecules. They went on to state that the most accurate predictions were obtained using the cc-pVTZ basis set. They then concluded that there was significant variation in the energies depending on functional and basis set combination. Gregory and Jenks employed different computational methods and basis set combinations to study the relative energies of vicinal disulfoxides and other sulfinyl radical dimers in 2003.[254] The authors asserted that within the limitations of the theoretical model chosen, the 6-311+G(3df,2p) basis set gave results that were very comparable to the extrapolated aug-cc-pV*x*Z limit. They further stated that the greatest effect among the Pople-type basis sets is that an increase in the number of *d*-polarisation functions stabilises the sulfoxides relative to the sulfenic esters. They went on to note that the addition of diffuse functions and an *f* function to the heavy atoms continued this trend but less dramatically. Su et al., in 2004 compared the energetics of large water clusters computed with the 6-31G**, 6-311++G** and aug-cc-pVTZ basis sets in combination with the X3LYP functional.[249] The authors showed that it was possible to use the functional in combination with smaller basis sets while preserving the accuracy in contrast to *ab initio* methods that require large basis sets. Pablo in 2005,[250] investigated the basis set requirements for sulfur compounds (SX where X = first or second row atom; SO_2 and SO_3) in DFT, comparing between correlation-consistent, polarisation-consistent and Pople-type basis sets in combination with B3LYP. The author asserted that the latter type of basis set gave very good geometries and atomisation energies and provided the best cost-results benefits considering that they have much fewer basis functions. They stated that the results computed at the 6-311+G(3df,2p) basis set were nearly of the aug-cc-pV(T+*d*) and aug-pc-2 quality. Klein and Zottola compared the ability of DFT and *ab initio* methods in combination with the aug-cc-pV*x*Z (*x* = D, T, Q) basis sets to reproduce the experimental spectroscopic bond lengths of some metal and non metal hydrides against their combination with the 6-311++G(2d,p) in 2006.[243] The authors found that the aug-cc-pV*x*Z (*x* = D, T, Q) basis sets combined with MP2 or CCSD performed less well than the DFT methods combined with the 6-311++G(2d,p) basis set. They then asserted that results produced by the MPW1PW91/6-311++G(2d,p) level of theory was only rivalled or bettered by combination with aug-cc-pV*x*Z (*x* = T, Q) at much reduced computational cost. Lastly, Jacquemin and Adamo investigated the basis set and functional effects on excited state properties of three bicyclic chromogens as working examples in 2012 using four Pople-type basis sets in combination with six DFT functionals.[252] The authors

asserted that the diffuse functions were necessary to obtain correct vertical transition energies. They also stated that the choice of functional impacted the energies but that difference in the vibrational energies between ground and excited states were almost functional and basis set independent.

4.1.1 Aim of Study

The aim of this work is to establish an optimum method and basis set combination for the accuracy and speed of computing the electronic structure and properties of sulfur clusters and hydrogen polysulfanes. This will be achieved by:

1. Basis set validation to obtain an appropriate basis set to adopt in the study.
2. Method evaluation and $\mathcal{T}_1$ Diagnostic test to determine the multi-configurational/reference character of species of interest.
3. Complete active space self-consistent field (CASSCF)[38] study of the singlet and triplet spin S_n (n = 1, 2) species for further evaluation of method.

4.2 Computational details

All calculations were performed using Gaussian 09.[24] Initially, the DFT method, ωB97XD[80] (used in Chapter 3 of this thesis) and CCSD(T)[44] method, together with a number of Pople[99] and Dunning correlation-consistent[100,116,255] basis sets, were employed to test the quality of the methodologies in reproducing the experimental geometry and bond dissociation energies of disulfane (HS_2H). This is because the molecule is the simplest compound that displays many factors important for the structure of polysulfur compounds.[256] In doing this, the neutral species in reaction (4.1) and (4.2) were fully optimised at the two levels of theory above to locate their energy minimum:[36]

$$HS_2H\ (^1A) \rightarrow 2HS\ (^2\Pi) \tag{4.1}$$

$$HS_2H\ (^1A) \rightarrow HS_2\ (^2A'') + H\ (^2A_{1g}) \tag{4.2}$$

i.e., singlet spin state species undergoing bond dissociation to produce doublet spin state species. Frequency calculations at 298.15 K and 1.0 atm were performed on all the optimised stationary points in this Chapter at the method of optimisation to characterise their nature and obtain the thermal and ZPE corrections to their equilibrium energies.[19,36,37] The absence of imaginary frequencies implies an energy minimum and the presence of a single imaginary frequency implies a first-order saddle point.[19,36,37] The DFT vibrational frequencies are uniformly scaled by a factor of 0.950[257] while unscaled ZPEs and CCSD(T) frequencies are used throughout. The $\mathcal{T}_1$ Diagnostic of

Lee and Taylor[3,53,54] was performed on the minimum points of the respective species in reaction (4.1) and reaction (4.2) optimised at *ω*B97XD and CCSD(T) using the CCSD(T)/aug-cc-pVQZ level of theory to determine the electron correlation character of the species. The $\mathcal{T}_1$ Diagnostic was also calculated for the *ω*B97XD optimised minimum points of *cis*- and *trans*-HS_3H and HS_4H. The geometries of the species in reaction (4.1) and reaction (4.2) were then re-optimised and characterised via frequency calculations using the DFT functionals; TPSS, CAM-B3LYP and M11, in combination with some basis sets to compare their performance with *ω*B97XD. In all the preliminary calculations, six (6) shared processors on a high performance computer (HPC) cluster were employed and %mem = 2GB was adopted for CCSD(T) computations. The performance of the optimum method on singlet and triplet spin state structures of the diatomic sulfur, S_n (n = 2) was determined. $\mathcal{T}_1$ Diagnostic was also calculated for the optimised singlet and triplet minimum stationary point of S_n (n = 2) using CCSD(T)/aug-cc-pVQZ.

Finally, the singlet and triplet spin S_n (n = 1, 2) species were investigated at the CASSCF[38] level of theory using the 6-31G(d) basis set. SPE calculations were performed on atomic sulfur (S) while for diatomic sulfur, the optimised geometry of the species at the *ω*B97XD/6-311++(2df,2p) level of theory was used as the starting structure for geometry optimisation, SPE and frequency calculation with the CASSCF method. CASSCF frequencies are used un-scaled. The canonical orbitals of the species adopted in the CASSCF study from which the active spaces, CAS(n,m: n = number of active electrons and m = number of active orbitals) were selected were generated from single-point calculations at the HF level of theory in combination with the STO-3G basis set using the pop=full keyword. Electron occupancies of the chosen orbitals obtained by examining the diagonal elements of the final symbolic one-electron density matrix were used to check the suitability of the active orbitals for a good description of the species. When the value of the occupancy is zero, the orbital is empty; occupancy of one means the orbital was singly occupied while occupancy of two implies a doubly occupied orbital. The composition of the final wavefunction of the systems was evaluated by examining the eigenvectors of the CI matrix.

4.3 Results and Discussion

4.3.1 Validation using HS_2H (Geometry and Dissociation Energy)

4.3.1.1 Basis Set Comparison using *ω*B97XD and CCSD(T)

The geometric parameters of HS_2H (^1A) computed at different basis set combinations with *ω*B97XD and CCSD(T) were compared with the experimental geometric parameters of the species:[258,259] bond lengths, r(S-H) = 1.342 (2) Å and r(S-S) = 2.056 (1) Å, bond angle, θ(SSH) =

97.9 (5) ° and torsion angle, τ(HSSH) = 90.3 (2) °. For all the methods considered, the computed r(S-H), θ(SSH) and τ(HSSH) are found to fall within the experimental error margins, respectively. To corroborate this, for instance, for the bond distances (r(S-S) and r(S-H)), the mean signed error (MSE) and mean unsigned error (MUE) analysis[10] for the bond distances is presented in **Figure 4.1**. Also included in **Figure 4.1** is the CPU time taken for frequency calculation for each methodology. Frequency calculation time is used instead of geometry optimisation time, as the latter is dependent on the initial guess geometry.

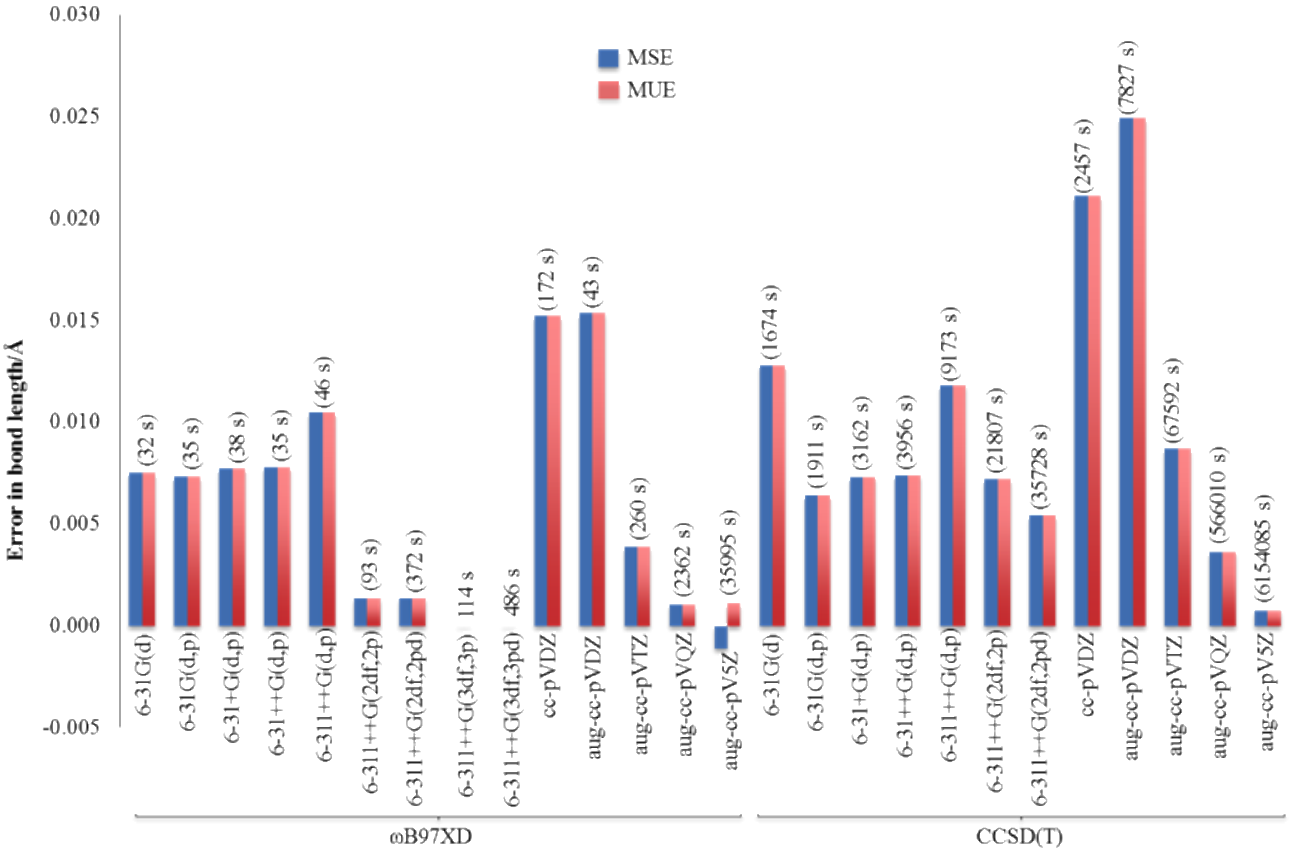

Figure 4.1. Comparison of the MSE and MUE analysis of the computed r(S-S) and r(S-H) of HS_2H and the CPU time in (in bracket) taken from frequency calculation on the moiety using different basis set combinations with ωB97XD and CCSD(T). Geometry optimisation and frequency calculations were performed at each methodology, respectively.

MSE is the average deviation of calculation (*calc.*) from experiment (*expt.*), eq. (4.2):

$$\mathrm{MSE} = \frac{1}{N}\sum_{i,j=1}^{N}\left(r_{ij}(calc.) - r_{ij}(expt.)\right) \tag{4.2}$$

while MUE is the absolute deviation from experiment, eq. (4.3):

$$\text{MUE} = \frac{1}{N}\sum_{i,j=1}^{N}\left|r_{ij}(calc.) - r_{ij}(expt.)\right| \quad (4.3)$$

where r_{ij} is the bond distance and N is the number of atoms in the molecule (including hydrogen). A careful inspection of **Figure 4.1** reveals that all the methodologies, except the CCSD(T)/cc-pVDZ and CCSD(T)/aug-cc-pVDZ levels of theory, reproduce the experimental geometry of HS_2H with MSE and MUE's of the bonded distances within 0.02 Å. The result further suggests that ωB97XD is computationally cheaper than the CCSD(T) method for all combinations. The accuracy of geometry optimisation and speed of frequency calculation at the ωB97XD/6-311++G(2df,2p) and ωB97XD/6-311++G(3df,3p) levels of theory is found to be more desirable in comparison to the other combinations. This result agrees with that of Klein and Zottola[243] who compared some Pople and Dunning-types of basis sets to assert that the Pople-type of basis sets outperformed the Dunning-type of basis sets in reproducing the experimental bond lengths of some group 1A metals and second row hydrides. Also in agreement with the results of these authors, it is found that all the methods and basis sets adopted herein uniformly give reasonable results in reproducing the experimentally determined bond angles and torsion angles for the studied moiety.

A comparison of the calculated bond dissociation energies ($\boldsymbol{D}_0$) resulting from reaction (4.1) and reaction (4.2) with the experimentally determined $\boldsymbol{D}_0$ of the species is summarised in **Table 4.1**.

Table 4.1. Comparison of bond dissociation energies ($\boldsymbol{D}_0$(S-S) & $\boldsymbol{D}_0$(S-H) in kJ mol^{-1}) of HS_2H computed at some of the methodologies in **Figure 4.1** with experiment. Also included is the CPU time in seconds taken for frequency calculations. $\Delta\boldsymbol{D}_0 = \boldsymbol{D}_0$(expt.) - $\boldsymbol{D}_0$(calc.).

Method	$\boldsymbol{D}_0$(S-S)	$\boldsymbol{D}_0$(S-H)	$\Delta\boldsymbol{D}_0$(S-S)	$\Delta\boldsymbol{D}_0$(S-H)	**CPU Time**
Experiment[260]	276.1 ± 8.4	292.9 ± 6.3	0.0	0.0	-
ωB97XD/6-31G(d)	245.8	295.0	21.9	4.2	32
ωB97XD/6-31+G(d,p)	242.4	303.8	25.3	-4.6	38
ωB97XD/6-311++G(d,p)	239.8	302.8	27.9	-3.6	46
ωB97XD/6-311++G(2df,2p)	264.8	301.4	2.9	-2.2	93
ωB97XD/6-311++G(2df,2pd)	264.8	302.3	2.9	-3.1	372
ωB97XD/6-311++G(3df,3p)	265.4	301.0	2.3	-1.8	114
ωB97XD/6-311++G(3df,3pd)	265.5	301.7	2.2	-2.5	486
ωB97XD/aug-cc-pVQZ	263.9	301.7	3.8	-2.5	2362
ωB97XD/aug-cc-pV5Z	267.2	301.5	0.5	-2.3	35995
CCSD(T)/6-311++G(2df,2p)	249.7	298.4	18.0	0.8	21807
CCSD(T)/6-311++G(2df,2pd)	250.0	305.7	17.7	-6.5	35728
CCSD(T)/aug-cc-pVTZ	249.6	306.0	18.1	-6.8	67592
CCSD(T)/aug-cc-pVQZ	261.8	308.0	5.9	-8.8	566010
CCSD(T)/aug-cc-pV5Z	268.6	308.5	-0.9	-9.3	6154085

Figure 4.1 and **Table 4.1** reveal that ωB97XD provides both accurate geometries and balanced description of D_0 when combined with at least 6-311++G(2df,2p) basis set while the largest basis sets are required for the CCSD(T) calculation. The best description of D_0 for both (S-S) and (S-H) bonds of HS_2H is found at ωB97XD/aug-cc-pV5Z as it was in good agreement with experiment; just 0.5 or 2.3 kJ mol^{-1} outside the respective experimental error margins of D_0 for (S-S) or (S-H).

4.3.1.2 Density Functionals Comparison using Optimum Basis Sets

Figure 4.2 presents the comparison of the MSE and MUE analysis of the computed *r*(S-S) of HS_2H and the CPU time taken to perform frequency calculation on the moiety using different density functionals in combination with the 6-31++G(d,p), 6-311++G(2df,2p) and 6-311++G(3df,3p). These basis sets were found to give good geometries at cheap computational expense in **Figure 4.1**.

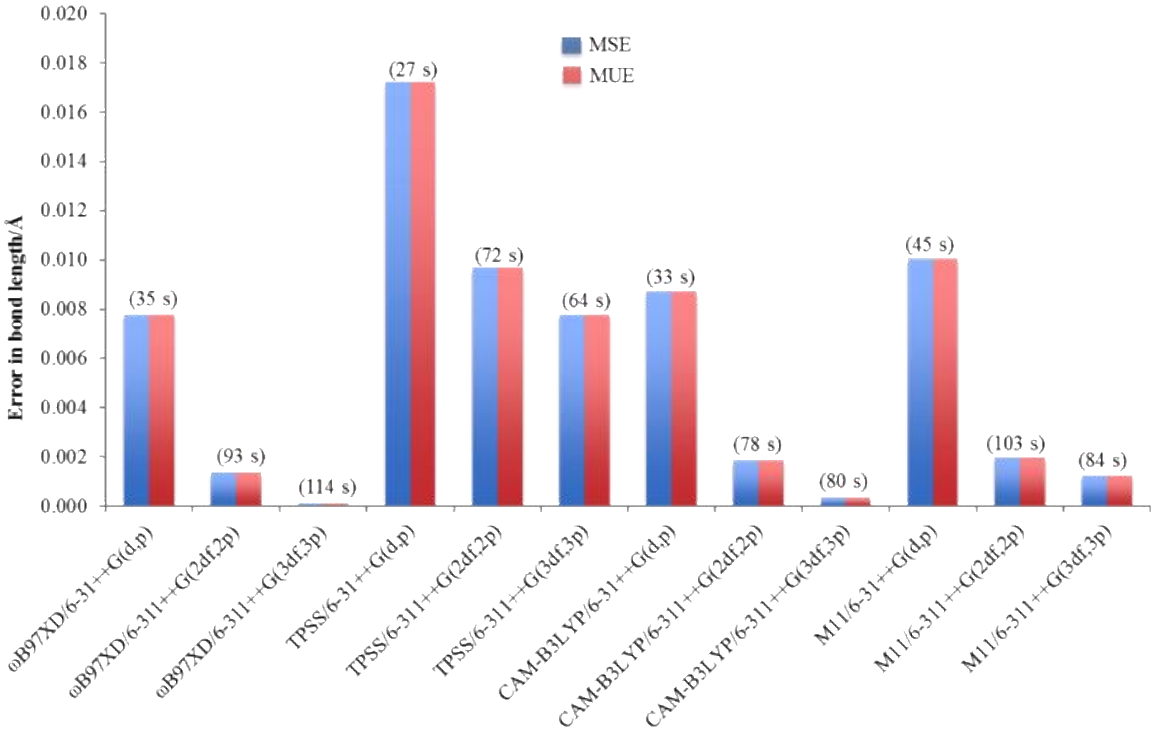

Figure 4.2. Comparison of the MSE and MUE analysis of the computed *r*(S-S) and *r*(S-H) of HS_2H and the CPU time in (in bracket) taken from frequency calculation on the moiety using different density functional methodologies.

The result in **Figure 4.2** suggests that all the methodologies give good geometry for HS_2H as the computed bond distances are all within experimental margins. Nevertheless, ωB97XD at the ωB97XD/6-311++G(2df,2p) and ωB97XD/6-311++G(3df,3p) methods are yet more desirable methods for calculating the geometries of the sulfur species of interest and/or their reactions.

A comparison of experimental $\boldsymbol{D}_0$ with that computed with the DFT/basis set combinations in **Figure 4.2** is summarised in **Table 4.2**.

Table 4.2. Comparison of bond dissociation energies ($\boldsymbol{D}_0$) of HS_2H in kJ mol^{-1} computed at various DFT methods with experiment, and the CPU time in seconds taken for frequency calculations. $\Delta\boldsymbol{D}_0 = \boldsymbol{D}_0$(expt.) - $\boldsymbol{D}_0$(calc.).

Method	$\boldsymbol{D}_0$(S-S)	$\boldsymbol{D}_0$(S-H)	$\Delta\boldsymbol{D}_0$(S-S)	$\Delta\boldsymbol{D}_0$(S-H)	CPU Time
Experiment[260]	276.1 ± 8.4	292.9 ± 6.3	0.0	0.0	-
ωB97XD/6-31++G(d,p)	242.6	300.4	25.1	-1.2	35
ωB97XD/6-311++G(2df,2p)	264.8	301.4	2.9	-2.2	93
ωB97XD/6-311++G(3df,3p)	265.4	301.0	2.3	-1.8	114
TPSS/6-31++G(d,p)	243.8	295.4	23.9	3.8	27
TPSS/6-311++G(2df,2p)	264.6	296.5	3.1	2.7	72
TPSS/6-311++G(3df,3p)	265.7	296.6	2.0	2.6	64
CAM-B3LYP/6-31++G(d,p)	223.8	298.6	43.9	0.6	33
CAM-B3LYP/6-311++G(2df,2p)	244.4	299.9	23.3	-0.7	78
CAM-B3LYP/6-311++G(3df,3p)	245.5	299.8	22.2	-0.6	80
M11/6-31++G(d,p)	242.1	304.0	25.6	-4.8	45
M11/6-311++G(2df,2p)	264.1	304.3	3.6	-5.1	103
M11/6-311++G(3df,3p)	265.6	303.6	2.1	-4.4	84

The results in **Table 4.2** indicate that all the DFT methodologies except CAM-B3LYP performs fairly well and in a similar manner considering at least, the DFT/6-311++G(2df,2p) level of theory. Taking into account the overall accuracy and computational speed so far, ωB97XD/aug-cc-pV5Z//ωB97XD/6-311++G(2df,2p) method is likely the desirable methodology (for SPE calculation//geometry optimisation and frequency calculation, respectively). Nevertheless, the other DFT/(basis set) combinations are also good. In addition, the dispersion term in ωB97XD may be important in describing other aspects of sulfur chemistry of interest in this thesis like the reactions of sulfur species with H_2S in which non-covalent interactions may be involved.

4.3.2 Method Evaluation using S and S_2

4.3.2.1 Performance of the Optimum Methodology Determined in 4.3.1 for Geometry of S_2

The triplet ground state and singlet excited state structures of S_2 have been experimentally determined to have r(S-S) = 1.8892 and 1.8983 Å, respectively.[261] Their vibrational frequencies have also been experimentally determined as 726 and 703 cm^{-1}, respectively.[261] S_2 belongs to the $D_{\infty h}$ point group. At the ωB97XD/6-311++G(2df,2p) level of theory, r(S-S) = 1.89 Å was computed for both the triplet ground state and singlet excited state. Similarly, the computed vibrational

frequencies of the species at this level of theory are 715 and 713 cm^{-1} for the triplet and singlet state S_2, respectively. The result suggests a good agreement between the present theoretical methodology and experiment.

4.3.2.2 CASSCF Study of S_n (n = 1, 2): Geometry and Energy Splitting

The expected electronic configuration for triplet spin state of atomic and diatomic sulfur[30,32,33,262] is: S - $[Ne]3s^2 3p^4$ and S_2 - $[core]4\sigma_g^2 4\sigma_u^{*2} 5\sigma_g^2 \{2\pi_u^2 2\pi_u^2\} \{2\pi_g^{*1} 2\pi_g^{*1}\}$ with $4s^0$ and $5\sigma_u^{*0} 6\sigma_g^0 6\sigma_u^{*0}$ as the immediate virtual orbitals for the species, respectively. The valence orbitals from the generated canonical orbitals of both species are presented in **Figure 4.3**.

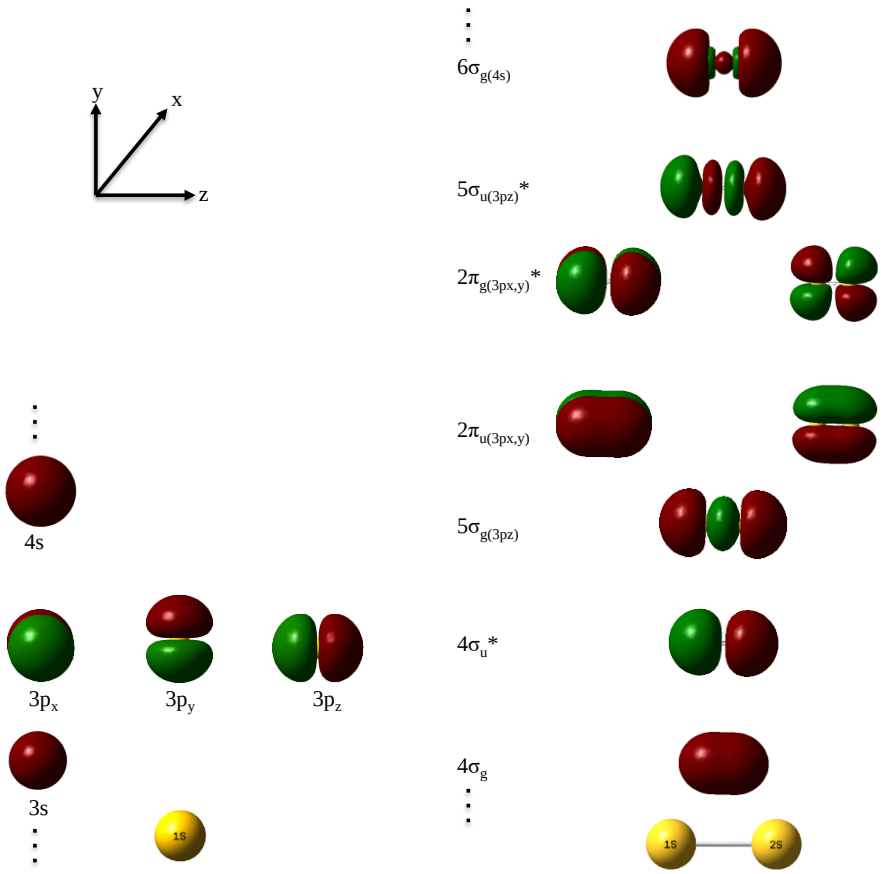

Figure 4.3. Valence canonical orbitals for: (a) atomic and (b) diatomic sulfur, based on expected electronic configuration. The *iso*-value for representative orbitals is 0.02. Dotted line above and below the presented orbitals represent virtual and core orbitals, respectively.

It is worth noting that S can adopt any of the degenerate valence configurations: $3s^2 3p_x^2 3p_y^1 3p_z^1$, $3s^2 3p_x^1 3p_y^2 3p_z^1$ or $3s^2 3p_x^1 3p_y^1 3p_z^2$.

The computed electronic configuration (or Hartree-Fock determinants) of singlet and triplet state S and S_2 are presented in **Figure 4.4**.

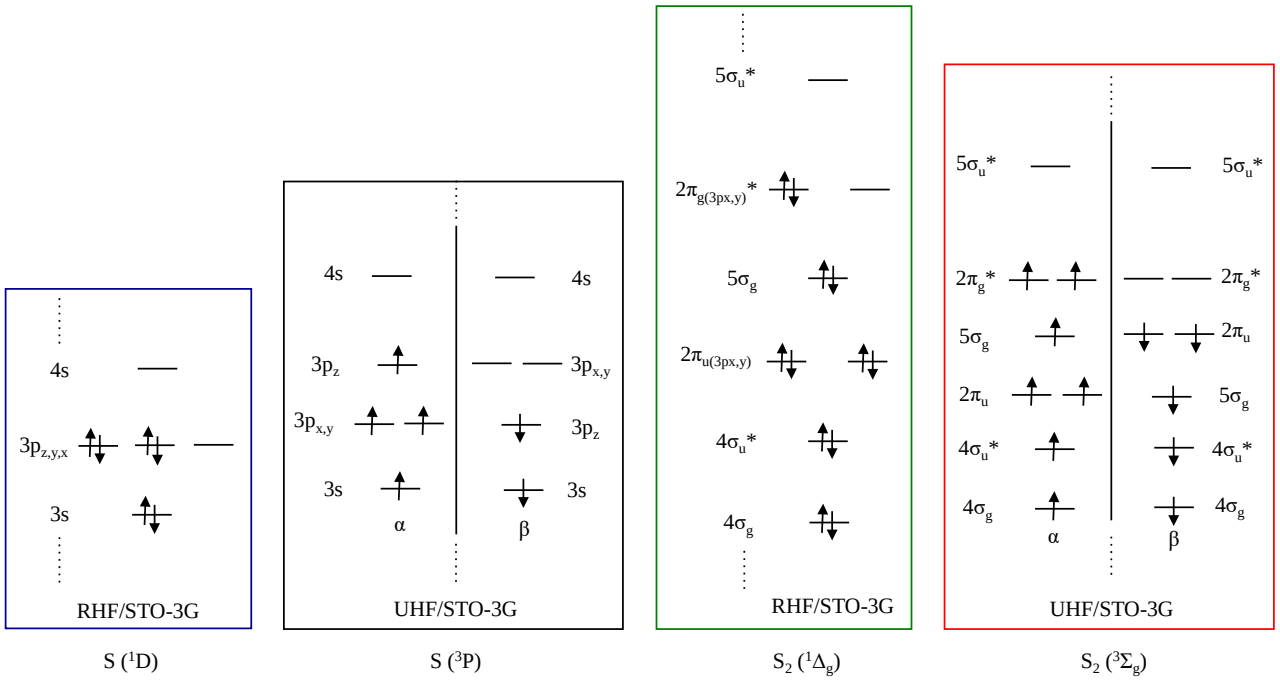

Figure 4.4. Computed valence electronic configuration of singlet and triplet S and S_2 using the HF method with a minimal basis set. The order of the orbitals is taken from the output of the code.

The orbitals in **Figure 4.3** or **Figure 4.4** correspond to the generated canonical orbitals: 6 to 10 for S and 11 to 19 for S_2. The active space in all cases, CAS(n,m), is chosen from orbitals 6 to 10 for S and 13 to 18 for S_2. In the notation, CAS(n,m), n denotes the number of active electrons while m represents the number of active orbitals. For S, CAS(4,3), CAS(4,4), CAS(6,4) and CAS(6,5) were considered. For S_2, CAS(4,4), CAS(8,6), and CAS(12,8) were considered.

Table 4.3 presents a comparison of the ωB97XD/6-311++G(2df,2p) and CAS(n,m)/6-31G(d) optimised geometry and computed vibrational frequencies of singlet and triplet S_2 with experiment.

Table 4.3. Equilibrium bond length, r(S-S) / Å and vibrational frequency, ω_e / cm^{-1} of singlet ($^1\Delta_g$) and triplet ($^3\Sigma_g$) S_2 computed at ωB97XD/6-311++G(2df,2p) and CAS(n,m)/6-31G(d) compared to experiment[261] (Expt.).

Method	r_e(S-S) $^3\Sigma_g$	r_e(S-S) $^1\Delta_g$	ω_e ($^3\Sigma_g$)	ω_e ($^1\Delta_g$)
Expt.	1.8892	1.8983	726	703
ωB97XD	1.89	1.89	715	713
CAS(4,4)	1.88	1.88	829	819
CAS(8,6)	1.95	1.96	677	640
CAS(12,8)	1.94	1.96	720	632

The results still suggest that the DFT method is better at reproducing the experiment geometry and frequencies. Nevertheless, the vibrational frequency of S_2 ($^3\Sigma_g$) computed at the CAS(12,8)/6-

31G(d) level is comparable with that computed at the DFT method in relation to their accuracy in reproducing its experimental value.

A summary of the singlet-triplet enthalpy, ΔH_{ST} and Gibbs free energy, ΔG_{ST} splitting for S and S_2 using single-reference and CAS(n,m)/6-31G(d) methods is presented in **Table 4.4**.

Table 4.4. Comparison of computed singlet-triplet energy splitting (ΔH_{ST} and ΔG_{ST}) of S and S_2 with the experiment; all CAS(n,m) employ the 6-31G(d) basis set.

Species	Method	ΔH_{ST} / kJ mol^{-1}	ΔG_{ST} / kJ mol^{-1}
S	ωB97XD/6-311++G(2df,2p)	158.6	161.3
	ωB97XD/aug-cc-pV5Z	158.7	161.4
	CCSD(T)/aug-cc-pVTZ	128.2	131.0
	CCSD(T)/aug-cc-pV5Z	125.1	127.8
	CAS(4,3)	161.7	164.5
	CAS(4,4)	103.1	105.8
	CAS(6,4)	164.2	166.9
	CAS(6,5)	183.0	185.7
	Experiment[263]	110.5	
S_2	ωB97XD/6-311++G(2df,2p)	93.4	96.1
	ωB97XD/aug-cc-pV5Z	93.3	96.0
	CCSD(T)/aug-cc-pVTZ	74.1	76.8
	CCSD(T)/aug-cc-pV5Z	72.1	74.8
	CAS(8,6)	57.8 (58.0)	60.2 (60.7)
	Experiment[261,264]	56.2 ± 9.6	

SPE, CAS(n,m)/6-31G(d)//ωB97XD/6-311++G(2df,2p), singlet-triplet energy splitting of S_2 are given in bracket.

The result in **Table 4.4** suggests that the CASSCF (CAS(4,4) for S and CAS(8,6) for S_2) method is the most accurate method for computing the singlet-triplet energy splitting of sulfur compounds. Nevertheless, CCSD(T) combined with at least the aug-cc-pVTZ basis set may also be employed for SPE calculation of S_n or its containing species of interest since its computed, ΔH_{ST} and ΔG_{ST} for S_2 is only 8 and 11 kJ mol^{-1} above experimental margins.

The CSFs with contributing weights ($w \geq 1.0$) of the configuration interaction coefficient (c) to the SPE total wavefunction of singlet and triplet S and S_2 at CAS(4,4) and CAS(8,6), respectively are presented in **Figure 4.5**.

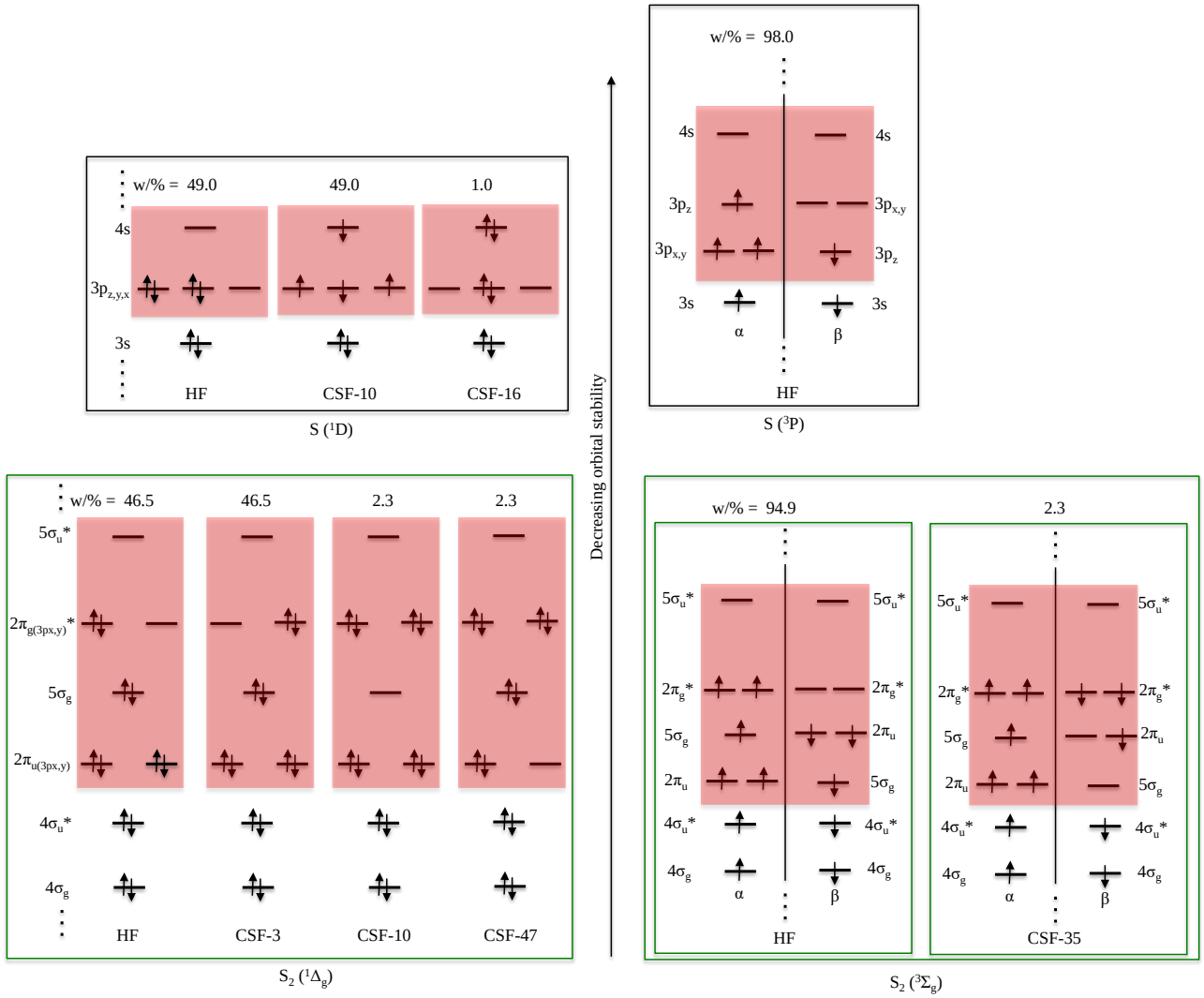

Figure 4.5. CSFs from the computed SPE wavefunctions of singlet and triplet S and S_2 using the CAS(4,4) and CAS(8,6) (brown regions), respectively: $w = c^2$.

Figure 4.5 suggests that the total wavefunction of singlet S and S_2 is made up of more than one CSF while that of triplet S and triplet S_2 is essentially the HF determinant with ($w \geq 95$ %). The total wavefunction of singlet S is made up of significant weight contributions ($w \geq 1$ %) from CSFs corresponding to single and double-electron distributions in addition to its reference HF determinant. The CSF (CSF-10) describing the single-electron distribution makes the most contribution (w = 49 %) amongst the two higher CSFs to the total wavefunction of S. CSF-35 which describes the single-electron distribution in the total wavefunction of triplet S_2 on the other hand makes negligible contribution (w = 2 %) to its total wavefunction. The contributions of these CSFs to the total wavefunction of singlet S provides a possible rationale to the discrepancies between the singlet-triplet energy splitting of the species computed using CCSD(T) and CASSCF levels of

theory with the DFT method. The total wavefunction of singlet S_2 is characterised by higher CSFs corresponding to only double-electron distributions in addition to its HF determinant.

The occupation of CAS(4,4) and CAS(8,6) orbitals in singlet and triplet S and S_2, respectively is summarised in **Table 4.5**.

Table 4.5. Occupation of CAS(4,4) and CAS(8,6) in singlet and triplet S and S_2

Species	Orbital	Occupation	Species	Orbital	Occupation
S (^{3}P)	4s	0.008	S_2 ($^3\Sigma_g$)	$5\sigma_u^*$	0.035
	3pz	1.000		$2\pi_g^*$	1.034
	3py	1.000		$2\pi_g^*$	1.034
	3px	1.992		$5\sigma_g$	1.965
				$2\pi_u$	1.966
S (^{1}D)	4s	1.000		$2\pi_u$	1.965
	3px	0.016			
	3py	1.984	S_2 ($^1\Delta_g$)	$5\sigma_u^*$	0.032
	3pz	1.000		$2\pi_g^*$	1.056
				$2\pi_g^*$	1.056
				$2\pi_u$	1.944
				$5\sigma_g$	1.970
				$2\pi_u$	1.944

The data in **Table 4.5** reveals that the CASSCF calculations for the respective species indeed involve small electronic re-distributions in the course of the computations as discussed above especially for singlet S, S_2 and triplet S_2.

4.3.3 $\mathcal{T}_1$ Diagnostic of Species

The computed $\mathcal{T}_1$ Diagnostic for all the species is less than 0.02 with the exception of HS_2, which has a value of 0.024. The $\mathcal{T}_1$ Diagnostic of species are presented in **Table 4.6**.

Table 4.6. $\mathcal{T}_1$ Diagnostic of species computed at the CCSD(T)/aug-cc-pVQZ method. Column *a* uses ωB97XD/6-311++G(2df,2p) stationary points and *b* CCSD(T)/aug-cc-pVQZ stationary points. - Implies not optimised at CCSD(T)/aug-cc-pVQZ.

	$\mathcal{T}_1$ Diagnostic	
Species	*a*	*b*
HS_2H (^{1}A)	0.0105	0.0115
H ($^2A_{1g}$)	0.0000	0.0000
HS ($^2\Pi$)	0.0116	0.0116
HS_2 (^{2}A″)	0.0236	0.0238
HS_3H (^{1}A)	0.0144	-
HS_4H (^{1}A)	0.0157	-
S_2 ($^1\Delta_g$)	0.0139 (0.0137)	-
S_2 ($^3\Sigma_g$)	0.0184 (0.0179)	-

Values in bracket are computed with CCSD(T)/aug-cc-pVTZ.

It has been asserted[57] that the $\mathcal{T}_1$ Diagnostic threshold value for open-shell systems that do not have significant multi-reference character should be 0.045 and not 0.02 to avoid misconstrued conclusions. It has also been argued that the $\mathcal{T}_1$ Diagnostic for open-shell reactions (systems) computed using the closed-shell formalism is likely to be higher than the threshold[56] of the formalism developed for open-shell systems. Furthermore, it was suggested[56] that when using the Gaussian Code on an open-shell species, the $\mathcal{T}_1$ Diagnostic could have values in excess of their upper limits without significant multi-configurational/reference character.

The CASSCF results (**4.3.2.2**) suggest that singlet state S and S_2 require multi-configurational methods, however the $\mathcal{T}_1$ Diagnostic (**Table 4.6**) suggest that single-reference/determinant methods are adequate enough for treating the electronic structure and properties of the species of interest. This is because the $\mathcal{T}_1$ Diagnostics are not large enough to suggest significant multi-configurational/reference character in the species of interest, i.e., all the calculated values are below the threshold for both open and closed-shell systems. A similar assertion has been made for S_4 ($^1A_1$) in the literature.[265] Nevertheless, to ensure that the electronic structure of open chain S_n structures is properly described, broken symmetry DFT (BS-DFT) calculations will also be performed in addition to closed-shell DFT calculations.

4.4 Conclusions

It is found on the overall from $\mathcal{T}_1$ Diagnostic, comparison with experiment, high-level theoretical calculations and previous literature[265–267] that the CCSD(T)/aug-cc-pVTZ//ωB97XD/6-311++G(2df,2p) method is computationally cheap and reliable for treating the electronic structure, vibrational frequencies and singlet-triplet energy splitting of sulfur species of interest. Nevertheless, to ensure proper description of the electronic structure of the S_n structures of interest, broken symmetry DFT (BS-DFT) calculations will also be performed in addition to closed-shell DFT calculations.

5 The electronic structure and stabilities of open chain and cyclic sulfur clusters

This chapter describes the computational investigation of the structure and thermodynamic stabilities of open chain and cyclic isomers of the sulfur clusters, S_n (n = 1 - 5 and 8) relative to their most stable structures using DFT and CCSD(T). The study reveals that all S_n ($n \leq 4$) possess open chain ground state structures while S_n (n = 5 and 8) have cyclic ground state structures. It is also found that all S_n (n = 3 - 5 and 8) considered have thermally accessible excited cyclic and open chain structures with either the same or different spin state. Some open chain structures are observed to exist in the singlet and triplet state with similar structures. For S_8 and S_5, the triplet state open chain isomers are found to be more stable than their singlet state analogues. This provides a likely explanation for the paramagnetic behaviour of liquid sulfur and the structures responsible for the behaviour. The stability studies of open chain structures of S_n suggest that as n increases, a switch in stability occurs at S_3 and S_4: from triplet S_2 to singlet S_3 and singlet S_4 to triplet S_5 ground state structures, respectively. This suggests the occurrence of two-state reactivity in gaseous sulfur and provides an explanation for observations in liquid sulfur. This in turn is likely to have implications on the viscosity behaviour of liquid sulfur and processes occurring during sulfur recovery in the thermal Claus process. The enthalpies of the triplet state open chains of S_8 relative to its cyclic ground state structure ($155 \leq \Delta H^{\circ}_{298} \leq 166$ kJ mol^{-1}) are computed in good agreement with the enthalpy of formation of radical sulfur species (154.4 ± 1.7 kJ mol^{-1}) determined from temperature dependent electron spin resonance measurements between $153 \leq T \leq 700$ °C.

5.1 Introduction

Sulfur (S_n) is a ubiquitous chemical species. Its indispensability ranges from industry, agriculture and biology to the atmosphere.[12,14,268–272] It is widely distributed in nature; occurs in the earth's crust and/or rocks, crude oil, petroleum, coal, natural gas and mineral sulfides.[12,260,269,270,273] In the

periodic table, sulfur belongs to the group 16 elements. This group of elements form a range of chemical species with variable geometrical structures (allotropes).[274] Sulfur in particular exhibits more allotropic forms than any other element in the periodic table, except carbon.[37,269,275] The solid cyclic crown-shaped sulfur, S_8 is the most stable and abundant allotrope near room temperature.[37,272]

In recent years, the modified thermal Claus process with the overall chemical reaction:[12,269]

$$3H_2S + \frac{3}{2}O_2 \rightarrow \frac{3}{8}S_8 + 3H_2O; \qquad \Delta H = -664.0\ \text{kJ mol}^{-1} \tag{5.1}$$

has become the most industrially and commercially attractive way of liquid sulfur production from hydrogen sulfide, H_2S for desired end uses.[12,14] This process is especially applicable to natural gas, coal, petroleum or oil refining which are the main sources of H_2S.[12,14] The process suffers a daunting H_2S elimination problem[13,14,269] due to the equilibrium:[14,276]

$$H_2S + S_n \rightleftharpoons H_2S_{n+1} \quad n \geq 8 \tag{5.2}$$

initially thought to be the reaction:[277,278]

$$H_2S + S_n \rightleftharpoons H_2S_n \quad n \geq 8 \tag{5.3}$$

but later modified to the reaction in eq. (5.2).

Eq. (5.3) was proposed from experimental studies of the viscosity changes of liquid sulfur in the absence and presence of H_2S, **Figure 5.1**.[277–279] This initiated a series of experimental and theoretical studies[14,276,280–286] aimed at explaining or understanding the reaction in eq. (5.3) and the viscosity changes of liquid sulfur. Much of the rapid increase in the viscosity at ca. 160 °C has since been attributed to the polymerisation of S_8 chains resulting from the rupture of S_8 rings.[14,276–278,284] However, a number of experimental and theoretical studies[275,287] suggest that liquid and gaseous sulfur are made up of an equilibrium between different sises of sulfur species, S_n (n = 2 - 8) which may be rings or open chains. Nevertheless, the structure and relative stabilities of singlet and/or triplet state open chains of S_8 to the most stable singlet state cyclic S_8 allotrope are less well known. Furthermore, liquid sulfur has been experimentally found to be paramagnetic[275,288] whereas the polysulfanes, $HS_{n+1}H$ formed in eq. (5.2) and eq. (5.3) are known from experiments and theoretical calculations to be diamagnetic.[258,259,282,289–291] The foregoing reports indicate the complexity and anomaly associated with the chemistry of sulfur recovery in the Claus process. As such, the question of the relative stability and structure of the lowest energy singlet or triplet open chain S_n species in eq. (5.2) to inform the unusual reversibility and influence the quality of recovered sulfur[13,14] arises.

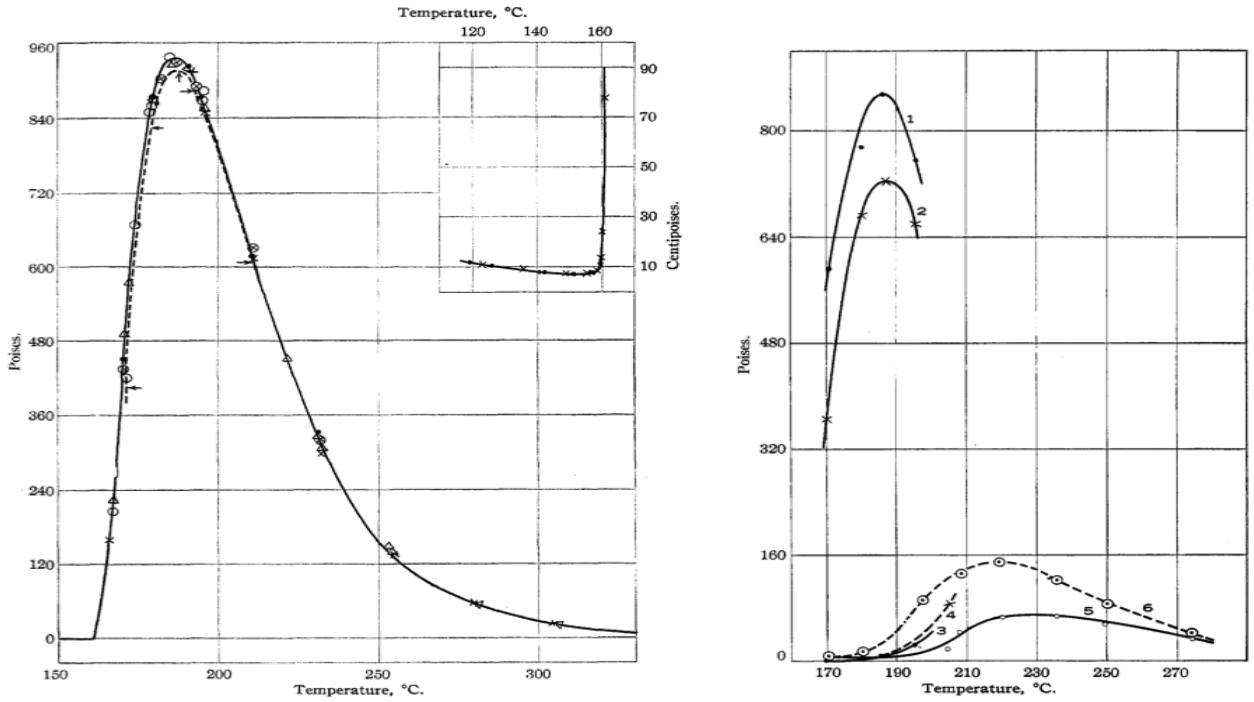

(a) (b)

Figure 5.1. Change in viscosity of liquid sulfur (S_n) with temperature; (a) in the absence and (b) in the presence of hydrogen sulfide. "Reprinted (adapted) with permission from Bacon, Fanelli, *J. Am. Chem. Soc.* **1943**, *65*, 639–648.[277] Copyright (1943), American Chemical Society."

Furthermore, the question of whether spin state interplay is involved in the reaction due to different spin states of the ground states of the S_n species also becomes important. It is on these grounds that this study finds its significance.

5.1.1 Literature Review

It is worth noting that a significant number of reports: reviews, experimental and theoretical studies of sulfur allotropes exist in the literature and will be summarised below.

Mass spectrophotometric study of equilibrium composition of sulfur vapour was reported in 1963.[287] The study asserted that measurable amounts of all possible sulfur molecules, S_n ($2 \leq n \leq 8$) and detectable amounts of S_n (n = 9 and 10) were present in sulfur vapour between room temperature and the boiling point of sulfur (445 °C). The authors further suggested that their high-temperature experiments were most concordant with the dissociation energy of S_2 (4.4 eV ≈ 424.5 kJ mol^{-1}). The report concluded that the enthalpy change for the reactions; $\left(\frac{n}{8}\right)S_8 \rightarrow S_n$ (n = 2, 3, 4, 5, 6, 7 and 8) at 400 K was 98.3, 94.1, 85.8, 59.8, 25.9 and 23.8 kJ mol^{-1}, respectively. A few years later (1968), the photo-ionisation mass spectrometric study of pure (> 99.999 %) orthorhombic sulfur was reported.[292] In this study, the efficiency curves of generated sulfur molecular species

were measured. The authors suggested that the ionisation potentials deduced for S_n (n = 2, 3, 5, 6, 7 and 8) were 903.1 ± 1.9, 934.0 ± 2.9, 829.8 ± 4.8, 868.4 ± 2.9, 836.5 ± 2.9 and 872.2 ± 2.9 kJ mol^{-1}, respectively. The authors went on to assert that no evidence of structures other than rings were obtained from their studies. No mention of the ionisation potential of S_4 was made in this study. The authors observed that the ionisation efficiencies of the S_4^+ species generated from two different sources was identical within experimental margins and so, indicated that the S_4 was present but in immeasurable amounts. Carleer and Colin published an estimate of the singlet-triplet energy splitting for S_2 as 56.2 ± 9.6 kJ mol^{-1} in 1970 from their flash photolysis and flash discharge experiments on the moiety.[264] It is mentioned in a 1976 review[293] that the experimental dissociation energy of cyclo-octasulfur (cyclic S_8) below 150 °C is 133.9 kJ mol^{-1} but 137.2 kJ mol^{-1} at higher temperatures and that the melting point of solid sulfur is 119.6 °C. Furthermore, the review asserted that at this temperature (119.6 °C), the composition of the liquid formed was unknown but a small concentration of spins was present in the liquid at 150 °C. The review concluded that equilibrium composition allowed for the existence of comparable concentrations of different sises of sulfur rings and chains in liquid sulfur at boiling temperature and above. In 1977, Kao predicted the triplet helical diradical structure of S_4 as the most stable S_4 structure from his *ab initio* studies of ten different conformational isomers of the species in their singlet and triplet spin states.[294] He however noted that the energetic comparison of singlet and triplet state species was uncertain because the single determinant theory he employed (Hartree-Fock (HF) method) is known to unduly favour triplet states. The cyclic (envelope-like) structure was also predicted from similar *ab initio* studies in the same year to be the most stable structure of S_5.[295]

The photoelectron spectroscopy of the S_3 anion together with other sulfur containing anions was reported in 1986.[296] The study revealed that the electron affinity of S_3 was 201.9 ± 2.4 kJ mol^{-1}. The authors further asserted that the S-S bond length in S_3 was 1.90 ± 0.05 Å after performing the Franck-Condon analysis of their spectra. The report did not mention however, whether the moiety was chain-like or cyclic but assumed the bond angle to be ≈ 120 ° suggestive of a bent chain structure. Therefore, Rice et al., in the same year investigated the structural isomers of S_3 using the analytic configuration interaction (CI), self-consistent field (SCF), complete active space self-consistent field (CASSCF) and multi-reference CI singles and doubles (MRCISD) methods.[297] Their SCF and CISD results revealed that the cyclic moiety was more stable than the chain structure by 38.9 kJ mol^{-1} (SCF) and 9.6 kJ mol^{-1} (CISD), respectively. Their results computed with CASSCF and MRCISD in combination with good basis sets on the other hand suggested that the open chain S_3 moiety was more stable than the cyclic structure by 37.2 kJ mol^{-1} (CASSCF) and 34.3 kJ mol^{-1} (MRCISD), respectively. They concluded that both forms of the species are experimentally

accessible. This study somehow closed the gap created by the results of the photoelectron spectroscopic studies of S_3 anion summarised above. The structure of orthorhombic sulfur (α-S_8) was refined by Rettig and Trotter using X-ray crystallography in 1987.[298] The authors asserted that the ring possessed an average S-S bond length of 2.055 (2) Å, average bond angle of 108.2 (6) ° and an average dihedral angle of 98.5 (19) °.

The first comprehensive theoretical study of the structure and stability of S_n (n = 2 - 13) was performed by Hohl et al., in 1988.[274] The study combined a parameter free density functional method, molecular dynamics (MD) and simulated annealing techniques to predict the ground state geometries of the sulfur species. The study revealed that the ground state structure for: S_2 had a triplet state; S_3 had an open chain (C_{2v}) singlet state but its singlet cyclic (D_{3h}) structure was 15.4 kJ mol^{-1} above the ground state structure and the lowest triplet S_3 (C_{2v}) structure was 67.5 to 77.2 kJ mol^{-1} above the ground state structure; S_4 had a rectangular (D_{2h}) singlet state with all triplet state structures of the species lying well above the D_{2h} structure and that S_5 to S_{13} possessed cyclic singlet ground state structures. Although this report was detailed, the ground state structure predicted for S_4 was in contrast to that predicted by Kao[294] thereby leading to a controversy about the ground state structure and its spin state for the moiety. The report[274] also did not consider the stability of the open chain structures of S_n ($n \geq 5$) relative to the cyclic structures. The second detailed theoretical study of sulfur clusters was performed in 1990 at the HF, MP*n* and the quadratic CI technique including perturbative triples (QCISD(T)) methods for S_n (n = 2 - 12).[37] The study revealed that *d*-type polarisation functions were extremely important in obtaining reliable geometries of S_n species. The authors suggested that S_n forms with $n \leq 4$ adopted open chain structures while those with $n \geq 5$ preferred cyclic structures. More interestingly, the report suggested that the ground state structure of S_3 was the singlet C_{2v} structure in agreement with the calculations of Hohl et al.,[274] but was inconclusive about the ground state structure of S_4 and suggested that the singlet D_{2h} structure of S_4 was not a minimum structure contrary to the report by Hohl et al. Notwithstanding, the study computed other forms of S_4 as minimum structures in the singlet and triplet state. In addition, singlet (C_s) and triplet (C_2) state open chain structures were computed in the study to be less stable than the cyclic structure of S_5, its global minimum, by 41.8 and 69.8 kJ mol^{-1}, respectively. The authors however, did not report open chain conformers for S_n ($6 \leq n \leq 12$).

In 1992, Hassanzadeh and Andrews reported the vibronic absorption spectra of S_3 and S_4 in solid Argon.[299] The authors asserted that S_4 showed two distinct electronic absorptions: a broad green band centred at 518 nm and a structured red band between 560 and 660 nm. They went on to state that the red-absorbing species converted to the green-absorbing one on irradiation with red light and that the green absorbing moiety converted to the red-absorbing isomer under green light photolysis.

They then assigned the bands to singlet state C_{2v} (open chain, green-absorbing) and C_s (branched three membered ring, red-absorbing) structures of S_4 on the basis of their CISD calculations. The authors further stated that the electronic spectra of S_3 showed sharper bands between 350 and 440 nm. They suggested that the electronic spectrum of S_3 was indicative of a singlet state, bent chain structure for the moiety. Hunsicker et al., in 1995 reported a density functional, simulated annealing and experimental investigation of anions formed from sulfur rings and chains of different sises (S_n, $1 \leq n \leq 9$).[300,301] The authors asserted that although ring structures were energetically more stable than chain structures, the environment used to generate the larger clusters, $n > 7$ favoured the chain structures. As such, Shimojo et al.,[302] performed an *ab initio* MD investigation of bond breaking in the S_8 ring in 1998. The authors asserted that a bond in cyclic S_8 is easily broken after an electron is excited from the highest occupied molecular orbital (HOMO) of the species to its lowest unoccupied molecular orbital (LUMO). The authors argued that bond breaking in cyclic S_8 occurred to stabilise the anti-bonding states occupied by the excited electron. The vibrational study and molecular structure investigation of two S_4 isomers in sulfur vapour was reported by Boumedien et al., in 1999.[303] The study assigned the green-absorbing (λ_{max} = 530 nm) chain-like S_4 moiety to a *trans* (C_{2h}) structure contrary to the assignment by Hassanzadeh and Andrews[299] but assigned the red-absorbing (λ_{max} = 560 - 660 nm) isomer to the branched ring structure in agreement with the report by Hassanzadeh and Andrews. Shimojo and co-workers again in 2000 published their combined DFT and MD simulation of S_8 ring rupture in liquid sulfur and subsequent polymerisation of the resulting chain species.[304] The authors suggested this time that the chain structures resulting from cyclic S_8 after electron excitation do not recombine to form cyclic S_8 but a long-lived 'tadpole' structure when electron excitation is stopped. They concluded therefore that photo-induced polymerisation occurs in liquid sulfur due to the presence of S_8 chains and tadpole structures that are close to each other.

In 2001, Chen et al., reported a DFT (B3LYP) study of the geometric structure and stability of neutral sulfur clusters with 3 - 11 sulfur atoms.[305] The authors suggested that in the 68 isomers of sulfur clusters for S_n (n = 3 - 11), sulfur atoms could be coordinated one, two and/or three-fold. They also asserted that S_n species with three-coordinate sulfur atoms were energetically less stable compared to species with one or two-fold coordinated sulfur atoms. They therefore concluded that it seemed difficult for sulfur to form cage structures with the involvement of three-fold coordinated atoms. Another *ab initio* study of sulfur clusters, S_n (n = 2 - 12), this time for their structure and polarisability was reported in 2001.[306] The study employed the B3LYP and coupled cluster at the CCSD(T) level. The authors stated that the binding energy per atom increased with sise of cluster and reached the asymptotic limit for a relatively small n value. They also asserted that no defined

correlation existed between the polarisability of the species, $\langle\alpha_n\rangle$, and hardness, η, but that the value of the difference, $\langle\alpha_n\rangle - n\langle\alpha_1\rangle$, correlated linearly with the atomisation energies of the species. They went on to suggest that in sulfur clusters, the polarisability principle does not hold, stating that the lone-pair electron polarisability is more diffuse hence more polarisable in cluster than in free atoms. They then concluded that pure vibrational effects on the $\langle\alpha_n\rangle$ were negligible. Also in this year, Cioslowski et al., investigated the conformational structures and thermodynamic properties of sulfur homocycles at the B3LYP/6-311G* and MP2/6-311G* levels of theory.[307] The authors asserted that the S_5 ring was confirmed to exist exclusively in a highly fluxional C_s conformation. They also suggested that two S_6 homocycles were linked via two transition states with the D_{4d} structure corresponding to a global energy minimum with the higher energy species possessing a C_{2v} symmetry. The authors went on to state that the S_7 ring was found to adopt one of the highly fluxional C_s conformations that are separated by a substantial energy barrier. They concluded that a complete set of S_8 conformers consisted of C_{2v}, C_2, C_s and possibly a C_{2h} structure in addition to the low-energy D_{4d} species that are yet to be uncovered. Steudel and co-workers in 2002[308] adopted *ab initio* calculations at the G3X(MP2) level to examine the structures and energies of isomers of the sulfur cluster, S_8. The authors asserted that a spiralling chain singlet cluster structure with 8 atoms and C_2 symmetry was less stable than the crown-shaped structure of S_8 (its global minimum) in energy by $\Delta G^{\circ}_{298} = 28.3$ kJ mol^{-1} ($\Delta H^{\circ}_{298} = 33.3$ kJ mol^{-1}). They stated that the less stable structure possessed three-coordinate atoms and a rectangular arrangement of four sulfur atoms at the chain-ends. They went on to suggest that the unusual geometry of the cluster could be rationalised in terms of a weak π*-π* bond between two π* orbitals at the chain-ends of the species. A year later, Jones and Ballone reported DFT and Monte Carlo studies of the structure and bonding in S_n rings (n = 2 - 18) and chains (n = 2 - 10).[309] They asserted that many isomers existed for both types of S_n structures (rings and chains). Later this same year, Wong and Steudel reported an *ab initio* study of the structure and spectra of S_4 employing the G3X(MP2), CCSD(T) and MRCI/CASSCF levels of theory.[310] The authors asserted that the *cis*-planar (C_{2v}) singlet structure of the species was its global minimum while its singlet D_{2h} structure was calculated as a transition state. This was the first clear assignment of the global minimum structure for S_4. They predicted the stability of various singlet state isomers of S_4 in the order $C_{2v} > C_{2h} > C_s > D_{2d} > D_{3h}$. The authors went on to state that their calculated electronic absorption spectra at CIS/6-311+G(3df) and vibrational spectra at B3LYP/6-31G(2df) indicated that the green-absorbing S_4 was its C_{2v} structure in agreement with the report of Hassanzadeh and Andrews[299] while the red-absorbing species was the C_{2h} structure of the species contrary to the reports by both Hassanzadeh and Andrews[299] and Boumedien et al.[303] Also in 2003, Steudel and co-workers in edited books[275,291] presented excellent reviews on solid, liquid

and gaseous sulfur species. The authors reiterated that crown-shaped S_8 was the most stable allotrope of sulfur in solid, liquid and gas phase and that liquid sulfur was paramagnetic. They also reiterated that at high temperatures ($200 \leq T \leq 1000$ °C), sulfur vapour was made up of S_n species with $n = 2$ - 10 with some existing as two or more isomers.

A communication of the first experimental geometry of S_3 by means of Fourier transformed microwave spectroscopy (FTMS) of a molecular beam was published in 2004.[311] The authors asserted that the S-S bond length of the species was 1.917 (1) Å and that its bond angle was 117.34 (6) °. The structure has a singlet spin state, is bent and has C_{2v} symmetry. This structure is found to be in close agreement with the structure of the species that was proposed from photoelectron spectra of S_3 anion[296] summarised above. The authors of this communication[311] acknowledged the important role of previous computational calculations in guiding their observation of the species. Later this same year, Wong et al., reported novel isomers of S_6 via high-level *ab initio* molecular orbital calculations.[312] The authors asserted that a prism structure of the species essentially made of three S_2 and connected through a six-center π*-π*-π* interaction was energetically less stable by $\Delta G^{\circ}_{298} = 41.9$ kJ mol^{-1} ($\Delta H^{\circ}_{298} = 52.4$ kJ mol^{-1}) than its global minimum (cyclic, chair form). They also noted that cyclo-S_6 required activation energy of $\Delta G^{\ddagger^{\circ}}_{298} = 137.8$ kJ mol^{-1} ($\Delta H^{\ddagger^{\circ}}_{298} = 149.7$ kJ mol^{-1}) for ring opening to occur. They concluded that the prism and singly branched isomers of S_6 were more reactive than its chair form and were potential sources of S_2 in chemical reactions involving elemental sulfur. The refined singlet structures of S_3 and S_4 by means of centimeter, millimetre and submillimetre FTMS were reported in 2005.[313] In this report, the recommended structures of S_3 and S_4 possess the parameters: S-S bond length, 1.914 (2) Å and bond angle, 117.33 (5) ° for S_3 and S-S bond lengths, 1.898 (5) Å (terminal) and 2.155 (10) Å (central) for S_4 while its bond angle is 104.2 (2) °. Also in 2005, Francisco et al., published a high-level *ab initio* study of the structure, vibrational spectra and energetics of S_3.[314] The authors reported that the S-S bond dissociation energy of the moiety was determined to be 254.8 ± 4.2 kJ mol^{-1}. A year later, Francisco and co-workers reported yet another *ab initio* study of S_3.[266] The authors calculated the low-lying singlet and triplet electronic states of the moiety using the MRCI+Q method. They assigned the strong experimentally observed absorption around 395 nm to the $1\ ^1B_2$ state of the species. They also predicted the isomerisation energy of cyclic (D_{3h}) and bent (C_{2v}) singlet state structures of S_3 to be 18.4 ± 2.1 kJ mol^{-1}.

Matus et al., studied the electronic structure and energetics of S_4 at the CCSD(T) level of theory in 2007.[265] The authors calculated the geometry of the ground state singlet C_{2v} isomer of the species to be in good agreement with its microwave[313] structure. They went on to suggest that the singlet D_{2h} isomer of the species was a transition state lying 6.7 kJ mol^{-1} above the C_{2v} global minimum

structure of the moiety and could interchange its long S-S bonds to give the C_{2v} isomer on adjacent sides. The authors also stated that S_4 had a low-lying triplet state isomer of D_{2h} symmetry that was less stable than its C_{2v} singlet structure by 45.2 kJ mol^{-1}. The authors further predicted the bond dissociation energy of the species into two triplet state S_2 moieties as 95.4 kJ mol^{-1} and the bond energy to form singlet S_3 + S (^{3}P) as 267.8 kJ mol^{-1}. Later this same year, Grant et al., reported an *ab initio* (CCSD(T)) study of the energetic properties of $S_2^x (x = 0, +1, 1)$.[267] They computed the heat of formation of neutral triplet state S_2 in the gas phase at 0 K to be 124.7 kJ mol^{-1} in good agreement with its experimental value (128.3 ± 0.3 kJ mol^{-1}) quoted in their report. They also calculated the adiabatic ionisation potential (IP) and electron affinity of the species at the same temperature to be 904.1 and 162.1 kJ mol^{-1}, respectively. The IP of S_2 calculated by these authors falls within the limits of the experimentally[292] deduced IP of S_2 (903.1 ± 1.9) kJ mol^{-1}. In 2010, Maron and co-workers studied the singlet D_{2h} and C_{2v} isomers of S_4 using *ab initio* (MD) and DFT methods[251] even though there were a lot of theoretical investigations in the literature on the species. They asserted that DFT method combination, BPW91/aug-cc-pVTZ, reproduced the relative energy differences computed by Matus et al.,[265] at the CCSD(T)/aug-cc-pVTZ level of theory between the isomers. Their findings also predicted the D_{2h} structure of the moiety as a transition state rather than a minimum structure. They then stated that the trajectories show that symmetric C_{2v} isomers interconvert via the D_{2h} transition structure without producing any three-dimensional isomers observed with tetraoxygen. Francisco and co-workers performed a kinetic study of the $S + S_2 \rightarrow S_3$ reaction by the chaperone mechanism using the CCSD(T)/aug-cc-pVTZ method in 2011.[272] The authors proposed that the recombination of sulfur atoms occurred in a stepwise manner from elemental sulfur to the most abundant sulfur molecule, S_8. They went on to suggest that the reaction is possibly a key step in the formation of sulfur aerosols in low-O_2 atmospheres. The authors further noted that the rate constant of the reaction at 298.15 K in Argon matrix was determined to be 2.66×10^{-33} cm^{-6} mol^{-1} s^{-1} while its second-order rate constant was 6.47×10^{-14} cm^{-3} mol^{-1} s^{-1} and its Arrhenius-type rate constant was $6.25 \times 10^{-14} \exp[450.15(1/T - 1/298.15)]$ cm^{-3} mol^{-1} s^{-1}. In addition, they asserted that the work provided key intermediate species for studies of sulfur formation in the modern Venus and Earth atmospheres. Lastly, a benchmark *ab initio* study of the stability of the cuboid singlet $(S_2)_4$ supermolecule using different levels of theory was reported in 2013.[315] The authors argued that unlike the van der Waals-like $(O_2)_4$ cluster, $(S_2)_4$ was found to be much more chemically bound. The went on to state that their best estimate of the decomposition of the cuboid $(S_2)_4$ into four triplet S_2 moieties was 272 kJ mol^{-1} and that the intermolecular distance between the S_2 moieties was 2.74 Å. In addition, they asserted that the singlet ground state of the species possessed much less multi-configurational (MC)

character than its oxygen analogue thereby allowing for reliable treatment of the species around its equilibrium geometry at the CCSD(T) level of theory. They concluded however, that further MR/MC studies of the species were required to correctly describe its stability as the moiety was characterised as a minimum structure at MP2/cc-pV*x*Z (*x* = D, T, Q) but a transition state at CCSD/aug-cc-pV*x*Z (*x* = D, T) level of theory.

5.1.2 Justification of Study

Although there are a significant number of reports on the structure and stability studies of sulfur allotropes (S_n) in the literature, very little mention is made of the stability and structure of the excited state isomers of S_n species relative to their ground state structures especially for $n \geq 3$. It is also important that n at which minimum cyclic S_n clusters begin to form is established. This is because experimental structures for open chain n = 2 - 4 previously predicted by theoretical calculations are available but theoretical predictions of thermally accessible cyclic S_3 and S_4 structures also exist in the literature. Peaks of the S_5 cation were observed using mass spectroscopy[268] and its neutral structure is predicted to have a cyclic ground state at low-level[37,295] and some high-level theory[309] but its experimental structure is yet to be established. All species of S_n for at least $6 \leq n \leq 8$ are known from experiments[268,287,292,298] and theory to have cyclic global minimum structures with S_8 established as the most stable and abundant form of S_n species in the solid, liquid and vapour phase. However, only scanty information is available in the literature on the structural variation or similarities of open chain isomers of S_n species in the same or different spin states. It is also not clear from the literature available whether a singlet or triplet open chain S_8 species is responsible for the unpaired spins in liquid sulfur above 120 °C giving rise to its paramagnetic behaviour at $T \geq 153$ °C. Nevertheless, it is proposed that open chains of S_8 are present in liquid sulfur and are responsible for its sudden viscosity change at 159 °C due to their self-polymerisation and reaction with other S_n species in the liquid to form polymeric sulfur chains.[14,275,277] In addition, industrial sulfur is recovered in liquid form using the thermal Claus process and is condensed in the presence of H_2S due to the thermodynamic limitations of the process.[13,14] Understanding the structural variations or similarities of singlet and triplet states of S_n species as well as their stabilities will therefore, go a long way in enhancing the understanding of the unusual reactivity of open chain S_n and H_2S to form $HS_{n+1}H$ thereby suppressing the viscosity of liquid sulfur.

5.1.3 Aim of Study

The aim of the work in this Chapter therefore, is to explore the structure and thermodynamic stability of open chain and cyclic S_n isomers using high-level quantum chemistry methodologies. The information that will be obtained will be useful in explaining, augmenting the understanding or complementing previous observations or predictions on S_n species and the behaviour of liquid sulfur. To achieve this aim, the following objectives are outlined:

1. Determination of the geometries of cyclic and open chain isomers of neutral singlet and triplet state sulfur clusters, S_n ($n \leq 5$ and 8).
2. Determination of the thermodynamic stability of the structural isomers relative to their global minimum structures and the singlet-triplet energy splitting between key open chain S_n structures with the same n.
3. Determination of the ring opening for structures with cyclic global minimum structures.

5.2 Computational Details

All the gas phase calculations were performed using the Gaussian 09 package.[24] Geometry optimisation of open chain and cyclic neutral singlet and triplet state sulfur clusters S_n ($n \leq 5$ and 8) were performed at the ωB97XD[80]/6-311++G(2df,2p)[99] level of theory. The nature of the stationary points was ascertained by frequency calculations at 298.15 K and 1.0 atm on the optimised stationary points using the same level of theory. Minimum points and first-order saddle points (transition states) were characterised by no and one imaginary frequencies, respectively.[19,36] All frequencies presented here are uniformly scaled by the fundamental scale factor of 0.950.[257,316] SPE calculations on the calculated stationary points were then performed at the CCSD(T)[44]/aug-cc-pVTZ[100,255] level of theory. Topological analysis of the electron density of the pentasulfur ring was performed using QTAIM[124–133] as implemented in the Multiwfn package.[203] In doing this, the ωB97XD/aug-ccpV5Z level of theory was employed to generate the wavefunction of the species.

5.3 Results and Discussion

5.3.1 Structures and Energetics of S_n ($2 \leq n \leq 5$ and 8)

5.3.1.1 S_n ($n = 2$)

The gas phase structure, spectroscopic and/or energetic parameters of the sulfur dimer, S_2, have been studied experimentally[261,264] and theoretically[5,37,266,267,274,309] in the past. The ground state of the species is known from experiment to be the $^3\Sigma_g$ state[261] just like its O_2 analogue. A comparison of the calculated structure and vibrational frequency of the ground state and excited singlet state of

the dimer with previous calculations and experiment is presented in **Table 5.1**. The excited singlet isomer of the dimer is rarely mentioned in theoretical studies in the literature even though it is known from experiments.

Table 5.1. Calculated equilibrium bond length (r_e) and vibrational frequency (ω_e) of triplet and singlet state S_2 compared to experiment.

State	Method	r_e / Å	ω_e / cm^{-1}	Ref.
$^3\Sigma_g$	HF/3-21G*	1.8680	825	[37]
	B3LYP/cc-pVDZ	1.9340	702	[306]
	MD/DFT	1.9400	665	[309]
	MRCI+Q/aug-cc-pV(5+d)Z	1.8987	720	[266]
	CCSD(T)/aug-cc-pV5Z	1.8952	729	[267]
	CCSD(T)/aug-cc-pV(5+d)Z	1.8939	730	[267]
	ωB97XD/6-311++G(2df,2p)	1.89	715	**This work**
	Experiment	1.8892	726	[261]
$^1\Delta_g$	MRCI+Q/aug-cc-pV(5+d)Z	1.9081	697.0	[266]
	ωB97XD/6-311++G(2df,2p)	1.89	713	**This work**
	Experiment	1.8983	703	[261]

The results in **Table 5.1** indicate that the adopted method is adequate for the investigation of ground and excited states of S_n structures. Although the calculation does not capture the slight increase in the bond length of the singlet state S_2 structure, there is a reasonably good agreement between the results computed using the determined method with experiment and high-level theoretical calculations. The excited singlet isomer of the dimer is rarely mentioned in theoretical studies in the literature even though it is known from experiments. The results in **Table 5.1** further indicate that the adopted method is adequate for the investigation of ground and excited states of S_n structures. This is because there is very good agreement between the results computed using the method with experiment and high-level theoretical calculations.

Both atomic (S) and diatomic sulfur (S_2) were computed to have triplet ground states in agreement with experiments.[261,263,264] A summary of the energy difference between their triplet ground and singlet excited state is presented in **Table 5.2**.

Table 5.2. Energy differences (electronic, ΔE, enthalpy, ΔH and Gibbs free energy, ΔG) between triplet ground and singlet excited state of atomic and diatomic sulfur computed at the CCSD(T)/aug-cc-pVTZ//ωB97XD/6-311++G(2df,2p) level of theory.

Species	ΔE / kJ mol^{-1}	ΔH / kJ mol^{-1}	ΔG / kJ mol^{-1}	Expt. / kJ mol^{-1}
S	128.2	128.2	131.0	110.5[263]
S_2	74.1	74.1	76.8	56.2 ± 9.6[261,264]

It is observed that although the energy difference for atomic sulfur differs (≥ 17 kJ mol^{-1}) significantly with experiment,[263] it agrees excellently with the ΔH values (127.9, 125.5 and 124.7 kJ mol^{-1}) computed at the CCSD(T)/aug-cc-pV(*x*+*d*) levels of theory[317] where *x* = T, Q and 5, respectively. The energy difference (ΔH) for diatomic sulfur on the other hand is overestimated by at most 11 kJ mol^{-1} above its experimental[261,264] margins and is also similar with the literature values (73.5, 72.4 and 72.0 kJ mol^{-1})[317] at the same level of theories above.

5.3.1.2 S_n (*n* = 3)

This allotrope of sulfur is calculated to have four minimum geometric structures, presented in **Figure 5.2**.

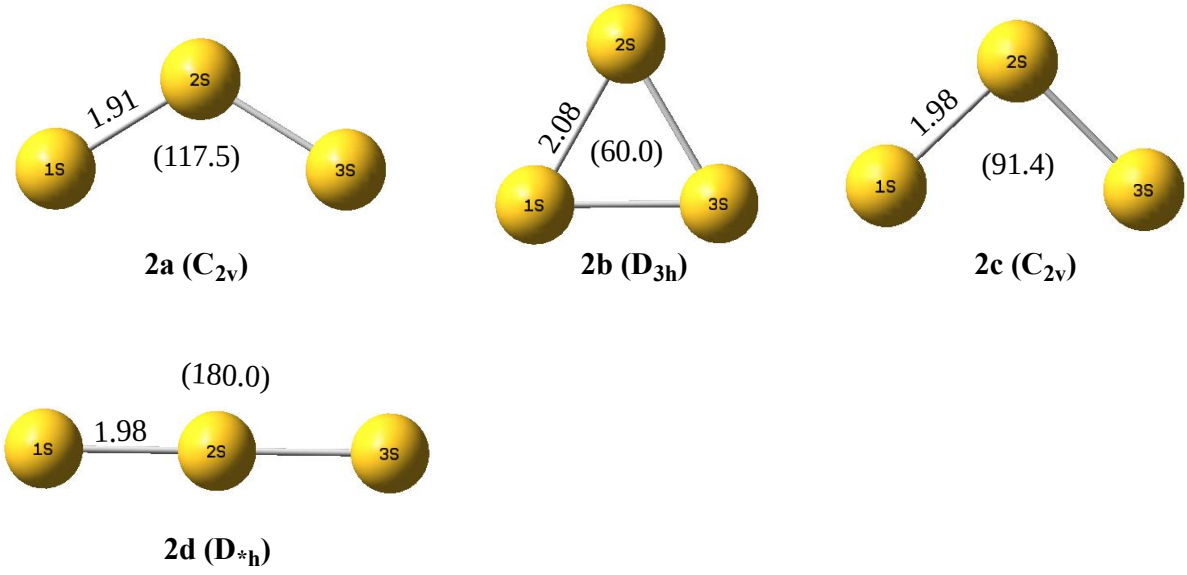

Figure 5.2. Optimised structural isomers of S_3 confirmed as minima: bond lengths are in angstroms (Å) and bond angles, enclosed in brackets, are in degrees (°). **2a** and **2b** are singlet state species while **2c** and **2d** are triplet state S_3 moieties. * stands for ∞.

The singlet structure of the allotrope, **2a**, is known from experiment[296,311,313] and together with **2b** have been reported in high-level theoretical studies.[37,266,274,297,305,306,309,314] However, little or no mention of **2c** and **2d** is made in the literature before now. Nevertheless, a non-minimum singlet state S_3 structure with similar structure to **2d** has been reported in literature from theoretical calculations for the purpose of comparison and discussion[305] and was also found in the present study as a saddle point structure (not shown).

The vibrational frequencies of the S_3 isomers in **Figure 5.2** are summarised in **Table 5.3**.

Table 5.3. The vibrational frequencies of the S_3 isomers in **Figure 5.2**.

Isomer	ω_e / cm^{-1}
2a	257 (a_1), 597 (a_1), 690 (b_2)
2b	449 (b_2), 449 (a_1), 606 (a_1)
2c	212 (a_1), 420 (b_2), 600 (a_1)
2d	202 (π_u), 419 (σ_g), 470 (σ_u), 1199 (π_u)

It is found that the computed bond length for **2a** agrees with that experimentally estimated (1.90 ± 0.05 Å)[296] or determined (1.914 ± 0.002 Å).[313] Its bond angle is also in good agreement with its experimental[313] value (117.33 ± 0.05 °). Furthermore, the calculated geometries of **2a** and **2b** agree with that computed at the CCSD(T)/aug-cc-pV5Z level of theory (S-S = 1.918 and 2.077 Å and S-S-S = 117.4 and 60.0 °, respectively) in the literature.[314] The geometry of **2c** is found to also agree with the structure (S-S = 1.972 Å and S-S-S = 94.3 °) computed at the HF/3-21G* method in the literature.[37] No information on **2d** has been reported in the literature. The calculated vibrational frequencies of **2a** are also found to agree with the harmonic frequencies (256 cm^{-1} (a_1), 585 cm^{-1} (a_1), 681 cm^{-1} (b_1)) calculated[313] at the CCSD(T)/cc-pVTZ level of theory.

A summary of the energies of the isomers of S_3 in **Figure 5.2** relative to the energetically most stable isomer of the allotrope (**2a**) is presented in **Table 5.4**.

Table 5.4. The energies (electronic, ΔE, enthalpy, ΔH and Gibbs free energy, ΔG) of the minimum S_3 isomers relative to the energies of **2a** computed at the CCSD(T)/aug-cc-pVTZ//ωB97XD/6-311++G(2df,2p) level of theory. The electronic energy of **2a** is computed as -1193.2044775 a.u.

Species	Spin state*	ΔE / kJ mol^{-1}	ΔH / kJ mol^{-1}	ΔG / kJ mol^{-1}
2a	S	0.0	0.0	0.0
2b	S	16.1	15.9	19.1
2c	T	81.2	81.8	77.6
2d	T	237.7	237.4	241.8

*S stands for singlet and T for triplet.

The results presented in **Table 5.4** indicate that although the singlet open chain **2a** structure of S_3 is the global minimum in agreement with experiment,[311,313] its singlet cyclic **2b** and triplet **2c** conformers may also be thermally accessible. It is observed that the computed ΔG of **2b** to **2a** agrees with previously computed values (18.8, 19.7 and 20.1 kJ mol^{-1}) at the CCSD(T)/aug-cc-pV*x*Z (*x* = T, Q and 5) levels of theory.[314] Furthermore, Raghavachari et al.,[37] computed the relative energy (ΔE) of **2c** to **2a** at the QCISD(T)/6-31G* level of theory as 80.8 kJ mol^{-1}. The information presented here is therefore important as the triplet bent (**2c**) and singlet cyclic (**2b**) structures of S_3 are yet to be experimentally established. It is worth noting that the triplet linear (**2d**)

structure of S_3 may also be thermally accessed but at greater energetic cost compared to the triplet bent (**2c**) and singlet cyclic (**2b**) structures of the species.

5.3.1.3 S_n (n = 4)

This is the most theoretically studied allotrope of sulfur in the literature. The most comprehensive high-level theoretical studies of the structure and stability of S_4 in the literature are those of Wong and Steudel,[310] Matus et al.,[265] and Ramírez-Solís et al.[251] The geometric structure of the singlet C_{2v} ground state of the species has been experimentally established.[313] The optimised minimum geometries of S_4 in the present study are presented in **Figure 5.3**.

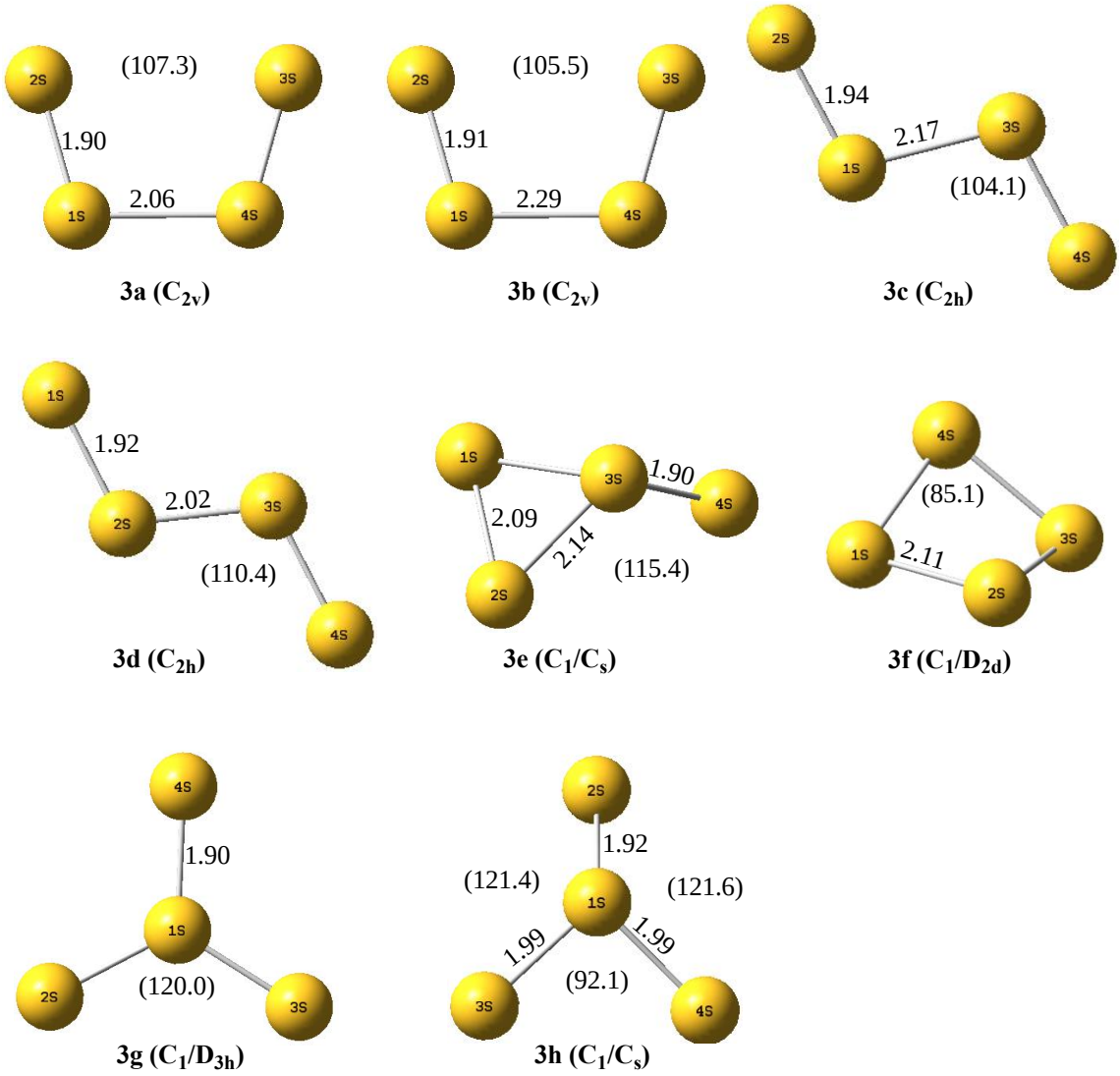

Figure 5.3. The optimised structural isomers of S_4 confirmed as minima: bond lengths are given in angstroms (Å) and bond angles, enclosed in brackets, are given in degrees (°). **3a** and **3d**-**3g** are singlet state S_4 isomers while **3b**, **3c**, and **3h** are triplet state structures of S_4. The ordering of the structures is based on their stabilities (discussed in **Section 5.3.2**)

The 2S-1S bond length of **3a** agrees with experiment (1.898 ± 0.005 Å)[313] while its 1S-4S bond is shorter than the experimental value (2.155 ± 0.01 Å)[313] by 0.09 Å. Nevertheless, the latter bond is found to agree with the geometry of the structure (2.083 Å) computed at the QCISD/cc-pVTZ level of theory.[310] Also, the calculated geometries of other structural isomers of S_4 e.g., **3b**-**3g** are found to agree very well with their geometries computed at the QCISD/cc-pVTZ level of theory.[310] No data on the structure of **3h** is found in the previous literature. The calculated vibrational frequencies of the S_4 structures in **Figure 5.3** are summarised in **Table 5.5**. The calculated vibrational frequencies of **3a** are found to agree very well with those computed[265] using the CCSD(T)/aug-cc-pVTZ, CCSD(T)/aug-cc-pV(T+d)Z and the CASSCF/aug-cc-pV(T+d)Z.

Table 5.5. The vibrational frequencies of the S_4 isomers in **Figure 5.3**.

Isomer	ω_e / cm^{-1}
3a	123 (a_1), 210 (a_2), 328 (b_2), 420 (a_1), 630 (b_2), 663 (a_1)
3b	21 (a_2), 118 (a_1), 265 (b_2), 278 (a_1), 628 (b_2), 641 (a_1)
3c	24 (a_u), 99 (b_u), 195 (a_g), 434 (a_g), 595 (b_u), 604 (a_g)
3d	86 (a_u), 126 (b_u), 237 (a_g), 514 (a_g), 614 (b_u), 639 (a_g)
3e	171 (a), 217 (a), 334 (a), 403 (a), 555 (a), 640 (a)
3f	195 (a), 294 (a), 443 (a), 443 (a), 468 (a), 520 (a)
3g	236 (a), 236 (a), 258 (a), 470 (a), 695 (a), 698 (a)
3h	178 (a), 182 (a), 221 (a), 454 (a), 476 (a), 630 (a)

The optimised structures of the first-order saddle-points of S_4 are presented in **Figure 5.4**.

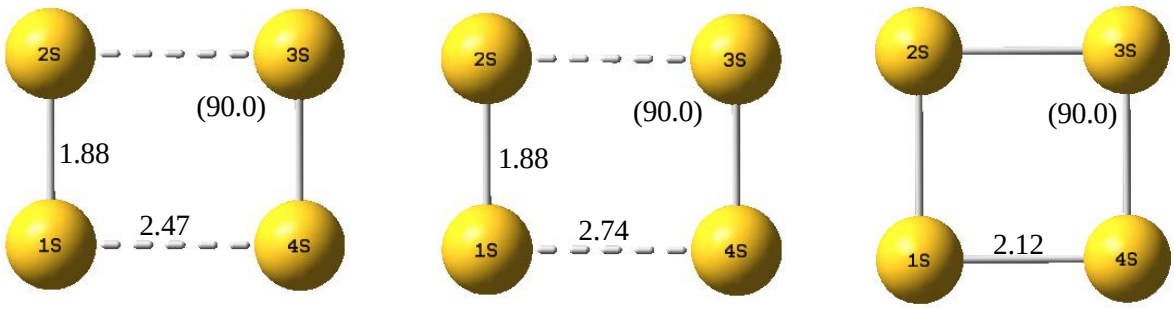

4a (D_{2h}) **4b (D_{2h})** **4c (Cs/D_{4h})**

Figure 5.4. Optimised geometries of the first-order saddle-points of S_4: bond lengths are given in angstroms (Å) and bond angles, enclosed in brackets, are in degrees (°). **4a** and **4c** are singlet state while **4b** is a triplet state species.

4a and **4c** are computed to be connected to isomers with similar structures as **3a** and **3f** (differing only in the connection or position of their atoms), respectively on their adjacent sides. **4b** on the other hand is found to be connected to isomers with similar structures as **3b** (differing only in the connection of their atoms), respectively on its adjacent sides. Contrary to the present calculations, it

is found that **4b** was computed as a minimum structure at the CCSD(T)/aug-cc-pV(T+*d*)Z level of theory.[265] The present calculation of the structure of **4b** at the CCSD/6-311++G(2df,2p) level of theory also optimised as a first-order saddle-point. The geometries of **4a** and **4b** are found to differ by 0.011 to 0.06 Å in comparison to those computed at the CCSD(T)/aug-cc-pV5Z and CCSD(T)/aug-cc-pV(Q+*d*)Z levels of theory.[265] The calculated imaginary frequency modes for **4a**, **4b** and **4c** are 215*i* cm^{-1}, 153*i* cm^{-1} and 162*i* cm^{-1}, respectively. The geometries of singlet and triplet state $D_{\infty h}$ S_4 (not presented) are calculated to be second-order saddle-points.

In the present study, 11 structures (**Figure 5.3** and **Figure 5.4**) of the species have been computed. Three of these are transition structures (**4a**-**4c**) and eight are minimum structures (**3a**-**3h**). The structures are ranked on the basis of their nature (minimum or transition state structures) and Gibbs free energies. It is found that the singlet C_{2v} structure of the species is the global minimum in agreement with experiment.[313] The relative energies of the optimised structures of S_4 are summarised in **Table 5.6**.

Table 5.6. The energies (electronic, ΔE, enthalpy, ΔH and Gibbs free energy, ΔG) of S_4 structures relative to the energy of **3a** computed at the CCSD(T)/aug-cc-pVTZ//ωB97XD/6-311++G(2df,2p) level of theory. The electronic energy of **3a** is computed as -1590.9537159 a.u.

Nature	Species	Spin state	ΔE / kJ mol^{-1}	ΔH / kJ mol^{-1}	ΔG / kJ mol^{-1}
Min.	**3a**	S	0.0	0.0	0.0
	3b	T	35.2	36.8	26.9
	3c	T	42.8	44.4	34.8
	3d	S	36.4	37.1	35.0
	3e	S	54.7	54.6	53.7
	3f	S	56.2	55.6	56.2
	3g	S	108.8	108.2	107.8
	3h	S	195.6	196.1	190.8
TS	**4a**	S	5.4	3.7	9.3
	4b	T	30.6	30.1	29.2
	4c	S	85.9	83.8	87.0

Min. and TS denotes minimum and transition state, respectively while S stands for singlet and T for triplet.

It is found that a triplet C_{2v} structure of S_4 (**3b**) is the next lowest-energy minimum structure of the species considering its ΔG°_{298} values relative to the singlet C_{2v} isomer (**3a**) of the species. The triplet (**3c**) and singlet (**3d**) C_{2h} isomers of the allotrope are found to lie just above the triplet C_{2v} (**3b**) isomer of the species by 8 kJ mol^{-1}. This indicates that these isomers of S_4 may thermally be accessed given that all the structures lie within $\Delta G^{\circ}_{298} \approx 40$ kJ mol^{-1} of the ground state. The cyclic isomers of the species (**3e** and **3f**) may also be accessed with similar but higher energetic costs

(ΔG°_{298} ≈ 55 kJ mol^{-1}) compared to **3b**-**3d** (ΔG°_{298} ≈ 30 kJ mol^{-1}) from **3a**. Likewise, **3g** and **3h** are high-energetic (ΔG°_{298} > 100 kJ mol^{-1}) isomers of the species relative to **3a**. The transition structure, **4a**, is determined to be just ΔG°_{298} = 9.3 kJ mol^{-1} (or ΔE°_{298}= 5.4 kJ mol^{-1}) above **3a** in perfect agreement with previous calculations at the CCSD(T)/aug-cc-pVTZ level of theory.[265,310] This implies that the energy barrier to inter-conversion between two iso-structural isomers similar in structure with **3a** is not significant. This is also true for inter-conversion between two iso-structural isomers of **3b** via a low-energy transition structure for which the PES is essentially flat, of $\Delta G^{\circ\ddagger}_{298}$ = 2.3 kJ mol^{-1}. The relative energies discussed above for **3b**-**3g** are also found to agree with previous calculations at the CCSD(T)/aug-cc-pVTZ//QCISD/cc-pVTZ level of theory.[310] **3h** however, has not been reported in the literature before now. The relative energy (ΔE°_{298}) of **4c** on the other hand was computed previously at the QCISD(T)/6-31G* level of theory to be 96 kJ mol^{-1}. The present calculations differ from this energy for **4c** with a smaller basis set by 10 kJ mol^{-1}. Inter-conversion between two iso-structural isomers similar in structure to **3f** via this transition state structure will therefore, encounter an energy barrier of $\Delta G^{\circ\ddagger}_{298}$ = 30.8 kJ mol^{-1}.

5.3.1.4 S_n (n = 5)

The optimised minimum structures of S_5 are presented in **Figure 5.5**.

The experimental structure of this sulfur allotrope is yet to be published. Nevertheless, it is predicted from the experimental observations of Berkowitz et al.,[287,292] that the cyclic conformer of the species is the most stable isomer of the species. It is found that **5a** is a non-planar ring structure with C_s symmetry. The bond angles of the ring are: 1S-2S-3S = 99.2 °, 5S-1S-2S = 101.5 ° and 2S-3S-4S = 91.6 ° while its dihedral angles are 5S-1S-2S-3S = 39.3 °, 2S-1S-5S-4S = 0.0 ° and 2S-3S-4S-5S = 63.0 °.

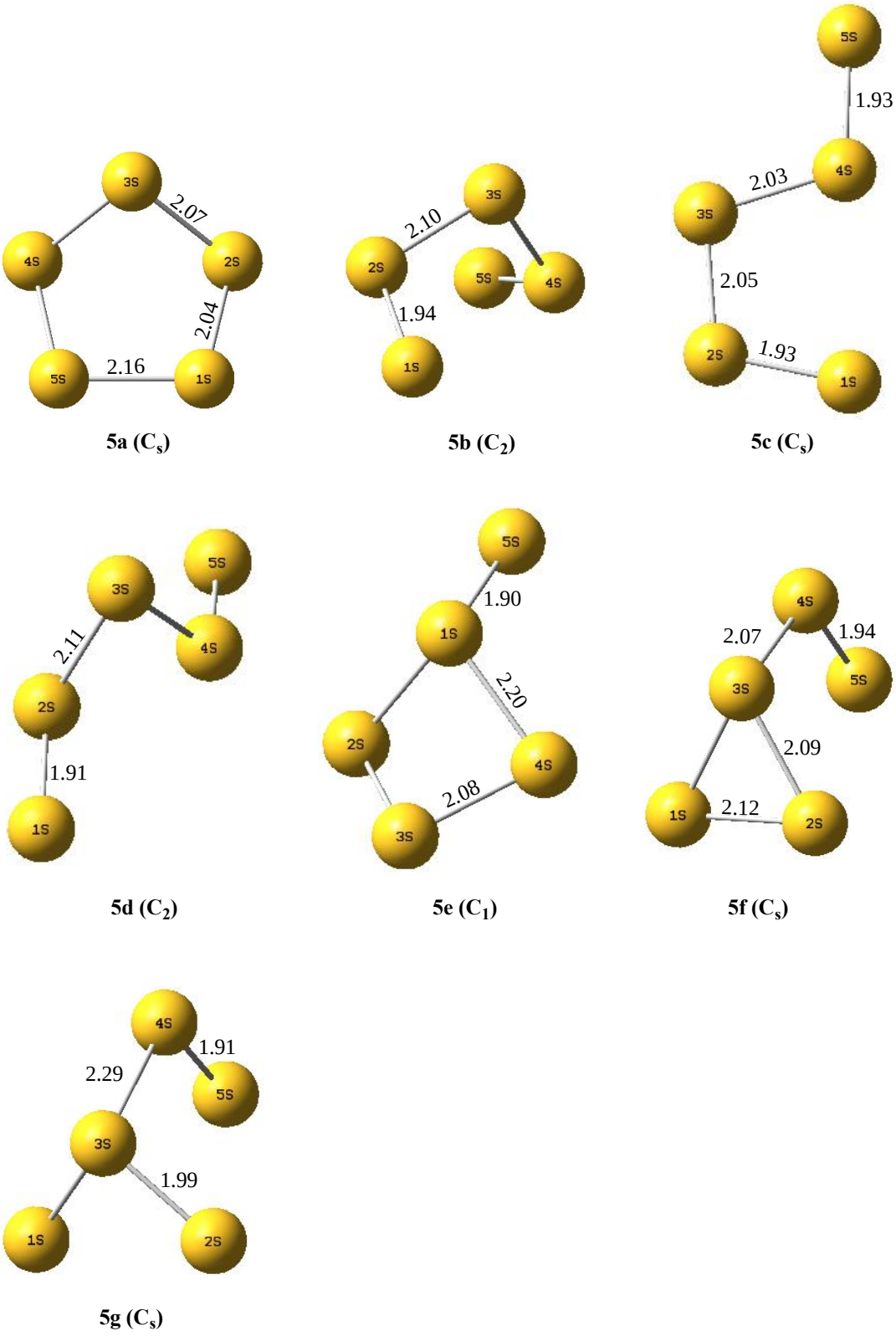

Figure 5.5. The confirmed minimum energy geometries of S_5: bond lengths are given in angstroms (Å). **5a** and **5c**-**5f** are singlet state whereas **5b** and **5g** are triplet state isomers.

In addition, the molecular graph of **5a** with the values of the $\rho(\boldsymbol{r})$ and $\nabla^2\rho(\boldsymbol{r})$ in a.u. at the bcp's and rcp is:

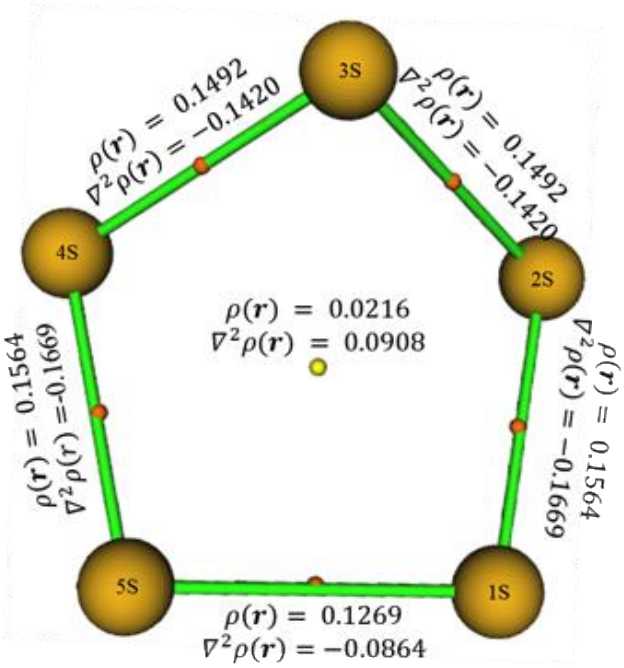

The computed values of the $\rho(\boldsymbol{r})$ and $\nabla^2\rho(\boldsymbol{r})$ at the bcp's (orange dots) and rcp (yellow dot) for this structure (**5a**) suggest that the electron density in the system is concentrated at the bcp's and is slightly delocalised over the ring. Furthermore, the bonds (solid green lines) in the system are all of covalent nature (all have $\nabla^2\rho(\boldsymbol{r}) < 0$)[134,138] and their strength and hence, bond length vary with the values of the $\rho(\boldsymbol{r})$; the higher the value of $\rho(\boldsymbol{r})$, the shorter the bond length.

A summary of the vibrational frequencies of the isomers of S_5 in **Figure 5.5** is presented in **Table 5.7** while the bond and dihedral angles of **5b**-**5g** are summarised in **Table A.1.2**.

Table 5.7. Calculated vibrational frequencies of the S_5 isomers in **Figure 5.5**.

Isomer	ω_e / cm^{-1}
5a	62 (a''), 231 (a'), 283 (a'), 285 (a''), 387 (a''), 390 (a'), 435 (a'), 505 (a'), 511 (a')
5b	27 (a), 50 (b), 125 (a), 223 (b), 229 (a), 399 (b), 428 (a), 574 (b), 578 (a)
5c	51 (a''), 120 (a'), 163 (a''), 180 (a'), 280 (a'), 452 (a'), 490 (a'), 585 (a'), 611 (a')
5d	87 (a), 97 (b), 186 (a), 229 (b), 313 (a), 367 (b), 495 (a), 623 (b), 653 (a)
5e	102 (a), 130 (a), 239 (a), 278 (a), 372 (a), 376 (a), 461 (a), 514 (a), 650 (a)
5f	45 (a''), 94 (a'), 185 (a''), 289 (a'), 290 (a''), 339 (a'), 448 (a'), 553 (a'), 588 (a')
5g	15 (a''), 113 (a'), 151 (a''), 208 (a'), 261 (a'), 285 (a'), 477 (a''), 562 (a'), 631 (a')

The optimised structures of the first-order saddle-points of S_5 are presented in **Figure 5.6**. These transition structures are found to possess similar imaginary vibrational frequencies namely: 66i cm^{-1} and 64i cm^{-1}, respectively.

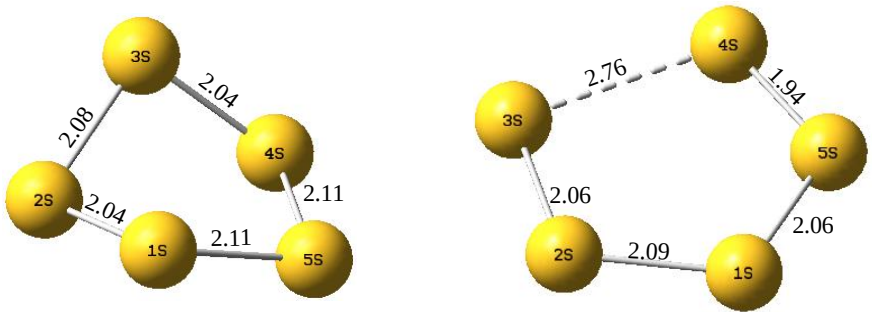

6a (C_2) **6b (C_s)**

Figure 5.6. Optimised geometries of the first-order saddle-points of S_5: bond lengths are given in angstroms (Å). **6a** is a singlet transition state while **6b** is a triplet transition state of S_5.

The structure of the most stable isomer of S_5 has not been experimentally established. The global minimum structure of the species is computed to be its cyclic C_s structure (**5a**, **Figure 5.5**) with singlet ground state in agreement with previous theoretical[37,305,309] studies. The computed energies of the structures of S_5 (**Figure 5.5** and **Figure 5.6**) relative to its energetically most stable conformer (**5a**) are presented in **Table 5.8**.

Table 5.8. The energies (electronic, ΔE, enthalpy, ΔH and Gibbs free energy, ΔG) of the structures of S_5 relative to the energy of its most stable structure, **5a** computed at the CCSD(T)/aug-cc-pVTZ//ωB97XD/6-311++G(2df,2p) level of theory.

Nature	Species	Spin state	ΔE / kJ mol^{-1}	ΔH / kJ mol^{-1}	ΔG / kJ mol^{-1}
Min.	**5a**	S	0.0	0.0	0.0
	5b	T	96.2	98.4	87.5
	5c	S	114.7	115.9	111.2
	5d	S	125.3	126.1	124.9
	5e	S	131.3	131.5	131.0
	5f	S	184.5	185.8	181.1
	5g	T	189.2	191.2	179.8
TS	**6a**	S	1.0	-1.2	6.0
	6b	T	223.9	222.4	222.6

Min. and TS denotes minimum and transition state, respectively while S stands for singlet and T for triplet.

The structures of S_5 (**Figure 5.5** and **Figure 5.6**) are also ranked on the basis of their nature (minimum or transition structures) and Gibbs free energies in **Table 5.8**. The iso-energetic structures, **5b** and **5c**, are computed as the next lowest-energy ($\Delta G^{\circ}_{298} \approx 86$ kJ mol^{-1} less stable than **5a**) minimum structures of S_5. All other minimum geometries of S_5 (**Table 5.9**, **Figure 5.5**) are significantly ($\Delta G^{\circ}_{298} > 100$ kJ mol^{-1}) less stable than its global minimum structure, **5a**. It is observed that the triplet open chain S_5 species (**5b**) is thermodynamically more stable than its singlet state

counterpart (**5d**) by ΔG°_{298} = 23.7 kJ mol^{-1}. In addition, it is found that the transition structure, **6a**, is essentially iso-energetic with **5a** (ΔG°_{298} = 6.0 kJ mol^{-1} or ΔE°_{298}= 1.0 kJ mol^{-1} above **5a**). All other structures (first or higher-order saddle-points) of S_5 are calculated to lie within $113 \leq \Delta G^{\circ}_{298} \leq 464$ kJ mol^{-1} above **5a**.

It is clear from the structural and energetic information discussed so far that S_5 is the first allotrope of sulfur to form a global minimum cyclic structure, even though the possibility of thermally accessing a local minimum cyclic structure exists for S_3 and S_4.

5.3.1.5 S_n (n = 8)

This is asserted to be the most common and abundant allotrope of sulfur[12,268–270,275,298] in the solid, liquid and gaseous state. The allotrope is established from experiments[275,298] to have a singlet ground state and a cyclic D_{4d} (crown-shaped) structure. Nevertheless, other cyclic structures of the species have been suggested to exist from theoretical studies.[307] Also, it is believed that the reactivity of the open chain species formed by this sulfur allotrope are responsible for the sudden change in the viscosity of liquid sulfur at 159 °C.[275,277] Furthermore, the open chains of this species are implicated in the paramagnetism of liquid sulfur but the structure of the species giving rise to this phenomenon still unknown. Consequently, the structures of some cyclic and open chain isomers of neutral S_8 in the singlet and triplet state have been computed.

The optimised singlet state minimum cyclic structures of S_8 are presented in **Figure 5.7**.

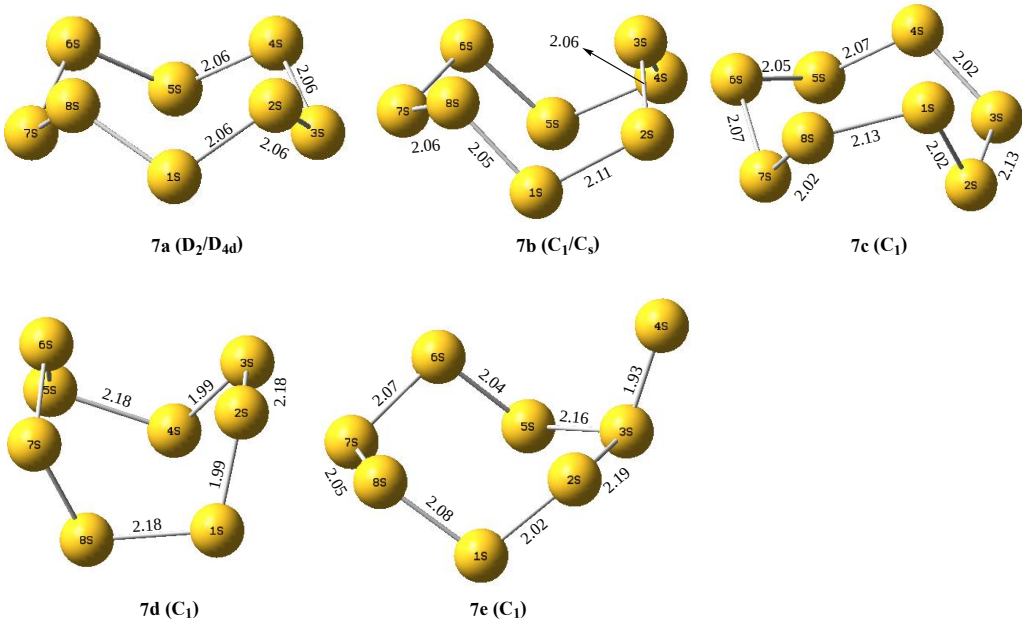

Figure 5.7. Optimised minimum energy geometries of the cyclic isomers of S_8: bond lengths are given in angstroms (Å). All these cyclic structures are singlet state species.

No triplet ground state minimum cyclic structure was found in the present study. These structures of S_8 have also been calculated previously at the B3LYP/6-31G(2df) level of theory.[308] However, the average experimental S-S bond length (2.055 ± 0.002 Å)[298] of **7a** is found to be reproduced excellently (2.06 Å) in the present study compared to previous calculation of the parameter (2.08 Å).[308] Also, an MP2/6-311G* calculation of the structure yielded an S-S bond length of 2.075 Å.[307] The optimised bond angle θ(SSS) = 107.8 ° and dihedral angle τ(SSSS) = 99.0 °) of **7a** are also within ± 0.5 ° of experiment (108.2 ± 0.6 and 98.5 ± 0.2 °, respectively).[298] It is found that the computed bond lengths of **7b**-**7e** are generally within 0.013 to 0.129 Å of the values computed with B3LYP/6-31G(2df) for similar structures of S_8 reported.[308]

Seven minimum open chain isomers of S_8 were computed. Four of the isomers are triplet spin species and three are singlet spin species. The optimised geometrical structures of open chain minima of S_8 are presented in **Figure 5.8**.

A singlet state open chain structure similar to triplet state isomer **8b** in **Figure 5.8** has been reported[308] in the literature from B3LYP/6-31G(2df) calculations but was not found in the present investigation. The singlet state structure **8e** was found instead. Also, an open chain isomer of S_8 similar in structure to **8c** and **8f** was reported as the immediate product of S_8 ring rupture from a combined DFT and MD simulation of the process after 263 fs.[304] However, neither the spin state nor the structural parameters of the species were specified. As may be seen in **Figure 5.8**, the structures of **8b** and **8e**, **8c** and **8f** and **8d** and **8g** are similar, even though each structure in each pair of similar structures possess different spin states.

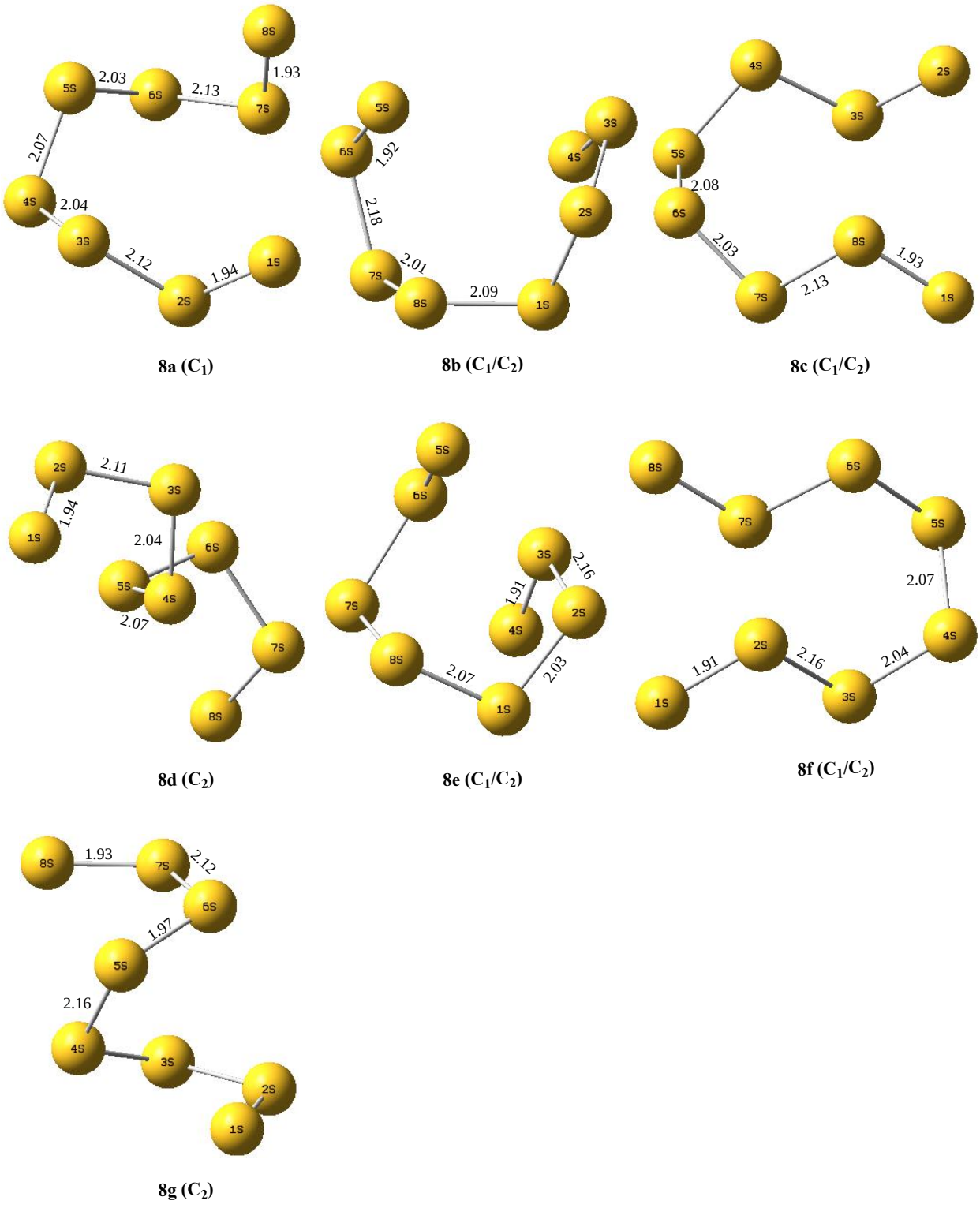

Figure 5.8. Optimised minimum energy geometries of the triplet (**8a**-**8d**) and singlet (**8e**-**8g**) state open chain isomers of S_8: bond lengths are given in angstroms (Å).

Two cyclic transition structures of S_8, presented in **Figure 5.9**, were also found in the triplet state.

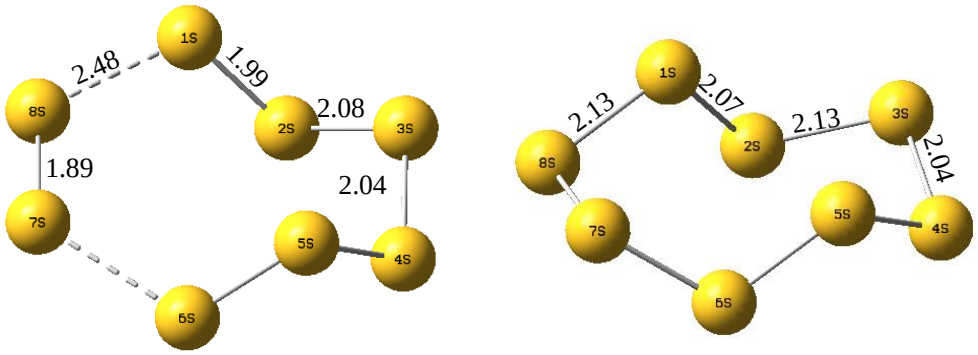

9a (C_2) **9b (D_2)**

Figure 5.9. Optimised geometries of the triplet state first-order saddle-points of S_8. Bond lengths are given in angstroms (Å).

The imaginary vibrational frequencies of **9a** and **9b** are calculated as 326*i* cm^{-1} and 192*i* cm^{-1}, respectively. The linear ($D_{\infty h}$) structures of S_8 (not shown) were calculated to be fifth and sixth-order saddle-points with triplet and singlet spin states, respectively.

The structure of the most stable isomer of S_8 is widely believed[305,308,309] and has been experimentally established[298] as the singlet ground state cyclic structure, **7a** (**Figure 5.7**). This structure is also found to be the global minimum structure of the species in the present calculations. The computed energies of S_8 structures (**Figure 5.7**, **Figure 5.8** and **Figure 5.9**) relative to **7a** are presented in **Table 5.9**. The structures are also ranked in a similar fashion as with structures of S_4 and S_5. It is observed that **7b** and **7c** are found to possess a similar energy (ΔG°_{298} = 33 ± 1 kJ mol^{-1}) above **7a** even though their geometries are not similar (see **Figure 5.7**). Wong et al.,[308] asserted that the next local minimum cyclic structures of S_8, **7b** and **7c** were ΔG°_{298} = 28 and 30 kJ mol^{-1}, respectively above **7a** at the G3X (MP2) level of theory. The present result is in good agreement with these literature values. **7d** and **7e** (**Table 5.10**, **Figure 5.7**) on the other hand, are ΔG°_{298} > 60.0 kJ mol^{-1} less stable than **7a** in contrast to the stability of the species in the same report,[308] wherein their stabilities relative to **7a** is underestimated by 23.6 and 17.5 kJ mol^{-1}, respectively in comparison to the present work. This is likely due to the varying degree of electron correlation accounted for in the methodologies adopted in the literature[308] computations. The present results suggest that the cyclic conformers of S_8 may be thermally accessible in sulfur vapour or sulfur melts as it is widely believed.[275,307] The minimum triplet open chain isomers of S_8 (**8a-8d**, **Figure 5.8**) are found to be essentially iso-energetically less stable (ΔG°_{298} = 139 ± 3 kJ mol^{-1}) than **7a** while the minimum singlet open chain isomers of S_8 (**8e-8g**, **Figure 5.8**) are at least ΔG°_{298} = 155 kJ mol^{-1} above **7a**. It is found that **8e** and **8f** have similar energies (only differing by ΔG°_{298} = 8 kJ mol^{-1}).

Table 5.9. The energies (electronic, ΔE, enthalpy, ΔH and Gibbs free energy, ΔG) of the structures of S_8 relative to the energy of its most stable structure, **7a** computed at the CCSD(T)/aug-cc-pVTZ//ωB97XD/6-311++G(2df,2p) level of theory.

Nature	Species	Spin state	ΔE / kJ mol^{-1}	ΔH / kJ mol^{-1}	ΔG / kJ mol^{-1}
Min.	**7a**	S	0.0	0.0	0.0
	7b	S	35.5	35.7	32.1
	7c	S	39.0	39.4	34.0
	7d	S	69.1	69.4	64.7
	7e	S	105.5	105.8	100.0
	8a	T	152.9	155.9	136.3
	8b	T	155.6	158.9	136.8
	8c	T	158.6	162.2	136.8
	8d	T	162.6	166.1	142.2
	8e	S	157.3	157.4	154.8
	8f	S	169.2	170.1	163.1
	8g	S	205.1	206.6	200.6
TS	**9a**	T	228.6	230.4	216.1
	9b	T	273.0	274.4	265.3

Min. and TS denotes minimum and transition state, respectively while S stands for singlet and T for triplet. **7a** to **7e** are cyclic structures, **8a** to **8g** are open chain structures.

This suggests that both structures of the species may be accessible from **7a** given ΔG°_{298} = 158 ± 5 kJ mol^{-1} via a possible spin-flip mechanism. A comparison of the stabilities of the open chain isomers of S_8 gives the $\Delta G^{\circ}_{ST,298}$ = 18.0 kJ mol^{-1} between **8b** and **8e** and $\Delta G^{\circ}_{ST,298}$ = 26.3 kJ mol^{-1} between **8c** and **8f**. A similar structure to **8c** and **8f** was reported as the immediate products of S_8 ring rupture from DFT-MD simulation of the process after 263 fs.[304] The information in **Table 5.10** therefore suggests that **7a** requires, on average, at least ΔG°_{298} = 158 ± 5 kJ mol^{-1} to rupture to an open chain structure on the singlet PES from which the more stable triplet analogue may be accessed via a favourable spin-flip. These observations may be true as it is widely believed that sulfur melts at 120 °C[277,279] leading to the formation of other ringed structures or open chain species and polymeric structures between 120 and 159 °C.[277–279,284,291] **9a** and **9b** are found to lie at ΔG°_{298} > 200 kJ mol^{-1} above **7a**.

5.3.2 Ring Opening Reaction of S_n (n = 5 and 8): Implications for Liquid Sulfur

The computed singlet PES for the ring opening reaction of S_5 and S_8 are presented in **Figure 5.10** and **5.11**, respectively.

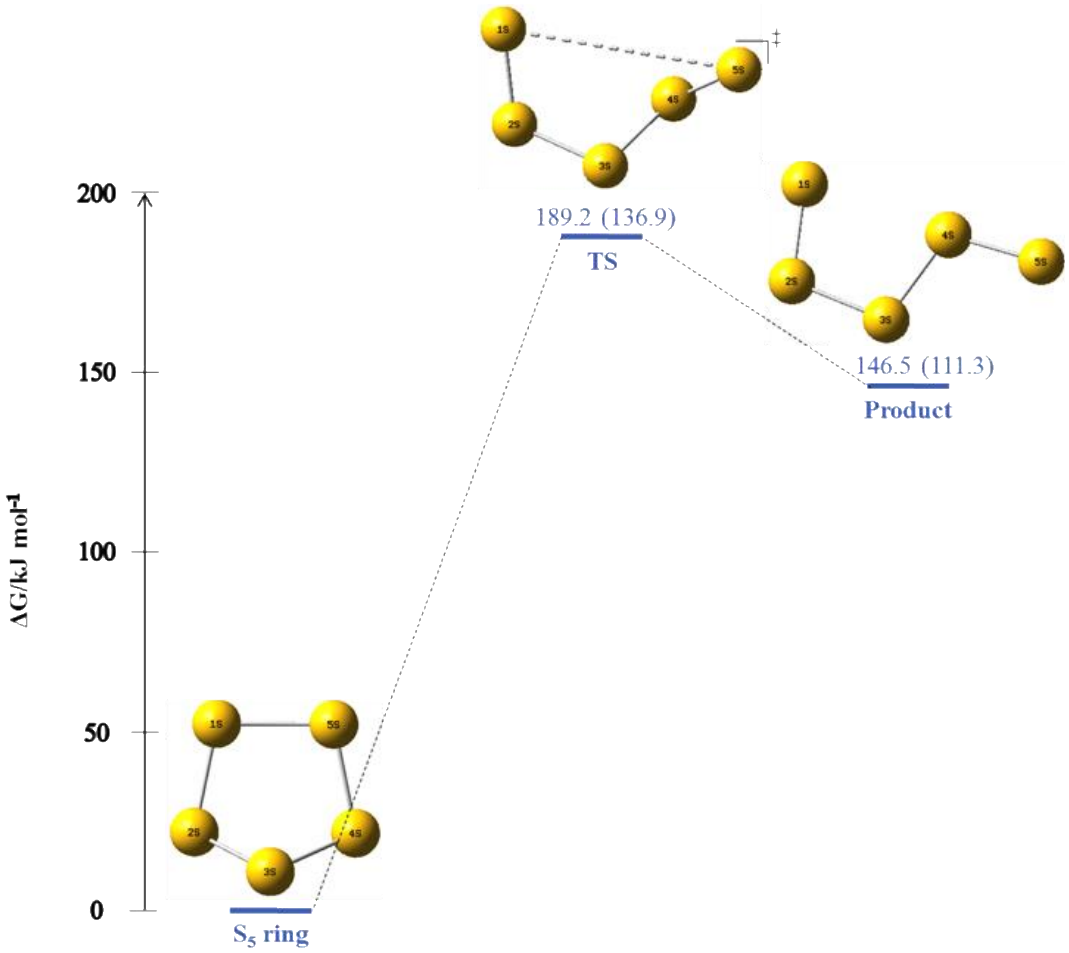

Figure 5.10. The singlet PES of the ring opening reaction of S_5. The free energies are obtained from geometry optimisation at ωB97XD/6-311++G(2df,2p) and SPE calculation (in brackets) at the CCSD(T)/aug-cc-pVTZ//ωB97XD/6-311++G(2df,2p) level of theory.

It is found that for both structures, S_5 and S_8, the ring opens to one of their computed open chain conformers (**5d** for S_5 and **8f** for S_8) in the preceding sections on the singlet PES.

The result in **Figure 5.10** indicates that the ring opening reaction of the cyclic structure of S_5 (**5a**) is an endergonic (uphill, ΔG°_{298} = 110 kJ mol^{-1}) process with an activation energy barrier of ΔG°_{298} = 137 kJ mol^{-1}. This suggests that the ring will likely persist even above the melting point of sulfur (120 °C). Nevertheless, once the structure is ruptured, the product will undergo a possible spin flip process to the more stable triplet open chain structure, **5b** or **5c**. Spin flip processes are asserted to be achievable through thermally activated delayed fluorescence especially for systems with small singlet-triplet energy gaps or via spin-orbital coupling.[318] In the same vein, spin flip is asserted to be favoured by heating that results from increasing temperature.[319] It is found that the singlet-triplet energy gap between **5d** and **5b** or **5c** is $\Delta G^{\circ}_{ST,298} \leq 25$ kJ mol^{-1}. It is therefore reckoned that a spin flip may be possible after ring rupture of **5a**.

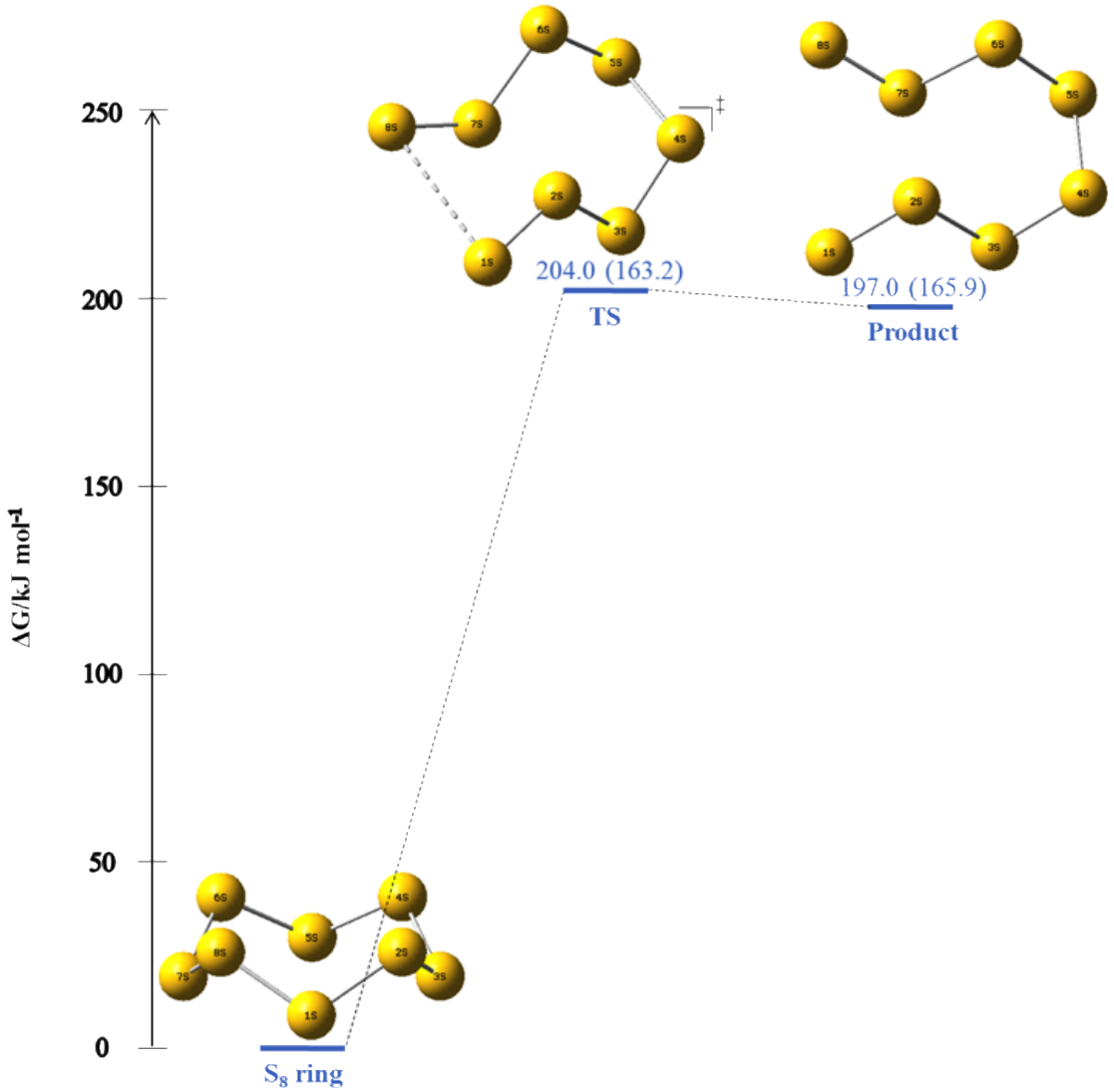

Figure 5.11. The singlet PES of the ring opening reaction of S_8. The free energies are obtained from geometry optimisation at ωB97XD/6-311++G(2df,2p) and SPE calculation (in brackets) at the CCSD(T)/aug-cc-pVTZ//ωB97XD/6-311++G(2df,2p) level of theory.

The PES for the S_8 ring opening process is observed to be essentially flat between the ring opening transition state and product of the process (**Figure 5.11**), which lie ΔG°_{298} < 8 kJ mol^{-1} apart at both levels of theory. Nevertheless, the initial ring opening barrier > 200 (or 160) kJ mol^{-1}. This suggests that the ring structure will persist even at high energies and most likely provides explanation to the assertions that it is the most stable structure in the gaseous, liquid and solid states.[275,291,320,321] As discussed above, the triplet open chain isomers of both allotropes are more stable relative to their global minimum structures compared to their singlet open chain analogues and by extension, the ring opening transition states on this PES. As sulfur melts at 120 °C[277,279] producing ringed and/or open chain structures which undergo polymerisation between 120 and 159°C,[277–279,284,291] the

results of these calculations indicate further that the thermal accessibility of both singlet and triplet open chain structures of S_5 and S_8 (**Figure 5.5** and **5.8**) is possible. Furthermore, it is found that the computed relative enthalpy for the open chain S_8 triplet species (**8c)** from singlet cyclic S_8 (**7a**), is ΔH°_{298} = 162 kJ mol^{-1} while that of the open chain S_8 singlet species (**8f)** is ΔH°_{298} = 170 kJ mol^{-1} (**Table 5.9**). This suggests greater stability for the triplet species (**8c**) compared to its singlet state analogue (**8f**) even though their enthalpies from **7a** are similar, differing only by 8 kJ mol^{-1}. As such, **8c** and **8f** may both be thermally accessible from **7a** given ΔH°_{298} = 165 ± 5 kJ mol^{-1}. The computed enthalpy for the triplet species, **8c** is found to agree better with the enthalpy of formation of radical sulfur species (154.4 ± 1.7 kJ mol^{-1})[322] determined from temperature dependent ESR measurements between 153 ≤ T ≤ 700 °C. Experiments such as this are reported to be spin state dependent.[240] The ring opening reaction together with the structure and stability analysis above provides a possible explanation for the paramagnetic behaviour and structural information of the species responsible for this behaviour in liquid sulfur. This is because the product of ring rupture, especially for S_8, can exist in both triplet (**8c**) and singlet (**8f**) spin states (**Figure 5.8**). The ring opening process as computed for S_8 correlates very well with the DFT-MD simulation[302,304] of the process. The authors however suggested that it was unlikely for the ring structure to reconstruct from the resulting open chain structure in the process. They went on to state that the formation of a tadpole species similar in structure to **8e** (**Figure 5.8**) was more likely from the chain structure[304] contrary to the present finding. No information is available in the literature about the ring opening reaction of S_5 for comparative purposes.

The structures of the transition states for ring rupture of S_5 and S_8 are presented in **Figure 5.12** and the imaginary vibrational frequencies of the species are 103*i* cm^{-1} and 109*i* cm^{-1}, respectively.

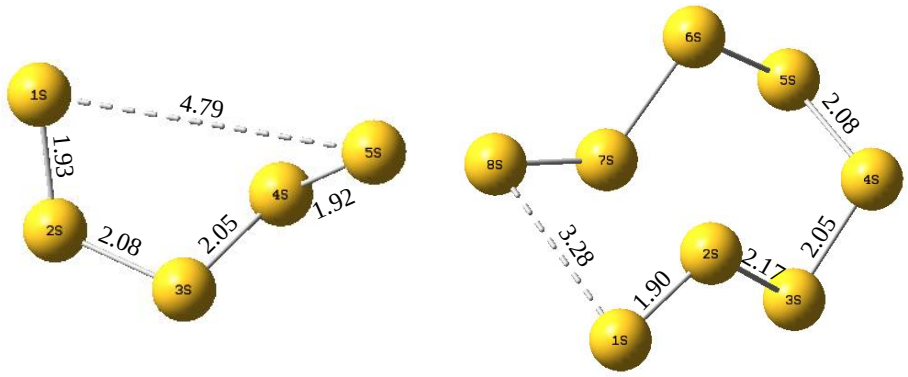

Figure 5.12. Optimised geometries of the singlet state first-order saddle-points of S_5 and S_8 ring rupture: bond lengths are given in angstroms (Å).

It is observed that the structure of the ring opening transition state for S_8 is similar to the product of the process for the species. The only significant difference between the structures is the bond distance between the atoms undergoing bond breaking to form the open chain S_8 species. This distance (1S-8S) is longer in the open chain S_8 produced in the process by 0.6 Å compared to the same bond distance in the transition structure. The transition structure for the ring opening process of S_5 is not planar while the product of the process is a planar, C_s structure. Nevertheless, their bond distances, except for 1S-5S, are similar (see structure of ring opening transition state, **Figure 5.12** and **5d**, **Figure 5.5**).

5.3.3 Stability of Low-Energy Singlet and Triplet Open Chains of S_n ($n \leq 5$ and 8)

The stability of low-energy, minimum singlet and triplet state open chain species of S_n ($n \leq 5$ and 8) is presented in **Figure 5.13**.

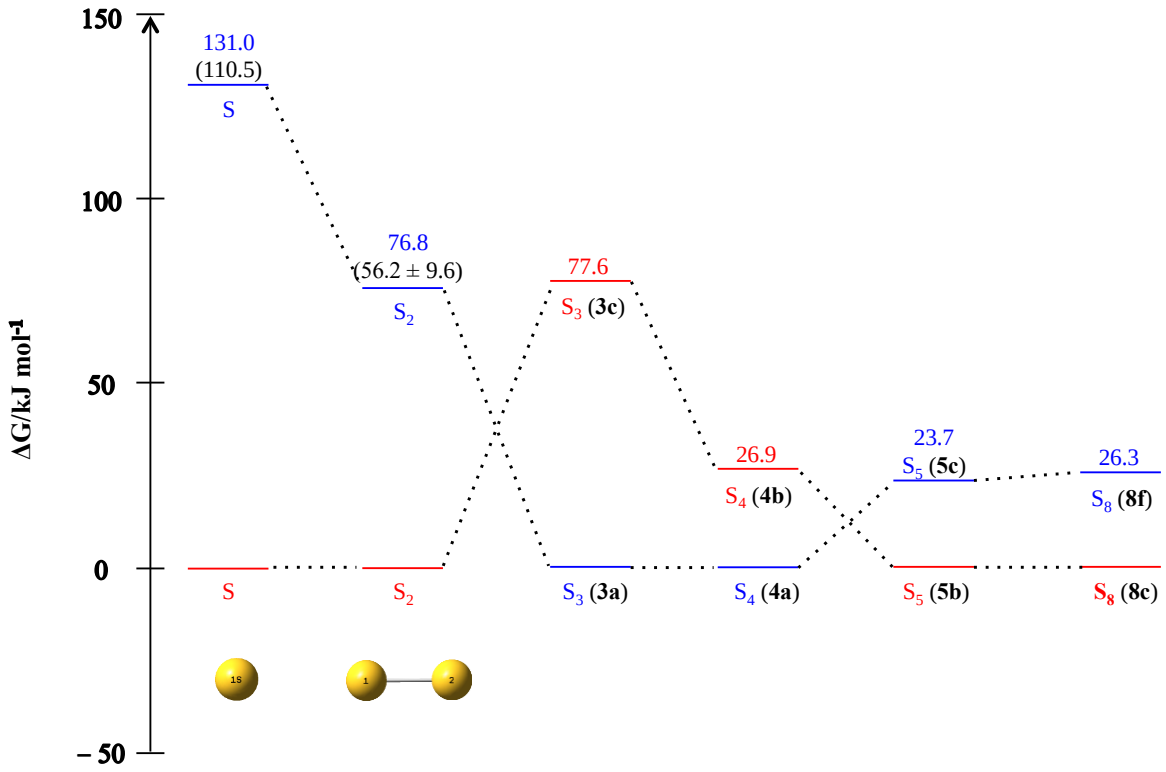

Figure 5.13. The stability of low-energy singlet and triplet state open chain species of S_n ($n \leq 5$ and 8): singlet-triplet energy splitting of the species. Values in brackets are experimentally determined for S[263] and S_2.[261,264]

It is observed that except for S_3 and S_4, all other open chain forms of sulfur considered have a triplet ground state. It is known from experiments[275,287,291,292] that liquid and sulfur vapour comprises sulfur complexes, S_n ($n \leq 10$) which may possess cyclic or open chain structures. It has also been

shown from experiments that all S_n ($n \leq 4$) possess open chain[261,263,313] structures while S_8 is determined to possess a cyclic ground state structure.[298] Information on the stability and structure of the low-energy open chain structures of these species is important, as it is crucial to the understanding of the viscosity behaviour of liquid sulfur, sulfur recovery and reactions in the thermal Claus process. This is because the species are widely believed to be present in liquid sulfur and hence, influencing the paramagnetic and viscosity behaviour[275,277,279] of the liquid and its reactivity with hydrogen sulfide to suppress both behaviours.[14,275,277–279] The results of the present computations show in agreement with experiments that S_n ($n \leq 4$) possess open chain structures while S_8 has a cyclic ground state structure. The results also suggest that excited state open chain forms of the species considered are thermally accessible relative to their ground state structures (cyclic or open chain). The calculations also reveal S_5 to have a cyclic ground state structure with thermally accessible excited state open chain structures. More so, the result in **Figure 5.13** indicates that the interplay of spin states (curve crossing or "two-state reactivity"[323]) is likely to be a key factor in the viscosity behaviour of (reactivity in) liquid sulfur.

5.3.3.1 Broken Symmetry Calclculations on Singlet Open Chains of S_n ($n \leq 5$ and 8)

To further describe the geometries and energetics of the singlet state open chain structures in **Figure 5.13**, broken symmetry (BS) calculations were performed using the UCCSD(T)/aug-cc-pVTZ//UωB97XD/6-311++G(2df,2p) on all the singlet state structures, S_n ($n \leq 5$ and 8) in **Figure 5.13**. The singlet state structure for S_4 and S_5 (similar to **3a** (**Figure 5.3**) and **5c** (**Figure 5.5**)) optimised using the BS-DFT methodology is presented in **Figure 5.14**.

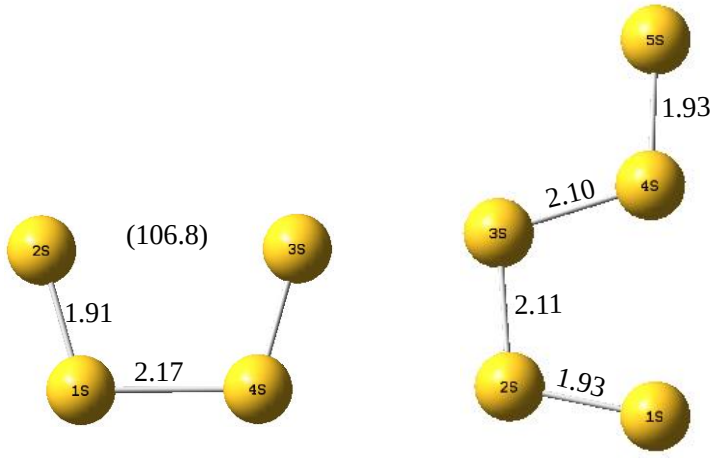

Figure 5.14. The BS-DFT optimised geometry of singlet state S_4 and S_5 confirmed as minima: bond lengths are given in angstroms (Å) and bond angles, enclosed in brackets, are given in degrees (°).

Figure 5.14 suggests that the inner *r*(S-S) for S_4 computed using the BS-DFT is found to be 0.11 Å longer than the same bond computed using the restricted DFT (RDFT-(*ω*B97XD/6-311++G(2df,2p))) approach (**3a**, **Figure 5.3**). This provides better agreement with its experimental value[313] (inner *r*(S-S) = 2.155 ± 0.01 Å) than that for **3a**, **Figure 5.3**. BS-DFT also gives longer inner *r*(S-S) for singlet state open chain S_5. The inner *r*(S-S) of S_5 computed using BS-DFT is found to be 0.07 Å longer than the same structure computed using the RDFT method. For S_2, S_3 and S_8, the BS-DFT geometry and that computed using the restricted DFT (RDFT) are in full agreement.

A comparison of the singlet-triplet energy splitting for the structures in **Figure 5.13** computed using BS and CCSD(T)/aug-cc-pVTZ//*ω*B97XD/6-311++G(2df,2p) is presented in **Table 5.10**.

Table 5.10. The singlet-triplet energies (enthalpy, ΔH_{ST} and Gibbs free energy, ΔG_{ST}) for the open chain S_n ($n \leq 5$ & 8) structures in **Figure 5.13** using CCSD(T)/aug-cc-pVTZ//*ω*B97XD/6-311++G(2df,2p) and BS calculation at UCCSD(T)/aug-cc-pVTZ//U*ω*B97XD/6-311++G(2df,2p) level of theory. Also included are the experimental values for S[263] and S_2.[261,264]

Species	CCSD(T)//RDFT		UCCSD(T)//BS-DFT		**Expt. / kJ mol^{-1}**
	ΔH_{ST} / kJ mol^{-1}	**ΔG_{ST} / kJ mol^{-1}**	**ΔH_{ST} / kJ mol^{-1}**	**ΔG_{ST} / kJ mol^{-1}**	
S	128.2	131.0	38.2	40.9	110.5
S_2	74.1	76.8	25.2	27.9	56.2 ± 9.6
S_3	81.8	77.6	67.6	65.7	
S_4	36.8	26.9	26.8	20.5	
S_5	17.5	23.7	9.0	15.9	
S_8	7.9	26.3	7.9	26.3	

The result summarised in **Table 5.10** suggests that the energy splitting computed using BS calculation is ∼20 kJ mol^{-1} below the experimental error limit for S_2 while the calculation employing CCSD(T)/aug-cc-pVTZ//*ω*B97XD/6-311++G(2df,2p) gives values that are only ∼10 kJ mol^{-1} above the experimental error margin. For longer S_n open chains, it is observed that both CCSD(T)/aug-cc-pVTZ//*ω*B97XD/6-311++G(2df,2p) and BS give energy splitting that are similar; differing by 13 ± 1 kJ mol^{-1} (for S_3), 10 or 6 kJ mol^{-1} (for S_4), ∼8 kJ mol^{-1} (for S_5) or ∼0 kJ mol^{-1} (for S_8). Furthermore, it is found that in all cases, regardless of whether the BS-DFT or RDFT is employed to investigate the singlet state open chain structures, the relative stabilities summarised in **Figure 5.13** remain unchanged. Nevertheless, for S, S_2 and S_5, the singlet state single point/structure computed using BS-DFT is more stable than that using RDFT by 90, 50 and 8 kJ mol^{-1}, respectively. For S_3 and S_4, the BS-DFT structures are computed to be less stable by at most 14 and 10 kJ mol^{-1}, respectively.

It was shown in **4.3.2.2** that singlet states of S and S_2 possessed multi-configurational character. Therefore in addition to the BS calculations, single point CAS(n,m)/6-31G(d)//HF/STO-3G

calculations (using CAS(4,3), CAS(4,5) and full valence (CAS(18,12))) were also performed on the RDFT optimised singlet (**2a** ($^1A_1$) **Figure 5.2**) and triplet (**2c** ($^3A_2$) **Figure 5.2**) state structures of S_3. This is performed to confirm whether thiozone possesses multi-configurational or diradical charater, as ozone (O_3, $^1A_1$ and $^3A_2$), its valence *iso*-electronic system, is known to possess multi-configurational and partial diradical character.[19,324–326] The valence configuration of the singlet ground state S_3 ($^1A_1$) computed using HF/STO-3G is $\ldots 8a_1^2 6b_2^2 9a_1^2 10a_1^2 7b_2^2 3b_1^2 8b_2^2 11a_1^2 2a_2^2$ with the unoccupied orbitals: $4b_1^0 12a_1^0 9b_2^0$. A summary of the CSF's and their contributing weights and configurations making up the total wavefunction of thiozone (S_3) for the CAS(n,m) employed is presented in **Table 5.11**.

Table 5.11. The contributing configuration state function (CSF) with weight (w) ≥ 1 % and electronic configuration in the computed total CAS(n,m)/6-31G(d) wavefunction of thiozone (S_3). In all cases, the UHF/STO-3G canonical orbitals of thiozone are employed. Occupation of the orbitals by single electrons with spin up are denoted α while those with spin down are denoted β.

State	CAS(n,m)	**CSF**	**w / %**	$8a_1$	$6b_2$	$9a_1$	$10a_1$	$7b_2$	$3b_1$	$8b_2$	$11a_1$	$2a_2$	$4b_1$	$12a_1$	$9b_2$
$^1A_1$	(4,3)	1	79.2								2	2	0		
		6	11.1								0	2	2		
		4	9.7								α	2	β		
	(4,5)	28	87.7								2	0	0	0	2
		1	10.7								2	2	0	0	0
	(18,12)	1	87.1	2	2	2	2	2	2	2	2	2	0	0	0
		21	5.8	2	2	2	2	2	2	2	0	2	0	2	0

State	CAS(n,m)	**CSF**	**w / %**	$8a_1$	$6b_2$	$9a_1$	$3b_1$	$10a_1$	$7b_2$	$11a_1$	$2a_2$	$8b_2$	$4b_1$	$9b_2$	$12a_1$
$^3A_2$	(4,3)	1	100.0								2	α	α		
	(4,5)	1	99.1								2	α	α	0	0
	(18,12)	708	86.9	2	0	2	2	2	2	2	2	α	α	2	0
		497	6.6	2	α	2	2	2	2	2	2	α	0	2	0

The result presented in **Table 5.11** indicates that both states of S_3 investigated possess multi-configurational character on the basis of the contributing CSF weights and electronic configurations in the total CAS(n,m) wavefunction of the systems. The result further suggests that S_3 ($^1A_1$) also possesses a diradical character in addition to its multi-configurational character. In addition, it was found that when the CAS(n,m) calculations are performed using HF canonical orbitals for S_3 ($^1A_1$) with the same active spaces as in **Table 5.11**, the sole contributing CSF's to its total CAS(n,m) wavefunction are CSF-1 ($\ldots 11a_1^2 2a_2^2 4b_1^0 12a_1^0 9b_2^0$, w ≈ 87 %) and CSF-3 ($\ldots 11a_1^2 2a_2^0 4b_1^2 12a_1^0 9b_2^0$, $6 \leq$ w ≤ 13 %) for all the CAS(n,m). This is also indicative of the system possessing multi-configurational character. The computed results discussed here therefore suggest that S_3 ($^1A_1$), just like the singlet state of S, S_2 (**4.3.2.2**) and O_3 ($^1A_1$),[19,324–326] is a multi-

configurational system with partial diradical character. In addition, S_3 ($^3A_2$), like O_3 ($^3A_2$),[324] is also computed to possess multi-configurational character when CAS(18,12) is employed. For the CAS(n,m) considered, the multi-configurational character is defined by CSF's corresponding to double-electron distribution and/or a diradical CSF with $6 \leq w \leq 13$ % or $w \approx 87$ % contribution to the total wavefunction of the system.

A summary of the thermally corrected singlet-triplet energy splitting for S_3 and O_3 using CCSD(T)//DFT and CAS(n,m) calculations is presented in **Table 5.12** for comparative purposes. The valence configuration of O_3 ($^1A_1$) computed with HF/STO-3G and used to form the active spaces used in the CAS(n,m) calculations is: $...3a_1^2 2b_2^2 4a_1^2 5a_1^2 1b_1^2 3b_2^2 4b_2^2 6a_1^2 1a_2^2 2b_1^0 7a_1^0 5b_2^0$.

Table 5.12. The singlet-triplet energy splitting (enthalpy, ΔH_{ST} and Gibbs free energy, ΔG_{ST}) of S_3 and O_3 using CCSD(T)/aug-cc-pVTZ//ωB97XD/6-311++G(2df,2p) and CAS(n,m)/6-31G(d). CAS(n,m) employ canonical orbitals for $^1A_1$ generated using RHF/STO-3G (or UHF/STO-3G for values in brackets).

System	Methodology	ΔH_{ST} / kJ mol^{-1}	ΔG_{ST} / kJ mol^{-1}
S_3	CCSD(T)//DFT	81.8	77.6
	CAS(4,3)	91.7 (89.1)	87.5 (84.9)
	CAS(4,5)	89.7 (89.5)	85.5 (85.4)
	CAS(18,12)	100.1 (95.2)	96.0 (91.0)
O_3	CCSD(T)//DFT	105.4	101.9
	CAS(4,3)	82.6 (91.0)	79.2 (87.5)
	CAS(4,5)	88.7 (95.0)	85.5 (91.5)
	CAS(18,12)	125.7 (118.6)	122.2 (115.1)
	MRMP*/aug-cc-pVTZ//CAS(18,12)/aug-cc-pVTZ[324]	86.8	
	CAS(18,12)/[4*s*3*p*2*dlf*][327]	139.9	
	CASPT2(18,12)/[4*s*3*p*2*dlf*][327]	92.6	
	CASPT2(g_2)(18,12)/[4*s*3*p*2*dlf*][327]	111.9	
	Experiment[328]	113.9	

*MRMP stands for multi-reference Møller-Plesset perturbation calculation.

Table 5.12 suggests that the energy splitting between S_3 ($^1A_1$) and S_3 ($^3A_2$) computed using CAS(4,3) and CAS(4,5) are only ~10 kJ mol^{-1} higher than the values computed using CCSD(T)//DFT. The energy splitting computed using CAS(18,12)/6-31G(d) on the other hand is 13 kJ mol^{-1} above CCSD(T)//DFT values when UHF is used to generate the canonical orbitals of S_3 ($^1A_1$), otherwise, it is 18 kJ mol^{-1} higher than the CCSD(T)//DFT values. In all cases, S_3 ($^1A_1$) is always computed to be more stable than S_3 ($^3A_2$) as presented in **Figure 5.13**. In addition, the energy difference between S_3 ($^1A_1$) calculated using canonical orbitals generated with RHF and UHF is found to be ≤ 5 kJ mol^{-1} for all CAS(n,m).

The results of the present computation of the structure and energies of $^1A_1$ and $^3A_2$ states of O_3 also indicate that the $^1A_1$ state of ozone is its ground state while its $^3A_2$ state is an excited state that is less stable than its ground state structure. This finding is in agreement with experimental[328] and high-level theoretical[324,327] investigations of the low-lying electronic states of ozone which suggest that the $^1A_1$ state is its ground state while the $^3A_2$ state is its next lowest excited state. The low-lying electronic states of O_3 considered in these investigations[324,327,328] are: $^3A_2$, $^3B_2$, $^3B_1$, $^1A_1$, $^1A_2$, $^1B_1$ and/or $^1B_2$. The result summarised in **Table 5.12** for O_3 suggests that CCSD(T)//DFT gives a reasonable description of the energy splitting between the lowest lying states of the system while the CAS(18,12)/6-31G(d) gives a more reliable description of the system. The energy splitting of O_3 computed using CCSD(T)//DFT is at most 12 kJ mol^{-1} below its experimental value while that computed using CAS(18,12)/6-31G(d) incorporating UHF canonical orbitals of the system is $\leq$ 5 kJ mol^{-1} above the experimental value. Going by this finding, the description of the $^1A_1$ and $^3A_2$ states of S_3 using CCSD(T)//DFT is reasonable as it is a valence *iso*-electronic system with ozone. Therefore, the results discussed above and summarised in **Table 5.12** further suggests that even though the CAS(n,m) calculation offers a more rigorous description of S_3 ($^1A_1$), CCSD(T)//DFT gives a reasonably balanced description of the energies.

In summary, a comparison of the results computed using CCSD(T)//DFT, BS and/or CAS(n,m) indicate that both closed and open shell (multi-configurational or diradical) singlet state structures of open chain S_n ($n \leq 5$) are likely to co-exist and be thermally accessed in gaseous and/or liquid sulfur. In addition, it is found that even though CAS(n,m)//DFT gives a more rigorous/reliable description of S_n ($n \leq 3$) (discussed here and in **4.3.2.2**), CCSD(T)//DFT gives a reasonable description and will be used to describe the chemistry in the next chapter.

5.4 Conclusions

The structures and thermodynamic stabilities of open chain and cyclic ground and excited state of sulfur S_n ($n \leq 5$ and 8) species have been investigated using high-level quantum theory methodologies. It is found in agreement with experiments[261,263,313] that all sulfur clusters S_n ($n \leq 4$) possess open chain ground state structures while S_8 has a cyclic ground state structure. The global minimum structure of S_5 is also found to be cyclic, indicating that it is the first sulfur allotrope to form a cyclic ground state. It is observed that excited state open chain isomers of all S_n considered are thermally accessible. Some of these open chain isomers may exist in the singlet and triplet state with similar geometric structures. The results indicate that both closed and open shell (multi-configurational or diradical) singlet state structures of open chain S_n are likely to co-exist in gaseous and/or liquid sulfur. It is found that even though CAS(n,m)//DFT gives a more reliable

description of open shains of S_n, CCSD(T)//DFT gives a reasonable description of the systems and will be used to describe the chemistry in the next chapter. For species with cyclic global minimum structures, it is found that their triplet state open chain structures are more stable than their singlet state analogues even though ring opening for the species occurs on the singlet PES. A likely explanation for this may be that the triplet state structures for such species may be thermally accessed via their higher energy singlet state analogues through favourable spin flip processes. This stability of the triplet state open chain structures especially for S_8 over their singlet state analogues provides a possible explanation for the paramagnetic behaviour[275,288,322] of liquid sulfur and the possible S_8 structures responsible for the behaviour. The switch in stability of the most stable open chain species at S_3 and S_4 suggests the participation of "two-state reactivity" in liquid and gaseous sulfur. This in turn may have implications on the viscosity behaviour of (the reactivity in) liquid sulfur above its melting point and processes occurring during sulfur recovery in the thermal Claus process.

6 Formation of hydrogen polysulfanes from sulfur clusters (S_n, $n \leq 5$ & 8) and hydrogen sulfide

In this chapter, the CCSD(T)/aug-cc-pVTZ//ωB97XD/6-311++G(2df,2p) method is used to describe the reaction of open chain sulfur clusters, S_n ($n \leq 5$ and 8) with H_2S on the singlet and triplet PESs to generate $HS_{n+1}H$. The study reveals that branched and unbranched $HS_{n+1}H$ are only formed in the course of the reaction(s) on the singlet PES. It is found that the unbranched $HS_{n+1}H$ are always formed in exergonic processes while the branched $HS_{n+1}H$ may be formed in either an exergonic or endergonic process. It is also found that the unbranched $HS_{n+1}H$ may be obtained via a direct (from reaction complex) or an indirect (through the branched species) reaction route. The results further reveal that the product of reaction on the triplet PES in all cases may best be described as weakly attracted doublet state species depending on n and are always formed in endergonic processes. In addition, it is found that the exergonicity of the reverse of the triplet PESs may provide an explanation for the observed residual H_2S in sulfur recovered in the thermal Claus process. It is observed that unbranched $HS_{n+1}H$ ($n \geq 2$) can exist in more than one conformational structure with general r(S-S) = 2.059 ± 0.003 Å and r(S-H) = 1.342 Å. Furthermore, the rotational barrier for transforming one isomer to another for a given unbranched $HS_{n+1}H$ is found to fall between 20 and 32 kJ mol^{-1} regardless of its sise. The forward and backward rotational energy barriers to transform one unbranched isomer to another are found to differ by at most 5 kJ mol^{-1}. This indicates that the different isomers of the species will undergo rapid interconversions at room temperature thereby making their isolation difficult.

6.1 Introduction

It has been established in **Chapter 5** that minimum energy singlet and/or triplet state open chain structures of S_n are thermally accessible from, or are, the global minimum structures. Spectroscopically accessible minimum energy structures of S_n ($n \leq 8$) are commonly produced in

the modified thermal Claus process with the overall chemical reaction,[12,269,275] summarised in reaction (5.1). This process has become the most industrially and commercially attractive way of liquid sulfur production from H_2S for desired end uses[12,14] in recent years. The process is especially applicable to natural gas, coal, petroleum or oil refining which are its main sources of H_2S.[12,14] However, it is known from experiments[13,14] that industrial liquid sulfur is condensed under small partial pressures of H_2S which in turn lead to high levels of residual H_2S in the liquid product (S_n) obtained in the thermal Claus process. This situation has prompted strict industrial guidelines stipulating that residual H_2S must be removed prior to the transportation of the recovered liquid sulfur or its solidification and application[14,15] as it may lead to pollution that is harmful to body organs.[273]

As a consequence of the small partial pressures of H_2S in the thermal Claus plants, sulfur recovery in the process suffers a daunting H_2S elimination problem[13,14,269] due to the equilibrium in eq. (5.2),[14,276] where the S_n is believed to be open chain species. Furthermore, liquid sulfur which contains mostly open chain S_n species has been experimentally found to be paramagnetic[275,288] whereas the hydrogen polysulfanes ($HS_{n+1}H$) formed in reaction (5.2) are known from experiments and theoretical calculations to be diamagnetic.[258,259,282,289–291] An understanding of the mechanism and nature of species involved in reaction (5.2) is therefore fundamental, as it may provide insights into the H_2S elimination[12–14,269] or temperature control difficulties[12] presently encountered in sulfur recovery plants. The reactivity of open chain sulfur species with H_2S and spin state interplay is therefore investigated to provide insights into the difficulties of H_2S elimination from S_n recovered in the thermal Claus process.[13,14,273] To do this, the singlet and triplet PESs of the S_n-H_2S reaction (5.2) for $n \leq 5$ & 8 are characterised; i.e., detailed mechanisms and energetics of $HS_{n+1}H$ formation on the singlet and triplet PESs are determined.

6.1.1 Review of Literature

The formation of polysulfanes (or persulfides) was first proposed by Bacon and Fanelli in 1943 from their experimental study of the viscosity changes of liquid sulfur in the absence and presence of H_2S (**Figure 5.1**).[277] The authors suggested that in heating sulfur containing oil, the compounds may form from direct action of sulfur on hydrocarbons or by reaction between nascent H_2S and sulfur. They went on to assert that the persulfides, H_2S_n were not particularly stable to heat but that H_2S_2 boils with little decomposition at about 75 °C. They also asserted that the formation of H_2S_n had a suppressing effect on the sudden viscosity changes of liquid sulfur at 160 °C. This lead Fanelli to further experimentally investigate the modifying effect of H_2S on the viscosity of liquid sulfur between 120 and 445 °C at atmospheric pressure in 1949.[278] The author suggested from his

study that H_2S reacts with sulfur to form the persulfides by the chemical reaction in eq. (5.3). He attributed the reactivity in eq. (5.3) to the formation of S_8 chains above 160 °C as a result of the rupture of S_8 rings which are predominant below 160 °C. The author asserted that hydrogen atoms took the terminal positions of the formed sulfur chains in liquid sulfur with generic structure in **Figure 6.1**;

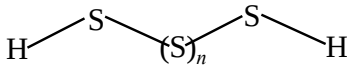

Figure 6.1. The generic structure of persulfides with terminal hydrogen atoms.

to inhibit their polymerisation into long sulfur chains at increasing temperature. The authors then asserted that the formation of the persulfides in turn suppressed the viscosity of liquid sulfur. Rubero reported a further experimental study of the viscosity reducing effect of H_2S on liquid sulfur in 1964.[285] The author suggested that the solubility/reactivity of H_2S in liquid sulfur was a function of temperature and pressure. He also noted that the suppressing effect of H_2S on the viscosity of liquid sulfur was extremely strong above 158 °C.

Eq. (5.3) was modified to eq. (5.2) in 1966 by Wiewiorowski and Touro from their experimental and theoretical consideration of the chemical equilibrium in eq. (5.3).[276] The authors asserted that the enthalpy and entropy changes involved in the formation of $HS_{n+1}H$ from sulfur chains and H_2S were $\Delta H = -30{,}900$ cal mol^{-1} and $\Delta S = -25.7$ cal deg^{-1} mol^{-1}. Later this same year, Hyne et al., studied the nuclear magnetic resonance (NMR) of $HS_{n+1}H$ in molten sulfur.[282] The authors reiterated that the dissolution and/or reactivity of H_2S in molten sulfur resulted in the formation of $HS_{n+1}H$ and that the so formed polysulfanes appeared to be mainly higher members of the homologous series with $n \geq 5$. They also asserted that shorter chain $HS_{n+1}H$ ($n \leq 4$) species may be formed as transient intermediates in the formation of the higher members of the $HS_{n+1}H$ species. In 1968, Muller and Hyne reported the proton NMR (^{1}H-NMR) and infrared (IR) study of hydrogen bonding (H-bonding) in sulfanes (H_2S_n).[329] The authors asserted that the position of the proton signals in the NMR spectrum of the species was dependent on sulfur chain length, $HS_{n+1}H$ concentration and temperature. They also noted that the position and appearance of the SH-absorption bands of the $HS_{n+1}H$ in the IR provided evidence of the existence of sulfane-solvent interactions. They then concluded that the species participated in H-bonding and suggested that a special type of intra-molecular H-bonding may be operative in H_2S_3. In addition, the authors found that the Raman and IR vibrational frequencies of the r(S-H) bonds for concentrated short-chain $HS_{n+1}H$ (n = 1 to 4) solutions were observed at 2498 to 2510 cm^{-1}. In the following year, the authors reported an NMR study of the thermal decomposition of $HS_{n+1}H$ (n = 2 and 3) at ca. 70 °C in the

absence of oxygen.[330] They asserted that H_2S and elemental sulfur (S_n) were the ultimate decomposition products of the species. They however demonstrated that the species do not decompose directly to H_2S and S_n but rather form a variety of sulfane intermediates. The authors then suggested a free-radical pathway for the decomposition of the species and/or formation of elemental S_n from sulfanes. In this same year, Wieser et al., reported the vibrational spectra and force field of $HS_{n+1}H$ (n = 2 and 3).[290] The authors asserted that both HS_3H and HS_4H had the C_2 symmetry on the basis of their IR and Raman spectra, temperature and concentration dependence. They went on to suggest that the derived valence force field for the species provided a least squares fit between the observed and calculated frequencies for both molecules simultaneously. Furthermore, the authors noted that the vibrational frequencies of the r(S-H) bonds for the species occurred at 2505 to 2540 cm^{-1} in dilute solutions. Also, Winnewisser reported the high resolution measurement of the IR absorption of HSSH between 2490 and 2650 cm^{-1} in 1970 using a vacuum grating spectrograph.[331] The author asserted that the high resolution spectrum of v_1 and v_5 of HSSH could be analysed as that of a true symmetric top molecule.

The composition of crude sulfane oil and identification of sulfanes (H_2S_n) from HS_9H to $HS_{35}H$ was reported by Hahn in 1985.[332] The author asserted that the position of the ^{1}H-NMR signals of the compounds depended on the sulfur chain length and sulfane concentration in benzene solution. He went on to suggest that under proper conditions, all sulfanes in a mixture are characterised by well-resolved NMR signals showing a downfield shift with increasing sulfur chain length. The author also noted that the shift differences between the higher homologues ($n > 8$) remain nearly constant, thus allowing the assignment of the signals up to H_2S_{35} and the determination of the complete sulfane distribution in crude oils. Later, Grein calculated the *cis*- and *trans*-rotational energy barriers for HSSH at the SCF/4-31G level of theory to be 33.6 kJ mol^{-1} and 23.2 kJ mol^{-1}, respectively.[333] Also the same year, Dixon et al.,[334] reported the barriers to internal rotation of HSSH calculated at the SCF and CI-SD in combination with the DZ+P basis set of the form (11s7p1d/4s1p)/[6s4p1d/2s1p] to be 31.4 ± 0.6 and 20.9 ± 0.6 kJ mol^{-1} for the *cis*- and *trans*-barriers, respectively with the error margins as the corrections for the difference in zero-point energies. In 1986, Hahn and Altenbach reported the synthesis of the silylsulfanes, $(MePh_2Si)_2S_n$ ($2 \leq n \leq 5$) by reacting $MePh_2SiSNa$ with iodine or chlorosulfanes, S_mCl_2 ($1 \leq m \leq 3$) in toluene solution.[335] The authors asserted that the compounds proved to be a convenient source for the generation of sulfanes H_2S_n and deuterosulfanes D_2S_n of definite chain length, $2 \leq n \leq 5$. Mauer et al., reported the detection of gas-phase trisulfane, HSSSH and its rotational absorption spectrum using the Cologne free-space-cell millimetre-wave spectrometer in 1988 for the first time.[336] The authors asserted that the molecule had no symmetry axis and so must be tightly locked in one

conformation. Based on their spectroscopic data, the authors assigned this conformation as the *cis*-conformation. The structure of *cis*-trisulfane is illustrated in **Figure 6.2**.

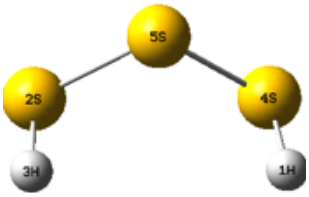

Figure 6.2. The *cis*-conformational structure of trisulfane.

In 1989, Herbst and Winnewisser used a variety of millimetre-wave and IR spectral data on the internal rotation of HSSH to derive its torsional barrier heights as 33.5 ± 1.1 and 23.8 ± 0.2 kJ mol^{-1} (*cis*- and *trans*-barriers, respectively).[337] The synthesis of HSSH from the cracking distillation of raw sulfane mixtures in a rotary evaporator and structure of the molecule was reported by Hahn et al., in 1991.[258] The authors determined the geometric parameters of the species from microwave spectroscopy as: r(S-S) = 2.0564 Å, r(S-H) = 1.3421 Å, τ(HSSH) = 90.34 ° and θ(SSH) = 97.88 ° for the first time. Later the same year, Behrend et al., reported a more refined molecular structure of HSSH from its rotational spectra measured in the millimetre-wave and far IR region with the following geometrical parameters: r(S-S) = 2.0564 (1) Å, r(S-H) = 1.3421 (2) Å, τ(HSSH) = 90.3 (2) ° and θ(SSH) = 97.88 (5) °.[259] The authors claimed that the bond lengths and angles, as given, represent a partial equilibrium structure since contributions from the torsional motions of the molecule were removed. Pelz et al.,[338] reanalysed the torsional potentials of HOOH and HSSH by fitting their calculated rotational constants to their observed values and the dependencies of their structural parameters on torsional angles in 1993. The authors asserted that internal rotation tunneling in the complexes occurred predominantly through the *trans*- rather than *cis*-configuration. They went on to suggest that upon passage through the *cis*- or *trans*-position, the internuclear S-S (O-O) distances increased by 0.1642 Å (0.0486 Å) while the θ(SSH) (θ(OOH)) closed by 3 ° compared to their equilibrium values. They also noted that the *trans*- barrier for HSSH was 24.4 kJ mol^{-1} and 4.6 kJ mol^{-1} for HOOH. This *trans*-barrier for HSSH agrees with that determined by Herbst and Winnewisser.[337] Later this same year, *trans*-HSSSH was detected and characterised in a mixture of *cis*- and *trans*-HSSSH using millimetre-wave and Fourier transformed IR (FTIR) spectroscopy together with *ab initio* calculations at the MP2/TZ+P and QCISD/TZ+P levels of theory by Liedtke et al.[289] The authors noted that the observed rotational constants in MHz were *trans*-HSSSH: **A** = 14098.89744 (42); **B** = 2750.15137 (15); **C** = 2371.69779 (14) and *cis*-HSSSH: **A** = 14103.20962 (25); **B** = 2752.75945 (11); **C** = 2373.86989 (12). They went on to suggest that the intensity alternation of *trans*-HSSSH was characteristic of asymmetric top rotors with C_2-

rotational symmetry. They also asserted that the calculated energy barrier of internal rotation from *trans*- to *cis*-HSSSH was 35 kJ mol^{-1}. In 1994, Mittler et al., reported another FTIR spectrum of the HSSH molecule in the *r*(S-H) stretching region.[339] The authors asserted that the origin of the ν_5 band in the gas-phase for the species was determined to be 2559 (89) cm^{-1}.

Drozdova et al., reported the *ab initio* investigation of the structures, energies, torsional barriers and vibrational spectra of three rotational isomers (rotomers) of tetrasulfane (HSSSSH) at the MP2/6-311G** level of theory in 1995.[340] They asserted from their calculations that the rotomers were energetically identical and had identical vibrational wavenumbers. They also noted that upon rotation about the central bond of the species, the torsional barriers were found to be 32 kJ mol^{-1} (*cis*-barrier) and 26 kJ mol^{-1} (*trans*-barrier). They went on to assert that the geometries of the two torsional transition states with τ(SSSS) = 0 ° and 180 ° may be explained by hyperconjugation between the lone pairs at the terminal sulfur atoms and the σ* molecular orbital of the central *r*(S-S) bond of the species. Yamada et al., reported the anomalous *K*-type doubling observed in the millimetre and submillimetre-wave spectra of HSSH in the K_a = 2 and 3 states in 1996.[341] The authors discussed the anomaly by applying the second-order perturbation theory to the Watson's *S*-reduced Hamiltonian. They then predicted that the anomaly does not occur for the levels $K_a \geq 4$. In 1997, Steudel et al., reported the *ab initio* study of the stability of various disulfanes (RSSR, R = H, Me, Pr, All), their branched isomers (R_2SS) and related isomerisation transition states using different levels of theory.[342] The authors asserted that at the MP2/6-311G** level of theory, H_2SS was 143 kJ mol^{-1} less stable than HSSH and that the species were separated by an activation energy barrier of 210 kJ mol^{-1}. The authors stated that when much higher levels of theory were used, the results were only slightly changed and that at the same level of theory, Me_2SS was 84 kJ mol^{-1} less stable than MeSSMe with the isomerisation transition state between the latter species lying 340 kJ mol^{-1} above MeSSMe. They therefore suggested that the thermal isomerisation of HSSH or MeSSMe may be excluded and that H_2SS and Me_2SS should be kinetically stable toward unimolecular isomerisation at low temperatures. They went on to propose that the bimolecular decomposition of Me_2SS to Me_2S and S_2 was exothermic but spin-forbidden in the case of triplet S_2 and endothermic but spin-allowed when singlet S_2 was formed. In addition to the structural descriptions of sulfanes considered by these authors, the structural definitions in **Figure 6.3** may be made for the series, $HS_{n+1}H$ ($n \geq 2$). Also in 1997, Liedtke et al., published the molecular structure of *cis*- and *trans*-HSSSH from the rotational spectra of the species obtained from microwave and millimetre-wave spectroscopy.[343] The authors asserted that the geometrical parameters of the molecules were: *r*(S-S) = 2.0530 (1) Å, *r*(S-H) = 1.3435 (14) Å, θ(SSS) = 106.919 (3) °, θ(SSH) =

97.37 (15) °, θ(SSS-SSH) = 90.82 (16) ° for *cis*-HSSSH and r(S-H) = 2.0539 (4) Å, r(S-H) = 1.3435 (14) Å, θ(SSS) = 107.02 (2) °, θ(SSH) = 97.2 (7) °, θ(SSS-SSH) = 87.7 (4) ° for *trans*-HSSSH.

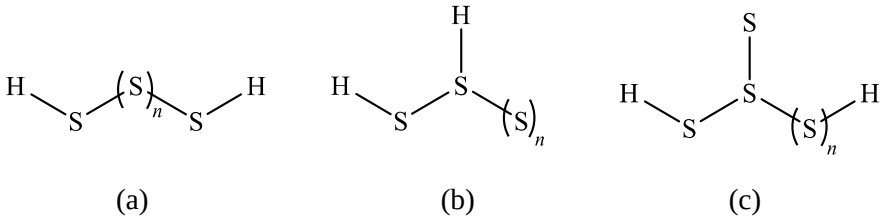

(a) (b) (c)

Figure 6.3. Structural definitions of $HS_{n+1}H$ ($n \geq 2$): (a) linear and terminal $HS_{n+1}H$, (b) linear but non-terminal $HS_{n+1}H$ and (c) non-linear but terminal $HS_{n+1}H$ with respect to the sulfur chain and position of H-atoms, respectively. (a) may also be described as unbranched $HS_{n+1}H$ while (b) and (c) may also be described as branched $HS_{n+1}H$.

They also suggested that the spectra of the species showed no effect of internal rotation in agreement with their previous *ab initio* calculation[289] of the energy barrier. Wong et al., reported the *ab initio* study of the protonation of various isomers of sulfur molecules, S_n ($2 \leq n \leq 8$) at the G3X(MP2) level of theory in 2004.[271] The authors asserted that smaller cations, $[HS_n]^+$ ($2 \leq n \leq 4$) were all chainlike with the hydrogen atom at the S_n chain end. They also noted that the singlet chain-like structures of $[HS_n]^+$ ($2 \leq n \leq 8$) with the hydrogen terminating the chain at one end were more stable than the corresponding triplet chains. They went on to suggest that the protonation of neutral sulfur molecules will always occur at the atom of highest negative charge. The authors also stated that the r(S-H) bond of the protonated species were calculated between 1.35 and 1.39 Å.

In 2005, Gargurevich presented in a review article, the major chemical paths in the combustion of H_2S and formation of S_n by molecular growth under conditions typical of the Claus furnace.[344] The author asserted that HSSH (or H_2S_2) seemed to have an important role in the combustion of H_2S while the higher molecular weight linear H_2S_n species had only a minor role in the combustion of H_2S. Zhou et al., in 2008 reported the theoretical study of hydrogen abstraction and sulfur insertion in the reaction of H_2S with atomic sulfur at the multi-reference configuration interaction (MRCI) level of theory.[345] The authors asserted that the presence of an intersystem crossing enabled the formation of $SH + SH$ on the singlet PES via S atom insertion, which bypassed the triplet energy barrier (19 kJ mol^{-1}) to H-abstraction. They however stated that the H-abstraction route will be competitive at higher temperatures due to a higher Arrhenius pre-exponential factor in comparison to that of the S atom insertion route. They went on to suggest that with a slightly higher transition-state barrier than that of the H-abstraction channel, the production of $S_2 + H_2$ is less favourable due to proceeding via intersystem crossing and insertion. They also noted that the formation of $HSS + H$ was energetically unfavourable relative to $SH + SH$ but that the recombination channels producing

H_2SS or the more stable HSSH were expected to occur under collisional stabilisation conditions at high pressures. Later this year, Marriott et al.,[14] suggested the possibility that some of the vibrational IR absorptions of H_2S_n molecules may arise from radical/doublet species (e.g., HS_n) formed from partial termination of diradical sulfur chains with hydrogen atoms. The authors made this observation after considering the vibrational IR spectra of sulfanes in the literature[290,329,339] while investigating the solubility/reactivity of H_2S in the liquid sulfur recovered from the Claus process using a new FTIR technique. A year later, Zhou et al., reported the characterisation of the PES for the H_2/S_2 system at the full valence MRCI+Davidson/aug-cc-pV(Q+*d*)Z level of theory using geometries optimised at the MRCI/aug-cc-pVTZ level of theory.[346] The authors considered reactions occurring entirely on the singlet and triplet PES as well as those involving an intersystem crossing. They asserted that of the SH recombined on the singlet surface, the stabilisation of HSSH occurs at the low-pressure limit at 1 bar but has a rate comparable to that of forming another major set of products ($H_2S + S$) via an intersystem crossing at temperatures below 1000 K. They went on to note that at higher temperatures, $HSS + H$ become the dominant products. They also suggested that for the reaction, $H_2S + S$, the presence of an intersystem crossing will allow for the formation of the singlet excited adduct H_2SS and that most of the adduct will rearrange and stabilise as HSSH under atmospheric conditions. The authors also observed that while the formation of $H_2S + S$ or $S_2 + H_2$ via an isomerisation or intersystem crossing, respectively were minor product channels, their rates were significantly higher than those of the corresponding direct triplet channels except at elevated temperatures. Hill and Butcher employed high level, coupled cluster and MRCI+Davidson, calculations to probe the properties of triplet excited states of a series of small molecules with two or more adjacent heteroatoms including disulfane, HSSH in 2014.[3] They predicted that HSSH, just like most of the investigated molecules, had a bound lowest triplet excited state that is either a (π^*, σ^*), (σ^*, π^*) or a Rydberg state. That is to say that the triplet state is formed by excitation of an electron from a doubly occupied *pi* anti-bonding orbital to an empty *sigma* anti-bonding orbital, (π^*, σ^*) or from a doubly occupied *sigma* anti-bonding orbital to an empty *pi* anti-bonding orbital (σ^*, π^*). The last category is the occupation of Rydberg type orbitals, which lie higher in energy than the anti-bonding orbitals in natural orbital analysis and their occupation numbers are typically small (0.01).[3] The authors also asserted that the heteroatom-heteroatom bond dissociation enthalpies (BDEs) of the triplet states ranged from very small values (e.g., as predicted for H_2O_2 or F_2) to BDEs around 33 to 38 kJ mol^{-1} and so should allow for the experimental observation of the triplet state of HSSH or H_2NF.

6.1.2 Justification of Study

It appears however from the available literature (summarised above) that only limited work to determine the mechanism of the reaction or spin state interplay in the $S_n + H_2S$ reaction for eq. (5.2) has been done. Nevertheless, a significant number of experimental studies on the suppressing effect of H_2S on the viscosity of liquid sulfur is readily available in the literature.[14,277–279,285,286,291] Furthermore, the available literature suggests that the linear and terminal $HS_{n+1}H$ (**Figure 6.1** and **Figure 6.3**) is the most studied/reported structural conformation of hydrogen polysulfanes. In addition, all the terminal $HS_{n+1}H$ and branched $HS_{n+1}H$ in the available literature are singlet state species. As a result, the mechanisms of formation of linear and terminal $HS_{n+1}H$ in the gas-phase for S_n ($n \leq 5$ & 8) on the singlet and triplet PES will be investigated. This will go a long way in providing an understanding of the mechanism and nature of species and the spin state interplay involved in reaction (5.2). This study is therefore likely to provide insights into the H_2S elimination difficulties[12–14,269] presently encountered in the modern thermal Claus process.

6.1.3 Aim of Study

This study is aimed at exploring the $S_n + H_2S$ reaction in eq. (5.2) using computational quantum chemistry methodologies to provide insights into the persistence of H_2S in sulfur recovered in the thermal Claus process. This will be provided using the optimum computational methodology determined in **Chapter 4**. This is because most of the species involved in the reaction may only be accessed via computational methodologies, as they may be elusive to observation by experimental techniques. To achieve this aim, the objectives are:

1. To elucidate the reaction mechanism(s) for the $S_n + H_2S$ ($n \leq 5$ & 8) on the singlet and triplet PESs using reaction (5.2) as a basis.
2. To determine the energetics of the elucidated mechanisms.
3. To provide a possible explanation for the source of residual H_2S in sulfur recovered in the thermal Claus process based on the findings.

6.2 Computational Details

DFT at the ωB97XD[80]/6-311++G(2df,2p)[99] level of theory as implemented in the Gaussian 09 package[24] was initially employed to study the $S_n + H_2S$ reaction for $n \leq 5$ & 8. Using this method, the neutral geometries of species in eq. (5.2) and the resulting intermediate and product species were optimised on the singlet and triplet PESs in the gas phase. In all cases, the singlet ground state of H_2S was considered. The nature of the optimised stationary points on the PESs was characterised

by frequency calculations at 298.15 K and 1.0 atm at the same level of theory. Minima were confirmed by absence of imaginary frequencies while the presence of an imaginary frequency confirmed first-order saddle points (transition states).[36,37] Thermal and ZPE corrections to the equilibrium energies of the stationary points were also obtained from the frequency calculations. The vibrational frequencies of the considered species were uniformly scaled by a factor of 0.950[257,316] while unscaled ZPEs were used throughout. The connectivity of the transition states to their adjacent minima was confirmed by eigenvector following calculations.[36,201,202] SPE calculations were thereafter, performed on the optimised geometries at the CCSD(T)[44]/aug-cc-pVTZ level of theory to obtain accurate energies. The method is summarised as CCSD(T)/aug-cc-pVTZ//ωB97XD/6-311++G(2df,2p). All the energies discussed/presented herein are computed at this level of theory. Topological analysis of the electron density of species was performed using QTAIM[124–133] as implemented in the Multiwfn package.[203] In doing this, the ωB97XD/aug-cc-pV5Z was employed to generate the wavefunctions of the investigated species.

6.3 Results and Discussion

The formation of the linear and terminal (unbranched) $HS_{n+1}H$ on the singlet PES from H_2S and S_n (reaction (5.2)) is found to occur directly or indirectly depending on S_n.

6.3.1 Direct Formation of Linear and Terminal $HS_{n+1}H$

The direct formation of linear and terminal (unbranched) $HS_{n+1}H$ from H_2S and singlet S_n is found to occur only when S_n ($2 \leq n \leq 4$) is involved and the calculated singlet PESs are presented in **Figure 6.4**. The computed reaction mechanisms are presented in **Scheme A.2.2** (path *a*) ($S_2 + H_2S$), **Scheme A.2.3** (path *a*) ($S_3 + H_2S$), and **Scheme A.2.4** ($S_4 + H_2S$) of **Appendix A.2**. The reaction is computed to proceed via three steps namely: co-ordination, 1,3 H-atom shift (for S_n, n = 2) or H-atom abstraction (for S_n, n = 3 and 4) and formation of linear and terminal $HS_{n+1}H$.

It is found that for all the reactions involving S_n ($2 \leq n \leq 4$) that lead to the direct formation of unbranched $HS_{n+1}H$, **Int1**, the co-ordination step is formed in an endergonic process with similar reaction energies, $\Delta G_r = 23 \pm 3$ kJ mol^{-1} **(Figure 6.4)**. The energy barrier ($\Delta G^{\ddagger}$) to generate the linear and terminal $HS_{n+1}H$ from **Int1** via **TS1** is found to increase with n from 65 kJ mol^{-1} for S_2 to 82 and 87 kJ mol^{-1} for S_3 and S_4, respectively. Nevertheless, the energy barrier for n = 3 and 4 differ by only 5 kJ mol^{-1}. Thus, the energy barrier for H-atom shift (when S_2 reacts) is significantly (ca. 20 kJ mol^{-1}) lower than that of H-atom abstraction (when S_3 or S_4 reacts). The overall reaction for the direct formation of linear and terminal $HS_{n+1}H$ is found to be exergonic in all cases with the exergonicity of the reaction decreasing with increasing n from ΔG_r = -101 kJ mol^{-1} for S_2 to -42 and

-46 kJ mol^{-1} for S_3 and S_4, respectively. The results in **Figure 6.4** suggest that the direct formation of the unbranched polysulfanes will be kinetically stabilised and thermodynamically less favourable as the S_n increases in sise (i.e., as *n* increases).

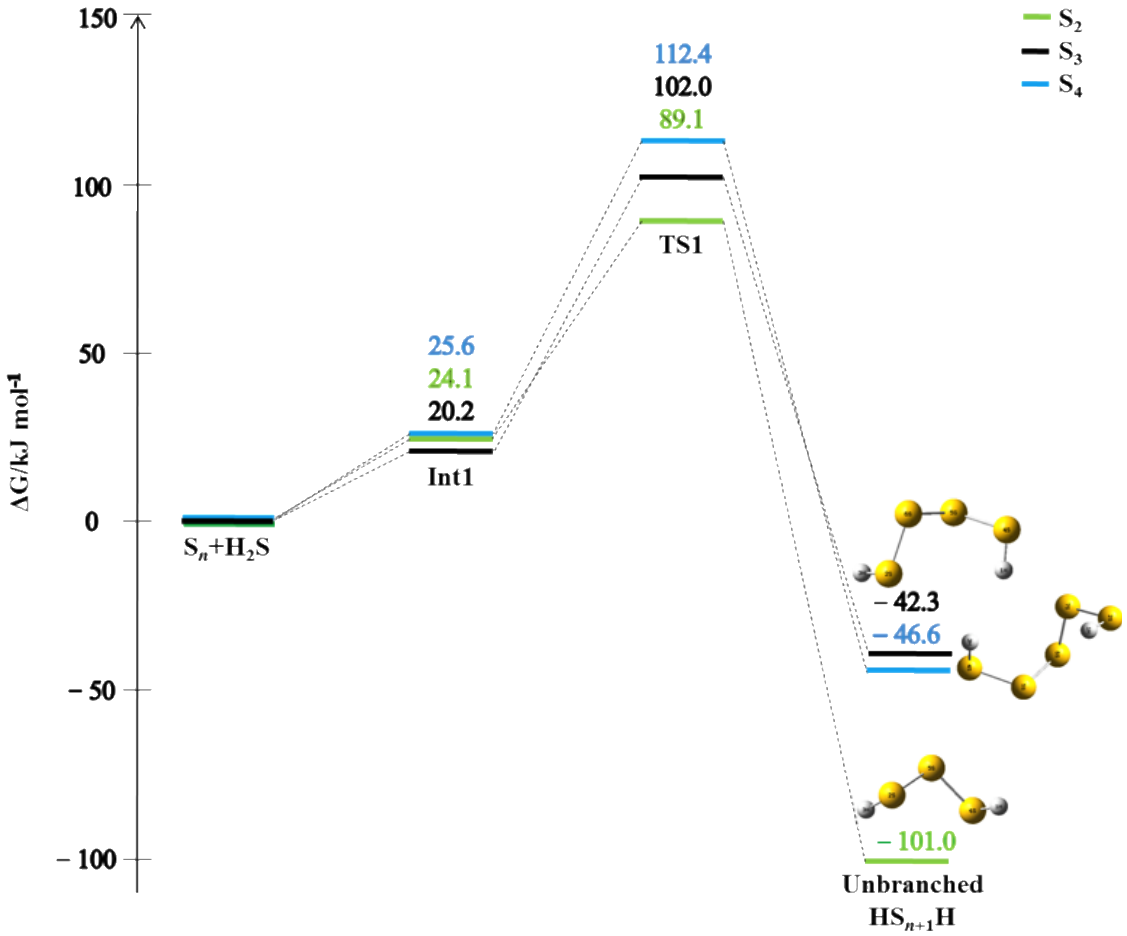

Figure 6.4. The combined singlet Gibbs free energy profiles (PESs) for the direct formation of linear and terminal (unbranched) $HS_{n+1}H$ from the reaction of S_n ($2 \leq n \leq 4$) with H_2S.

6.3.2 Indirect Formation of Linear and Terminal $HS_{n+1}H$

Here, the formation of a linear but non-terminal (when S_n ($n \leq 3$) reacts with H_2S) or non-linear but terminal $HS_{n+1}H$ (when S_n (n = 5 or 8) reacts with H_2S) is found to occur prior to the formation of the linear and terminal $HS_{n+1}H$. The indirect process is found to occur for all the S_n considered except S_4.

The calculated singlet PESs for the indirect formation of linear and terminal $HS_{n+1}H$ from S_n ($n \leq 3$) and H_2S are presented in **Figure 6.5** while the computed reaction mechanisms are presented in **Scheme A.2.1** ($S + H_2S$), **Scheme A.2.2** (path *b*) ($S_2 + H_2S$) and **Scheme A.2.3** (path *b*) ($S_3 + H_2S$) of **Appendix A.2**.

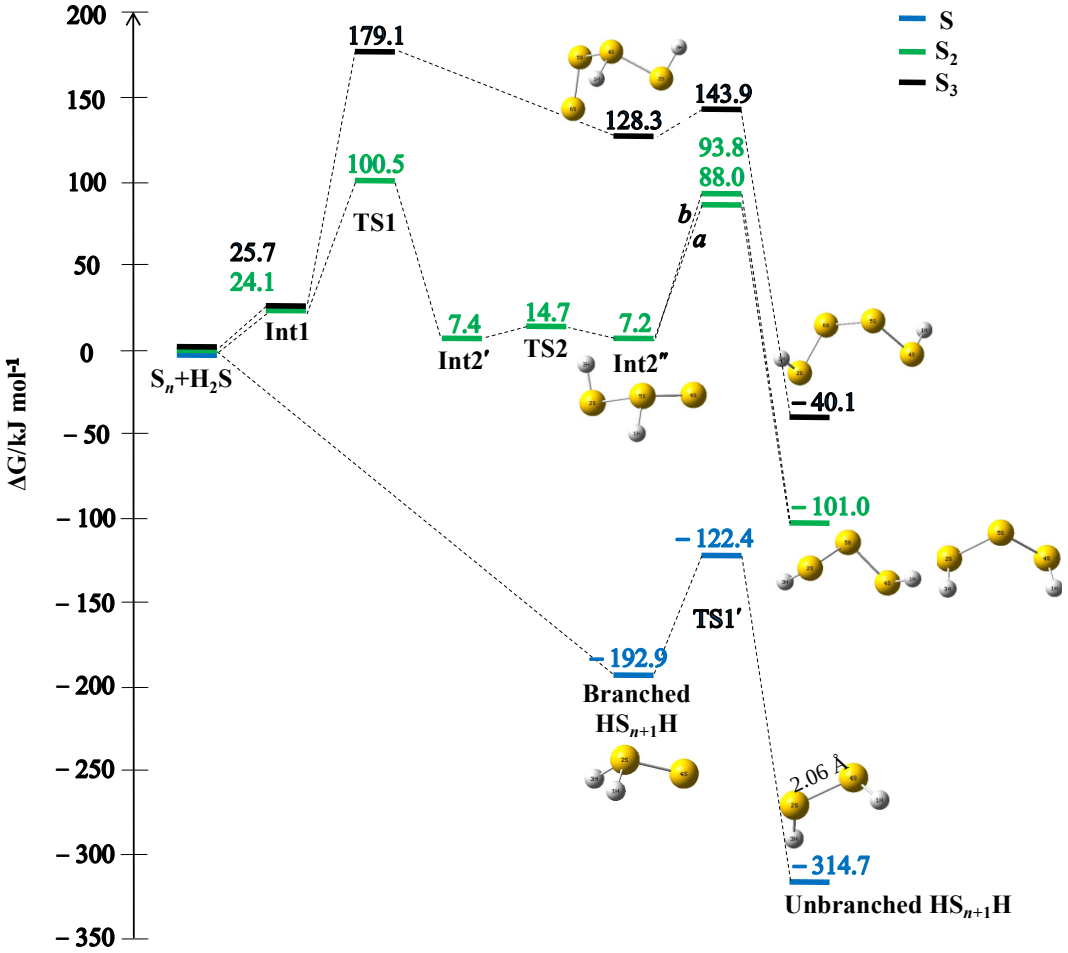

Figure 6.5. The combined singlet PES for the indirect formation of linear and terminal $HS_{n+1}H$ from the reaction of S_n ($n \leq 3$) with H_2S: path ***a*** leads to *trans*-HS_3H while path ***b*** leads to *cis*-HS_3H.

The indirect routes involving S_n ($n \leq 3$) are found to result in the prior formation of the linear but non-terminal $HS_{n+1}H$ (for S_2 or S_3) or the branched disulfane previously reported in the literature[342] (for S_n, n = 1). It is found that the indirect reaction involving S_2 or S_3 proceeds by the formation of the reaction complex (**Int1**) in an uphill process with similar reaction energy of $\Delta G_r = 25$ kJ mol^{-1}. This is followed by the formation of the linear but non-terminal $HS_{n+1}H$ (**Int2″**) which is 7 and 128 kJ mol^{-1} for S_2 and S_3, respectively above the reactants. For S_2, **Int2″** is found to be formed from **Int2′** via rotational isomerisation. The energy barrier to generate **Int2″** via 1,2 H-atom shift (**TS1**) is computed as $\Delta G^{\ddagger} = 76$ and 153 kJ mol^{-1} for S_2 and S_3, respectively. For S, the branched disulfane is formed from the reactants in an exergonic (ΔG_r = -192 kJ mol^{-1}) and barrier-free process. The linear and terminal $HS_{n+1}H$ is formed in an exergonic process of ΔG_r = -314, -101 and -40 kJ mol^{-1} for the indirect reaction involving S, S_2 and S_3, respectively. The energy barrier to generate the unbranched $HS_{n+1}H$ from its branched isomer via a 1,2 (for S and S_2) or 1,3 (for S_3) H-atom shift is

computed as 70 kJ mol^{-1} for S, 80/86 kJ mol^{-1} (to *trans*-/*cis*-products) for S_2 or 16 kJ mol^{-1} for S_3. The computed electronic energy barrier (71 kJ mol^{-1}) to generate the unbranched HS_2H from the branched HS_2H in the reaction involving S is found to be underestimated by only 5 kJ mol^{-1} in comparison with the literature value[345] computed at the MRCI+Davidson/aug-cc-pV(Q+*d*)Z level of theory. The computed stability of the stationary points in the reaction involving S in terms of electronic energy suggests that the linear and terminal $HS_{n+1}H$ is more stable than its branched isomer by 121 kJ mol^{-1}. This is also found to be within 5 kJ mol^{-1} of the value computed[345] at the MRCI+Davidson/aug-cc-pV(Q+*d*)Z level of theory.

The computed singlet PESs for the reaction involving the open chain S_n (n = 5 and 8) are presented in **Figure 6.6** while their mechanisms of reaction are summarised in **Scheme A.2.5** and **Scheme A.2.6** of **Appendix A.2**.

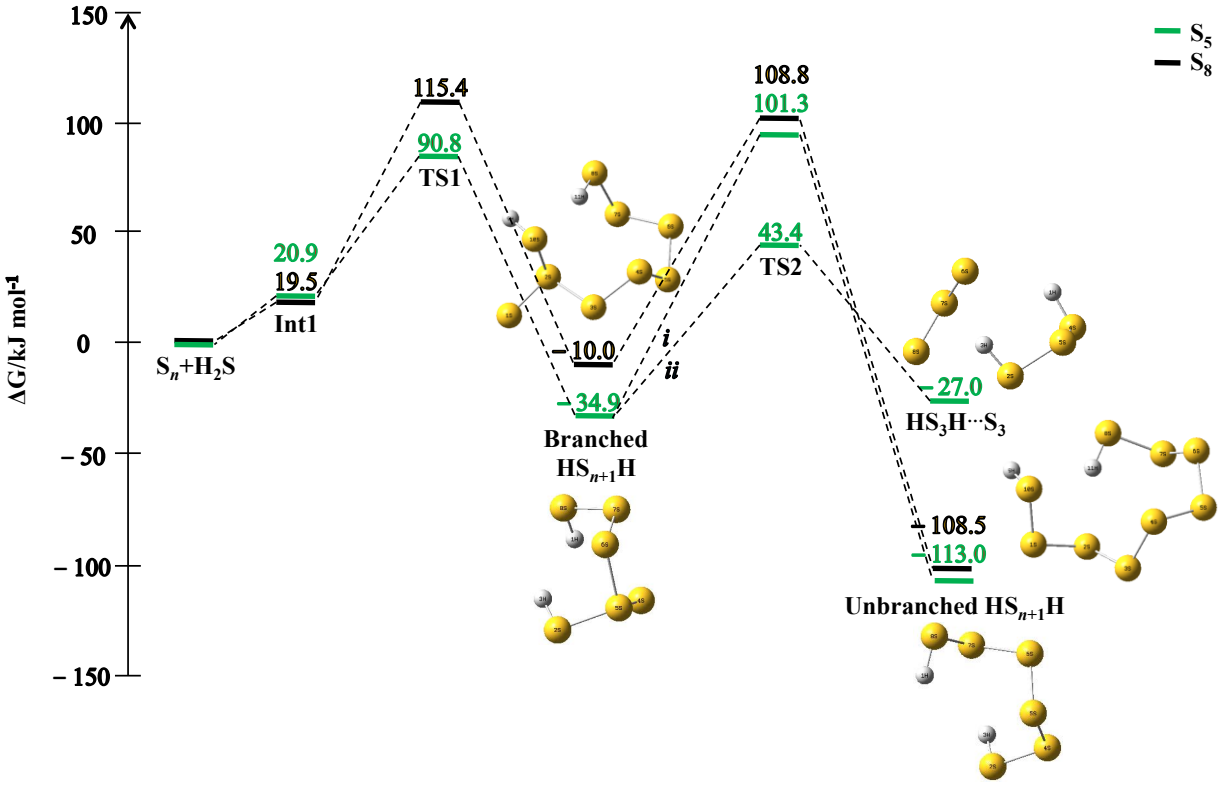

Figure 6.6. The singlet PESs for the indirect formation of linear and terminal (unbranched) $HS_{n+1}H$ from the reaction of S_n+H_2S reaction; n = 5 (green) and 8 (black). Also included is the formation of the weak complex, $HS_3H\cdots S_3$, path ***ii*** of the S_5+H_2S reaction; path ***i*** of this reaction produces the unbranched $HS_{n+1}H$.

The reaction involving S_5 and S_8 to form the unbranched $HS_{n+1}H$ is found to proceed by the formation of the reaction complex (**Int1**) which is 20 kJ mol^{-1} above the reactants for both systems. **Figure 6.6** and the elucidated reaction mechanisms for the process involving S_5 and S_8 suggest that

the branched $HS_{n+1}H$ is generated via the reaction complex (**Int1**) in an exergonic process of $\Delta G_r =$ -35 and -10 kJ mol^{-1}, respectively. The H-atom abstraction (**TS1**) barrier to the formation of the branched $HS_{n+1}H$ is computed as $\Delta G^{\ddagger} = 70$ and 96 kJ mol^{-1} for the reaction involving S_5 and S_8, respectively. It is observed that **Int2** (branched $HS_{n+1}H$) transforms to the unbranched $HS_{n+1}H$ in an exergonic process of $\Delta G_r =$ -113 and -108 kJ mol^{-1} via a 1,2 HS-group migration transition state (**TS2**) with $\Delta G^{\ddagger} = 136$ and 119 kJ mol^{-1} for the reaction involving S_5 and S_8, respectively. In addition, it is found that the branched $HS_{n+1}H$ for the process involving S_5 can also lead to the formation of the weakly bound complex, $HS_3H \cdots S_3$ (dissociation into component moieties is computed as $\Delta G = 18$ kJmol^{-1}) in an exergonic process of $\Delta G_r =$ -27 kJmol^{-1} via H-atom abstraction, **TS2-*ii***. The energy barrier to generate this complex from the **Int2** (branched $HS_{n+1}H$) in the indirect reaction of S_5 and H_2S is computed as $\Delta G^{\ddagger} = 78$ kJ mol^{-1}. This suggests that **Int2** in the process involving S_5 is kinetically stable to HS-group migration (**TS2-*i***) but labile to H-atom abstraction even though the formation of the unbranched $HS_{n+1}H$ from the moiety via the HS-group transfer is thermodynamically more facile.

In summary, the indirect route of unbranched $HS_{n+1}H$ formation is found to proceed via:

1. co-ordination of reactants for $n > 1$,
2. branched $HS_{n+1}H$ formation,
3. H-atom shifts (1,2 shifts for reactions involving S_n, $n = 1$ and 2 but 1,2 and 1,3 shifts for reactions involving S_n, $n = 3$) and
4. formation of the unbranched $HS_{n+1}H$ for reactions involving S_n, $n \leq 3$.

For S_5 and S_8, it proceeds via the co-ordination of reactants, H-atom abstraction, branched $HS_{n+1}H$ formation and HS-group transfer to form the unbranched $HS_{n+1}H$. It is also found that in all the elucidated indirect reactions, the unbranched $HS_{n+1}H$ is always more stable than the branched (linear but non-terminal or non-linear but terminal) $HS_{n+1}H$.

6.3.3 Triplet State Reaction of S_n and H_2S

The computed triplet PESs for the reaction of the considered S_n and H_2S are presented in **Figure 6.7** while their mechanisms of the reaction are presented in **Scheme A.3.1** to **Scheme A.3.6** of **Appendix A.3**. The triplet PESs in **Figure 6.7** suggest that the reaction of S_n with H_2S on the triplet PES proceed in three steps namely: co-ordination, H-atom abstraction and formation of the triplet state product of reaction for the considered S_n species. The coordinated complex (**Int1**) is formed from the reactants in an endergonic process of $\Delta G_r = 18$, 18, 22, 23, 24 and 31 kJmol^{-1} for the reactions involving S, S_2, S_3, S_4, S_5 and S_8, respectively.

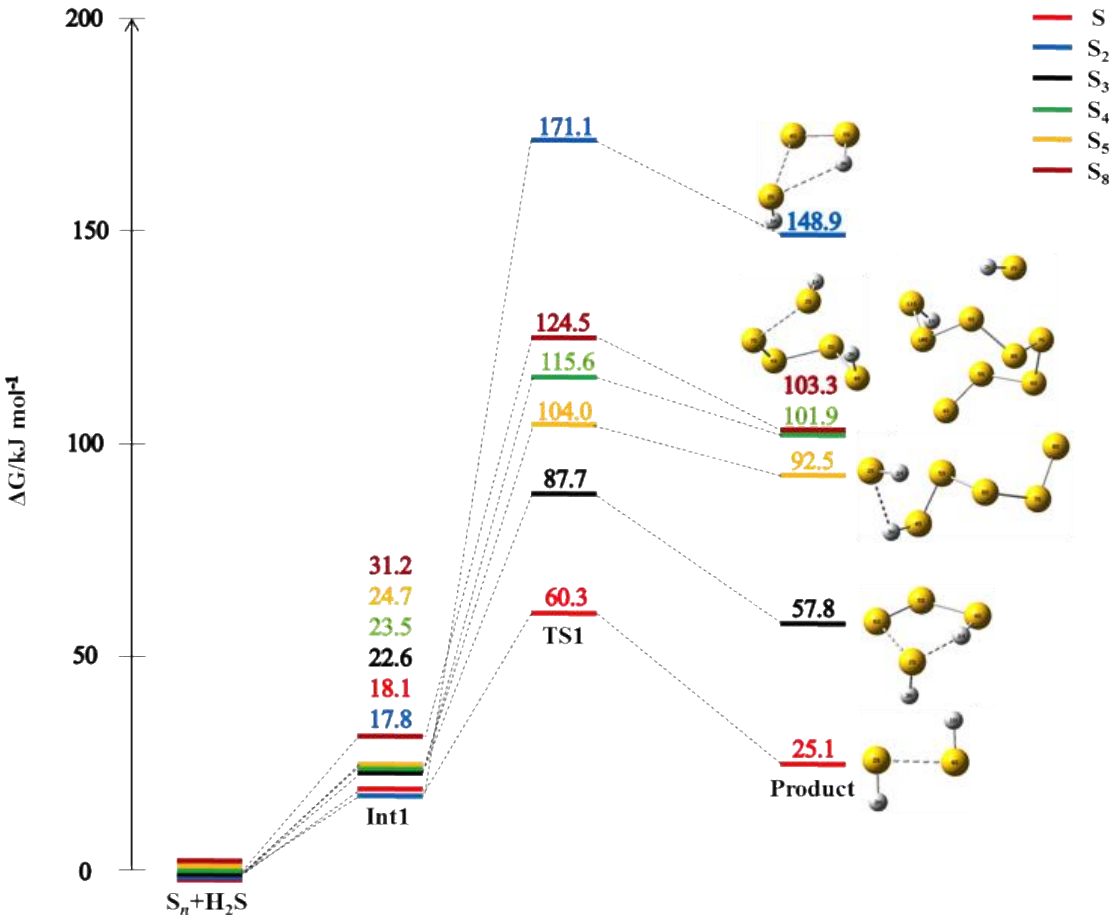

Figure 6.7. The triplet PESs for the reaction of S_n ($n \leq 5$ and 8) with H_2S: the r(S-S) of all the S ⋯ S bonds is > 2.06 Å, the normal[269,293,298] r(S-S) and the r(S-H) of all the S ⋯ H is > 1.34 Å.

The H-atom abstraction transition state (**TS1**) is also calculated to be formed in an endergonic process and is located above **Int1** at ΔG_r = 42, 153, 65, 92, 79 and 93 kJ mol^{-1} for the process involving S, S_2, S_3, S_4, S_5 and S_8, respectively. Furthermore, the triplet product for all the reactions involving the considered S_n species is generated in an endergonic process of 25, 149, 58, 102, 93 and 103, respectively from the reactants. Nevertheless, there is no clear trend in the overall reaction energies on the triplet PES for the species considered unlike the trends obtained for the singlet state reactions of the S_n species with H_2S as n increases. It is found that the energy barrier to generate the product of reaction and the overall reaction energy for the triplet process involving S is within 3 kJ mol^{-1} of the values computed at the MRCI+Davidson/aug-cc-pV(Q+*d*)Z level of theory.[345]

A QTAIM analysis was performed to determine the nature of the bonding in of the triplet products and their molecular graphs are presented in **Figure 6.8**. On the basis of **Figure 6.8**, the product of reaction on the triplet PES in all cases may best be described as weakly attracted doublet state species of the form: HS ⋯ S_nH, SH ⋯ S_nH or [HS] ⋯ [S_nH] depending on the n.

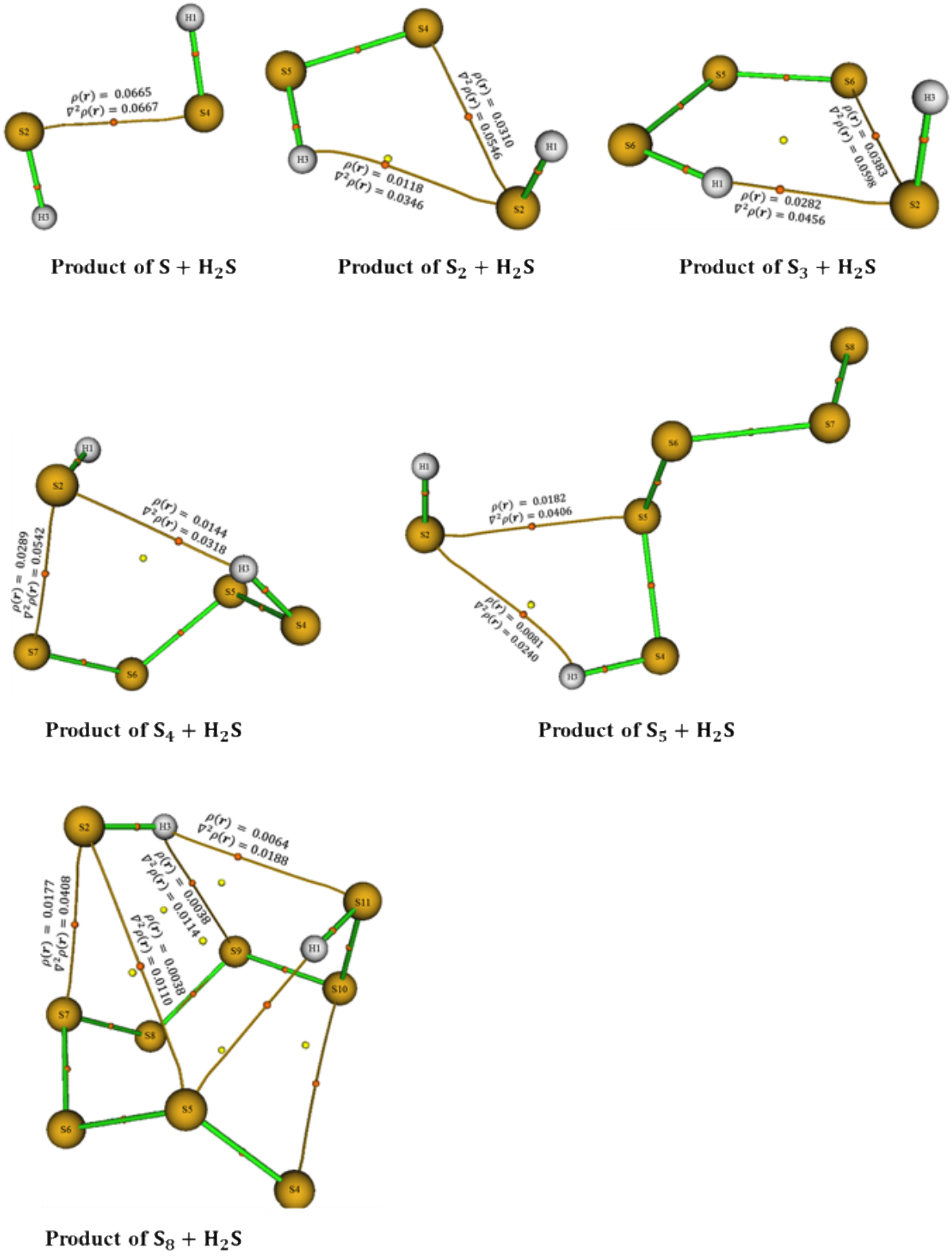

Figure 6.8. Molecular graphs for the product of reactions of S_n ($n \leq 5$ and 8) with H_2S on the triplet PES. The values of $\rho(\boldsymbol{r})$ and $\nabla^2\rho(\boldsymbol{r})$ at the bcp's on the bond paths between the fragments of the triplet products are in a.u.

This is because the magnitude of the $\rho(\boldsymbol{r})$ and $\nabla^2\rho(\boldsymbol{r})$ at the bcp's (orange dots) along the bond paths between the fragments suggests that electron density is depleted at the bcp's; $\rho(\boldsymbol{r}) < 0.1$ a.u. and $\nabla^2\rho(\boldsymbol{r}) > 0$ in all cases. These values indicate that the interactions are weak, non-covalent interactions.[134,138] Furthermore, the computed dissociation energy, $\Delta G_r = ([G([HS] + [S_nH])] - [G([HS] \cdots [S_nH])])$ of the respective products into their constituent doublet species is: 3, 13, 20, 16, 20 and 19 kJ mol^{-1} for the triplet state S_n+H_2S process involving S, S_2, S_3, S_4, S_5 and S_8. Hill and Bucher[3] computed the *r*(S-S) BDE of triplet state C_{2h} disulfane $HS \cdots SH$ as $\Delta H_r = 35$ kJ mol^{-1} at the CCSD(T)/aug-cc-pVQZ level of theory. It is found that the that the BDE of the triplet state C_{2h} disulfane $HS \cdots SH$, with an *r*(S-S) = 2.492 Å formed from triplet S and singlet H_2S, computed at the CCSD(T)/aug-cc-pVTZ level of theory in this study is in excellent agreement with the results of Hill and Bucher. The triplet state C_{2v} disulfane has also been reported to exist but less stable in comparison to its C_{2h} analogue.[3,345] Only the triplet state, C_{2h} disulfane was found to be involved in the triplet state reaction between S and H_2S probably because it is more stable compared to its C_{2v} analogue.

6.3.4 Singlet-Triplet PESs for the Reaction of S_n and H_2S

The singlet-triplet PESs for the $S_n + H_2S$ ($n \leq 5$ and 8) reactions are presented in **Figure 6.9** to **Figure 6.14**, respectively.

Comparatively, it is found that the thermodynamically most stable and ultimate reaction products lie on the singlet PES for the considered $S_n + H_2S$ reactions and are always generated from the reactants in a downhill process. Furthermore, it is found that the product of the triplet state reactions using eq. (5.2) as a basis is always generated in an uphill process. This implies that the reverse of the singlet state reactions will always be endergonic processes while that of the triplet state reactions will always be exergonic processes. The exergonicity of the reverse of the triplet PESs may therefore provide an explanation for the observed residual H_2S in sulfur recovered from natural gas or crude oil etc.,[13–15] in the thermal Claus process. Except for the PESs in **Figure 6.12** (for the reactions involving S_4), the singlet and triplet curves for the $S_n + H_2S$ reactions are found to cross. This occurrence indicates the likelihood of the participation of "two-state reactivity"[323] in the reactions to favour the formation of the singlet state reaction product(s), $HS_{n+1}H$. "Two-state reactivity" has been asserted to act as a means to low energy paths to otherwise difficult processes while spin inversion junctions are asserted to act as rate bottlenecks and mechanistic distributors in product formation.[323] Spin inversion and/or "two-state reactivity"[323] is therefore likely to affect the thermochemistry of the $S_n + H_2S$ reaction(s). In addition, it is found that more than one conformational isomer of unbranched $HS_{n+1}H$ may be accessed from these reactions, especially for

the reactions involving S_n ($2 \leq n \leq 5$ and 8) on the singlet PES. Finally, the thermodynamically more stable $HS_{n+1}H$ species are always computed to form on the singlet PES whereas the thermodynamically more stable reactants may lie on the triplet or singlet PES depending on *n* and the electronic structure of the species.

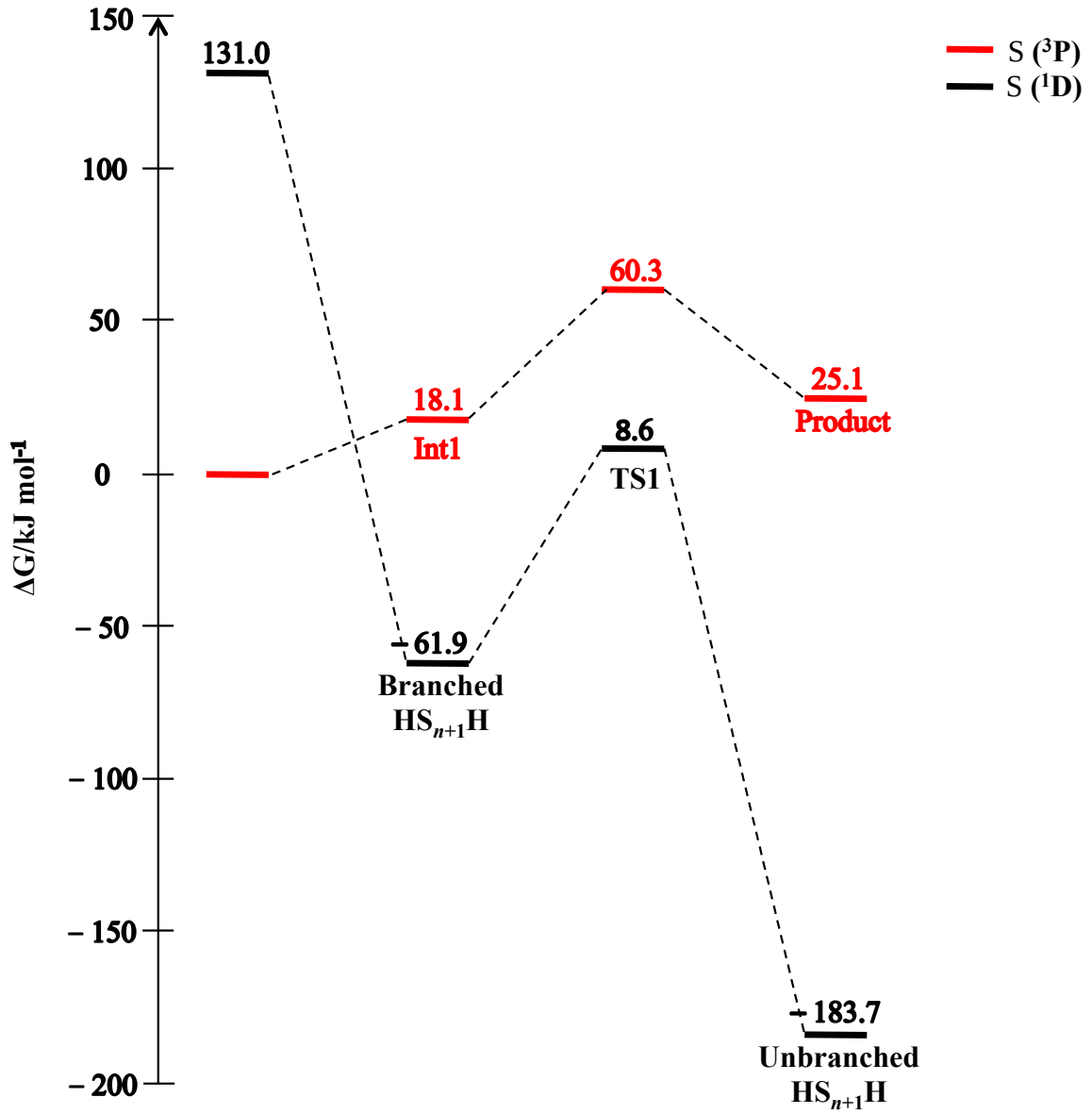

Figure 6.9. The singlet (black) and triplet (red) PESs for the reaction of S_n (n = 1) with H_2S.

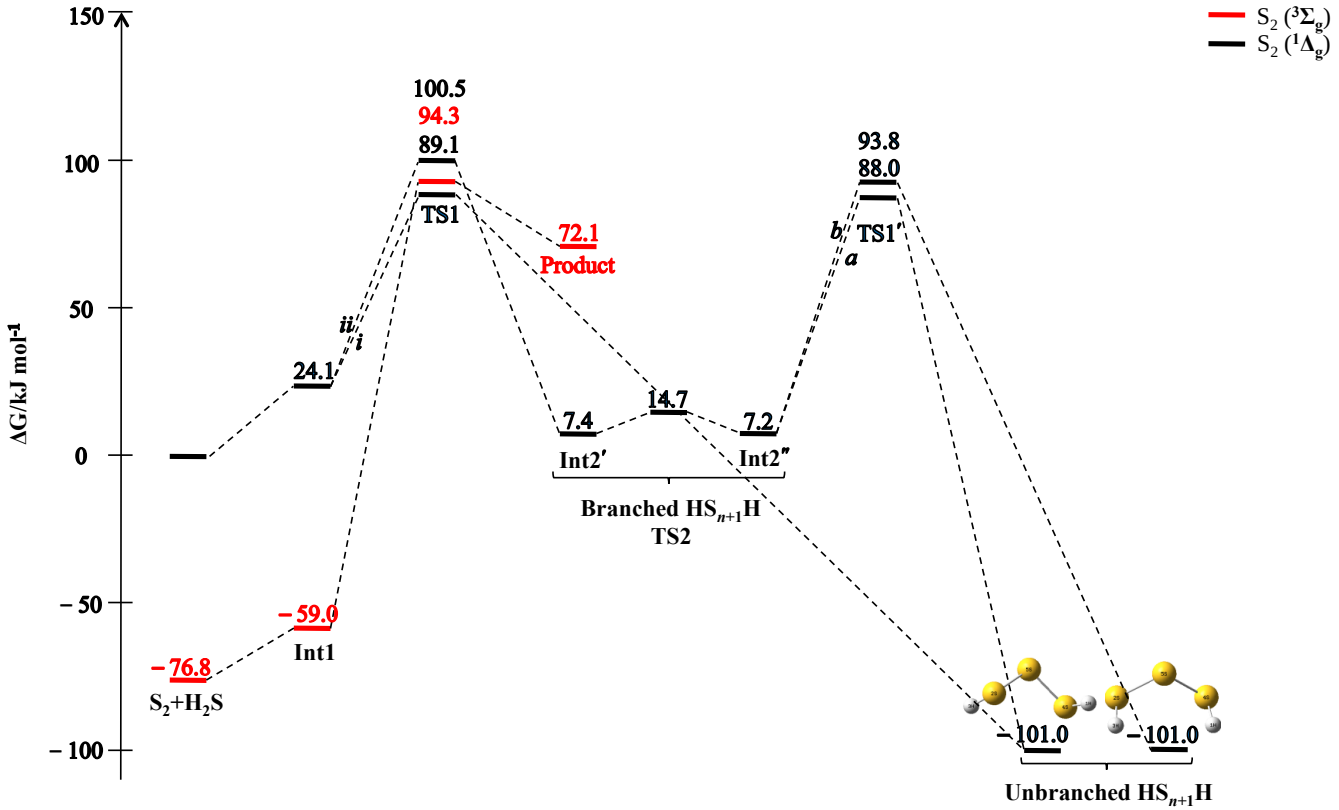

Figure 6.10. The combined singlet (black, with channel ***i*** and ***ii*** corresponding to the direct and indirect routes to the unbranched $HS_{n+1}H$) and triplet (red) PESs for the reaction of S_n (n = 2) with H_2S. Channel ***ii*** on the singlet PES leads to two different conformational isomers of the unbranched HS_3H: path ***a*** of the channel produces the *trans*- while path ***b*** generates the *cis*- isomer of the species.

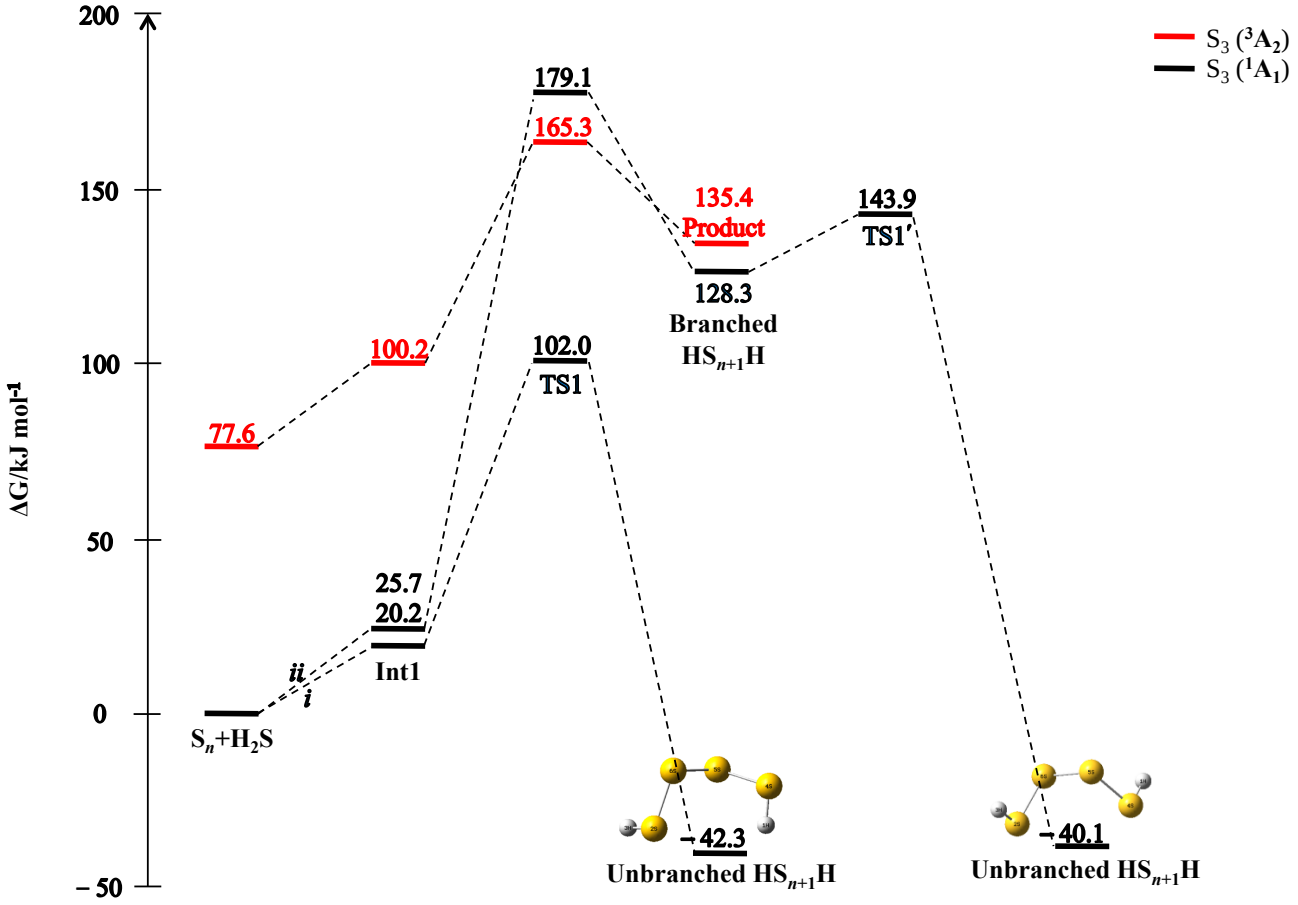

Figure 6.11. The combined singlet (black, with channel ***i*** and ***ii*** corresponding to the direct and indirect routes to the unbranched $HS_{n+1}H$) and triplet (red) PESs for the reaction of S_n (n = 3) with H_2S. The unbranched HS_4H formed in channel ***i*** and ***ii*** on the singlet PES are different conformational isomers of the species.

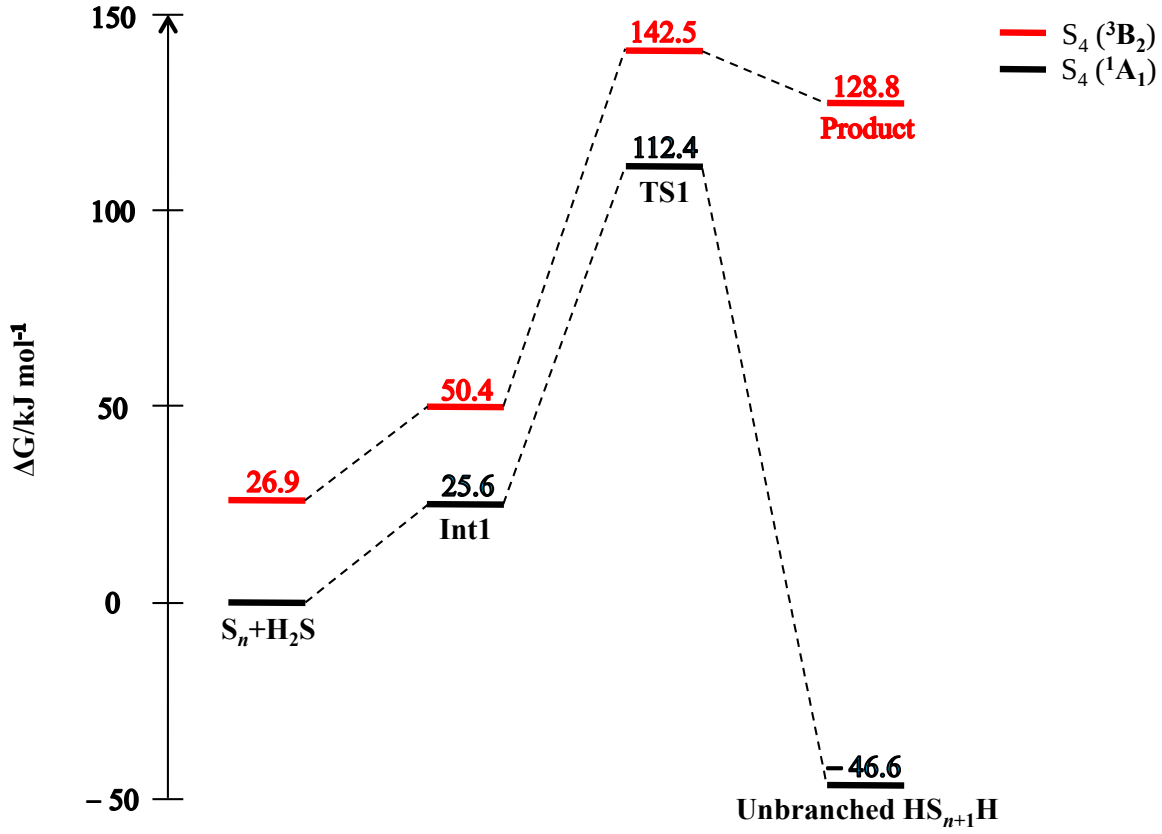

Figure 6.12. The singlet (black) and triplet (red) PESs for the reaction of S_n (n = 4) with H_2S.

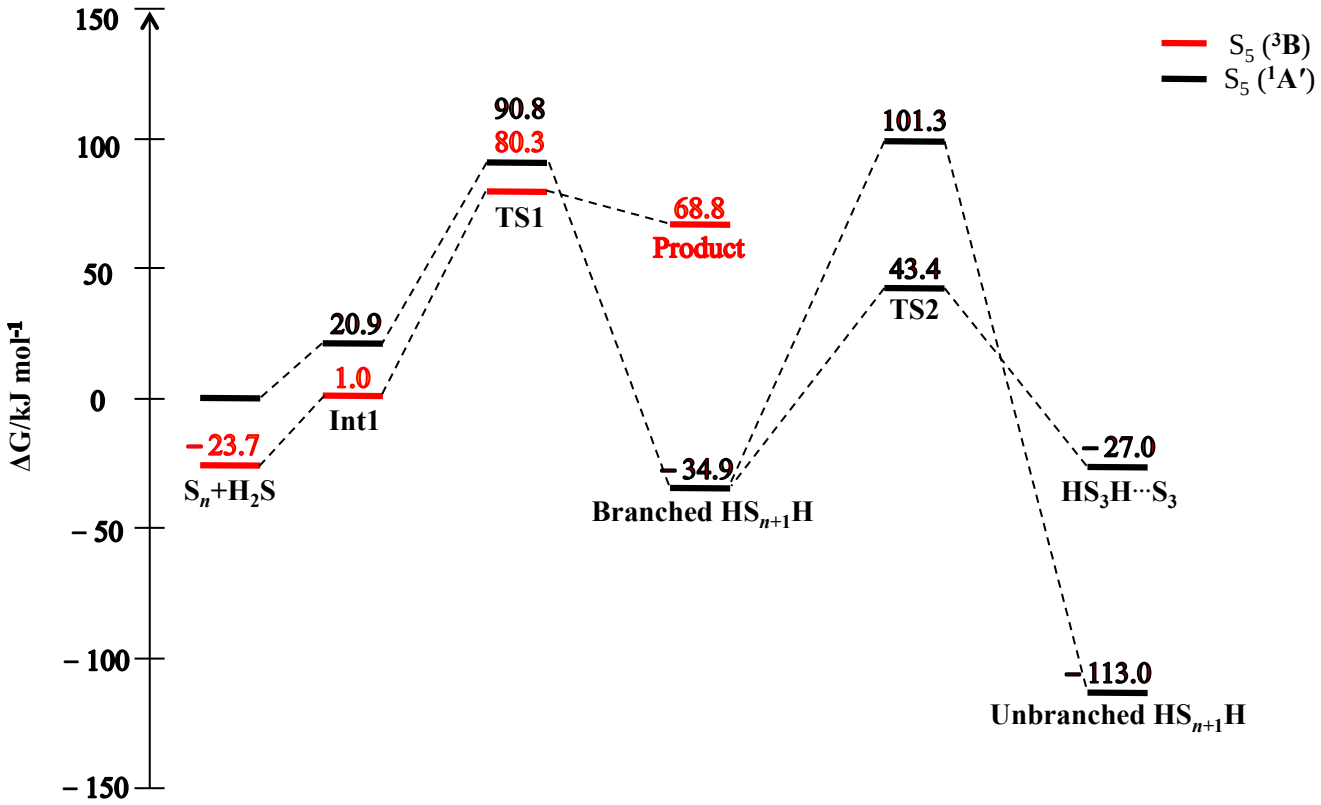

Figure 6.13. The singlet (black) and triplet (red) PESs for the reaction of S_n (n = 5) with H_2S.

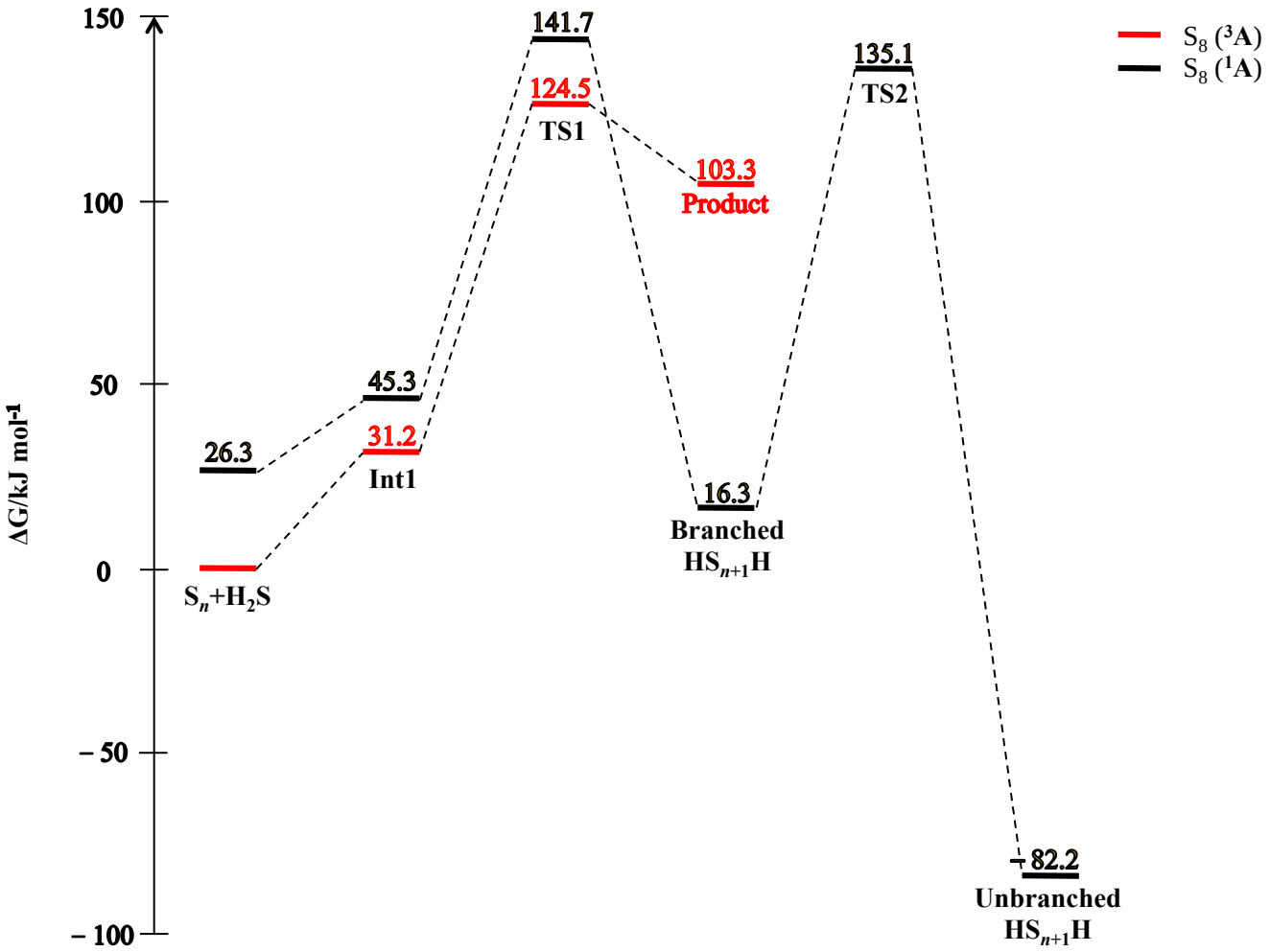

Figure 6.14. The singlet (black) and triplet (red) PESs for the reaction of S_n (n = 8) with H_2S.

6.3.5 Conformational Isomerism in Singlet State Unbranched $HS_{n+1}H$

The results discussed above suggest that the structure of the unbranched $HS_{n+1}H$ computed to form via the direct route is always different from that formed via the indirect route of the $S_n + H_2S$ reaction(s). The products of reaction exemplify this, for instance, for S_2 and S_3 (**Figure 6.10** and **Figure 6.11**) when the reaction proceeds in more than one route. This observation is therefore suggestive of the existence of structural variation in the polysulfane(s) (unbranched $HS_{n+1}H$, $n \geq 2$) formed in the $S_n + H_2S$ reaction(s); i.e., one structure of the species may undergo isomerisation to one or more other isomers. This is in line with the experimental observation of more than one conformational structure for polysulfanes, such as HS_3H with two conformational isomers[289,343] and the computation of three conformational isomers of HS_4H.[340] Such structures may include helical (C_2) structures (e.g., (**d**) in **Figure 6.15**) especially when $n \geq 3$.[291,347]

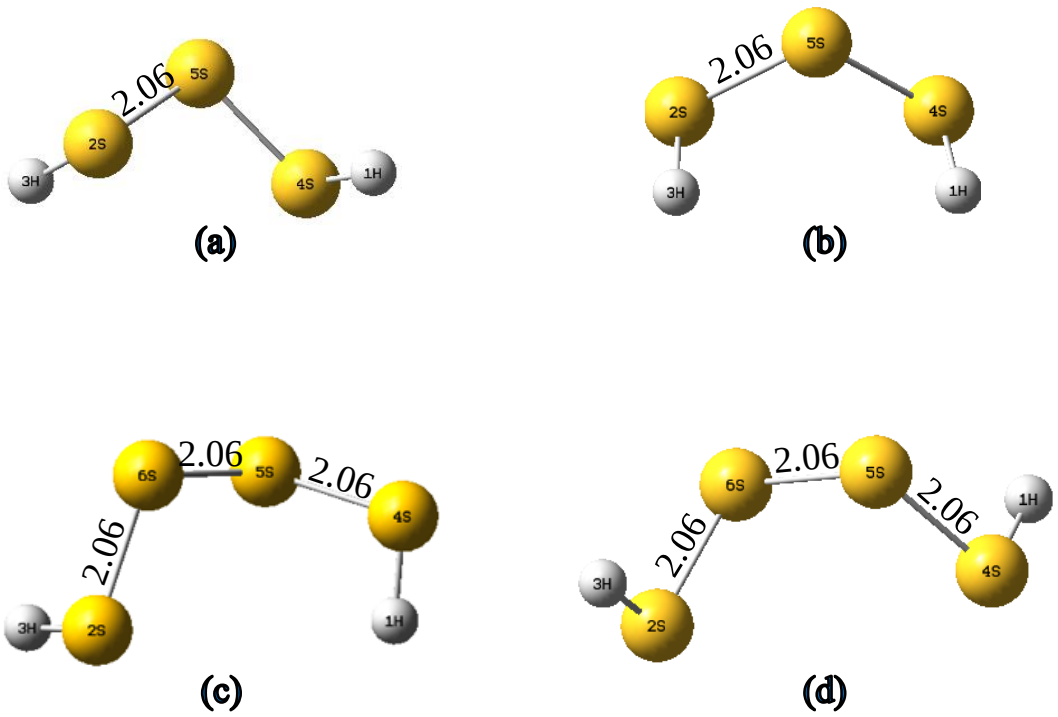

Figure 6.15. The optimised conformational structures of the unbranched $HS_{n+1}H$ formed in the direct; (**a**, C_1/C_2) and (**c**, C_1) and indirect; (**a**, C_1/C_2), (**b**, C_1) and (**d**, C_1/C_2) reaction routes of the reaction of S_2 and S_3 with H_2S. Bond lengths are in angstroms (Å).

As such, one or more conformational isomer(s) of the unbranched $HS_{n+1}H$ were computed to exist between the first unbranched reaction product and the helical (C_2) structure of the species especially for unbranched $HS_{n+1}H$ with $n \geq 3$. Only the conformational structure of HS_2H (as in **Figure 6.5**) was found in the $S + H_2S$ reaction. Also, only the two isomers (**Figure 6.15** (**a**, C_1/C_2) and (**b**, C_1)) were computed for HS_3H in agreement with experimental[343] observations. The computations suggest that there are three structural isomers for unbranched HS_4H, HS_5H and HS_6H (**Figure 6.16**) and seven conformational structures for unbranched HS_9H (**Figure 6.17**). It should be noted however, that the structures in **Figs. 6.16** and **6.17** optimised as C_1 structures.

It is found that all the isomers of each of the unbranched $HS_{n+1}H$ with the same n possess similar formation energies relative to their reactants. The isomers of HS_3H, HS_4H, HS_5H, HS_6H and HS_9H, are computed to be formed in exergonic processes of ΔG_r = -101.0, -41.2 ± 1.2, -45.0 ± 2.0, -112.0 ± 1.0 and -110.0 ± 2.0 kJ mol^{-1}, respectively. The results discussed here imply that unbranched $HS_{n+1}H$ ($n \geq 3$) exist as mixtures of non-helical and helical conformers with similar thermodynamic stabilities per series.

The rotational barriers between the respective isomers of HS_3H, HS_4H, HS_5H, HS_6H and HS_9H are summarised in **Table 6.1**.

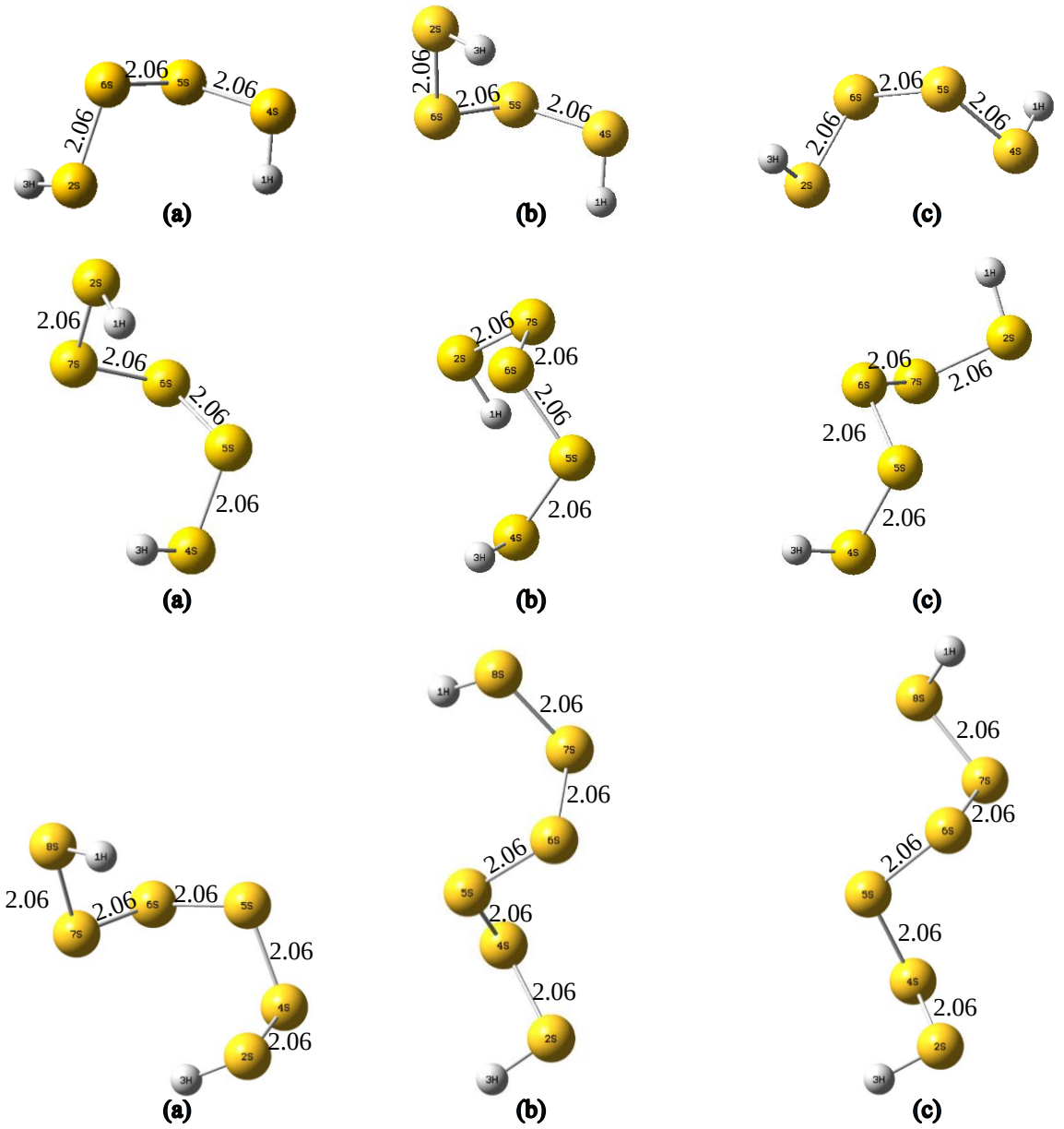

Figure 6.16. The optimised conformational structures of the unbranched $HS_{n+1}H$: HS_4H (top), HS_5H (middle) and HS_6H (bottom). The isomers are presented in order of their connectivity the transition states along reaction path. Bond lengths are in Å.

The data in **Table 6.1** suggests that regardless of the sise of the unbranched polysulfane(s), the rotational barrier for transforming from one isomer to another for a given unbranched polysulfane falls between 20.0 and 32.0 kJ mol^{-1}. This observation agrees with reports in the literature[333,334,340] which suggest that calculated torsional barriers to internal rotation for HSSH and HSSSH are calculated between 20.0 and 35.0 kJ mol^{-1}, with the *cis*-barrier always higher than the *trans*-barrier.

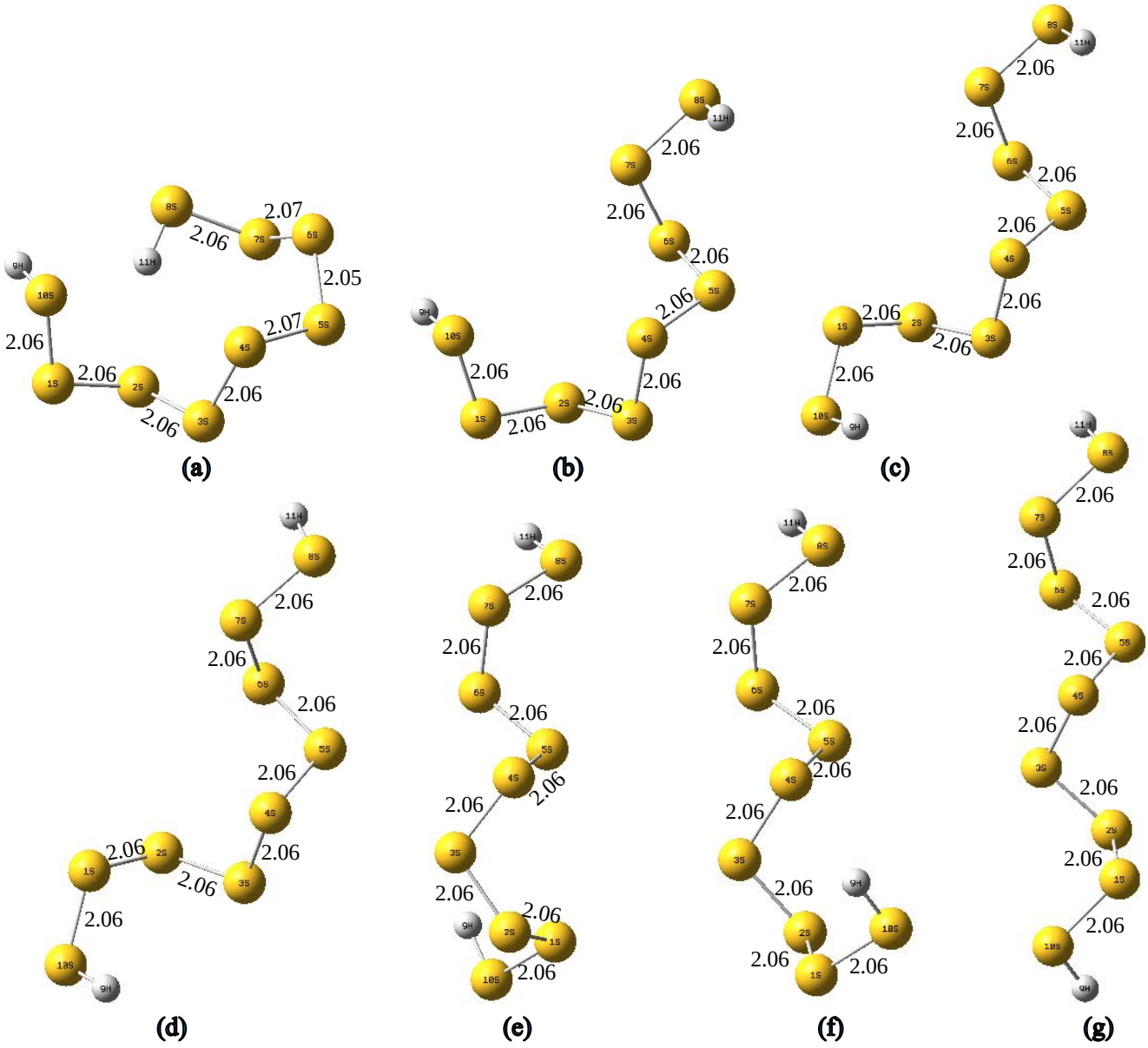

Figure 6.17. The conformational structures of the unbranched HS_9H; conformers are presented in order of their connectivity to the transition states along reaction path. Bond lengths are in Å.

Table 6.1. The forward (reverse) rotational barriers ($\Delta G^{\ddagger}$ / kJ mol^{-1}) between the isomers of unbranched $HS_{n+1}H$: HS_3H, HS_4H, HS_5H and HS_6H and HS_9H.

Species	$\Delta G^{\ddagger}_{(a)}$	$\Delta G^{\ddagger}_{(b)}$	$\Delta G^{\ddagger}_{(c)}$	$\Delta G^{\ddagger}_{(d)}$	$\Delta G^{\ddagger}_{(e)}$	$\Delta G^{\ddagger}_{(f)}$
HS_3H	23.4 (23.4)					
HS_4H	25.7 (25.8)	29.7 (28.7)				
HS_5H	27.0 (26.8)	26.6 (23.1)				
HS_6H	24.3 (24.7)	29.9 (27.5)				
HS_9H	23.6 (26.9)	25.2 (25.6)	21.9 (21.9)	29.1 (29.2)	31.1 (26.4)	27.7 (29.0)

Furthermore, Drozdova et al.,[340] computed the torsional barriers to rotation about the central S-S bond of HSSSSH as 32.0 (*cis*-barrier) and 26.6 kJ mol^{-1} (*trans*-barrier) at the MP2/6-311G** level of theory. The only experimental data available for internal rotation barriers in $HS_{n+1}H$ species are those for HSSH: 33.5 ± 1.1 and 23.8 ± 0.2 kJ mol^{-1} (*cis*- and *trans*-barriers respectively)[337] and 24.4 kJ mol^{-1} (*trans*-barrier).[338] The results in **Table 6.1** indicate that it will be difficult to separate the different structures of the respective homologous series of unbranched polysulfanes at room temperature as their interconversions will occur rapidly. This is because the rotational energy barriers to the isomerisation of a given isomer of unbranched polysulfane to another and vice versa are similar, differing only by at most 5.0 kJ mol^{-1}.

Another interesting feature of the S_n and SH units in the unbranched $HS_{n+1}H$ worthy of note is that the *r*(S-S) in all the species are of similar length, 2.06 ± 0.01 Å while all the *r*(S-H) are approximately 1.34 Å.

6.4 Conclusions

The reaction of open chain sulfur clusters, S_n ($n \leq 5$ and 8) with H_2S to generate hydrogen polysulfanes ($HS_{n+1}H$) has been investigated using the CCSD(T)/au-cc-pVTZ//ωB97XD/6-311++G(2df,2p) level of theory on the singlet and triplet PESs. The study reveals that the $HS_{n+1}H$ species are formed only on the singlet PES while the products of reaction on the triplet PES may best be described as weakly attracted species of the form: $HS\cdots S_nH$, $SH\cdots S_nH$ or $[HS]\cdots[S_nH]$ depending on *n*. It is found that both branched and unbranched $HS_{n+1}H$ may be formed in the reaction process on the singlet PES with the unbranched species always thermodynamically more stable than their branched analogues. The unbranched $HS_{n+1}H$ are found to always form in exergonic processes from the respective reaction complexes (direct route) or their branched analogues (indirect route), whereas the branched $HS_{n+1}H$ are generated in either endergonic or exergonic processes from the reaction complexes. This indicates that there is a possibility of experimentally observing branched $HS_{n+1}H$ in addition to their unbranched analogues as they are either generated in a downhill process or at a relatively low energetic cost. It is observed that in most cases, the product on the singlet PES is generated from a likely participation of "two-state reactivity"[323] in the course of reaction. The reaction products on the triplet PES on the other hand are all computed to be formed in endergonic processes: i.e., the triplet PES of the reactions is either energetically unfavourable or relatively flat. This implies that the reverse of the singlet state reactions will always be endergonic processes while that of the triplet state reactions will always be exergonic processes. The exergonicity of the reverse of the triplet PESs may therefore provide an explanation for the observed residual H_2S in sulfur recovered from natural gas or crude oil[13–15,260]

etc. in the thermal Claus process. This is because the thermodynamically more stable $HS_{n+1}H$ are always formed on the singlet PES whereas the thermodynamically more stable reactants may lie on the triplet or singlet PES depending on *n* and the electronic structure of the S_n species. It is observed that only the reaction involving S_4 does not produce a branched $HS_{n+1}H$. The overall reaction energy for the formation of unbranched $HS_{n+1}H$ on the singlet PES is found to decrease from $\Delta G_r = -314$ kJ mol^{-1} when S_n ($n = 1$) reacts through -101 kJ mol^{-1} when S_2 reacts to -41 kJ mol^{-1} when S_3 reacts after which it increases gradually to -108 and -113 kJ mol^{-1} when S_5 and S_8 react, respectively. This study suggests that unbranched $HS_{n+1}H$ with $n \geq 2$ formed in these reactions may exist in more than one structural conformation. It also reveals that regardless of the sises of the unbranched $HS_{n+1}H$, the rotational barrier for transforming from one isomer to another for a given unbranched $HS_{n+1}H$ falls between 20.0 and 32.0 kJ mol^{-1}. Furthermore, the results indicate that the forward and backward rotational energy barrier for transforming one isomer of an unbranched $HS_{n+1}H$ to another may differ by, at most 5.0 kJ mol^{-1}. This indicates that their separation at room temperature will be difficult, as their interconversions will occur rapidly. Finally, the study reveals that the *r*(S-S) in all the unbranched $HS_{n+1}H$ species are very similar: 2.06 ± 0.01 Å.

7 Electron correlation of atomic systems using a re-parameterised Colle and Salvetti formula

This chapter describes the re-parametrisation of the Colle and Salvetti (CS) correlation formula using the least squares fitting procedure in combination with accurately computed 25-term Laguerre-based Hartree-Fock (HF) wavefunctions for the helium atom and the hydride ion. Detailed determination and analysis beginning with fitting to helium atom HF densities reveals that the optimum constants for fitting to helium atom densities are; $a = 0.01628$, $b = 0.18438$, $c = 0.57594$ *and* $d = 0.80562$. *These values are found to be similar to the CS constants. The results further suggest that the optimum constants for fitting to the hydride ion densities are;* $a = 0.02578$, $b = 0.10943$, $c = 1.49357$ *and* $d = 1.22388$. *Application of the hydride fitting constants to a form of the Lee-Yang-Parr (LYP) correlation functional in combination with standard HF wavefunctions for several atomic systems suggests that resulting correlation energies are only accurate for the hydride ion. This implies that fitting to the accurately computed hydride ion densities does not improve the correlation energies nor account for the long range low density behaviour for atomic systems, especially anions. Nevertheless, the correlation energies of anions in particular are found to be especially accounted for by the fitting constants optimised from fitting to the helium atom densities. It may therefore be reckoned that long range correlation, characteristic of anionic systems, is accounted for by fitting to the computed helium atom densities. Finally, the results reveal that the variation of the approximated* $H(\beta, W)$ *function proposed by CS with nucleus-electron distance follows a decay pattern similar to that of intracule densities with inter-electronic distance for the helium atom and hydride ion, respectively. A discernible link between the variation of the two functions is however, yet unknown.*

7.1 Introduction

The Lee-Yang-Parr (LYP) correlation functional[27] is one of the widely used[348–351] inexpensive computational approaches in DFT to treat the spin independent correlated motion of electrons

(Coulomb correlation).[16–18] This motion of electrons is ignored by the HF theory.[16,18] The HF theory accounts only for the correlated motion of electrons of the same spin (Fermi correlation) via the anti-symmetry of the HF wavefunction.[16–18] The energy of the ignored correlated motion of the electrons in a system, E_c, as defined by Löwdin,[39,40] is a measure of the error in the HF method, i.e., the difference between the exact, non-relativistic energy of a system and its energy computed at the HF level of theory. This is summarised as $E_c = E_{exact} - E_{HF}$, where E_c is the correlation energy, E_{exact} is the exact, non-relativistic energy (or fully correlated energy[16–18]) and E_{HF} is an upper bound to the E_{exact} of the system thereby making E_c always negative. Computing E_{exact} however is computationally demanding except for small systems[352–360] which is why approximate approaches to compute the E_c of a system such as the Colle and Salvetti (CS)[26] formula become important. The LYP correlation functional is based on the approximate correlation energy formula derived by Colle and Salvetti (CS).[26] This formula has however been criticised over the years for a variety of reasons.[351,361–364] Nevertheless, the CS correlation formula and the LYP correlation functional is still, very successful in computing the correlation energies of systems, especially neutral atoms, atomic cations and small molecules.[26,27,351] However these formulae were not extensively tested on atomic or molecular anionic systems. It is noteworthy that the correlation energy of a system controls most of its chemical properties.[364] There is therefore room for improvement of the CS correlation formula to also account for the E_c's of atomic anionic systems. To achieve this, a first step could be to understand the physics captured or re-adjustment of the parameters in the model.[351] When this is done, it is likely to enhance the robustness of the formula in predicting E_c's for a wide range systems.

7.1.1 The Colle and Salvetti Correlation Energy Formula: Review of Literature

The approximate expression for computing the correlation energy, E_c of closed-shell systems derived by CS in 1975, beginning from a correlated wavefunction of the systems is expressed as:[26]

$$E_c = -\frac{1}{2}\int P_{2\mathrm{HF}}(\boldsymbol{R},\boldsymbol{R})\left(\int \frac{P_{2\mathrm{HF}}(\boldsymbol{r_1},\boldsymbol{r_2})}{P_{2\mathrm{HF}}(\boldsymbol{R},\boldsymbol{R})}\left(2\exp^{(-\beta^2 r^2)}\left(1-\Phi(\boldsymbol{R})\left(1+\frac{r}{2}\right)\right)\right.\right.$$
$$\left.\left.-\exp^{(-2\beta^2 r^2)}\left(1-\Phi(\boldsymbol{R})\left(1+\frac{r}{2}\right)\right)^2\right)\frac{d\boldsymbol{r}}{r}\right)d\boldsymbol{R} \qquad (7.1)$$

where $P_{2\mathrm{HF}}(\boldsymbol{r_1},\boldsymbol{r_2})$ is the HF two-electron density matrix without spin calculated at point $\boldsymbol{r_1}$ and $\boldsymbol{r_2}$, $r = |\boldsymbol{r}_i - \boldsymbol{r}_j|$ and $\boldsymbol{R} = {(\boldsymbol{r}_i + \boldsymbol{r}_j)}/{2}$. To formulate this expression, CS started from the knowledge of the $P_{2\mathrm{HF}}(\boldsymbol{R},\boldsymbol{R})$ and $\rho_1(\boldsymbol{R}) \equiv \rho(\boldsymbol{R}) = \rho$, i.e., the HF two-electron and one-electron density matrices, respectively. These density matrices are related by:

$$P_{2\mathrm{HF}}(\boldsymbol{R},\boldsymbol{R}) = \frac{1}{2}\rho(\boldsymbol{R})^2 \tag{7.2}$$

CS calculated these matrices by employing the HF method and the HF wavefunctions of atomic systems derived by Clementi.[365,366] CS formed the $\rho(\boldsymbol{R})$ of a given system by using the system's Clementi HF wavefunction[365,366] through the expression:[367]

$$\rho(\boldsymbol{R}) \equiv \rho_1(\boldsymbol{R}) = \sum_{i=1}^{N/2} n_i \cdot |\psi_i(\boldsymbol{R})|^2 \tag{7.3}$$

where N is the number of electrons in the system and n_i represents the occupancy of each spatial orbital (ψ_i). CS wrote the correlated wavefunction for a closed-shell system as:[26]

$$\Psi(\boldsymbol{x}_1,\boldsymbol{x}_2,\dots,\boldsymbol{x}_N) = \Psi_{\mathrm{HF}}(\boldsymbol{x}_1,\boldsymbol{x}_2,\dots,\boldsymbol{x}_N)\prod_{i>j}\Big(1-\varphi\big(\boldsymbol{r}_i,\boldsymbol{r}_j\big)\Big) \tag{7.4}$$

where $\boldsymbol{x}_i, i = 1,2,\dots,N$ indicates the spatial and spin coordinates of electron i, $\boldsymbol{r}_i$ represents all the spatial coordinates of electron i and $\Psi_{\mathrm{HF}}(\boldsymbol{x}_1,\boldsymbol{x}_2,\dots,\boldsymbol{x}_N)$ is the N-electron HF determinant. The latter is written as:[32,368]

$$\Psi_{\mathrm{HF}}(\boldsymbol{x}_1,\boldsymbol{x}_2,\dots,\boldsymbol{x}_N) = \left(\frac{1}{N!}\right)^{1/2}\det|\psi_1(\boldsymbol{x}_1)\psi_2(\boldsymbol{x}_2)\dots\psi_N(\boldsymbol{x}_N)| \tag{7.5}$$

These spatial orbitals are expanded in terms of basis functions, χ_i (or ϕ_j as used in eq. (2.21)) in the Roothaan-Hartree-Fock[366,369–371] method as:[19,32]

$$\psi_i = \sum_{i=1}^{M} c_{ij}\chi_i \tag{7.6}$$

with χ_i denoting the i^{th} basis function, c_{ij} as the orbital expansion coefficients and M representing the overall number of basis functions of the orbitals. The basis functions are defined as:[366]

$$\chi_i \equiv \chi_{p\lambda\alpha}(r,\theta,\phi) = R_{\lambda p}(r)Y_{\lambda\alpha}(\theta,\phi) \tag{7.7}$$

where $\lambda \equiv l$ and $\alpha \equiv m_l$, $Y_{\lambda\alpha}(\theta,\phi)$ is the spherical harmonics in complex form while $R_{\lambda p}(r)$ is the radial part of the basis functions. $R_{\lambda p}(r)$ is defined as:[366,371]

$$R_{\lambda p}(r) = \left[(2\eta_{\lambda p})!\right]^{-1/2}\left(2\xi_{\lambda p}\right)^{\eta_{\lambda p}+1/2} r^{\eta_{\lambda p}-1}e^{-\xi_{\lambda p}r} \tag{7.8}$$

where $\eta_{\lambda p} \geq \lambda + 1$ is an index for the principal quantum number, p denotes the p^{th} basis function of symmetry λ, $\xi_{\lambda p}$ is the orbital exponent chosen to give the best energy, r is the separation of an electron from an atomic nucleus.

CS defined $\varphi\big(\boldsymbol{r}_i,\boldsymbol{r}_j\big)$, the correlation factor in eq. (7.4) as:

$$\varphi\big(\boldsymbol{r}_i,\boldsymbol{r}_j\big) = \exp(-\beta^2 r^2)\left(1-\Phi(\boldsymbol{R})\left(1+\frac{r}{2}\right)\right) \tag{7.9}$$

The authors approximated $\Phi(\boldsymbol{R})$ by $\frac{\sqrt{\pi}\beta}{1+\sqrt{\pi}\beta}$ while computing β from the exclusion volume (Coulomb hole) via the Wigner's formula[372,373] as:[26]

$$\beta = \left(\frac{\sqrt{\pi}}{\sqrt[3]{\hbar_e}}\right) \cdot \rho(\boldsymbol{R})^{1/3} = q \cdot \rho(\boldsymbol{R})^{1/3} \tag{7.10}$$

where $\hbar_e$ represents the average number of electrons in the volume and q is a proportionality constant. CS determined q as 2.29 for the helium atom. To simplify eq. (7.1), CS made the approximation:

$$\int \frac{P_{2\mathrm{HF}}(\boldsymbol{r_1},\boldsymbol{r_2})}{P_{2\mathrm{HF}}(\boldsymbol{R},\boldsymbol{R})}\left(2\exp^{(-\beta^2 r^2)}\left(1-\Phi(\boldsymbol{R})\left(1+\frac{r}{2}\right)\right)-\exp^{(-2\beta^2 r^2)}\left(1-\Phi(\boldsymbol{R})\left(1+\frac{r}{2}\right)\right)^2\right)\frac{d\boldsymbol{r}}{r}$$
$$= \frac{4\pi}{\rho(\boldsymbol{R})}H(\beta,W) \tag{7.11}$$

in which:

$$H(\beta,W) = a\frac{1+bW\exp^{(-c/\beta)}}{1+{}^{d}/_{\beta}} \tag{7.12}$$

where:[26,363]

$$W(\boldsymbol{R}) = 0.7628 \cdot \rho(\boldsymbol{R})^{-8/3} \cdot \left[\nabla_{\boldsymbol{r}}^2 P_{2\mathrm{HF}}\left(\boldsymbol{R}+\frac{\boldsymbol{r}}{2},\boldsymbol{R}-\frac{\boldsymbol{r}}{2}\right)\right]_{\boldsymbol{r}=0} \tag{7.13}$$

and $\nabla_{\boldsymbol{r}}^2 P_{2\mathrm{HF}}$ is the Laplacian of the two-electron density matrix. The authors asserted that by finding the function, $H(\beta,W)$ one may compute the correlation energy of a closed-shell system as:[26]

$$E_c = -a\pi\int \rho(\boldsymbol{R})\frac{1+bWe^{\left(-c/\beta\right)}}{1+{}^{d}/_{\beta}}d\boldsymbol{R} \tag{7.14}$$

where $d\boldsymbol{R} = R^2\sin(\theta)\,d\theta d\phi dr$ with $0 \le \theta \le \pi$ and $0 \le \phi \le 2\pi$.[34,367,374] As such, only the $\rho(\boldsymbol{R})$ and constants a, b, c and d are necessary to compute the correlation energy for a given system. CS determined eq. (7.12) by numerically integrating the left hand side (LHS) of eq. (7.11) at different distances within $0.3 \le R \le 2$ a.u.[26,349] from the nucleus of the helium atom. To determine eq. (7.12), CS formed $\rho(\boldsymbol{R})$ from the Clementi HF wavefunction of the helium atom[365,366] and applied it to eq. (7.11). They then fitted the $H(\beta,W)$ function to the result of the integration thereby arriving at the values of a, b, c and d as; $a = 0.01565$, $b = 0.173$, $c = 0.58$ and $d = 0.8$.[26]

CS went on to derive an analogous formula to eq. (7.14) for open-shell systems in 1979[375] by developing the $P_{2\mathrm{HF}}(\boldsymbol{r}_1,\boldsymbol{r}_2)$ in eq. (7.1) up to second order. The expression for open-shell systems written as:[375]

$$E_c = -2\pi \int \frac{P_{2\mathrm{HF}}(\boldsymbol{R},\boldsymbol{R})}{\beta^3}\left(a\left(\frac{1+bW\exp^{\left(-c/\beta\right)}}{1+d/\beta}\right)\right)d\boldsymbol{R} \tag{7.15}$$

where $a = 0.18794$, $b = 0.173$, $c = 0.58$ and $d = 0.8$.[375] Cohen et al., in 1980[376] derived a CS-type formula by imposing the Schrödinger equation via the quantum density matrix hierarchy equations. The authors stated that by solving the equation for the helium atom, they obtained the same functional form as CS. In 1983, CS reported a detailed analysis of the methods in eq. (7.14) and eq. (7.15), outlining their advantages over the configuration interaction techniques.[377] To summarise, CS asserted that eq. (7.14) and eq. (7.15) were computationally less time demanding, easier to use and produced the same level of accuracy in calculating the total electronic energies of ground and excited states of systems. They also stated that the methods allowed evaluation of the contribution to the total correlation energy from different electronic shells. Three years later, Cohen et al.,[378] again showed that using the CS formula, the correlation energies of systems could be computed from a Slater determinant developed for computing the exact density of crystals by applying the method to the beryllium atom.

Eq. (7.14) was converted to the correlation energy functional of the electron density by Lee Yang and Parr (LYP) in 1988.[27] This, they expressed as:

$$E_c = -a\int \frac{1}{1+d\rho^{-1/3}}\left\{\rho + 2b\rho^{-2/3}\left[C_F\rho^{5/3} - 2t_W + \left(\frac{1}{9}t_W + \frac{1}{18}\nabla^2\rho\right)\right]\exp^{-c\rho^{-1/3}}\right\}d\boldsymbol{R} \tag{7.16}$$

Eq. (7.16) was formulated from eq. (7.14) by setting:[27]

$$\left[\nabla_{\boldsymbol{r}}^2 P_{2\mathrm{HF}}\left(\boldsymbol{R}+\frac{\boldsymbol{r}}{2},\boldsymbol{R}-\frac{\boldsymbol{r}}{2}\right)\right]_{\boldsymbol{r}=0} = \rho(\boldsymbol{R})[t_{\mathrm{HF}}(\boldsymbol{R}) - 2t_W(\boldsymbol{R})] \tag{7.17}$$

where the local HF kinetic energy density ($t_{\mathrm{HF}}(\boldsymbol{R})$) and the Weizsacker kinetic energy density ($t_W(\boldsymbol{R})$) are defined as:

$$t_{\mathrm{HF}}(\boldsymbol{R}) = \frac{1}{8}\sum_i \frac{|\nabla\rho_i(\boldsymbol{R})|^2}{\rho_i(\boldsymbol{R})} - \frac{1}{8}\nabla^2\rho(\boldsymbol{R}) = t_{\mathrm{TF}}(\boldsymbol{R}) + \left(\frac{1}{9}t_W + \frac{1}{18}\nabla^2\rho(\boldsymbol{R})\right) \tag{7.18}$$

$$t_W(\boldsymbol{R}) = \frac{1}{8}\frac{|\nabla\rho(\boldsymbol{R})|^2}{\rho(\boldsymbol{R})} - \frac{1}{8}\nabla^2\rho(\boldsymbol{R}) \tag{7.19}$$

respectively. The Thomas-Fermi kinetic energy density is defined as $t_{\mathrm{TF}}(\boldsymbol{R}) = C_F\rho^{5/3} = \left(\frac{3}{10}(3\pi^2)^2\right)\cdot\rho^{5/3}$ where C_F is a constant; $\nabla^2\rho(\boldsymbol{R})$ is the Laplacian of the one-electron density matrix. LYP determined the constants in eqn. (7.16) as:[27] $a = 0.04918$, $b = 0.132$, $c = 0.2533$ and $d = 0.349$. Eq. (7.14) and eq. (7.16) rely on the correlation factor, $\varphi(\boldsymbol{r}_i,\boldsymbol{r}_j)$ that satisfies the electron-electron cusp condition and the constants, a, b, c and d.[16,26,27] In 1989, Miehlich et al.,[379] compared the performance of the Becke 1988 correlation functional (B88)[380] and the LYP

functional by using them to compute the correlation energies of the first-row atoms, ions and molecules. It is worth noting that the B88 correlation functional is a uniform electron gas (UEG) functional[380] while the LYP is not.[348] They found that correlation contributions to ionisation energies, electron affinities and dissociation energies obtained by the two models were comparable to other density functionals.[379] The authors also reported similar correlation energies for the systems considered using the two formalisms with the LYP performing better in most cases. CS again in 1990 generalised eq. (7.1) to treat electron correlation in systems with many-determinant wavefunction.[381] The authors asserted that the generalised method resulted in energies that were only a few tenths of the milli-hartree (10^{-4} a.u.) less accurate in comparison to the experimental, non-relativistic electronic energies for atomic and diatomic systems. Later this same year, Flocco et al.,[382] tested the limits of the validity of the CS formalism eq. (7.14), by applying same to a series of helium and beryllium *iso*-electronic ions and reported that the approximation breaks down for sufficiently high nuclear charge, Z. Then in 1991, Moscardó and San-Fabián deduced an approximate CS-type functional from a wavefunction within the correlation factor approach.[383] The authors stated that the functional omitted terms that depended on the gradient of the density but included inhomogeneity effects and showed the simplicity of local density functionals without spin. They also suggested that the functional stressed the validity of the expression adopted by CS for building the correlation factor. The authors then concluded that their functional therefore provides an avenue for gaining insights into the deficiencies of functionals resulting from a perspective of the Hohenberg and Kohn (HK) theorem. Later that same year, the authors showed that the limitations in functionals derived from the HK theorem were due to the absence of non-local two-body effects.[384] They therefore stated that a complete description of the two-body problem required the incorporation of the two-electron density. The authors then used simple approximations to incorporate two-body density explicitly into equations of the density functional and concluded that their behaviour was improved considerably.

In 1997, Tsuneda and Hirao[364] asserted that all the previously proposed CS-type correlation methods, CS[26] and LYP,[27] do not obey the distinct treatment of paired-spin and unpaired-spin correlations due to fitting to the helium atom, a paired-spin system. This led the authors to propose a new, spin-polarised CS-type dynamical correlation functional that satisfies this condition to treat paired and unpaired-spin electron correlation in systems.[364] This, they summarised for paired-spin as:

$$E_c^{\sigma_1\sigma_2} = -\int \left(\frac{\rho_{\sigma_1}^{1/3}}{K_{\sigma_1}} + \frac{\rho_{\sigma_2}^{1/3}}{K_{\sigma_2}}\right)^3 \frac{0.04488}{1+\left(\frac{0.7826}{\beta_{\sigma_1\sigma_2}}\right)} d^3\boldsymbol{R} \quad \text{for } \sigma_1 \neq \sigma_2 \tag{7.20}$$

and for unpaired spin as:

$$E_c^{\sigma\sigma} = -0.07614 \int \left(\frac{\rho_\sigma}{K_\sigma^3}\right) W_{\sigma\sigma} d^3\boldsymbol{R} \tag{7.21}$$

where

$$\beta_{\sigma\sigma'} = q_{\text{new}}^{\sigma\sigma'} \frac{\rho_\sigma^{1/3} \rho_{\sigma'}^{1/3} K_\sigma K_{\sigma'}}{\rho_\sigma^{1/3} K_\sigma + \rho_{\sigma'}^{1/3} K_{\sigma'}} \tag{7.22}$$

and

$$W_{\sigma\sigma} = \frac{\left[\nabla_{\boldsymbol{r}}^2 P_{2\text{HF}}^{\sigma\sigma}\left(\boldsymbol{R} + \frac{\boldsymbol{r}}{2}, \boldsymbol{R} - \frac{\boldsymbol{r}}{2}\right)\right]_{\boldsymbol{r}=0}}{\rho(\boldsymbol{R})^2 \beta_{\sigma\sigma}(\boldsymbol{R})^2} \tag{7.23}$$

The authors asserted that $q_{\text{new}}^{\sigma\sigma'}$ determined the correlation length in a system while K_σ is a constant determined from Becke's exchange functional[64] as $K_\sigma = \left[3\left(\frac{3}{4\pi}\right)^{1/3} + 2\zeta \frac{x_\sigma^2}{1+6\zeta x_\sigma \sinh^{-1} x_\sigma}\right]$; $x_\sigma = |\nabla\rho_\sigma|/\rho_\sigma^{4/3}$ and $\zeta = 0.0042$ a.u. They determined that for unpaired-spin using a beryllium wavefunction, $q_{\text{new}}^{\sigma\sigma'} = 2.60$ while for paired-spin using a helium atom wavefunction, $q_{\text{new}}^{\sigma\sigma'} = 2.68$. The authors then suggested that the new method gave good results for the total correlation energies of atomic systems in both excited and ground state, thus leading to an accurate estimation of the energy difference between two states. Tsuneda and Hirao also noted that the constants, a, b, c and d in the CS correlation potential factor, i.e., the $H(\beta, W)$ function (eq. (7.12)), were positive fitting parameters and went on to determine same using the least squares fitting (LSF) procedure.[364] Two years later, Tsuneda et al.,[363] reported the one-parameter CS-type correlation functional:

$$E_c^{\text{OP}} = -\int \rho_\alpha \rho_\beta \frac{1.5214\beta_{\alpha\beta} + 0.5764}{\beta_{\alpha\beta}^4 + 1.1284\beta_{\alpha\beta}^3 + 0.3183\beta_{\alpha\beta}^2} d^3\boldsymbol{R} \tag{7.24}$$

where $\beta_{\alpha\beta}$ is defined as in eq. (7.22) with the subscript as $\alpha \equiv \sigma$ and $\beta \equiv \sigma'$. To propose this functional (eq. (7.24)), the authors argued that the CS formula, eq. (7.14) could be separated into two expressions:

$$E_c^{no\,W} = -a\pi \int \rho(\boldsymbol{R}) \frac{1}{1 + {}^{d}/_{\beta}} d^3\boldsymbol{R} \tag{7.25}$$

and

$$E_c^{W} = -a\pi \int \rho(\boldsymbol{R}) \frac{bW e^{\left({}^{-c}/_{\beta}\right)}}{1 + {}^{d}/_{\beta}} d\boldsymbol{R} \tag{7.26}$$

They suggested then that eq. (7.26) was not necessary in computing the correlation energies of systems as it led to increase in the E_c's of light atoms and decrease in the E_c's of atoms heavier than carbon. However, eq. (7.24) as formulated gave good correlation energies for atoms heavier than

carbon but wrong energies for atoms lighter than carbon when they used it to compute the correlation energies of He to Ar.[363] This same year, Singh et al., analysed the CS formula to assert that:[361]

1. The formula is not normalised.
2. The corresponding Coulomb hole structure is inaccurate.
3. The formula violates the Coulomb hole sum rule.
4. The Coulomb component of the Kohn-Sham (KS) correlation potential in the formula is inaccurate and so the KS correlation potential is erroneous.
5. The Coulomb correlation and correlation-kinetic-energy components of the KS correlation energy are in error.

The authors then concluded that the physics of the electron correlation described by the formula was inaccurate therefore, results obtained by the CS formula or those based on it are not well founded.

In 2000, Caratzoulas and Knowles reported a critical review of the CS model (eq. (7.14)) after applying the formalism to two-electron problem and comparing with a variational wavefunction.[362] They found that the Coulomb hole was too short ranged in agreement with the earlier report of the inaccuracies associated with the Coulomb hole in the formalism by Singh et al.[361] Caratzoulas and Knowles therefore asserted that the CS model was biased towards regions of large electron density while neglecting pair correlations that are long ranged. They went on to note that the correlation energy per electron was found to be singular at the nucleus and that the error due to neglect of the single-particle operators was of the order of magnitude of the correlation energy itself. The authors concluded that the CS model predicts inaccurate pair correlations and should be used with great care. Tao et al., in 2001[385] suggested that the most fundamental approximation in the CS model, eq. (9) in the CS paper:[26,349]

$$E = E_{\mathrm{HF}} + \frac{1}{2}\int P_{2\mathrm{HF}}(\boldsymbol{r_1},\boldsymbol{r_2})\left(\phi^2(\boldsymbol{r_1},\boldsymbol{r_2}) - 2\phi(\boldsymbol{r_1},\boldsymbol{r_2})\right) \times \frac{1}{r_{12}} d\boldsymbol{r_1} d\boldsymbol{r_2} \tag{7.27}$$

gave rise to 25 % of the true correlation of a UEG and not 100 % as previously believed. The authors went on to state that while short-range correlations were described surprisingly well by the CS approach, important long-range correlations were not accounted for by the model. Cohen and Handy in 2001 mentioned that even though the LYP functional is one of the most often used correlation functional, it is not a UEG functional, is designed for unlike-pair (opposite-spin) correlation but gives zero correlation energy for hydrogen atom correctly.[348] These observations agree with those made by Tsuneda and Hirao.[364] It is noteworthy that for UEG functionals, the key is that parameterisations involve simulations such that:[348]

$$E_{\mathrm{tot}} = T_s[\rho] + E_{\mathrm{x}}[\rho] + E_c[\rho] \tag{7.28}$$

where the total energy of a system, E_{tot} is deduced from the simulations, while the kinetic energy functional, T_s and the exchange energy functional, $E_{\mathrm{x}}[\rho]$ are analytically known. The authors[348] went on to assert that the major error of the LYP approach is that its form gives zero correlation energies for like-spin (parallel-spin) correlation while also over appropriating correlation contributions to the unlike-spin. In 2002, Handy and Cohen examined the CS derivation of the LYP functional in detail while searching for a justifiable form for a molecular dynamic correlation functional.[349] The authors argued that the reasonable expression for correlation energy for this formalism:

$$E_c = \int P_{2\mathrm{HF}}(\boldsymbol{r_1}, \boldsymbol{r_2})\left(\phi^2(\boldsymbol{r_1}, \boldsymbol{r_2}) - 2\phi(\boldsymbol{r_1}, \boldsymbol{r_2})\right) \times \frac{1}{r_{12}} d\boldsymbol{r_1} d\boldsymbol{r_2} \tag{7.29}$$

where 2ϕ is the dominant term, should account for paired-spin correlation. The authors therefore combined this argument and others made in their paper to formulate a four parameter generalised gradient correlation functional, CS1. They suggested that this functional performed nearly as well as the LYP functional. They went on to state that unlike the LYP functional, CS1 had two identifiable terms for opposite-spin and two identifiable terms for parallel-spin correlation. They concluded that it may not be possible to find a local functional that was significantly more accurate for chemistry applications than the commonly used generalised gradient approximation (GGA) functionals. Later this same year, Imamura et al.,[350] investigated the behaviour of the CS model using helium as a case study. They analysed the correlation hole and energy contributions to reveal that correlation effects were not taken into account appropriately due to missing kinetic correlation. They also stated that the simplified form of the CS model, eq. (7.14) also had some problems. The authors then addressed these issues by constructing a new CS-type correlation functional based on $P_{2\mathrm{HF}}$ that included correlation effects and kinetic energy via an adiabatic connection formula. Furthermore, the authors asserted that the opposite and parallel-spin correlations were treated independently. They also suggested that their functional reproduced accurate correlation energies for the atoms, hydrogen to argon.

In 2003, Sancho-García and Moscardó[386] examined the behaviour of the CS formalism for strongly correlated systems with negligible non-dynamic effects. The authors used the CS model in conjunction with a multi-configurational wavefunction and were able to accurately reproduce multi-reference coupled-cluster results for automerisation of cyclobutadiene. They also asserted that they were able to provide the correct energy profiles for dissociating diatomic molecules. They then suggested that the results confirmed the quality of the CS model for complicated chemical problems even though it did not satisfy some known exact properties. Ragot and Cortona modified the CS

formalism to explicitly include the kinetic contribution to the correlation energy in 2004.[387] The authors achieved this by applying a many-electron wavefunction and including correlation effects through the Jastrow factor (used by CS):

$$f(\boldsymbol{r}_1, \boldsymbol{r}_2) = \left[1 - \Phi(\boldsymbol{R})\left(1 + \frac{r_{12}}{2}\right)\right] \exp^{\left(-\beta(\boldsymbol{R})^2 r_{12}^2\right)} \tag{7.30}$$

By applying eq. (7.30) to a UEG, they re-wrote the equation as:

$$f(r_{12}) = \left[1 - \Phi\left(1 + \frac{r_{12}}{2}\right)\right] \exp^{\left(-\beta^2 r_{12}^2\right)} \tag{7.31}$$

they derived an analytical expression for the kinetic correlation energy. Thereafter, they deduced an expression for the total correlation energy of systems. They suggested that unlike the CS approach, the parameters entering their expressions were determined analytically therefore leading to a satisfactory agreement with the Perdew and Wang[388] correlation energy functional based on UEG.

Two years later, Moscardó et al.,[389] studied the CS correlation factor by comparing the behaviour of three different correlation functionals. The authors used the three functionals to analyse the: i.) normalisation, ii.) sum rule, iii.) Coulomb hole, iv.) correlation energy integrand and v.) the Wigner exclusion hole. They then noted that the correlation factor proposed by CS was very good for modelling electron correlation in atoms. They also suggested that the limitations in the CS model were mainly due to inadequate use of the first mean value theorem of integral calculus. Then in 2007, Moscardó[390] applied the CS wavefunction model to the UEG model using different levels of approximations. He asserted that contrary to previous assertions by Tao et al.,[385] the CS formalism was able to semi-quantitatively reproduce the properties of the UEG. He went on to state that the requirement for this outcome was the choice of the parameter, q, entering the CS wavefunction. The author also put forward a simple functional for the correlation energy and asserted that the results obtained from its application to the UEG were reasonable. He concluded that the CS wavefunction remained a good option to build the correlation component of an N-electron system in an approximate way. Later this same year, Pittalis et al., suggested a remedy for the inability of the exchange-correlation functionals to reproduce the degeneracy of different ground states of open-shell atoms.[391] To do this, the authors presented an analysis of the problem by investigating functionals that explicitly depended on the KS orbitals. They then went beyond the exact-exchange approximation by adding correlation in the form of the CS model to show how current-dependent terms enter the CS expression and evaluated their relevance. The authors concluded that very good description of the degeneracy of ground states for atoms of the first and second row was obtained. In 2008, Imamura et al., proposed a CS-type electron-nucleus correction in the nuclear orbital and molecular orbital theory.[392] The authors suggested that the correction was designed to correct the cusp condition for the electron-nucleus interaction. Furthermore, they asserted that since the

correction is expressed in terms of the electron and nucleus densities, the evaluation was computationally feasible. Also in this same year, Pittalis et al.,[393] derived a local CS-type approximation for the correlation energy in two-dimensional (2-D) electronic systems by considering a Gaussian approximation for the pair density. The authors introduced an *ad hoc* modification of the CS model and claimed that it better accounted for both long-range correlation and the kinetic energy contribution to the correlation energy. They also asserted that their functional was local and depends parametrically on the number of electrons in a system. They went on to apply the formulated functional to the UEG and a set of 2-D quantum dots covering a wide range of electron densities. They then suggested that in all their test cases, they found an excellent agreement between their results and the exact correlation energies. Handy published a paper in 2009 titled; the importance of the CS paper for computational DFT.[351] In this paper, the author showed the importance of the CS model (eq. (7.1) and eq. (7.14)) in the development of modern computational DFT. To do this, the author discussed several topics but most importantly the development of the LYP dynamic correlation functional from the CS model. In doing so, he asserted that the method and allied models could be improved by re-adjusting the value of the four constants; a, b, c and d in eq. (7.12) by fitting to atomic correlation energies of helium to argon. It is worthy of note that Tsuneda and Hirao also determined the values of these constants by means of the LSF procedure by fitting to the helium atom data.[364]

In 2010, Ragot[394] derived the one-electron reduced density matrix underlying their earlier derived model[387] in closed form. He alluded that the density matrix was parameter-free by construction but not N-representable due to the approximations used in the Ragot-Cortona[387] approach. The went on to assert that the resulting density matrix formally corrected the short- and long-range expansions. Udagawa et al., proposed an electron-nucleus CS-type correlation functional for multicomponent DFT in 2014.[395] They demonstrated that the functional quantitatively reproduced the quantum mechanical effects of protons and the effective potential energy curve for the H_2 molecule. They then asserted that the strategy employed to develop the functional could be applied as a recipe to deduce new functionals for the potentials of other particle interactions such as the electron-positron and electron-muon interaction since it was derived without unphysical assumptions. Three years later, Yang et al., formulated the electron-proton correlation functional, epc17 by extending the CS formalism and implemented it within the nuclear-electronic orbital (NEO) framework.[396] The authors asserted that the NEO-DFT (epc17) method efficiently produced accurate proton densities and is promising for diverse applications. A year later in 2018, Brorsen et al., asserted that multicomponent DFT allows the consistent quantum mechanical treatment of both electrons and nuclei.[397] The authors derived yet another electron-proton functional denoted epc18

using a different form for the parameter interpreted as representing the correlation length for electron-proton interaction. They then asserted that epc18 performed similarly to epc17 in predicting 3-D proton densities and affinities. Then in 2019, Patra and Samal constructed CS-type energy functionals for dynamical correlation for 2-D quantum systems.[398] The authors assessed the proposed functionals through parabolic quantum dot systems to compare exact correlation energies along with self-consistent results. They then asserted that the computed correlation energies agreed well with reference results having minimum errors.

In all the available literature summarised above, no rational re-adjustment or re-determination of the constants in eq. (7.12) has been reported. There is also, little or no correlation energies for anions (atomic or molecular) computed when testing CS or allied functionals as almost all the reported correlation energies are for neutral atoms or cations. It is on these grounds that this work finds its significance.

7.1.2 Justification of Study

It is proposed that the CS models can be improved upon by re-determining the constants, a, b, c and d in eq. (7.12) using a fitting procedure. In addition, it has been asserted that the CS model fails to account for important long-range correlations.[362,385] It was mentioned that the LSF approach was used to determine the constants while fitting to the helium atom density.[364] However, no report exists in the available literature for addressing the long-range correlation behaviour nor rational and/or systematic determination of the constants by fitting to anionic densities. It is in this regard that this work hopes to capture the long-range correlation behaviour by rational and systematic fitting to the hydride ion HF densities. The HF wavefunction for the hydride ion is likely to possess properties that will represent the long-range behaviour asserted to be lacking[362,385] in the CS formalism. This is because the density and Coulomb hole curves arising from accurate HF and fully correlated wavefunctions for the helium atom and hydride ion reveal that the densities die out faster for the helium atom than the hydride ion. This is summarised in the density and Coulomb hole distributions with inter-electronic separation in **Figure 7.1** for the helium atom and hydride ion as reported by Cox et al.[18] The Coulomb hole curves in **Figure 7.1** were calculated as $\Delta D(r) = D_{\mathrm{FC}}(r) - D_{\mathrm{HF}}(r)$.[18] It can also be seen from **Figure 7.1** that the Coulomb hole and density of the helium atom is less diffuse in comparison to that of the hydride ion. It is therefore reasonable to conclude that the Coulomb hole for the helium atom represents very well the short-range[362] correlation behaviour while that for the hydride ion is likely better to capture the long-range correlation behaviour. Hence, the β parameter for these systems will also be different; likewise, the fitting constants; a, b, c and d.

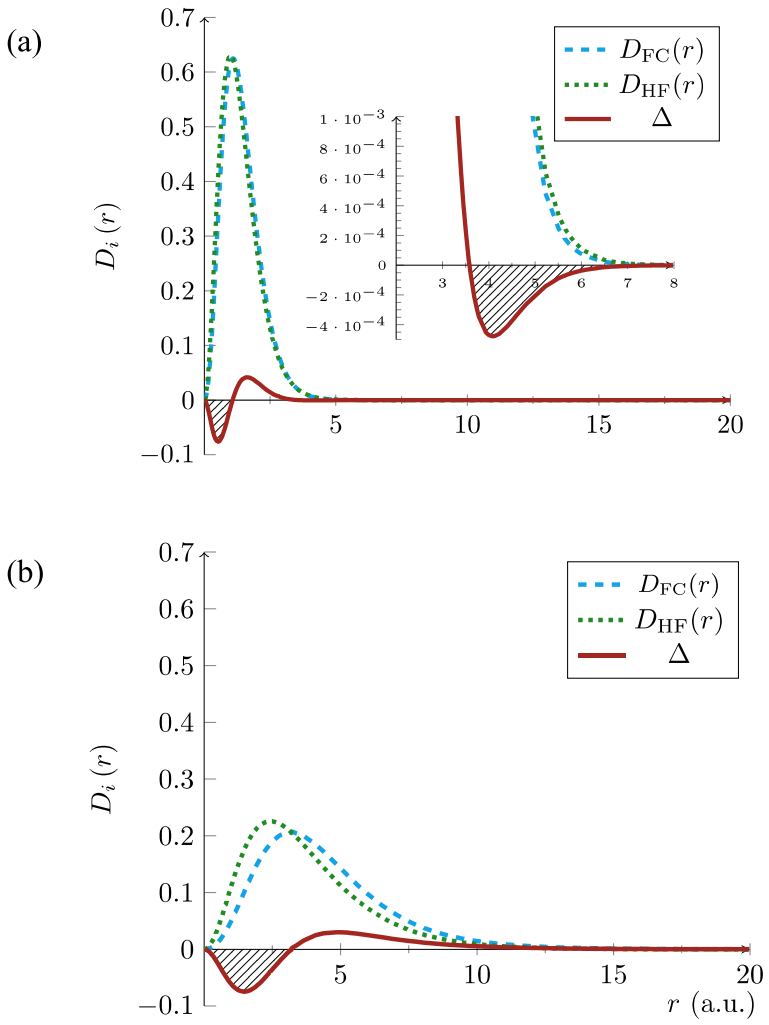

Figure 7.1. Variation of the intracule densities, $D_i(r)$ with inter-electronic distance $r = r_{12}$ for: (a) the helium atom and (b) the hydride ion. Blue dashed lines are for densities computed with the fully correlated method ($D_{\mathrm{FC}}(r)$) and green dotted lines represent densities computed with the HF method ($D_{\mathrm{HF}}(r)$). Also included is the Coulomb hole (shaded portion) for the systems, respectively (red solid lines); the inset in (a) is a secondary Coulomb hole. Adapted from Baskerville, King, Cox, *R. Soc. Open Sci.* **2019**, *6*, 181357.[18]

7.1.3 Aim of Study

The aim of the work presented in this chapter is to re-parameterise eq. (7.12) in the CS formalism using the HF densities for the helium atom with an accurate helium wavefunction and test the workability of the in-house implementation of the formula using the determined constants. The HF density for the hydride ion will then be used to determine the constants in eq. (7.12) with the hope of capturing the long-range correlation behaviour in the CS model. To do this, the objectives are:

1. Accurate Laguerre-based HF wavefunction will be computed for the helium atom and the hydride ion.[16]

2. The wavefunctions will be used to compute the densities required to determine the constants, a, b, c and d in eq. (7.12) for the helium atom or hydride ion via the LSF[399,400] procedure.
3. The determined constants in combination with Koga et al.,[401] HF wavefunctions for systems will be used to compute the correlation energies of several atomic systems including anions.

7.2 Computational Details

All computations presented in this chapter were performed using an in-house Python and/or Maple[402] code.

7.2.1 The Laguerre-Based HF Wavefunctions for Helium Atom or Hydride Ion

The singlet ground state of the helium atom and hydride ion within the fixed nucleus approximation are computed using an accurate in-house implementation of the HF method using a Laguerre-based wavefunction.[16,18] Here, the HF wavefunction (also in eq. (2.14)) is taken as:[16,18,19,32]

$$\psi_{\mathrm{HF}}(r_1, r_2) = \psi(r_1)\psi(r_2) \tag{7.32}$$

where the required anti-symmetry of the total wavefunction is embedded in the spin part which has been integrated out. $\psi(r_i)$ has the form:[16,18]

$$\psi(r_i) = e^{-\left(\frac{1}{2}\right)Ar_i} \sum_{\mathrm{q}=0}^{\infty} C(\mathrm{q}) L_{\mathrm{q}}(Ar_i) \left(\cong \sum_{q=0}^{M-1} c_{\mathrm{q}i}\phi_{\mathrm{q}} \right), \quad i = 1 \text{ or } 2 \tag{7.33}$$

where A is treated as a non-linear variational parameter (NLP) and is introduced to increase the convergence for a given basis set sise. The infinite sum is solved in truncated form with M basis functions ϕ_{q} (χ_i as used in eq. (7.6)) taken to be the normalised Laguerre functions, $e^{-x/2}L_{\mathrm{q}}(x)$ of degree (or order) q. These Laguerre functions are defined from 0 to ∞ as:[16,17,105,106]

$$\int_0^{\infty} e^{-x}\left[L_{\mathrm{q}}(x)\right]^2 dx \equiv \int_0^{\infty} e^{-x} L_{\mathrm{p}}(x) L_{\mathrm{q}}(x) dx = \delta_{\mathrm{pq}} = \begin{cases} 1 \text{ (when p = q)} \\ 0 \text{ (when p} \neq \text{q)} \end{cases} \tag{7.34}$$

where δ_{pq} is the Kronecker delta. The two-electron system lies in the plane of the two axes of a right-handed system with the third axis perpendicular to the plane of the two-electron system.[106] As such, the internal coordinates are chosen to be the inter-particle distances, r_1, r_2 and r_{12}. The r_i's are therefore obtained by choosing the translationally invariant Cartesian coordinates of the particles:[16,106]

$$\underline{t}_1 = \left(\underline{x}_{electron_1} - \underline{x}_{nucleus}\right) \quad \text{and} \quad \underline{t}_2 = \left(\underline{x}_{electron_2} - \underline{x}_{nucleus}\right) \tag{7.35}$$

to be:

$$r_i = \left|\underline{t}_i\right| \quad i = 1,2 \quad \text{and} \quad r_{12} = \left|\underline{t}_2 - \underline{t}_1\right| \tag{7.36}$$

To evaluate the internal coordinate part of the Jacobian, the Cartesian coordinates are transformed via:[16,105]

$$dx_1^3 dx_2^3 = 8\pi^2 r_1 r_2 r_{12} dr_1 dr_2 dr_{12} \tag{7.37}$$

By so doing, the integration is over $dr_1 dr_2 dr_{12}$ as the r_{12} in the Jacobian is easily cancelled by the $\frac{1}{r_{12}}$ in two-electron integrals. For systems considered, the $\psi(r_i)$ are independent of the angle as they have ^{1}S ground state. This wavefunction is chosen to complement work in the Cox group on fully correlated systems.

For these two-electron atoms, i.e., systems having the form $\{e_1^- \; e_2^- \; m_N^{Z+}\}$, the general form of the non-relativistic, time independent Schrödinger equation in its simplest form[106] is expressed as in eq. (2.1); $\hat{H}\psi = E\psi$. In the fixed nucleus approximation (i.e., the mass of the nucleus, $m_N = \infty$), the Hamiltonian for these systems, $\hat{H}$ is a sum of the kinetic and potential energy terms expressed in atomic units ($m_e = e = (4\pi\epsilon_0)^{-1} = \hbar = a_0 = 1$) as:[16,17]

$$\hat{H} = -\frac{1}{2m_1}\nabla_1^2 - \frac{1}{2m_2}\nabla_2^2 - \frac{Z}{r_1} - \frac{Z}{r_2} + \frac{1}{r_{12}} \tag{7.38}$$

where $r_i, i = 1,2$ are the nucleus-electron distances, r_{ij} denotes the inter-electron distances, $m_i = 1$ represents the masses of the electrons while the Z stands for the nuclear charge. As discussed in Chapter 2, the HF equations have the form $\hat{F}\psi_i(1) = \varepsilon_i\psi_i(1)$ where:

$$\hat{F} = \hat{H}^{core}(1) + \sum_{j=1}^{N}\left(2\hat{J}_j(1) - \hat{K}_j(1)\right), \quad \hat{H}^{core}(1) = -\frac{1}{2m_1}\nabla_1^2 - \frac{Z}{r_1}$$

The core Hamiltonian is solved using the series solution method[17] by substituting eq. (7.33) into the HF equations and solving $\left(\hat{H}^{core} - E\right)\psi = 0$. Here, the Laguerre recurrence relations:[16,17,105]

$$xL_{\mathrm{q}}(x) = -(\mathrm{q}+1)L_{\mathrm{q}+1}(x) + (2\mathrm{q}+1)L_{\mathrm{q}}(x) - \mathrm{q}L_{\mathrm{q}-1}(x) \tag{7.39}$$

$$xL'_{\mathrm{q}}(x) = \mathrm{q}L_{\mathrm{q}}(x) - \mathrm{q}L_{\mathrm{q}-1}(x) \tag{7.40}$$

$$xL''_{\mathrm{q}}(x) = (x-1)L'_{\mathrm{q}}(x) - qL_{\mathrm{q}}(x) \tag{7.41}$$

are employed to eliminate all the derivatives and powers of the variables r_i arising from $\hat{H}^{core}$ and the overlap.[16,106] The primes denote the derivatives (first ($'$) and second ($''$) derivatives) with

respect to x.[105] This leads to a 5-term[105] recursion relation between the $C(q)$ in eq. (7.33) summarised as:[16,17]

$$\sum_{\alpha=-2}^{+2} R_\alpha(\mathrm{q}) C(\mathrm{q}+\alpha) = 0 \tag{7.42}$$

This is used to form a sparse secular determinant that is solved in truncated form to give the eigenvalues.[403] This recursion relation represents a set of linear equations for determining $C(q)$ and the vanishing of their determinant gives the hydrogen-like core energy eigenvalues of the systems. These one-electron terms are very fast to calculate using the series solution method explicitly.[16–18] The recursion relation is calculated once and then used to determine the M^2 matrix elements for a given matrix sise, M (which in the present work is $M = 25$, i.e., a 25-term wavefunction). It is not possible to use this method for the two-electron integrals arising from $\hat{J}$ and $\widehat{K}$, as they give rise to terms that do not satisfy the Laguerre orthogonality condition (eq. (7.34)). Nevertheless, these integrals are analytically solved by exploiting the properties of the Laguerre polynomials, $L_\mathrm{q}(x)$ defined as:[16,17]

$$L_\mathrm{q}(x) = \frac{1}{\mathrm{q}!} e^x \frac{d^\mathrm{q}}{dx^\mathrm{q}}(x^\mathrm{q} e^{-x}) = \sum_{\mathrm{q}_i=0}^{\mathrm{q}} (-1)^{\mathrm{q}_i} \binom{\mathrm{q}}{\mathrm{q}_i} \frac{x^{\mathrm{q}_i}}{\mathrm{q}_i!} \tag{7.43}$$

To do this, the integral is converted to *perimetric* coordinates, z_i (**Figure 7.2**):

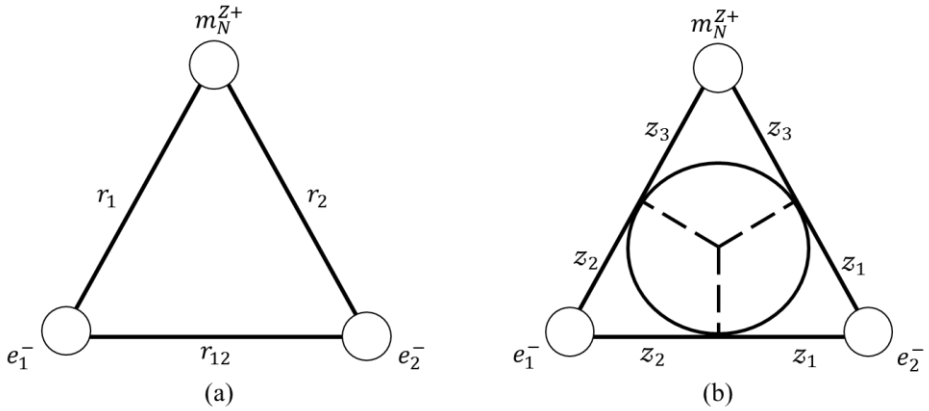

Figure 7.2. Inter-particle r_i (a) and perimetric z_i (b) coordinate systems used for unit charged two-electron atoms; the circle inside the system represented by (b) gives rise to the *perimetric* coordinates as the subdivisions of the sides of a triangle. In atomic system, r_1 and r_2 are the nucleus-electron separation while r_{12} is the electron-electron separation. Similarly, z_1 and z_2 are the electron coordinates while z_3 involves the nuclear coordinate. "Reprinted (Adapted) from *Advances in Quantum Chemistry*, 77, H. Cox, A.L. Baskerville, *The Series Solution Method in Quantum Chemistry for Three-Particle Systems*, Copyright (2018), 40[17] with permission from Elsevier."

where $z_i = r_j + r_k - r_i$ with $\{i, j, k\}$ denoting the cyclic permutation of $\{1, 2, 12\}$ such that;

$$z_1 = r_2 + r_{12} - r_1 \tag{7.44}$$

$$z_2 = r_1 + r_{12} - r_2 \tag{7.45}$$

$$z_3 = r_1 + r_2 - r_{12} \tag{7.46}$$

to give independent integration domains where:

$$r_i = \frac{z_j + z_k}{2} \tag{7.47}$$

When this is done, the internal coordinate part of the Jacobian is evaluated by transforming the Cartesian coordinates to the inter-particle and then to the *perimetric* coordinates, i.e.,[16,105]

$$dx_1^3 dx_2^3 = 8\pi^2 r_1 r_2 r_{12} dr_1 dr_2 dr_{12} = \frac{\pi^2}{4}(z_2 + z_3)(z_3 + z_1)(z_1 + z_2) dz_1 dz_2 dz_3 \tag{7.48}$$

The polynomials in eq. (7.43) are then solved using the standard integral:[17]

$$\int_0^\infty x^n e^{-ax} \mathrm{d}x = \Gamma(n+1) a^{-n-1} \tag{7.49}$$

The sum of the one-electron and two-electron matrix elements is then used to form the Fock matrices to solve the Fock equations as a generalised eigenvalue problem to determine the HF energy and the coefficients of the new wavefunction.

7.2.1.1 Quality of Wavefunction and Expectation Values

The quality of the wavefunction obtained by solving the HF equations using a wavefunction of the form in eq. (7.33) can be assessed by computing various expectation values that satisfy the virial and cusp conditions.[16–18] The virial condition depends on the entire space of the system while the cusp condition defines the behaviour of the wavefunction at the singularities of the Coulomb potential where two or more particles coalesce.[17,106] As such, good energies and cusps suggest good wavefunctions.[17]

7.2.1.1.1 The Virial Condition

For particles interacting via Coulomb forces, if the Hamiltonian describing the system in which they interact is $\widehat{H} = \widehat{K} + \widehat{V}$, where the expectation value of the Hamiltonian for the system is $\langle \widehat{H} \rangle \equiv E = \langle \widehat{K} \rangle + \langle \widehat{V} \rangle$, i.e., the sum of the expectation values of the kinetic and potential energy operators, the virial theorem for the Coulomb potential is:[18,106,404]

$$\frac{\langle \hat{V} \rangle}{\langle \hat{K} \rangle} = -2 \tag{7.50}$$

As such, the factor η can be defined for these systems as:[16,18,404]

$$\eta = \frac{\langle \hat{V} \rangle}{\langle \hat{K} \rangle} + 2 = 0 \tag{7.51}$$

The extent to which this equation is satisfied determines the quality of the wavefunction.

7.2.1.1.2 The Cusp Condition

For coalescing two-body Coulomb systems, the potential energy becomes singular (discontinuous) but must remain self-adjoint and bounded.[405] This change in the potential energy is compensated for by the kinetic energy at the singularity.[405] For such systems, the exact value of a two-particle cusp, ν_{ij} is defined as:[406,407]

$$\nu_{ij} = Z_i Z_j \frac{m_i m_j}{m_i + m_j} \tag{7.52}$$

The ratios of the cusps are determined by the gradient of the wavefunction at coalescence as:[406,408,409]

$$\nu_{ij} = \langle \hat{\nu}_{ij} \rangle = \frac{\left\langle \psi \left| \delta(\boldsymbol{r}_{ij}) \left(\frac{\partial}{\partial(\boldsymbol{r}_{ij})} \right) \right| \psi \right\rangle}{\langle \psi | \delta(\boldsymbol{r}_{ij}) | \psi \rangle} \tag{7.53}$$

where $\delta(\boldsymbol{r}_{ij})$ is the two-particle Dirac delta function, used to evaluate the effect of correlation and gives the probability of $\boldsymbol{r}_{ij} = 0$ for each value of r (e.g., **Figure 7.1**) along the radial distance of the electrons from the nucleus.[18,410] The exact value of the electron-electron cusp is $\nu_{12} = \nu_{21} = -0.5$ but for HF calculations, $\nu_{12} = \nu_{21} = 0$ while the value of the nucleus-electron cusp is $\nu_{31} = \nu_{32} = -Z$.[16,411] The difference between the computed value of the cusps and its exact value (eq. (7.52)) gives an indication of the quality of a wavefunction. It should be noted nevertheless that good cusps cannot guarantee good energies as the energies depend on the entire space whereas the cusp values are point based.[17,106] Therefore, good energies and good cusps are required to guarantee that a wavefunction is of high quality.

7.2.2 Standard HF Wavefunctions for Helium Atom or Hydride Ion

The standard HF wavefunctions determined by Clementi et al.,[365,366] and/or Koga et al.,[401] are used to form the $\rho(\boldsymbol{R})$ of systems with two or more electrons in order to compute their correlation energies. In order to form the standard HF wavefunctions for the systems of interest in this thesis, eq. (7.6) is re-written as:

$$\psi_i = \psi_{p\lambda\alpha} = \sum_{p=1}^{M} c_{p\lambda\alpha} \left[\left(\left[(2\eta_{\lambda p})! \right]^{-1/2} (2\xi_{\lambda p})^{\eta_{\lambda p}+1/2} r^{\eta_{\lambda p}-1} e^{-\xi_{\lambda p} r} \right) Y_{\lambda\alpha}(\theta, \phi) \right] \qquad (7.54)$$

where $c_{p\lambda\alpha}$ are the orbital expansion coefficients, $\lambda \equiv l$ (the angular momentum quantum number and gives the symmetry of the function/orbital), $\alpha \equiv m_l$ and M represents the overall number of basis functions. $Y_{\lambda\alpha}(\theta, \phi)$ are the normalised spherical harmonics of the basis functions in complex form (its angular part) and are always kept constant in the course of a computation.[16,366,371] Every other symbol retains its meaning as in **7.1.1**. To form these wavefunctions, the $c_{p\lambda\alpha}$'s and $\xi_{\lambda p}$'s are then extracted from the atomic function tables of Clementi[366,371] or Koga et al.,[401] and incorporated for the expansion of $\psi_{p\lambda\alpha}$ as in eq. (7.54). Once this expansion (eq. (7.54)) is performed for the respective orbitals of a given system, its complete wavefunction on the basis of eq. (7.5) is computed by incorporation of the result of eq. (7.54). The expansion in eq. (7.54) is illustrated below by application of the $c_{p\lambda\alpha}$'s and $\xi_{\lambda p}$'s taken from the Clementi atomic function tables[371] for neutral helium and boron atoms. This same notation/format is used in the Koga et al., atomic functions tables.[401] **Figure 7.3** is an annotation to explain the components of typical atomic function tables.

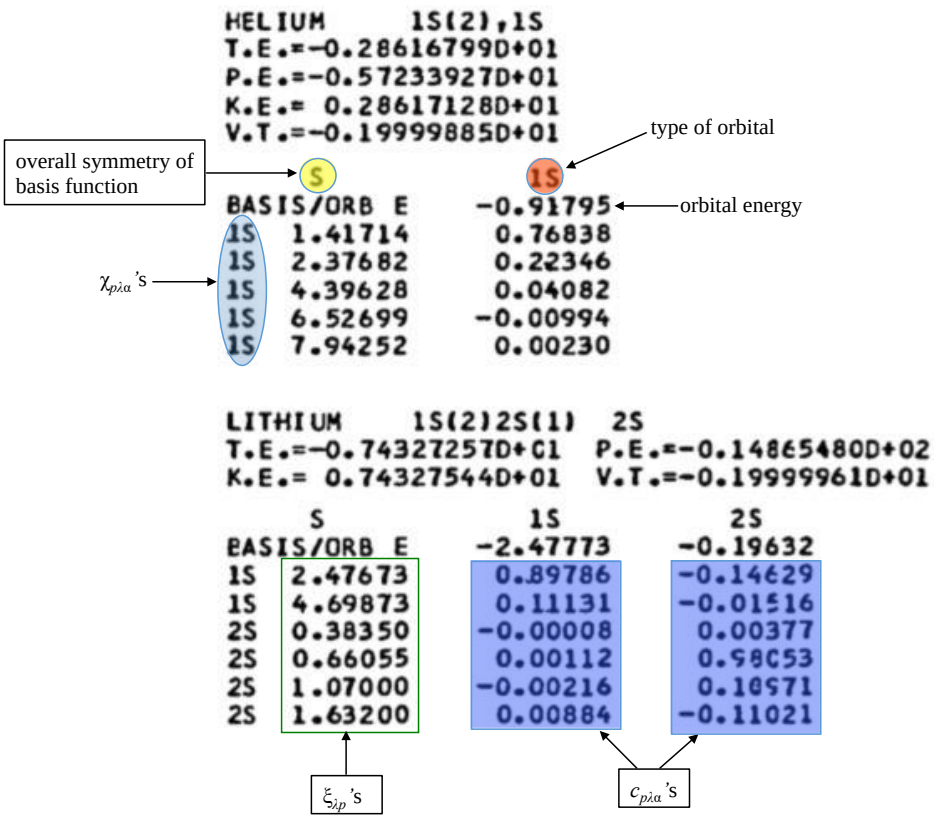

Figure 7.3. Annotation of the atomic function tables for neutral helium and lithium atoms: At the top of each atomic function table is a summary of the name of the system, its electronic configuration, its spin state, its total HF energy (T.E), its potential energy (P.E), its kinetic energy (K.E) and its virial term (V.T). D+01 or D+02 represents $\times 10^1$ or $\times 10^2$, respectively."Reprinted (Adapted) from Atomic Data and Nuclear Data Tables, 14, E. Clementi, C. Roetti, *Roothaan-Hartree-Fock atomic wavefunctions Basis functions and their coefficients for ground and certain excited states of neutral and ionised atoms, $Z \leq 54$*, Copyright (1974), 302[371] with permission from Elsevier."

The $c_{p\lambda\alpha}$'s and $\xi_{\lambda p}$'s taken from the Clementi atomic function tables[371] for the neutral helium atom (with electronic configuration, $1s^2$) comprising five basis functions for the $1s$ orbital of the atom (i.e., $p = 1, 2, \ldots, 5$) corresponding to each p of the $\chi_{p\lambda\alpha}$ are presented in **Table 7.1**.

Table 7.1. The orbital expansion coefficients and exponents corresponding to the respective basis function of the $1s$ orbital of helium atom.[371]

p	$\chi_{p\lambda\alpha}$	$c_{p\lambda\alpha}$	$\xi_{\lambda p}$
1	$1s$	0.76838	1.41714
2	$1s$	0.22346	2.37682
3	$1s$	0.04082	4.39628
4	$1s$	-0.00994	6.52699
$M = 5$	$1s$	0.00230	7.94252

For the basis functions in **Table 7.1**, $\eta_{\lambda p} = 1$. The 1*s* orbital of helium therefore can be written upon inclusion of the $c_{p\lambda\alpha}$'s and $\xi_{\lambda p}$'s in Table **Table 7.1** in in eq. (7.54) as:

$$\begin{aligned}\psi_{1s} = 0.76838\times&\left[\left((2!)^{-1/2}\times(2\times1.41714)^{1.5}\times r^{0}e^{-(1.41714\times r)}\right)\times Y_{0,0}(\theta,\phi)\right]\\ &+ 0.22346\times\left[\left((2!)^{-1/2}\times(2\times2.37682)^{1.5}\times r^{0}e^{-(2.37682\times r)}\right)\times Y_{0,0}(\theta,\phi)\right]\\ &+ 0.04082\times\left[\left((2!)^{-1/2}\times(2\times4.39628)^{1.5}\times r^{0}e^{-(4.39628\times r)}\right)\times Y_{0,0}(\theta,\phi)\right]\\ &- 0.00994\times\left[\left((2!)^{-1/2}\times(2\times6.52699)^{1.5}\times r^{0}e^{-(6.52699\times r)}\right)\times Y_{0,0}(\theta,\phi)\right]\\ &+ 0.00230\times\left[\left((2!)^{-1/2}\times(2\times7.94252)^{1.5}\times r^{0}e^{-(7.94252\times r)}\right)\times Y_{0,0}(\theta,\phi)\right]\end{aligned} \tag{7.55}$$

For the neutral boron atom having the electronic configuration, $1s^2 2s^2 2p^1$, the $c_{p\lambda\alpha}$'s and $\xi_{\lambda p}$'s taken from the Clementi atomic function tables[371] for the atom for the 1*s*, 2*s* and 2*p* orbitals of the atom with six, six and four basis functions corresponding to each p of the $\chi_{p\lambda\alpha}$ for the respective orbitals are presented in **Table 7.2**.

Table 7.2. The orbital expansion coefficients and exponents corresponding to the respective basis function of the 1*s*, 2*s* and 2*p* orbitals of boron atom.[371]

$\boldsymbol{p}$	$\boldsymbol{\chi_{p\lambda\alpha}}$	$\boldsymbol{\xi_{\lambda p}}$	$\boldsymbol{1s}$	$\boldsymbol{2s}$	$\boldsymbol{\chi_{p\lambda\alpha}}$	$\boldsymbol{2p}$	
		$\boldsymbol{1s}$ & $\boldsymbol{2s}$	$\boldsymbol{c_{p\lambda\alpha}}$	$\boldsymbol{c_{p\lambda\alpha}}$		$\boldsymbol{\xi_{\lambda p}}$	$\boldsymbol{c_{p\lambda\alpha}}$
1	$1s$	4.44561	0.92705	-0.19484	$2p$	0.87481	0.53622
2	$1s$	7.91796	0.07780	-0.01254	$2p$	1.36992	0.40340
3	$2s$	0.86709	0.00088	0.06941	$2p$	2.32262	0.11653
4	$2s$	1.21924	-0.00200	0.75234	$2p$	5.59481	0.00821
5	$2s$	2.07264	0.00433	0.31856			
$\boldsymbol{M} = 6$	$2s$	3.44332	0.00270	-0.12642			

It is noteworthy that the $\xi_{\lambda p}$ are the same for the same p^{th} basis function for a given orbital symmetry, regardless of its principal quantum number, i.e., each corresponding p^{th} basis function of s-symmetry will have the same $\xi_{\lambda p}$ and every corresponding p^{th} basis function of p-symmetry will possess the same $\xi_{\lambda p}$. This is exemplified by the exponents of the p^{th} basis functions in the $1s$ and $2s$ columns of **Table 7.2**. Therefore, putting the $c_{p\lambda\alpha}$'s and $\xi_{\lambda p}$'s in **Table 7.2** into eq. (7.54), the orbital expansion for the respective orbitals of the neutral boron atom will be:

$$\begin{aligned}\psi_{1s} = 0.92705\times&\left[\left((2!)^{-1/2}\times(2\times4.44561)^{1.5}\times e^{-(4.44561\times r)}\right)\times Y_{0,0}(\theta,\phi)\right]\\ &+ 0.07780\times\left[\left((2!)^{-1/2}\times(2\times7.91796)^{1.5}\times e^{-(7.91796\times r)}\right)\times Y_{0,0}(\theta,\phi)\right]\\ &+ 0.00088\times\left[\left((4!)^{-1/2}\times(2\times0.86709)^{2.5}\times r\times e^{-(0.86709\times r)}\right)\times Y_{0,0}(\theta,\phi)\right]\\ &- 0.00200\times\left[\left((4!)^{-1/2}\times(2\times1.21924)^{2.5}\times r\times e^{-(1.21924\times r)}\right)\times Y_{0,0}(\theta,\phi)\right]\\ &+ 0.00433\times\left[\left((4!)^{-1/2}\times(2\times2.07264)^{2.5}\times r\times e^{-(2.07264\times r)}\right)\times Y_{0,0}(\theta,\phi)\right]\\ &+ 0.00270\times\left[\left((4!)^{-1/2}\times(2\times3.44332)^{2.5}\times r\times e^{-(3.44332\times r)}\right)\times Y_{0,0}(\theta,\phi)\right]\end{aligned} \tag{7.56}$$

$$\begin{aligned}\psi_{2s} = -0.19484\times&\left[\left((2!)^{-1/2}\times(2\times4.44561)^{1.5}\times e^{-(4.44561\times r)}\right)\times Y_{0,0}(\theta,\phi)\right]\\ &- 0.01254\times\left[\left((2!)^{-1/2}\times(2\times7.91796)^{1.5}\times e^{-(7.91796\times r)}\right)\times Y_{0,0}(\theta,\phi)\right]\\ &+ 0.06941\times\left[\left((4!)^{-1/2}\times(2\times0.86709)^{2.5}\times r\times e^{-(0.86709\times r)}\right)\times Y_{0,0}(\theta,\phi)\right]\\ &+ 0.75234\times\left[\left((4!)^{-1/2}\times(2\times1.21924)^{2.5}\times r\times e^{-(1.21924\times r)}\right)\times Y_{0,0}(\theta,\phi)\right]\\ &+ 0.31856\times\left[\left((4!)^{-1/2}\times(2\times2.07264)^{2.5}\times r\times e^{-(2.07264\times r)}\right)\times Y_{0,0}(\theta,\phi)\right]\\ &- 0.12642\times\left[\left((4!)^{-1/2}\times(2\times3.44332)^{2.5}\times r\times e^{-(3.44332\times r)}\right)\times Y_{0,0}(\theta,\phi)\right]\end{aligned} \tag{7.57}$$

$$\begin{aligned}\psi_{2p} = 0.53622\times&\left[\left((4!)^{-1/2}\times(2\times0.87481)^{2.5}\times r\times e^{-(0.87481\times r)}\right)\times Y_{1,0}(\theta,\phi)\right]\\ &+ 0.40340\times\left[\left((4!)^{-1/2}\times(2\times1.36992)^{2.5}\times r\times e^{-(1.36992\times r)}\right)\times Y_{1,0}(\theta,\phi)\right]\\ &+ 0.11653\times\left[\left((4!)^{-1/2}\times(2\times2.32262)^{2.5}\times r\times e^{-(2.32262\times r)}\right)\times Y_{1,0}(\theta,\phi)\right]\\ &+ 0.00821\times\left[\left((4!)^{-1/2}\times(2\times5.59481)^{2.5}\times r\times e^{-(5.59481\times r)}\right)\times Y_{1,0}(\theta,\phi)\right]\end{aligned} \tag{7.58}$$

The spherical harmonics for the basis functions of s-symmetry are:[16,32,371]

$$Y_{0,0}(\theta,\phi) = \frac{1}{2}\left(\frac{1}{\pi}\right)^{1/2} \tag{7.59}$$

while those for the basis functions of p-symmetry are:[32,371]

$$Y_{1,0}(\theta,\phi) = \frac{1}{2}\cdot\left(\frac{3}{\pi}\right)^{1/2}\cdot\cos\theta \tag{7.60}$$

7.2.3 Formation of the One-Electron Densities of Atomic Systems from HF Wavefunctions

The total electron density ($\rho(\boldsymbol{R})$) for a given system is computed in this thesis as the sum of the product of the occupation number of an orbital and the square of that orbital for all the orbitals in the system. This may be summarised mathematically in general as:[19,32,367,368]

$$\rho(\boldsymbol{R}) = \sum_{i=1}^{N_{occ}} n_i\cdot|\psi_i(\boldsymbol{R})|^2 = n_i\sum_{i=1}^{N_{occ}}\psi_i^*\psi_i = n_i\sum_{r=1}^{M}\sum_{s=1}^{M}\sum_{i=1}^{N_{occ}}c_{rj}^*c_{sj}\chi_r^*\chi_s \tag{7.61}$$

where N_{occ} is the number of orbitals occupied by the N-electrons in the system. For a closed-shell system, $N_{occ} = \frac{N}{2}$ and M is the overall number of basis functions in the system. For the helium atom and hydride ion with two electrons and one spatial orbital expressed for e.g., for the helium atom in eq. (7.55) and an electronic configuration of $1s^2$, eq. (7.61) becomes:

$$\rho(\boldsymbol{R}) = 2 \cdot |\psi_{1s}(\boldsymbol{R})|^2 \tag{7.62}$$

For the helium atom and hydride ion, our computed Laguerre-based HF wavefunction for the respective system is also applicable in eq. (7.62). For lithium with three electrons, 2 spatial orbitals ($1s$ and $2s$) and an electronic configuration of $1s^2 2s^1$, its electron density is computed as:

$$\rho(\boldsymbol{R}) = 2 \cdot |\psi_{1s}(\boldsymbol{R})|^2 + 1 \cdot |\psi_{2s}(\boldsymbol{R})|^2 \tag{7.63}$$

For boron with five electrons, 3 spatial orbitals; $1s$, $2s$ and $2p$, expressed in eq. (7.56) to eq. (7.58), respectively, the total one-electron density of the system is computed as:

$$\rho(\boldsymbol{R}) = 2 \cdot |\psi_{1s}(\boldsymbol{R})|^2 + 2 \cdot |\psi_{2s}(\boldsymbol{R})|^2 + 1 \cdot \left|\psi_{2p}(\boldsymbol{R})\right|^2 \tag{7.64}$$

These densities are then used to form the two-electron HF density matrices on the basis of eq. (7.2) for the respective systems.

7.2.4 Fitting Procedure

7.2.4.1 Fitting to the Helium Atom and Testing of the CS Formula and LYP Functional

To determine the constants (a, b, c, d) in eq. (7.12) and use the determined constants to test the reproducibility of atomic correlation energies, the relevant CS equations (eq. (7.11), eq. (7.12) and eq. (7.14)) and a form of the LYP expression for correlation energy (eq. (7.16)) discussed in **7.1.1** were implemented in in-house Maple and Python codes. First, a 25-term Laguerre-based HF wavefunction was computed for the helium atom as described in **7.2.1** by using a 25×25 determinant of the form in eq. (7.33) to solve the HF equations ($\hat{F}\psi_i(1) = \varepsilon_i\psi_i(1)$). To do this, the electronic and nuclear charge of the system, the guess NLP, A = 2, method (RHF, as implemented[16,17]), spin multiplicity ($2S + 1 = 1$) and mass of the nucleus set to infinity were specified in the input for optimisation. This code uses Maple for the one-electron integrals and Python and C++ for the two-electron integrals to form the Fock matrices. The computed wavefunction was employed to compute the electron density ($\rho(\boldsymbol{R})$) of the system as described in **7.2.3**. The computed $\rho(\boldsymbol{R})$ was then used to form the two-electron density of the atom ($P_{2\mathrm{HF}}(\boldsymbol{R}, \boldsymbol{R})$) on the basis of eq. (7.2). This was initially performed using a Maple code to test the formula and later implemented in an in-house Python code. Both densities were then employed to perform the numerical integration of the left-hand-side (lhs) of eq. (7.11) to obtain the 'exact' value of the equation for the system within $0.3 \leq R \leq 2$ a.u. using the in-house Python code. This range was determined earlier[349] from the first table in the CS[26] paper.

The function, $H(\beta, W)$ on the right-hand-side (rhs) of eq. (7.11) was then fitted to the results of the numerical integration using an implementation of the simple, least squares fitting algorithm[399,400] to obtain the calculated value ($H(\beta, W)^{\text{Calc.}}$) for the atom. The fitting constants in eq. (7.12) were then determined by optimisation, first using different optimisation methods to minimise the square of the error:

$$Square\ error = \sum (Exact - Calculated)^2 \tag{7.65}$$

where $Exact$ refers to the result of the numerical integration of the lhs of eq. (7.11) and $Calculated$ stands for the value of the rhs of eq. (7.11) obtained from the fitting procedure. The optimisation methods initially explored to determine the constants in eq. (7.12) are the: scipy.optimise least_squares,[412–417] BOBYQA,[418,419] Nelder-Mead[420,421] and conjugate gradient (CG)[422] methods. In this step, the optimisers were tested for consistency by varying the guess values of the constants and tolerance for successful termination of calculation, with and/or without boundary constraints. Constraints are either imposed on the constants or not for the scipy.optimise least_squares method while no constraints are imposed when the BOBYQA, Nelder-mead or CG method is employed. The most consistent optimiser and optimum tolerance were then used to determine the constants under different conditions. To do this, different guess values of the constants were first adopted and the optimisation performed within $0.3 \leq R \leq 2$ a.u. Thereafter, suitable guess values were employed and the optimisation was performed with different ranges of R. In all these computations, $q = 2.29$ as determined by CS in their 1975 paper[26] was employed. The optimised constants in each optimisation were then applied to the implemented form of LYP expression for correlation energy (eq. (7.16)) in combination with the Koga et al.,[401] HF wavefunctions for H^-, He, Li^+, Be, B^+ and Ne to compute the correlation energies of the systems. These systems were chosen to validate the implementation of the CS formulae against the results of CS[26] and to test how well the formalism reproduces the correlation energy of the hydride ion. The computed correlation energies are also compared to their exact values[16] or their fixed nucleus non-relativistic experimental estimates.[423,424]

7.2.4.2 Fitting to the Hydride Ion and Testing of the CS Formula and LYP Functional

The procedure described in **7.2.4.1** was repeated but using the computed 25-term Laguerre-based HF wavefunction for the hydride ion to determine new a, b, c and d parameters. The most stable optimiser and optimum tolerance determined in **7.2.4.1** were used to determine the new a, b, c and d, which were then used to compute the corresponding correlation energies of some closed-shell systems. To do this, different guess values of the constants were first adopted and the optimisation

performed within $0.3 \leq R \leq 2$ a.u. Thereafter, suitable guess values were employed and the optimisation was performed with different ranges of R. In addition to $q = 2.29$ for He, q for H^- was also determined and used in the calculations. To do this, the computed Laguerre-based HF wavefunction for H^- was used to form $\rho(\boldsymbol{R})$ and $P_{2\mathrm{HF}}(\boldsymbol{R},\boldsymbol{R})$. β for H^- was then computed from the exponential term of the correlation energy in eq. (7.1) by setting the correlation energy of the system to the exact value[16] and varying q until the equation was satisfied. q for H^- was thereafter computed from the expression for β, eq. (7.10). This resulted in an optimised value of $q = 1.93985$ for the hydride ion.

The optimised constants in each optimisation were then applied to the implemented form of the LYP expression for correlation energy (eq. (7.16)) in combination with the Koga et al.,[401] HF wavefunctions for H^-, He, Li^+, Be, B^+ and Ne to compute the correlation energies of the closed-shell systems. The computed correlation energies were compared to the results of CS[26] and their exact values[16] or fixed nucleus non-relativistic experimental estimates.[423,424]

7.2.5 Correlation Energies of Atomic Systems using Fitting Constants and HF Wavefunctions

The optimised constants (a, b, c, d) determined in the present work and those determined by CS[26] were applied to the implemented form of the LYP expression for correlation energy (eq. (7.16)) in combination with the Koga et al.,[401] HF wavefunctions for several atomic systems (including anions) to compute the correlation energies of the systems. The computed correlation energies were then compared to their exact values[16] and/or their fixed nucleus non-relativistic experimental estimates.[423,424]

7.3 Results and Discussion

7.3.1 Testing the Implementation of the CS Formulae and LYP Functional

To validate our implementation of the CS equations (eq. (7.14)) and the form of the LYP expression for the correlation energies (eq. (7.16)) for closed-shell systems, the reproducibility of the CS results[26] for the correlation energies of He, Li^+, Be, and B^+ was initially tested in a Maple code and later, He, Li^+, Be, B^+ and Ne in an in-house Python code. To do this, the CS constants; $a = 0.01565$, $b = 0.173$, $c = 0.58$, $d = 0.8$ and Clementi[366] HF wavefunctions for He, Li^+, Be, and B^+ were employed in the Maple code while the CS constants and the Koga et al.,[401] HF wavefunctions for He, Li^+, Be, B^+ and Ne were employed in the in-house Python code. The computed correlation energies of He, Li^+, Be, B^+ and Ne, are summarised in **Table 7.3**. The CS

values,[26] the exact values[16] and the fixed-nucleus, non-relativistic experimental estimates[423,424] of the correlation eneries of these systems are also included in **Table 7.3**.

The results in **Table 7.3** suggest that our implementation of the CS formula and the LYP expression for the correlation energies of closed-shell systems is accurate. This is because the computation of correlation energies for some of the closed-shell systems tested by CS using the implemented expressions in combination with different HF wavefunctions for the systems reproduced the results of CS. It should be noted that CS employed the Clementi wavefunctions in obtaining their results.

Table 7.3. The correlation energies (E_c / a.u.) of some closed-shell systems computed with an implementation of the CS formula, E_c^{CS} (eq. (7.14)) in Maple code and the CS and a form of the LYP functional, E_c^{LYP} (eq. (7.16)) in an in-house Python code. Calculations in the Maple code employ the Clementi[366] HF wavefunctions of the systems (like CS) while that in the Python code employ the Koga et al.,[401] HF wavefunctions. Also included are literature values of the correlation energies.

System	$E_c^{\mathrm{Calc.}}$ / a.u. (Maple)	$E_c^{\mathrm{Calc.}}$ / a.u. (Python)		E_c^{CS}[26]	E_c^{Exact}[16] or $E_c^{\mathrm{Expt.}}$[423,424] / a.u.
	E_c^{CS}	E_c^{CS}	E_c^{LYP}		
He	-0.041560	-0.041560	-0.041560	-0.0416	**-0.042044**
Li^+	-0.043883	-0.043884	-0.043884	-0.0438	**-0.043498**
Be	-0.092602	-0.092596	-0.092596	-0.0926	**-0.09434**
B^+	-0.105961	-0.105959	-0.105959	-0.106	**-0.11134**
Ne		-0.375313	-0.375313	-0.374	**-0.39047**

7.3.2 Accuracy of the Calculated Laguerre-based HF Wavefunctions

The computed HF energy, $E_{\mathrm{HF}}^{\mathrm{Calc.He}} = -\mathbf{2.861\,679\,995\,612\,2}38\,877$ a.u. for the 25-term Laguerre-based HF wavefunction of the helium atom computed using the method[16,17] described in **7.2.1** is found to be accurate to 10^{-13} a.u. in comparison to the 'exact' value of $-\mathbf{2.861\,679\,995\,612\,21}$ a.u. in the literature.[425] For the hydride ion, the energy is $E_{\mathrm{HF}}^{\mathrm{Calc.H^-}} = -\mathbf{0.487\,929\,734\,37}0\,831\,313$ a.u. and is accurate to 10^{-11} a.u. in comparison to the most accurate literature value, $-\mathbf{0.487\,929\,734\,372}$ a.u.[426] A summary of the computed expectation values of the nucleus-electron distances and their Dirac delta functions in atomic units, virial factor, NLP (A) used to improve convergence and the two-body cusp values for these wavefunctions are summarised in **Table 7.4**. The values in **Table 7.4** are accurate to the number of digits presented. This was determined by comparing the computed values against the convergence data in the supplementary information of the papers by Cox and co-workers.[16,18] It is worthy of note that $\langle r_1 \rangle = \langle r_2 \rangle$ due to the symmetry of the calculated wavefunctions.

The properties of the computed Laguerre-based HF wavefunctions in **Table 7.4** further ascertains the accuracy of the wavefunctions especially the value of the virial factor and two-body cusps for the respective wavefunctions.

Table 7.4. Properties of the computed Laguerre-based HF wavefunction for He and H^-.

Property	$\psi_{\mathrm{HF}}^{\mathrm{He}}$	$\psi_{\mathrm{HF}}^{\mathrm{H}^-}$
$\langle r_1 \rangle$	0.927 273 404 731 49	2.503 959 63
$\langle r_{12} \rangle$	1.362 124 383 676 07	3.739 274 00
$\langle \delta(r_1) \rangle$	1.797 959 1	0.154 59
$\langle \delta(r_{12}) \rangle$	0.190 603 997 806 5	0.012 983 476 397
A	6.192 708	2.013 386
η	-1.092×10^{-22}	2.287×10^{-20}
ν_{31}	$-1.999\,999\,8$	$-1.000\,005$

The value of η in both calculations is close to zero, the exact value,[16,18,404] while $\nu_{31} \approx -2$ for the helium atom and $\nu_{31} \approx -1$ for the hydride ion, i.e., $-Z$[16,18] for the systems. These values of the virial and cusp conditions for the computed Laguerre-based HF wavefunctions for the helium atom and the hydride ion are indicative of the accuracy (quality) of the wavefunctions and are a considerable improvement ($\sim 10^{-6}$ a.u.) over the results of Clementi[366] and Koga et al.[401] The accuracy of this computation is also an improvement on the results reported earlier by Cox and co-workers[16] who used a 20×20 determinant to compute the Laguerre-based HF wavefunction for the helium atom and its iso-electronic series.

7.3.3 Comparison of the Fitting of $H(\beta, W)^{\mathrm{Calc.}}$ and $H(\beta, W)^{\mathrm{CS}}$ to the Numerically Integrated Results (Exact Data)

The computed Laguerre-based HF wavefunction for the He atom was used to form $\rho(\boldsymbol{R})$ and $P_{2\mathrm{HF}}(\boldsymbol{R}, \boldsymbol{R})$ for the atom. These were then employed to numerically integrate the lhs of eq. (7.11). A fit of the $H(\beta, W)$ function to the numerically integrated (exact) results within $0.01 \leq R \leq 4$ a.u. was then performed using the scipy.optimise least_squares[412–417] fitting procedure. In doing this, no boundary conditions were imposed while the guess values were set at $a = b = c = d = 0.1$ and the tolerance at 10^{-6}. The boundary constraints were imposed in order to open up more space for the optimiser and to reduce the influence of outlier residuals on the optimisation/solution[412–415] to explore the possibility of reproducing the CS constants.

The variation of the calculated $H(\beta, W)$ function ($H(\beta, W)^{\mathrm{Calc.}}$) with R was then compared with that of the CS $H(\beta, W)$ function ($H(\beta, W)^{\mathrm{CS}}$), computed using the CS constants in the same range of R. A plot of the variation of the numerically integrated (exact) results, $H(\beta, W)^{\mathrm{Calc.}}$ and $H(\beta, W)^{\mathrm{CS}}$ arising from the computed Laguerre-based HF helium atom densities with R within $0.01 \leq R \leq 4$ a.u. is presented in **Figure 7.4**.

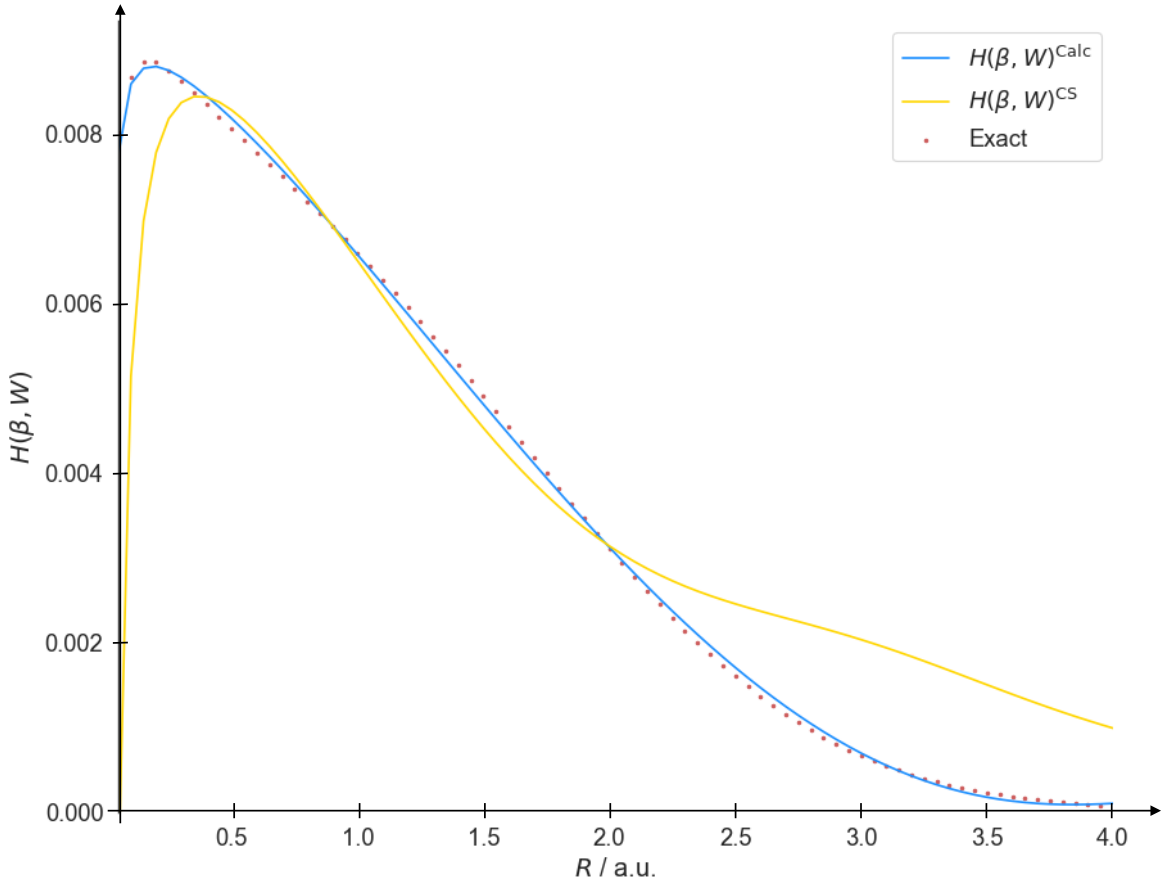

Figure 7.4. Variation of the $H(\beta, W)$ function with R for the helium atom within $0.01 \leq R \leq 4$ a.u. using a tolerance of 10^{-6}. The red dots represent the numerically integrated (exact) result; blue curve represents the calculated function ($H(\beta, W)^{\text{Calc.}}$) while the yellow curve is a plot of the CS function, $H(\beta, W)^{\text{CS}}$.

The results in **Figure 7.4** suggests that the calculated function has an almost exact (accurate) fit to the 'exact' data while the CS function gave a poor fit. This is especially noticeable with the position of the curve maxima and when $R \geq 2$ a.u. The maximum of the 'exact' data curve is found to be located at $R \approx 0.2$ a.u. while that of the CS function curve is found at $R \approx 0.4$ a.u. The calculated $H(\beta, W)$ function ($H(\beta, W)^{\text{Calc.}}$) in **Figure 7.4** led to the fitting constants, $a = 0.01212$, $b = 0.03163$, $c = 0.11764$ and $d = 0.74324$ which are found to be quite different from the CS constants, $a = 0.01565$, $b = 0.173$, $c = 0.58$ and $d = 0.8$. Applying the optimised constants to the implemented form of the LYP expression for closed-shell systems led to the correlation energy for He, Li^+ and Be as -0.042353 a.u., -0.048845 a.u. and -0.084308 a.u., respectively. These correlation energies are found to be in error by 0.7 %, 12.3 % and 10.6 % for He, Li^+ and Be, respectively in comparison with the exact[16] and experimentally estimated[423,424] values. The CS constants led to the correlation energies; -0.041560 a.u., -0.043884 a.u. and -0.092596 a.u. for He, Li^+ and Be with

errors of 1.2 %, 0.9 % and 1.8 %, respectively. This suggests that a poor fit of the $H(\beta, W)$ function is preferable to obtain good constants for accurate correlation energies for non-helium systems. It is also found from **Figure 7.4** that the calculated curve and the CS curve possess a somewhat similar fit to the 'exact' data between $R \approx 0.3$ a.u. and $R = 2$ a.u. This range was determined earlier[349] from the first table in the CS[26] paper to be where CS fitted the $H(\beta, W)$ function to their numerically integrated results to obtain the fitting constants. It may therefore be reckoned that relaxing the fit (by varying the tolerance) and focusing optimisation within $0.3 \leq R \leq 2$ a.u. or varying the range, tolerance limits and/or sundry conditions may improve the accuracy of the optimised fitting constants with respect to the accuracy of the correlation energies they generate.

7.3.4 Validation of Optimiser and Tolerance

Four optimisation methods; the BOBYQA,[418,419] Nelder-Mead,[420,421] CG[422] and the scipy.optimise least_squares[412–417] and the effect of tolerance limit on the optimised constants are investigated. In each case, the corresponding correlation energies for H^-, He, Li^+, Be, B^+ and Ne are computed using the optimised constants and the implemented form of the LYP expression for closed-shell systems (eq. (7.16)). In addition, the energies are compared with their exact values (in green),[16] fixed nucleus non-relativistic experimental estimates (in blue)[423,424] or those computed by CS.[26] Furthermore, in each case, the Koga et al.,[401] HF wavefunctions are employed in the computation of the correlation energies of the systems.

In **Table 7.5**, a summary of the effect of the tolerance limit on the fitting constants optimised using the BOBYQA method within $0.3 \leq R \leq 2$ a.u. using a total of 80 points, $q = 2.29$ and the computed Laguerre-based HF wavefunction for the helium atom is presented. The CS values of the constants are used as the guess values in the optimisation.

The results presented in **Table 7.5** suggest that the constants computed using BOBYQA method with a tolerance of 10^{-2} and 10^{-3} are essentially the same even when the code is run more than once. However, the output becomes inconsistent when a tolerance of 10^{-4} is employed to compute the constants with BOBYQA. This is reflected by the values in red for running the code three times with a tolerance of 10^{-4}. It is found that the consistent values of the optimised constants are close to those of CS for a and d but different for b and c by 0.09931 and 0.01412, respectively. The correlation energies of the systems corresponding to the consistent/reproducible constants in **Table 7.5** are found to be better or worse than the CS values by 0.3 to 0.8 % in comparison with the computed exact[16] or experimentally estimated[423,424] values except for hydride ion. For the hydride ion, the computed correlation energy is in error by 21.6 %. Nevertheless, the results indicates that a lower tolerance leads to improved helium atom and non-helium systems except the hydride ion.

Table 7.5. Effect of tolerance on fitting constants (a, b, c, d) optimised using the BOBYQA method. Guess values are in **bold** under the constants. Correlation energies in green are the calculated exact values[16] while those in blue are experimentally estimated.[423,424] The optimised constants in red are inconsistent (i.e., not reproducible) for the tolerance.

Tolerance	a	b	c	d	E_c / a.u.					
					H^-	He	Li^+	Be	B^+	Ne
	0.01565	**0.173**	**0.58**	**0.8**	**-0.039821**	**-0.042044**	**-0.043498**	**-0.09434**	**-0.11134**	**-0.39047**
1×10^{-2}	0.01570	0.18712	0.67931	0.79963	-0.031209	-0.041808	-0.043657	-0.091882	-0.105430	-0.377327
1×10^{-3}	0.01570	0.18712	0.67931	0.79963	-0.031209	-0.041808	-0.043657	-0.091882	-0.105430	-0.377327
1×10^{-4}	0.01481	0.16098	0.67691	0.78600	-0.030447	-0.041864	-0.044624	-0.089737	-0.102460	-0.355381
1×10^{-4}	0.01502	0.16436	0.67640	0.79959	-0.030473	-0.041892	-0.044610	-0.090086	-0.102997	-0.359217
1×10^{-4}	0.01282	0.08799	0.56554	0.72706	-0.028979	-0.042070	-0.046806	-0.085830	-0.096608	-0.308201
CS[26]	**0.01565**	**0.173**	**0.58**	**0.8**		**-0.0416**	**-0.0438**	**-0.0926**	**-0.106**	**-0.374**

The effect of the tolerance limit on the fitting constants optimised using the Nelder-Mead method within $0.3 \leq R \leq 2$ a.u. using a total of 80 points, $q = 2.29$ and the computed Laguerre-based HF wavefunction for the helium atom is summarised in **Table 7.6**. In a similar manner as in **Table 7.5**, the CS values of the constants are used as the guess values of the constants in the optimisation.

It is observed from the results in **Table 7.6** that the Nelder-Mead method is only stable when the tolerance is 10^{-2}. The output for the constant, c (in red) is found to be negative for tolerances $\geq 10^{-3}$ thereby leading to infinite (unreliable/undesirable) correlation energies for the considered systems. It is observed that the optimised constants at tolerance of 10^{-2} are similar to the CS values by 0.0008 for a, 0.00153 for b, 0.0607 for c and 0.07119 for d. However, although the helium fit is slightly better than with respect to the corresponding correlation energy of the system, the optimised constants do not improve on the CS results.

Table 7.6. Effect of tolerance on fitting constants (a, b, c, d) optimised using the Nelder-Mead method. Guess values are in **bold** under the constants. Correlation energies in green are the computed exact values[16] while those in blue are experimentally estimated.[423,424] The optimised constants in red are unreliable for the same tolerance as the expected constants do not have negative values.

Tolerance	a	b	c	d	E_c / a.u.					
	0.01565	**0.173**	**0.58**	**0.8**	H^-	He	Li^+	Be	B^+	Ne
					-0.039821	**-0.042044**	**-0.043498**	**-0.09434**	**-0.11134**	**-0.39047**
1×10^{-2}	0.01485	0.17147	0.64070	0.72881	-0.031314	-0.041778	-0.043782	-0.091434	-0.104150	-0.363587
1×10^{-3}	0.01139	0.01014	-0.29068	0.70802	∞	∞	∞	∞	∞	∞
1×10^{-4}	0.01139	0.01014	-0.29068	0.70802	∞	∞	∞	∞	∞	∞
1×10^{-5}	0.01139	0.01014	-0.29068	0.70802	∞	∞	∞	∞	∞	∞
CS[26]	**0.01565**	**0.173**	**0.58**	**0.8**		**-0.0416**	**-0.0438**	**-0.0926**	**-0.106**	**-0.374**

The results computed using the CG method[422] within $0.3 \leq R \leq 2$ a.u. employing a total of 80 points, $q = 2.29$ and the computed Laguerre-based HF wavefunction for the helium atom are summarised in **Table 7.7**.

For this method, it is found that stable constants are computed for the tolerances 10^{-2} to 10^{-5} but not for tolerances $\geq 10^{-6}$. It is found that for a tolerance of 10^{-2}, no optimisation is performed by the CG method, i.e., the method returns the CS constants as the optimum values. It is also observed that the method generates constants with values close to the CS constants when the tolerance is 10^{-3} and 10^{-4} especially with respect to b, c and d. The constants, a and b computed at a tolerance of 10^{-5} differ from the CS values by 0.0019 and 0.05898, respectively while c and d are essentially the same as those of CS. For the constants at 10^{-2}, the corresponding computed correlation energies are the same with those computed by CS for He, Li^+, Be, B^+ and Ne. It is observed that as the tolerance is increased, the accuracy of the correlation energies corresponding to the optimised constants is slightly improved for H^-, He, Be, B^+ and Ne from 10^{-2} to 10^{-4} in comparison to the exact[16] or estimated[423,424] values. The accuracy of the corresponding energy for Li^+ on the other hand is found to decrease for the same tolerance range. At a tolerance of 10^{-5}, only the correlation energy of He corresponding to the optimised constants is accurate (0.1 % error) in comparison to exact[16] value. The CG method is found to show better promise of giving good results so far. For this reason, the optimisation using this method was re-run with the guess value for all the constants set to 0.01. The result is presented in **Table 7.8.**

Table 7.7. Effect of tolerance on fitting constants (a, b, c, d) optimised using the CG method. Guess values are in **bold** under the constants. Correlation energies in green are the computed exact values[16] while those in blue are experimentally estimated.[423,424] The optimised constants in red are inconsistent (i.e., not reproducible) for the tolerance.

Tolerance	a	b	c	d	E_c / a.u.					
					H^-	He	Li^+	Be	B^+	Ne
	0.01565	**0.173**	**0.58**	**0.8**	**-0.039821**	**-0.042044**	**-0.043498**	**-0.09434**	**-0.11134**	**-0.39047**
1×10^{-2}	0.01565	0.17300	0.58000	0.80000	-0.030724	-0.041560	-0.043884	-0.092596	-0.105959	-0.375313
1×10^{-3}	0.01581	0.17299	0.58000	0.80000	-0.031040	-0.041988	-0.044336	-0.093547	-0.107048	-0.379165
1×10^{-4}	0.01581	0.17299	0.58000	0.80000	-0.031040	-0.041988	-0.044336	-0.093547	-0.107048	-0.379165
1×10^{-5}	0.01375	0.11402	0.61486	0.78382	-0.029226	-0.042069	-0.046380	-0.087352	-0.099024	-0.326655
1×10^{-6}	0.01181	0.04777	0.21614	0.63663	-0.028715	-0.042142	-0.047520	-0.085275	-0.094816	-0.289380
1×10^{-6}	0.01172	0.04247	0.17626	0.63817	-0.028535	-0.042136	-0.047671	-0.084882	-0.094337	-0.286527
1×10^{-6}	0.01174	0.04137	0.17487	0.64661	-0.028441	-0.042148	-0.047764	-0.084767	-0.094258	-0.286166
CS[26]	**0.01565**	**0.173**	**0.58**	**0.8**		**-0.0416**	**-0.0438**	**-0.0926**	**-0.106**	**-0.374**

Table 7.8. Effect of tolerance and guess values on fitting constants (a, b, c, d) optimised using the CG method. Guess values are in **bold** under the constants. Correlation energies in green are the calculated exact values[16] while those in blue are experimentally estimated.[423,424] The optimised constants in red are inconsistent (i.e., not reproducible) for the tolerance.

Tolerance	a	b	c	d	E_c / a.u.					
					H^-	He	Li^+	Be	B^+	Ne
	0.01	**0.01**	**0.01**	**0.01**	**-0.039821**	**-0.042044**	**-0.043498**	**-0.09434**	**-0.11134**	**-0.39047**
1×10^{-2}	0.00669	0.01904	0.00975	0.01241	-0.037777	-0.038225	-0.038295	-0.079547	-0.079986	-0.208824
1×10^{-3}	0.00888	0.07475	0.00687	0.02594	-0.038353	-0.037933	-0.037648	-0.092971	-0.093880	-0.276405
1×10^{-4}	0.01107	0.05824	0.14372	0.45130	-0.030686	-0.041769	-0.045630	-0.087193	-0.095444	-0.289399
1×10^{-4}	0.01239	0.02350	0.27823	0.86003	-0.026696	-0.042433	-0.049658	-0.082925	-0.093257	-0.281741
1×10^{-4}	0.01226	0.04958	0.22283	0.69797	-0.028304	-0.042260	-0.048008	-0.085720	-0.095727	-0.294727
CS[26]	**0.01565**	**0.173**	**0.58**	**0.8**		**-0.0416**	**-0.0438**	**-0.0926**	**-0.106**	**-0.374**

For this optimisation, the CG method also becomes inconsistent and the consistent values are neither better nor similar constants to the CS constants. Application of the consistent optimised constants in the computation of the correlation energies is found to favour the H^- in comparison to the exact value (error of 5.1 % for constants obtained with tolerance of 10^{-2} and for constants optimised with tolerance of 10^{-3}, the error is 3.7 %). The error in the computed E_c for constants optimised with tolerance of 10^{-2} and 10^{-3} is found to be: He (9.1 and 9.8 %), Li^+ (12.0 and 13.4 %), Be (15.7 and 1.5 %), B^+ (28.2 and 15.7 %) and Ne (46.5 and 29.2 %), respectively. It may therefore be reckoned that the values of the CS constants or values in the neighbourhood of the CS constants are to be sought as the guess values in the calculations upon comparison of the results in **Table 7.7** against those in **Table 7.8**.

The optimisation using scipy.optimise least_squares, within $0.3 \leq R \leq 2$ a.u. with a total of 80 points, $q = 2.29$ and the computed Laguerre-based HF wavefunction for the helium atom without constraints is summarised in **Table 7.9**.

Table 7.9. Effect of tolerance and guess values on fitting constants (a, b, c, d) optimised using the scipy.optimise least_squares method without boundary constraints. Guess values are in **bold** under the constants. Correlation energies in green are the computed exact values[16] while those in blue are experimentally estimated.[423,424] The optimised constants in red are unreliable as the expected constants do not have negative values.

Tolerance	a	b	c	d	E_c / a.u.					
					H^-	He	Li^+	Be	B^+	Ne
	0.01565	**0.173**	**0.58**	**0.8**	**-0.039821**	**-0.042044**	**-0.043498**	**-0.09434**	**-0.11134**	**-0.39047**
1×10^{-2}	0.01565	0.17300	0.58000	0.80000	-0.030724	-0.041560	-0.043884	-0.092596	-0.105959	-0.375313
1×10^{-3}	0.01580	0.17299	0.58000	0.80000	-0.031025	-0.041969	-0.044315	-0.093504	-0.106999	-0.378990
1×10^{-4}	0.01580	0.17299	0.58000	0.80000	-0.031025	-0.041969	-0.044315	-0.093504	-0.106999	-0.378990
1×10^{-5}	0.01374	0.11427	0.61519	0.78348	-0.029219	-0.042045	-0.046344	-0.087318	-0.098987	-0.326609
1×10^{-6}	0.01138	0.01110	-0.26234	0.70095	∞	∞	∞	∞	∞	∞
1×10^{-7}	0.01138	0.01111	-0.26210	0.70094	∞	∞	∞	∞	∞	∞
CS[26]	**0.01565**	**0.173**	**0.58**	**0.8**		**-0.0416**	**-0.0438**	**-0.0926**	**-0.106**	**-0.374**

The results presented in **Table 7.9** are similar to those computed using the CG method (**Table 7.7**) differing only in the fact that in **Table 7.9**, the constant, c becomes negative for tolerances $\geq 10^{-6}$ while in **Table 7.7**, the method becomes inconsistent for tolerances $\geq 10^{-4}$.

The optimisation using scipy.optimise least_squares,[412–417] within $0.3 \leq R \leq 2$ a.u. with a total of 80 points, $q = 2.29$ and the computed Laguerre-based HF wavefunction for the helium atom with constraints is presented in **Table 7.10**. The boundary constraints imposed on the constants are $(-1 \leq a \leq 5)$, $(0 \leq b \leq 5)$, $(0 \leq c \leq 5)$ and $(0 \leq d \leq 5)$.

It is found that the results presented in **Table 7.10** for tolerances 10^{-2} to 10^{-6} are similar to those summarised in **Table 7.9** for tolerances 10^{-2} to 10^{-5} but differ for tolerances $\geq 10^{-7}$ for which all the optimised constants are both consistent and positive valued. It is observed that the optimised constant, c tends to a negative at a tolerance of 10^{-10}. Also, the constants optimised with boundary constraints are all consistent, regardless of the number of times the code is run and the tolerance used within $10^{-2} \leq \text{tolerance} \leq 10^{-10}$. The results further suggest that tolerances $\leq 10^{-6}$ give constants that are similar to those of CS while tolerances of 10^{-7} to 10^{-9} give constants that differ with those of CS especially for a and b and a tolerance of 10^{-10} give different values for all the constants in comparison with CS constants. It is noteworthy that Handy and Cohen[349] asserted that the sensitivities of the constants was in the order $a > b > c > d$. It is therefore not very surprising that a and b are being more sensitive in our computations. The authors also suggested that the accuracy of a was especially vital for accuracy of the corresponding correlation energies for a given set of the constants. It is observed that the accuracy of the corresponding energies for the optimised constants in comparison with the exact[16] or estimated[423,424] values decreases $(6 \leq \text{error} \leq 31\ \%)$ for constants optimised with tolerances $\geq 10^{-7}$ except for He. For He, the computed value approaches the exact value (error ≤ 0.2 %).

It can therefore be reckoned that the LSF procedure using the scipy.optmise least_squares method with boundary restrictions and a tolerance of 10^{-6} is the optimum method for computation of the constants in eq. (7.12) as all the other methods are found to be inconsistent or gave poor correlation energies for other systems. As a consequence, this method has been employed to investigate the effect of variation of the range of R and guess values on the value of the optimised constants. In addition, corresponding correlation energies are investigated to determine whether their accuracy will be increased when compared to the exact[16] or estimated[423,424] values. The tolerance, 10^{-6} is chosen as a compromise for accuracy of the correlation energies of all the systems under consideration.

Table 7.10. Effect of tolerance and guess values on fitting constants (a, b, c, d) optimised using the scipy.optimise least_squares method with boundary constraints. Guess values are in **bold** under the constants. Correlation energies in green are the calculated exact values[16] while those in blue are experimentally estimated.[423,424]

Tolerance	a	b	c	d	E_c / a.u.					
					H^-	He	Li^+	Be	B^+	Ne
	0.01565	**0.173**	**0.58**	**0.8**	**-0.039821**	**-0.042044**	**-0.043498**	**-0.09434**	**-0.11134**	**-0.39047**
1×10^{-2}	0.01565	0.17300	0.58000	0.80000	-0.030724	-0.041560	-0.043884	-0.092596	-0.105959	-0.375313
1×10^{-3}	0.01580	0.17299	0.58000	0.80000	-0.031025	-0.041969	-0.044315	-0.093504	-0.106999	-0.378990
1×10^{-4}	0.01580	0.17299	0.58000	0.80000	-0.031025	-0.041969	-0.044315	-0.093504	-0.106999	-0.378990
1×10^{-5}	0.01580	0.17299	0.58000	0.80000	-0.031025	-0.041969	-0.044315	-0.093504	-0.106999	-0.378990
1×10^{-6}	0.01580	0.17299	0.58000	0.80000	-0.031025	-0.041969	-0.044315	-0.093504	-0.106999	-0.378990
1×10^{-7}	0.01394	0.12153	0.61088	0.78554	-0.029369	-0.041970	-0.046049	-0.087830	-0.099679	-0.331702
1×10^{-8}	0.01375	0.11437	0.61517	0.78353	-0.029221	-0.042045	-0.046340	-0.087325	-0.098997	-0.326681
1×10^{-9}	0.01375	0.11437	0.61517	0.78353	-0.029221	-0.042045	-0.046340	-0.087325	-0.098997	-0.326681
1×10^{-10}	0.01145	0.02481	0.00000	0.65724	-0.027643	-0.042004	-0.048159	-0.083180	-0.092483	-0.277043
CS[26]	**0.01565**	**0.173**	**0.58**	**0.8**		**-0.0416**	**-0.0438**	**-0.0926**	**-0.106**	**-0.374**

7.3.5 Effect of Guess Values, Variation of R, Number of Points with R and Tolerance on Fitting Constants for Helium Atom

Here, the scipy.optimise least_squares[412–417] method is used to compute the fitting constants to investigate the effects of different guess values of the constants, different ranges of R and different tolerance limits on the optimised constants. In each case, the corresponding correlation energies for H^-, He, Li^+, Be, B^+ and Ne are computed using the optimised constants and the implemented form of the LYP expression for closed-shell systems (eq. (7.16)). In addition, the energies are compared with their exact values (in green),[16] fixed nucleus non-relativistic experimental estimates (in blue)[423,424] or those computed by CS.[26] Furthermore, in each case, the Koga et al.,[401] HF wavefunctions are employed in the computation of the correlation energies of the systems.

7.3.5.1 Effect of Guess Values on Fitting Constants for Helium Atom within $0.3 \leq R \leq 2$ a.u.

A summary of the effect of guess values on the constants optimised using the scipy.optimise least_squares method with a total of 80 points, $q = 2.29$, a tolerance of 10^{-6}, the computed Laguerre-based HF wavefunction for the helium atom and boundary constraints is presented in **Table 7.11**.

The results in **Table 7.11** further supports the suggestion that guess values close to the CS or the same as CS constants are to be sought in the optimisation of the constants in eq. (7.12). It is found that the constants optimised from the set of parameters labelled **x** give more accurate correlation energies for the same systems than the CS constants even though the optimised constants are similar to those of CS. For these systems, the error is found to be 0.3 % for He, 0.8 % for Li^+, 0.6 % for Be, 2.3 % for B^+ and 0.1 % for Ne. CS computed the errors as 1.0 % for He, 0.7 % for Li^+, 1.5 % for Be, 5.0 % for B^+ and 0.5 % for Ne.[26] The guess values, **x** are therefore employed for further computations.

Table 7.11. Effect of guess values on fitting constants (a, b, c, d) optimised using the scipy.optimise least_squares method with boundary constraints; **y, x** and **z** represent guess values of the constants. For **y**, $a = b = c = d$, for **x**, $a = 0.08$, $b = 0.16$, $c = 0.58$ and $d = 0.8$ while for **z**, $a = 0.01565$, $b = 0.173$, $c = 0.58$ and $d = 0.8$. Correlation energies in green are the computed exact values[16] while those in blue are experimentally estimated.[423,424]

					E_c / a.u.					
y	***a***	***b***	***c***	***d***	**H^-**	**He**	**Li^+**	**Be**	**B^+**	**Ne**
					-0.039821	**-0.042044**	**-0.043498**	**-0.09434**	**-0.11134**	**-0.39047**
1	0.01569	0.28411	0.60474	0.33582	-0.042545	-0.040740	-0.034021	-0.110765	-0.122509	-0.450919
0.1	0.00979	0.09145	0.13064	0.12144	-0.038209	-0.040475	-0.040267	-0.095487	-0.098888	-0.293880
0.01	0.00636	0.01021	0.01000	0.01006	-0.037365	-0.037860	-0.037954	-0.077177	-0.077536	-0.198723
x	0.01628	0.18438	0.57594	0.80562	-0.031406	-0.041937	-0.043850	-0.094865	-0.108785	-0.390922
z	0.01580	0.17299	0.58000	0.80000	-0.031025	-0.041969	-0.044315	-0.093504	-0.106999	-0.378990
CS[26]	**0.01565**	**0.173**	**0.58**	**0.8**		**-0.0416**	**-0.0438**	**-0.0926**	**-0.106**	**-0.374**

7.3.5.2 Effect of Variation of R on Fitting Constants for Helium Atom

The results computed using the scipy.optimise least_squares method with $R_{initial} \equiv R_i = 0.3$ a.u., $R_{final} \equiv R_f = 2, 3, \ldots, 8$ a.u., a total of 80 points, $q = 2.29$, a tolerance of 10^{-6}, the computed Laguerre-based HF wavefunction for the helium atom and boundary constraints is presented in **Table 7.12**.

The results in **Table 7.12** suggests that extending R_f beyond 2 a.u. does not improve the constants nor lead to improved accuracy of the corresponding correlation energies of the systems computed.

Table 7.12. Effect of extension of R_f beyond 2 a.u. but fixing R_i at 0.3 a.u on fitting constants (a, b, c, d) optimised using the scipy.optimise least_squares method with boundary constraints. Guess values are in **bold** under the constants. Correlation energies in green are the calculated exact values[16] while those in blue are experimentally estimated.[423,424]

R_i	R_f	a	b	c	d	E_c / a.u.					
		0.08	**0.16**	**0.58**	**0.8**	**H^-**	**He**	**Li^+**	**Be**	**B^+**	**Ne**
						-0.039821	**-0.042044**	**-0.043498**	**-0.09434**	**-0.11134**	**-0.39047**
0.3	2	0.01628	0.18438	0.57594	0.80562	-0.031406	-0.041937	-0.043850	-0.094865	-0.108785	-0.390922
0.3	3	0.01550	0.17485	0.57682	0.80371	-0.030257	-0.040869	-0.043101	-0.091342	-0.104577	-0.371472
0.3	4	0.01142	0.01474	0.52983	0.85630	-0.025205	-0.040263	-0.047217	-0.077391	-0.086964	-0.259390
0.3	5	0.01487	0.17153	0.57742	0.80317	-0.029141	-0.039516	-0.041796	-0.087949	-0.100638	-0.356045
0.3	6	0.01483	0.17129	0.57747	0.80312	-0.029089	-0.039458	-0.041743	-0.087793	-0.100455	-0.355294
0.3	7	0.01482	0.17117	0.57748	0.80310	-0.029068	-0.039435	-0.041723	-0.087729	-0.100379	-0.354972
0.3	8	0.01481	0.17109	0.57749	0.80309	-0.029053	-0.039418	-0.041708	-0.087683	-0.100326	-0.354753
CS[26]		**0.01565**	**0.173**	**0.58**	**0.8**		**-0.0416**	**-0.0438**	**-0.0926**	**-0.106**	**-0.374**

A summary of the results computed with the scipy.optimise least_squares method using $R_i = 0.3, 0.25, 0.20, \ldots, .0.0$ a.u., $R_f = 2$ a.u., a total of 80 points, $q = 2.29$, a tolerance of 10^{-6}, the computed Laguerre-based HF wavefunction for the helium atom and boundary constraints is presented in **Table 7.13**.

It is observed from the results in **Table 7.13** that extending the range of R by decreasing R_i from 0.3 to 0.0 a.u. in steps of 0.05 a.u. does not lead to improved accuracy of the corresponding correlation energies for the systems computed. The optimum constants remain those optimised within $0.3 \leq R \leq 2$ a.u., when the corresponding correlation energies are compared with the exact and estimated values. Nevertheless, the accuracy of the corresponding correlation energies for the H^- and B^+ are increased with increasing range from $R_i = 0.25$ to 0.05 a.u. but declines sharply at $R_i = 0.0$ a.u.

Table 7.13. Effect of increasing the range of R by decreasing R_i in steps of 0.05 from 0.3 to 0.0 a.u. but fixing R_f at 2 a.u on fitting constants (a, b, c, d) optimised using the scipy.optimise least_squares method with boundary constraints. Guess values are in **bold** under the constants. Correlation energies in green are the computed exact values[16] while those in blue are experimentally estimated.[423,424]

R_i	R_f	a	b	c	d	E_c / a.u.					
		0.08	**0.16**	**0.58**	**0.8**	**H^-**	**He**	**Li^+**	**Be**	**B^+**	**Ne**
						-0.039821	**-0.042044**	**-0.043498**	**-0.09434**	**-0.11134**	**-0.39047**
0.3	2	0.01628	0.18438	0.57594	0.80562	-0.031406	-0.041937	-0.043850	-0.094865	-0.108785	-0.390922
0.25	2	0.01636	0.18555	0.57588	0.80575	-0.031503	-0.042004	-0.043872	-0.095161	-0.109145	-0.392773
0.2	2	0.01648	0.18724	0.57573	0.80594	-0.031680	-0.042151	-0.043955	-0.095703	-0.109798	-0.395934
0.15	2	0.01670	0.18995	0.57543	0.80627	-0.031989	-0.042417	-0.044117	-0.096649	-0.110933	-0.401345
0.1	2	0.01639	0.17928	0.57727	0.80392	-0.031847	-0.042785	-0.044942	-0.096131	-0.110137	-0.393274
0.05	2	0.01660	0.17963	0.57730	0.80385	-0.032235	-0.043286	-0.045453	-0.097298	-0.111480	-0.398233
0.0	2	0.01185	0.02239	0.58768	0.80238	-0.027006	-0.042327	-0.049163	-0.081599	-0.091527	-0.273903
CS[26]		**0.01565**	**0.173**	**0.58**	**0.8**		**-0.0416**	**-0.0438**	**-0.0926**	**-0.106**	**-0.374**

The constants optimised with the scipy.optimise least_squares method using $R_i = 0.0$ a.u., $R_f = 1, 2, \ldots, 8$ a.u., a total of 80 points, $q = 2.29$, a tolerance of 10^{-6}, the computed Laguerre-based HF wavefunction for the helium atom and boundary constraints are summarised in **Table 7.14**.

Inspection of the results summarised in **Table 7.14** reveal that the value of the constants are generally not improved and there is no discernible trend in the value of the optimised constants with increasing R_f from 1 to 5 a.u. Nevertheless, the values of the optimised constants within $0.0 \leq R \leq 6$ a.u. are very similar to the CS values. These values become less similar to the CS values for $R_f \geq 7$ a.u. The corresponding correlation energies computed within $0.0 \leq R \leq 6$ a.u. are found to have errors of; 1.7 % for He, 0.5 % for Li^+, 2.3 % for Be, 5.3 % for B^+ and 4.3 % for Ne in comparison with the exact or experimental estimates. This suggests that the energies are less accurate than the CS values by about 0.5 % for He, Be and B^+ but are of similar accuracy as CS values.

As a result of the similarity of the optimised constants and allied correlation energies for the constants optimised within $0.0 \leq R \leq 6$ a.u., the variation of the calculated $H(\beta, W)$ function and the CS $H(\beta, W)$ function with R is ploted to further investigate their similarity. To do this, a plot of the integrated (exact) results, calculated and CS $H(\beta, W)$ function arising from the computed Laguerre-based HF helium densities against R within $0.0 \leq R \leq 6$ a.u. is presented in **Figure 7.4**.

Table 7.14. Effect of increasing the range of R by increasing R_f in steps of 1 a.u. but fixing R_i at 0.0 a.u on fitting constants (a, b, c, d) optimised using the scipy.optimise least_squares method with boundary constraints. Guess values are in **bold** under the constants. Correlation energies in green are the calculated exact values[16] while those in blue are experimentally estimated.[423,424]

R_i	R_f	**a**	**b**	**c**	**d**	E_c / **a.u.**					
		0.08	**0.16**	**0.58**	**0.8**	**H^-**	**He**	**Li^+**	**Be**	**B^+**	**Ne**
						-0.039821	**-0.042044**	**-0.043498**	**-0.09434**	**-0.11134**	**-0.39047**
0.0	1	0.01177	0.01559	0.58567	0.80652	-0.026915	-0.042450	-0.049478	-0.081433	-0.091289	-0.271322
0.0	2	0.01185	0.02239	0.58768	0.80238	-0.027012	-0.042335	-0.049172	-0.081615	-0.091545	-0.273957
0.0	3	0.01161	0.02427	0.57804	0.80715	-0.026319	-0.041238	-0.047886	-0.079648	-0.089380	-0.268150
0.0	4	0.01116	0.00854	0.56924	0.82233	-0.025391	-0.040419	-0.047340	-0.077187	-0.086529	-0.255611
0.0	5	0.01112	0.00523	0.57443	0.81574	-0.025499	-0.040625	-0.047611	-0.077370	-0.086672	-0.254989
0.0	6	0.01559	0.17256	0.57760	0.80302	-0.030532	-0.041350	-0.043695	-0.092140	-0.105448	-0.373505
0.0	7	0.01554	0.17266	0.57768	0.80290	-0.030434	-0.041211	-0.043544	-0.091840	-0.105106	-0.372329
0.0	8	0.01552	0.17244	0.57772	0.80285	-0.030403	-0.041180	-0.043520	-0.091746	-0.104995	-0.371836
CS[26]		**0.01565**	**0.173**	**0.58**	**0.8**		**-0.0416**	**-0.0438**	**-0.0926**	**-0.106**	**-0.374**

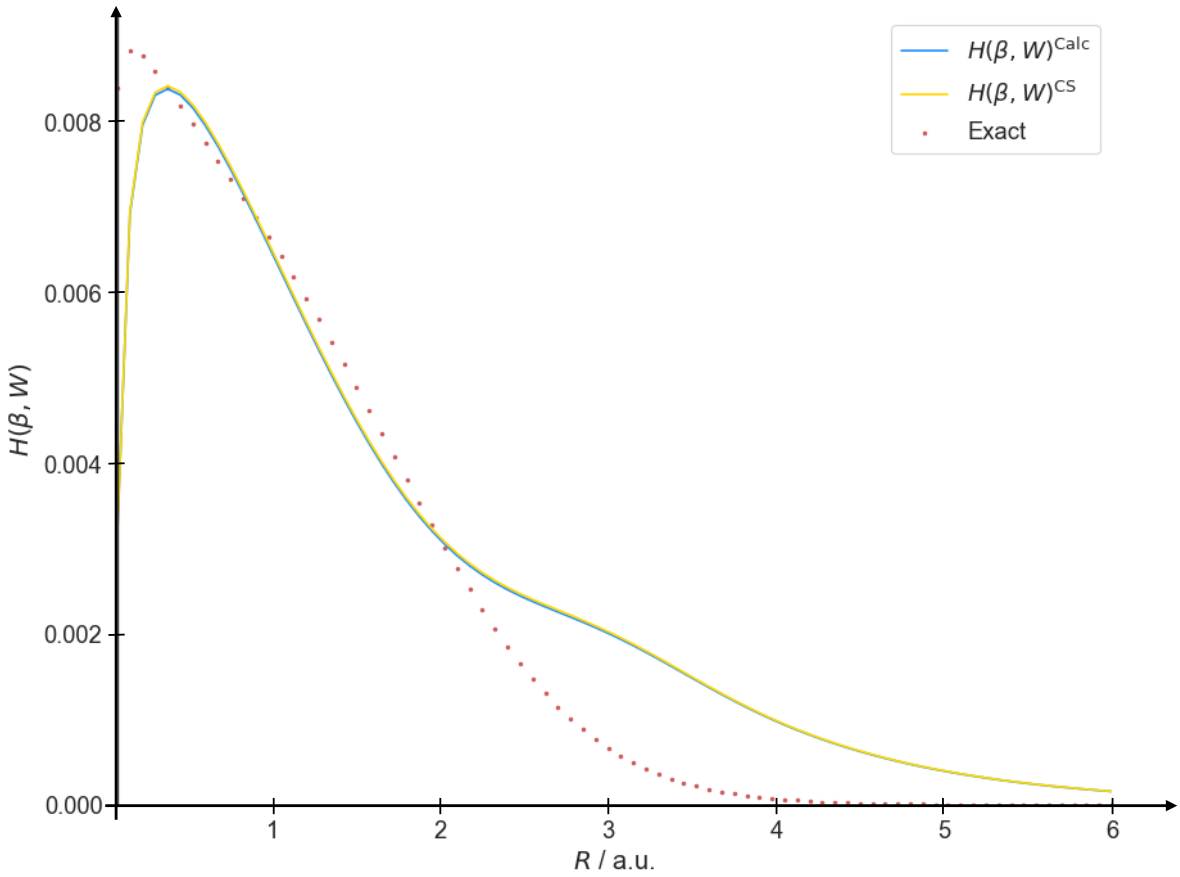

Figure 7.5. Variation of the $H(\beta, W)$ function with R for the helium atom within $0.0 \leq R \leq 6$ a.u. using a tolerance of 10^{-6}. The red dots represent the exact numerically integrated result; blue curve represents the approximated function ($H(\beta, W)^{\text{Calc.}}$) while the yellow curve is a plot of the CS function, $H(\beta, W)^{\text{CS}}$.

It is observed that the approximated and CS $H(\beta, W)$ function overlay each other almost exactly with only a marginal difference around their maximum. This is likely the region that is sensitive and that is reflected in sensitivity of the value of constant a. Even though the calculated curves look similar, the corresponding optimised constants within this range of R give slightly less accurate corresponding correlation energies especially for He, Be and B^+. This may be attributed to the behaviour around the maximum of the approximated curve or sensitivity of its constant a in agreement with the assertion by Handy and Cohen.[349]

In summary, it is found on the overall that increasing the range of R does not necessarily improve the optimised constants nor the correlation energies resulting from application of the optimised constants to the implemented form of the LYP exression for correlation energies.

7.3.5.3 Effect of Variation of the Number of Points with R on the Fitting Constants for Helium

The constants computed with the scipy.optimise least_squares method using $R_i = 0.3$ a.u., $R_f = 2, 3, 4, \ldots, 8$ a.u., a total of 80, 120, 160, …, 320 points, $q = 2.29$, a tolerance of 10^{-6}, the computed Laguerre-based HF wavefunction for helium and boundary constraints are summarised in **Table 7.15**.

The results summarised in **Table 7.15** suggest that increasing the number of points with increasing R_f decreases the accuracy of constant a and hence, the accuracy of the corresponding correlation energies even though the value of constant b, c and d is essentially unchanged on the overall.

It is found that the most accurate constants in general considering the accuracy of the corresponding correlation energies are $a = 0.01628$, $b = 0.18438$, $c = 0.57594$ and $d = 0.80562$. These constants are computed in the range, $0.3 \leq R \leq 2$ a.u. with a total number of points, $R_{\text{num}} = 80$, a tolerance of 10^{-6} and guess values: $a = 0.08$, $b = 0.16$, $c = 0.58$ and $d = 0.8$. The accuracy of the correlation energies computed by applying these optimised constants is found to be slightly higher than the CS values in comparison with exact values[16] or fixed nucleus non-relativistic experimental estimates.[423,424]

Table 7.15. Effect of increasing number of points (R_{num}) with R_f but fixing R_i at 0.3 a.u on fitting constants (a, b, c, d) optimised using the scipy.optimise least_squares method with boundary constraints. Guess values are in **bold** under the constants. Correlation energies in green are the calculated exact values[16] while those in blue are experimentally estimated.[423,424]

R_{num}	R_f	a	b	c	d	E_c / a.u.					
		0.08	**0.16**	**0.58**	**0.8**	**H^-**	**He**	**Li^+**	**Be**	**B^+**	**Ne**
						-0.039821	**-0.042044**	**-0.043498**	**-0.09434**	**-0.11134**	**-0.39047**
80	2	0.01628	0.18438	0.57594	0.80562	-0.031406	-0.041937	-0.043850	-0.094865	-0.108785	-0.390922
120	3	0.01563	0.17830	0.57610	0.80456	-0.030377	-0.040863	-0.042965	-0.091735	-0.105088	-0.374870
160	4	0.01559	0.18804	0.57369	0.80740	-0.029884	-0.039729	-0.041404	-0.090357	-0.103686	-0.374374
200	5	0.01548	0.18682	0.57395	0.80725	-0.029717	-0.039569	-0.041285	-0.089843	-0.103075	-0.371611
240	6	0.01543	0.18619	0.57410	0.80711	-0.029649	-0.039509	-0.041247	-0.089633	-0.102823	-0.370414
280	7	0.01541	0.18578	0.57420	0.80700	-0.029621	-0.039492	-0.041245	-0.089544	-0.102713	-0.369829
320	8	0.01539	0.18548	0.57427	0.80693	-0.029605	-0.039485	-0.041249	-0.089490	-0.102647	-0.369453
CS[26]		**0.01565**	**0.173**	**0.58**	**0.8**		**-0.0416**	**-0.0438**	**-0.0926**	**-0.106**	**-0.374**

7.3.5.4 Effect of Variation of Tolerance within $0.3 \leq R \leq 2$ a.u. on the Fitting Constants for Helium

The results of optimisation of constants within $0.3 \leq R \leq 2$ a.u. using a total of 80 points, $q = 2.29$, $10^{-2} \leq \text{tolerance} \leq 10^{-10}$, the computed Laguerre-based HF wavefunction for helium and boundary constraints are summarised in **Table 7.16**.

Table 7.16. Effect of variation of tolerance within $0.3 \leq R \leq 2$ a.u. on fitting constants (a, b, c, d) optimised using the scipy.optimise least_squares method with boundary constraints. Guess values are in **bold** under the constants. Correlation energies in green are exact values[16] while those in blue are experimentally estimated.[423,424]

Tolerance	a	b	c	d	E_c / a.u.					
					H^-	He	Li^+	Be	B^+	Ne
	0.08	**0.16**	**0.58**	**0.8**	**-0.039821**	**-0.042044**	**-0.043498**	**-0.09434**	**-0.11134**	**-0.39047**
1×10^{-2}	0.01658	0.18432	0.57595	0.80560	-0.031971	-0.042694	-0.044645	-0.096570	-0.110739	-0.397915
1×10^{-3}	0.01658	0.18432	0.57595	0.80560	-0.031971	-0.042694	-0.044645	-0.096570	-0.110739	-0.397915
1×10^{-4}	0.01628	0.18438	0.57594	0.80562	-0.031406	-0.041937	-0.043850	-0.094865	-0.108785	-0.390922
1×10^{-5}	0.01628	0.18438	0.57594	0.80562	-0.031406	-0.041937	-0.043850	-0.094865	-0.108785	-0.390922
1×10^{-6}	0.01628	0.18438	0.57594	0.80562	-0.031406	-0.041937	-0.043850	-0.094865	-0.108785	-0.390922
1×10^{-7}	0.01629	0.18437	0.57595	0.80562	-0.031411	-0.041943	-0.043857	-0.094879	-0.108800	-0.390975
1×10^{-8}	0.01629	0.18437	0.57595	0.80562	-0.031411	-0.041943	-0.043857	-0.094879	-0.108800	-0.390975
1×10^{-9}	0.01376	0.11418	0.61896	0.78763	-0.029183	-0.042047	-0.046373	-0.087261	-0.098947	-0.326549
1×10^{-10}	0.01376	0.11418	0.61896	0.78763	-0.029183	-0.042047	-0.046373	-0.087261	-0.098947	-0.326549
CS	0.01565	0.173	0.58	0.8		-0.0416	-0.0438	-0.0926	-0.106	-0.374

On inspection of the result in **Table 7.16**, it is found that there is no discernible trend in the value of the constants optimised in this range of R. It is also observed that tolerances of 10^{-4} to 10^{-6} all give the same constants. The corresponding correlation energies of the optimised constants for these tolerances are found to have smaller errors than the CS values in comparison with the exact values[16] and/or fixed non-relativistic experimental estimates.[423,424] In addition, it is found that the optimised constants at tolerances $\geq 10^{-9}$ lead to highly accurate correlation energies for only helium ($\text{error} = 0.0$ %) but inaccurate energies ($\text{error} \geq 6.6$ %) for every other system considered.

On the basis of the results considered so far, the optimum optimised constants for fitting to helium atom are $a = 0.01628$, $b = 0.18438$, $c = 0.57594$ and $d = 0.80562$. The errors for the corresponding correlation energies of the investigated closed-shell systems in comparison with exact and/or estimated values are: 21.1 % for H^-, 0.3 % for He, 0.8 % for Li^+, 0.6 % for Be, 2.3 % for B^+ and 0.1 % for Ne. The CS constants are $a = 0.01565$, $b = 0.173$, $c = 0.58$ and $d = 0.8$. Their corresponding correlation energies are found to have the errors: 1.1 % for He, 0.7 % for Li^+, 1.8 % for Be, 4.8 % for B^+ and 4.2 % for Ne. The computed constants in the present work therefore offer higher accuracy for computation of correlation energies.

A plot of the behaviour of the exact results, calculated and CS $H(\beta, W)$ function arising from the computed Laguerre-based HF helium densities against R corresponding to the optimum constants and the most accurate constants for helium is presented in **Figure 7.6**.

It is observed that the approximated and CS function curves corresponding to the optimum constants are poorly fitted to the exact data. For the fitting in **Figure 7.6b**, the approximated function has a better fit than that of the CS to the exact data. It may therefore be reckoned that for a robust set of constants, the poor fit is desirable as accurate fitting results in constants that lead to accurate correlation energies for only the helium atom.

It is worth noting that the constants optimised by fitting the $H(\beta, W)$ function to the numerically integrated helium data do not give good correlation energy for the hydride ion including the optimum and best constants. For this system, it is found that the smallest error is 20 %. On the basis of **Figure 7.1** and this result, it may considered to this extent that the CS formalism does not account for the long range low density behaviour of the hydride ion in agreement with literature assertions[362,385] of this anomaly. One may therefore expect that the optimum constants for fitting to the hydride ion data will not fall in the same range of R as those of the helium atom as the HF densities in the form of the the 'exact' data for the hydride ion is likely to have a larger radial extent than the helium atom just as in **Figure 7.1**.

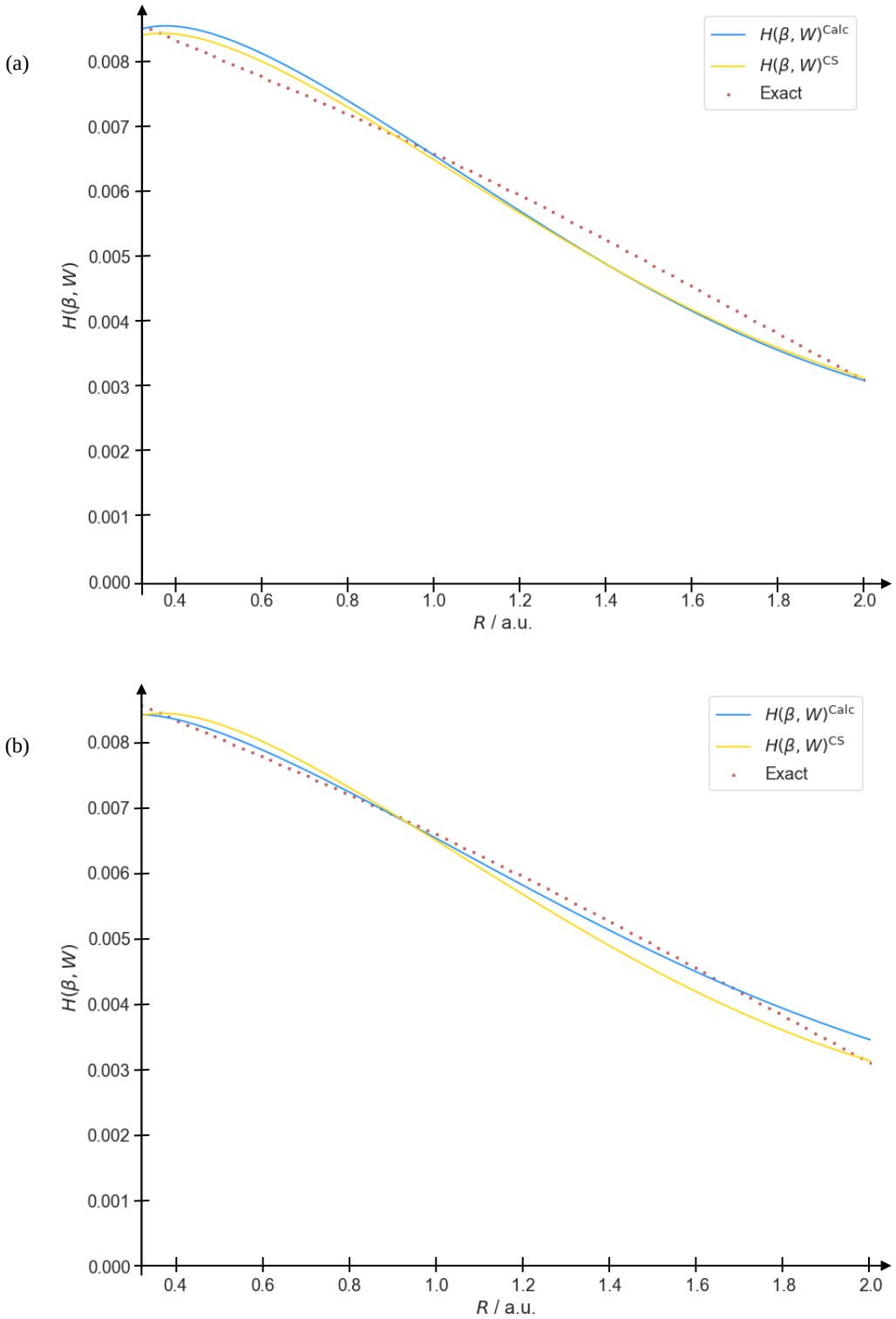

Figure 7.6. Variation of the $H(\beta, W)$ function with R for the helium atom within $0.3 \leq R \leq 2$ a.u. using a tolerance of: (a) 10^{-6} and (b) 10^{-10}. The red dots represent the exact numerically integrated result; blue curve represents the approximated function ($H(\beta, W)^{\text{Calc.}}$) while the yellow curve is a plot of the CS function, $H(\beta, W)^{\text{CS}}$.

The determination of the optimum constants for fitting to the hydride ion data is therefore considered next in an attempt to account for the long range low density behaviour asserted to be lacking[362,385] in the CS model.

7.3.6 Fitting Constants for the Hydride Ion

Following a detailed rational search for the optimum fitting constants for the hydride ion, only the summary of computed results consisting of the effect of the constant q and the most accurate results for the system are presented in this section. All other computational results with respect to the hydride ion are summarised in **Appendix A.4**. Just as in the preceeding sections, the corresponding correlation energies are computed for each set of optimised constants using the implementation of a form of the LYP functional (eq. (7.16)) and the Koga et al.,[401] HF wavefunctions. In addition, the exact[16] or fixed nucleus non-relativistic experimentally estimated[423,424] correlation energies of the respective closed-shell systems are employed to test the accuracy of the CS model for the optimised constants.

7.3.6.1 Effect of q, Guess Constant Values and Boundary conditions on the Fitting Constants for the Hydride Ion

Table 7.17 presents a summary of the optimised fitting constants for the fitting to the hydride ion density using different guess values and $q = 1.93985$ for H^-, determined in **7.2.4.2** in addition to $q = 2.29$ (that was derived from He), is employed within $0.3 \leq R \leq 2$ a.u. with a total of 80 points and a tolerance of 10^{-6}. To do this, the scipy.optimise least_squares approach with and without boundary constraints and the computed 25-term Laguerre-based HF wavefunction for the hydride ion were employed.

The results summarised in **Table 7.17** suggest that for the fitting to the computed hydride ion densities, the fitting constants optimised using $q = 1.93985$ without boundary constraints are more promising regardless of the guess values of the constants. This is observed especially in the accuracy of the corresponding computed correlation energies for the hydride ion, as the fitting to the hydride ion densities necessarily has to reproduce its correlation energy for it to be accurate. Consequently, $q = 1.93985$, no boundary constraints and guess constants; $a = 0.01$, $b = 0.17$, $c = 0.58$ and $d = 0.8$ are employed for further optimisations.

Table 7.17. Effect of q and boundary conditions on fitting constants (a, b, c, d) from fitting to the hydride ion densities optimised using the scipy.optimise least_squares method within $0.3 \leq R \leq 2$ a.u. and a total of 80 points employing. Four sets of guess values for the constants are employed. Correlation energies in green are the calculated exact values[16] while those in blue are experimentally estimated.[423,424]

q	**Boundary Constraints**	**a**	**b**	**c**	**d**	E_c / a.u.					
						H^-	**He**	**Li^+**	**Be**	**B^+**	**Ne**
		0.01	**0.17**	**0.58**	**0.8**	**-0.039821**	**-0.042044**	**-0.043498**	**-0.09434**	**-0.11134**	**-0.39047**
2.29	None	0.01192	0.01245	0.59148	0.81792	-0.027123	-0.043003	-0.050256	-0.082323	-0.092308	-0.273698
	Imposed	0.01448	0.16992	0.58001	0.79997	-0.028515	-0.038717	-0.040993	-0.085943	-0.098300	-0.346921
1.93985	None	0.02424	0.05184	0.57460	1.06007	-0.040209	-0.066294	-0.078578	-0.133492	-0.153613	-0.501289
	Imposed	0.02518	0.16962	0.58008	0.79990	-0.043261	-0.056425	-0.057048	-0.130171	-0.151967	-0.586863
q	**Boundary Constraints**	**a**	**b**	**c**	**d**	E_c / a.u.					
						H^-	**He**	**Li^+**	**Be**	**B^+**	**Ne**
		0.08	**0.16**	**0.58**	**0.8**	**-0.039821**	**-0.042044**	**-0.043498**	**-0.09434**	**-0.11134**	**-0.39047**
2.29	None	0.01213	0.01610	0.58565	0.83945	-0.027090	-0.043056	-0.050363	-0.082710	-0.092882	-0.276985
	Imposed	0.01456	0.17234	0.57766	0.80557	-0.028471	-0.038595	-0.040805	-0.085974	-0.098404	-0.348573
1.93985	None	0.02424	0.05172	0.57190	1.05947	-0.040210	-0.066293	-0.078580	-0.133511	-0.153628	-0.501259
	Imposed	0.02518	0.16962	0.58008	0.79990	-0.043261	-0.056425	-0.057048	-0.130171	-0.151967	-0.586863
q	**Boundary Constraints**	**a**	**b**	**c**	**d**	E_c / a.u.					
						H^-	**He**	**Li^+**	**Be**	**B^+**	**Ne**
		0.0	**0.0**	**0.0**	**0.0**	**-0.039821**	**-0.042044**	**-0.043498**	**-0.09434**	**-0.11134**	**-0.39047**
2.29	None	0.01291	0.02565	0.31483	0.90661	-0.026936	-0.043195	-0.050750	-0.084612	-0.095397	-0.289874
	Imposed	0.01078	0.00000	0.00000	0.68435	-0.027422	-0.042336	-0.048939	-0.080006	-0.088925	-0.257075
1.93985	None	0.02376	0.04490	0.40860	1.01330	-0.040225	-0.066185	-0.078557	-0.134356	-0.154074	-0.497619
	Imposed	0.01708	0.00000	0.00000	0.64042	-0.041105	-0.064741	-0.075509	-0.122592	-0.136820	-0.398235
q	**Boundary Constraints**	**a**	**b**	**c**	**d**	E_c / a.u.					
						H^-	**He**	**Li^+**	**Be**	**B^+**	**Ne**
		0.1	**0.1**	**0.1**	**0.1**	**-0.039821**	**-0.042044**	**-0.043498**	**-0.09434**	**-0.11134**	**-0.39047**
2.29	None	0.01314	0.03321	0.64235	0.94579	-0.026945	-0.043308	-0.050848	-0.084349	-0.095402	-0.292125
	Imposed	-0.00257	2.19488	0.00000	0.74790	-0.033042	-0.057841	-0.071552	-0.037741	-0.038065	0.090153
1.93985	None	0.02442	0.05706	0.69480	1.08267	-0.040180	-0.066266	-0.078401	-0.132567	-0.152811	-0.502181
	Imposed	-0.00341	1.63468	0.00000	0.50639	-0.052276	-0.088344	-0.107345	-0.056646	-0.057905	0.124745

7.3.6.2 Effect of Simultaneous Variation of R_i and R_f on the Fitting Constants for the Hydride Ion

The optimum fitting constants for the hydride ion were computed by varying both initial and final values of R simultaneously to increase the range of R. These values were obtained by using the scipy.optimise least_squares approach without boundary conditions, a total of 80 points, a tolerance of 10^{-6} and the computed 25-term Laguerre-based HF wavefunction for the hydride ion. The guess constant values employed for this optimisation were $a = 0.01$, $b = 0.17$, $c = 0.58$ and $d = 0.8$. The result of this optimisation is presented in **Table 7.18**.

It is found that for all the computed fitting constants in **Table 7.18**, the only system whose energy is reproduced correctly is the hydride ion whose correlation energy is within 1 % of its exact value. The correlation energies for all other systems are ≥ 28.3 % less accurate in comparison with the exact or experimentally estimated values. For the hydride ion in particular, the optimum fitting constants are computed as $a = 0.02578$, $b = 0.10943$, $c = 1.49357$ and $d = 1.22388$. These constants are optimised for the system within $0.1 \leq R \leq 6$ a.u. This range of R for the hydride is different from the range of R within which the optimum fitting constants were optimised for the helium atom as anticipated.

A plot of the integrated results, approximated and CS $H(\beta, W)$ functions arising from the computed Laguerre-based HF hydride ion densities against R corresponding to the optimum constants for the system is presented in **Figure 7.7**. It is observed from **Figure 7.7** that the $H(\beta, W)^{\text{Calc.}}$ is very accurately fitted to the exact data while the $H(\beta, W)^{\text{CS}}$ which uses the values of the CS constants is very poorly fitted to the exact data. As observed for helium in **7.3.2**, the excellent accuracy of the fitting for $H(\beta, W)^{\text{Calc.}}$ in **Figure 7.7** is a likely reason for the poor performance of the optimised a, b, c and d in the computation of correlation energies for non-hydride systems. As summarised in **Table A.4.4** of **Appendix A.4**, varying the tolerance to lower the accuracy of the fit does not improve the optimised constants nor the corresponding correlation energies in general.

Table 7.18. Effect of increasing the range of R by varying both initial and final values of R on fitting constants (a, b, c, d) optimised for the hydride ion using the scipy.optimise least_squares method without boundary restrictions. Correlation energies in green are exact values[16] while those in blue are experimentally estimated.[423,424]

R_i	R_f	**a**	**b**	**c**	**d**	E_c / **a.u.**					
		0.01	**0.17**	**0.58**	**0.8**	**H^-**	**He**	**Li^+**	**Be**	**B^+**	**Ne**
						-0.039821	**-0.042044**	**-0.043498**	**-0.09434**	**-0.11134**	**-0.39047**
0.3	2	0.02424	0.05184	0.57460	1.06007	-0.040209	-0.066294	-0.078578	-0.133492	-0.153613	-0.501289
0.25	3	0.02459	0.05341	0.57757	1.08198	-0.040170	-0.066383	-0.078764	-0.133929	-0.154301	-0.505553
0.2	4	0.02563	0.05660	0.58325	1.14862	-0.040053	-0.066739	-0.079506	-0.135287	-0.156364	-0.517216
0.15	5	0.02685	0.05868	0.59372	1.23223	-0.039905	-0.067271	-0.080624	-0.136895	-0.158759	-0.529557
0.1	6	0.02578	0.10943	1.49357	1.22388	-0.039825	-0.065826	-0.076525	-0.125969	-0.145885	-0.511579
0.05	7	0.02600	0.10401	1.52715	1.25014	-0.039689	-0.066248	-0.077529	-0.126829	-0.146837	-0.511384
0.0	8	0.02537	0.09131	1.59038	1.22461	-0.039516	-0.066498	-0.078397	-0.127192	-0.146827	-0.500849

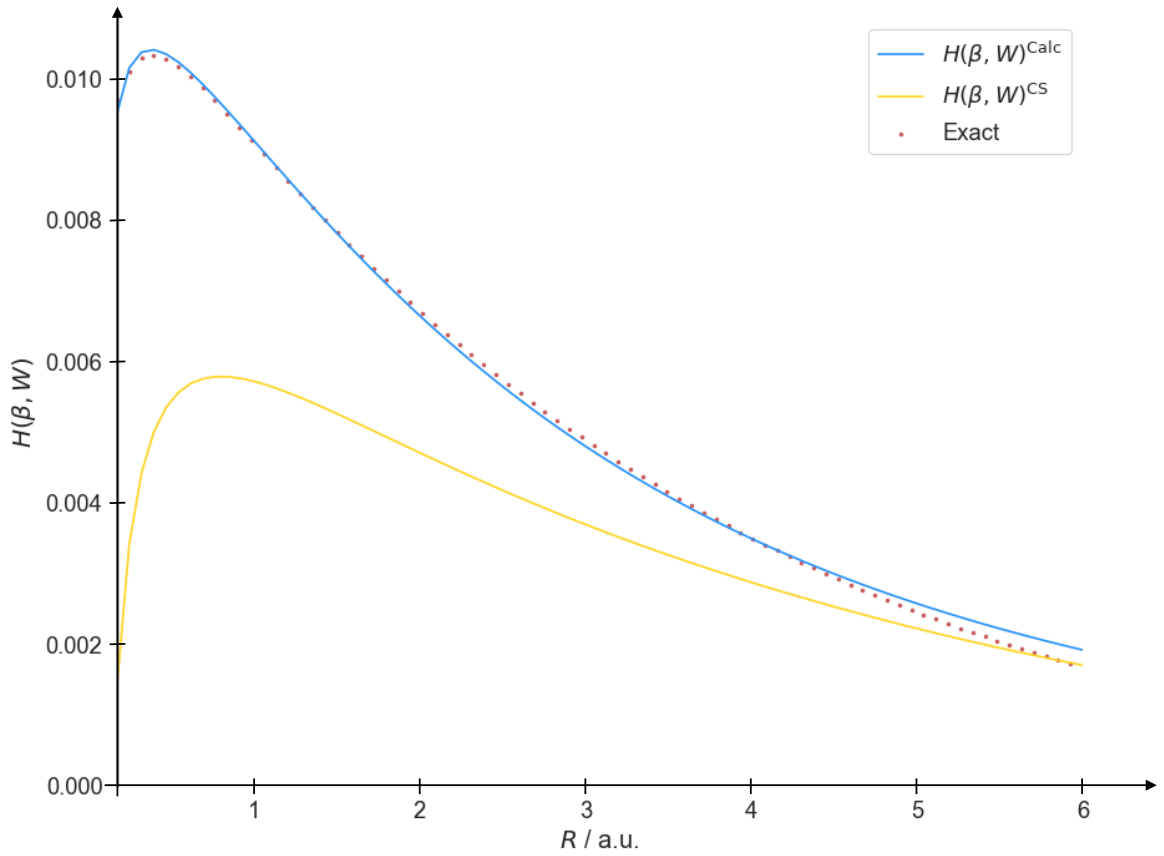

Figure 7.7. Variation of the $H(\beta, W)$ function with R for the hydride ion within $0.1 \leq R \leq 6$ a.u. using a tolerance of 10^{-6}. The red dots represent the exact numerically integrated result; blue curve represents the approximated function ($H(\beta, W)^{\text{Calc.}}$) while the yellow curve is a plot of the CS function, $H(\beta, W)^{\text{CS}}$.

In order to visualise the behaviour of the $H(\beta, W)$ at long range for both system, the 'exact' data of the systems is plotted against R in **Figure 7.8**.

The plots in F**igure 7.8** reveals that the $H(\beta, W)$ function has a shorter radial extent for the helium atom (**Figure 7.8(a)**) and a larger radial extent for the hydride ion (**Figure 7.8(b)**) as it decays faster for the helium atom (at $\sim 5\, a_0$) but slower for the hydride ion ($\sim 13\, a_0$). This is similar to the behaviour captured in **Figure 7.1**. However, in **Figure 7.1**, the densities are physically meaningful whereas the $H(\beta, W)$ function does not have a physical interpretation. In addition, the functions are plotted against inter-electronic and nucleus-electron distances, respectively and so are not directly comparable. So far therefore, no discernible link exists between the **Figure 7.8** and **Figure 7.1** except that the two functions decay in a similar manner. Thus, the $H(\beta, W)$ function is likely to have captured the long range low density behaviour of the hydride ion. Nevertheless, it is not very clear why the constants determined for the hydride ion are not accurate when other correlation

energies are computed. A possible explanation is that the hydride ion is predicted to be unbound at the HF level.[16,18] This is likely to be the reason for the success of the determined helium parameters in reproducing accurate correlation energies for neutral and cationic atomic systems. It may therefore be reckoned that a bound atomic anion, e.g., $Z_C^{\mathrm{HF}[16]}$ may perform better.

In the next section, the optimum constants for these species are used to compute the correlation energies for several atomic systems including atomic anions to determine which of the two sets of constants better reproduces their correlation energies.

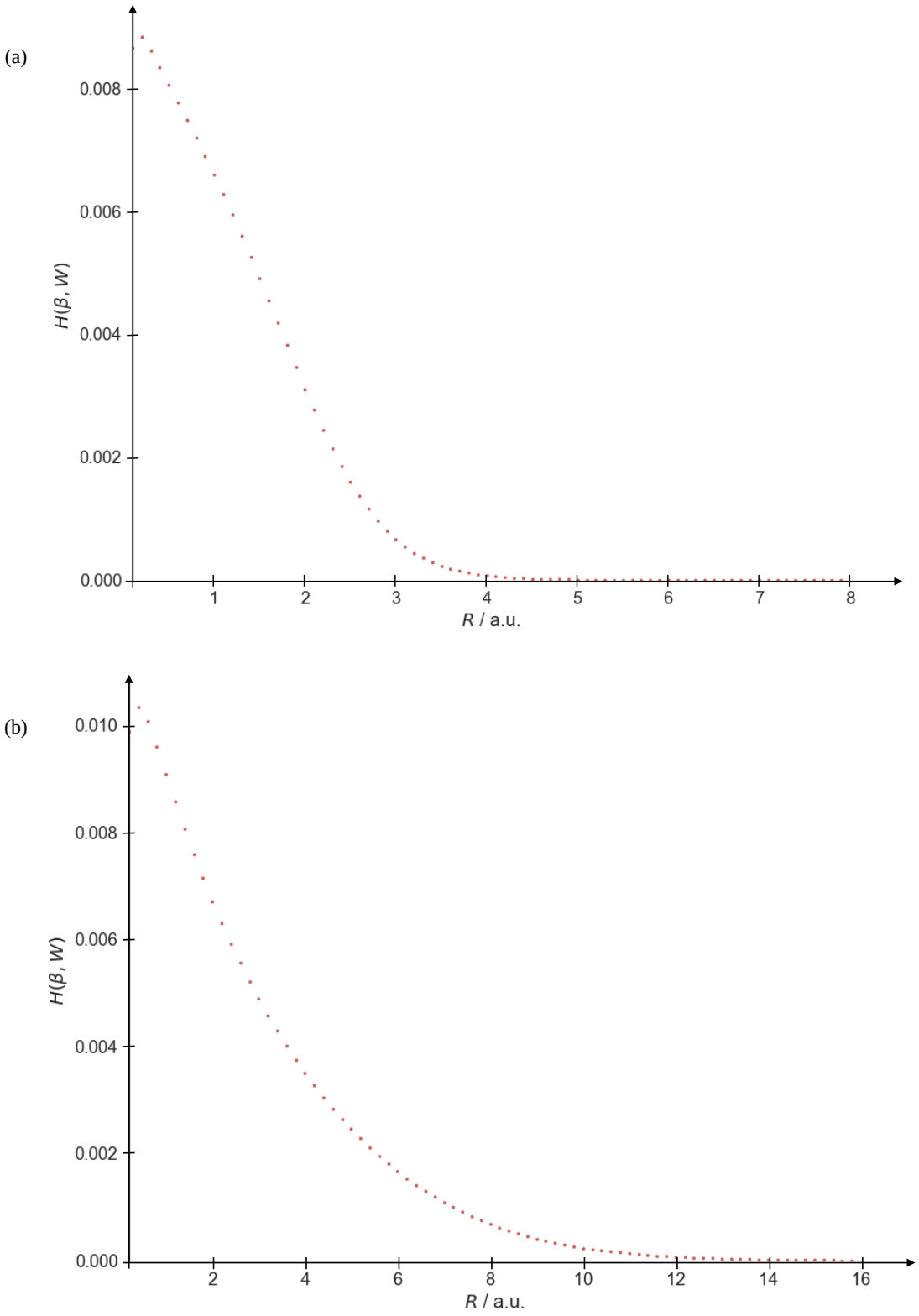

Figure 7.8. Variation of the exact numerically integrated result with R for the: (a) helium atom within $0.0 \leq R \leq 8$ a.u. and (b) hydride ion within $0.0 \leq R \leq 16$ a.u. using a tolerance of 10^{-6}.

7.3.7 Correlation Energies of Atomic Systems using Optimum Fitting Constants for the Helium Atom and the Hydride Ion

A summary of the correlation energies computed using the CS constants (**CS Fit**), optimum computed fitting constants for helium atom (**He Fit**) and optimum computed fitting constants for the hydride ion (**H⁻ Fit**) is presented in **Table 7.19**. The respective constants are: $a = 0.01565$, $b = 0.173$, $c = 0.58$ and $d = 0.8$ for **CS Fit**, $a = 0.01628$, $b = 0.18438$, $c = 0.57594$ and $d = 0.80562$ for **He Fit** and $a = 0.02578$, $b = 0.10943$, $c = 1.49357$ and $d = 1.22388$ for **H⁻ Fit**.

Table 7.19. Correlation energies of atomic systems computed using the CS Fit, He Fit and H⁻ Fit constants in combination with the respective Koga et al.,[401] HF wavefunctions. Correlation energies in green are the computed exact values[16] while those in red[427] and blue[423,424] are experimentally estimated.

System	$E_c^{\text{Calc.}}$ / a.u.			$E_c^{\text{Lit.}}$ / a.u.	Absolute Error / %		
Anions	**CS Fit**	**He Fit**	**H⁻ Fit**		**ΔCS Fit**	**ΔHe Fit**	**ΔH⁻ Fit**
H^-	-0.030724	-0.031398	-0.039821	**-0.039821**	22.8	21.2	0.0
Li^-	-0.070081	-0.071349	-0.098827	**-0.073**	4.0	2.3	35.4
B^-	-0.136152	-0.140800	-0.172398	**-0.145**	6.1	2.9	18.9
C^-	-0.167977	-0.174568	-0.210922	**-0.183**	8.2	4.6	15.3
N^-	-0.237865	-0.247407	-0.303009	**-0.265**	10.2	6.6	14.3
O^-	-0.299123	-0.311267	-0.389259	**-0.331**	9.6	6.0	17.6
F^-	-0.354303	-0.368911	-0.469486	**-0.400**	11.4	7.8	17.4
Cations							
Li^+	-0.043884	-0.043838	-0.076518	**-0.043498**	0.9	0.8	75.9
Be^+	-0.058123	-0.059085	-0.087871	**-0.04737**	22.7	24.7	85.5
B^+	-0.105959	-0.108756	-0.145873	**-0.11134**	4.8	2.3	31.0
C^+	-0.144020	-0.148939	-0.191051	**-0.13880**	3.8	7.3	37.6
N^+	-0.175908	-0.182818	-0.230547	**-0.16661**	5.6	9.7	38.4
O^+	-0.202159	-0.210769	-0.265414	**-0.19423**	4.1	8.5	36.6
F^+	-0.276579	-0.288051	-0.372880	**-0.26109**	5.9	10.3	42.8
Neutrals							
He	-0.041560	-0.041925	-0.065821	**-0.042044**	1.2	0.3	56.6
Li	-0.050302	-0.050877	-0.078798	**-0.04533**	11.0	12.2	73.8
Be	-0.092596	-0.094840	-0.125958	**-0.09434**	1.8	0.5	33.5
B	-0.128190	-0.132305	-0.166631	**-0.12485**	2.7	6.0	33.5
C	-0.160596	-0.166654	-0.205565	**-0.15640**	2.7	6.6	31.4
N	-0.188301	-0.196106	-0.241497	**-0.18831**	0.0	4.1	28.3
O	-0.261061	-0.271775	-0.342863	**-0.25794**	1.2	5.4	32.9
F	-0.321662	-0.334827	-0.431658	**-0.32453**	0.9	3.2	33.0
Ne	-0.375313	-0.390819	-0.511537	**-0.39047**	3.9	0.1	31.0
Average % Error					**6.3**	**6.7**	**35.7**

The results summarised in **Table 7.19** suggest that the optimum fitting constants for the helium atom give more accurate correlation energies for the atomic anions in comparison with the exact or experimental estimates except for the hydride ion as indicated by the percent errors. The CS

constants are found to give better correlation energies for the cationic and neutral atomic systems except for B^+, He, Be and Ne for which the computed constants for helium outperforms the results of CS. This suggests that long range, low density behaviour which is characteristic of anionic systems (due to their diffuse densities) is likely accounted for by the CS model, especially through our computed fitting constants for the helium atom. Moscardó et al.,[389] had earlier asserted that the correlation factor proposed by CS was very good for modelling electron correlation in atoms. Therefore, the CS results for neutral systems is expected. Moscardó[390] also suggested that contrary to previous assertions by Tao et al.,[385] the CS formalism was able to semi-quantitatively reproduce the properties of the UEG. He went on to state that the requirement for this outcome was the choice of the parameter, q, entering the CS wavefunction. The optimised parameters/constants employed in computing correlation energies of the anionic systems in this work are likely in agreement with this assertion, i.e, varying q improved the results slightly.

In summary, the accuracy of the computed constants from fitting to accurate helium atom HF densities do not improve on the constants computed by CS as reflected in the average % errors in **Table 7.19**. The fitting to the hydride ion data does not improve the accuracy of the computed correlation energies for non-hydride systems, including other anionic systems.

7.4 Conclusions

The Colle and Salvetti (CS)[26] correlation formula has been re-parameterised using the least squares fitting procedure in combination with an accurately computed 25-term Laguerre-based Hartree-Fock (HF) wavefunction for the helium atom or hydride ion. The helium fitting was to test if the quality of the wavefunction used in the fitting procedure improved the resulting correlation energies. The fitting to the hydride wavefunction, which has not been tried previously, was an attempt to account for long range correlation asserted[362,385] to be missing in the model. It is found from detailed determination and analysis of the fitting parameters that the optimum parameters computed from fitting to the helium atom densities are $a = 0.01628$, $b = 0.18438$, $c = 0.57594$ and $d = 0.80562$. These values are found to be similar to those computed by CS and that they arise from a low tolerance fit to the 'exact' data. The constants are found to offer slightly greater accuracy than those of the CS for correlation energies of atomic anions using a form of the Lee-Yang-Parr (LYP)[27] density correlation functional. Nevertheless, the CS constants give better correlation energies for most neutral and atomic cations. In computing correlation energies for the atomic systems using a form of the LYP density functional, the Koga et al.,[401] HF wavefunctions for atomic systems are employed to form the HF densities of the respective system. The optimum constants computed from fitting to the hydride ion densities are; $a = 0.02578$, $b = 0.10943$, $c =$

1.49357 and $d = 1.22388$. The result of computation of correlation energies using these derived constants in the implemented form of the LYP density functional in combination with Koga et al.,[401] HF wavefunctions for atomic systems suggests that they are only accurate for the hydride ion. As such, it may be reckoned that long range correlation is accounted for by the optimum constants from fitting to helium atom densities as they lead to accurate correlation energies for atomic anions. The results reveal that to obtain optimum fitting constants from fitting to helium HF densities that give good correlation energies, guess values in the neighbourhood of the CS constants, boundary constraints and low tolerance are required. This is because it is found that all guess values outside the neighbourhood of the CS constants lead to inaccurate optimised constants and by extension, correlation energies. For the fitting to hydride HF densities, the boundary constraints are not required and the fit must be tight. In addition, the results reveal that fitting to the hydride ion does not improve the correlation energies of non-hydride systems, including anions. Finally, it is found that the plot of the $H(\beta, W)$ function against nucleus-electron distance, R follows a similar decay pattern as the plot of intracule densities against inter-electronic distance for helium atom and hydride ion, respectively.

8 Summary of thesis and concluding remarks

It has been the focus of this thesis to use computational quantum chemistry methodologies to elucidate the structure, stability and reactivity of some inorganic complexes and electron correlation in atomic systems. To do this, density functional theory (DFT) and/or coupled cluster (CCSD(T)) theory, the quantum theory of atoms in molecules (QTAIM) and/or the polarisable continuum model (PCM) were employed.

The theoretical background and mathematical basis of the chemistry used or described in this thesis is summarised in **Chapter 2**. Here, the principles or approximations behind the computational quantum chemistry methodologies employed to investigate the chemistry covered in this thesis are discussed. In **Chapter 3**, the theoretical investigation of the structure and reaction mechanisms of the unsymmetrical SCN pincer palladacycle for the formation of Pd(0), using already validated[28] DFT methodology, QTAIM and PCM is presented. Analysis of the energy profiles of the elucidated reaction mechanisms reveals that Pd(0) formation from pincer palladacycles involve four main steps namely: a transmetallation step (TM), two de-coordination steps and a reductive elimination step (RE) with TM and RE as the key steps. The results also suggest that the process requires a base to occur. The results were used to rationalise the catalytic activity observed experimentally[29] for Suzuki-Miyaura carbon-carbon (C-C) cross-coupling reactions and the findings were published in the Journal of Organometallic Chemistry.[11] **Chapter 4** summarises the determination of a suitable and/or reliable computational methodology for the calculation of the geometry, vibrational frequencies and energies of sulfur clusters (S_n) and hydrogen polysulfanes ($HS_{n+1}H$). The determined methodology, CCSD(T)/aug-cc-pVTZ//ωB97XD/6-311++G(2df,2p) and QTAIM are used to investigate the electronic structure and stability of cyclic and open chain S_n ($n \leq 5$ and 8) (**Chapter 5**) and the reactivity of stable open chains of sulfur clusters with hydrogen sulfide (H_2S) (**Chapter 6**). This methodology is determined by analysing the performance of different DFT methods and CCSD(T) in combination with different basis sets in reproducing the experimental

geometry, vibrational frequencies and energies of sulfur species in comparison with multi-configurational (complete active space) self-consistent field (CASSCF) calculations. In addition, the suitability and/or reliability of the methodology, a single-reference methodology, is ascertained via the $\mathcal{T}_1$ Diagnostic test[54] of Lee and Taylor. In **Chapter 5**, it is found that all S_n, $n \leq 4$ have open chain ground state structures while S_n, $n = 5$ and 8 have cyclic ground state structures with S_5 as the first allotrope of sulfur to form a cyclic ground state structure. Allotropes of sulfur with singlet state, cyclic global minimum structures (S_5 and S_8) are found to possess a more stable triplet state open chain structure even though their ring opening reactions occur on the singlet PES. This suggests that triplet state open chain structures of sulfur may be thermally accessed via higher energy singlet state open chain structures via favourable spin flip or inter-system crossing. This finding provides an explanation for the experimentally observed paramagnetism[288] of liquid sulfur. Furthermore, some of the sulfur allotropes possess open chain isomers with singlet and triplet spin state having similar structures that are thermally accessible from one another. Also, open chain structures of S, S_2, S_5 and S_8 are computed to have triplet spin ground states while open chain structures of S_3 and S_4 are found to have singlet spin ground states. The open chains of S_n are found to be a key factor in liquid and/or gaseous sulfur reactions/phenomena in the absence (viscosity/paramagnetism) and presence ($HS_{n+1}H$ formation) of H_2S. The existence of some of the open chains in the singlet and triplet state and the fact that a switch in relative stability of the open chains of S_n occurs at S_3 and S_4 is indicative of the involvement of spin state interplay in sulfur systems.

In **Chapter 6**, the mechanisms for formation of $HS_{n+1}H$ from the reaction of open chains of sulfur and singlet H_2S are summarised. It is found that thermodynamically stable branched and unbranched $HS_{n+1}H$ are only formed on the singlet PES with the unbranched $HS_{n+1}H$ found to be more stable. The thermodynamically more stable unbranched $HS_{n+1}H$ are either formed directly or indirectly from the reactants depending on the sise of n. Indirect formation of unbranched $HS_{n+1}H$ is found to involve the prior formation of the branched analogue. In all cases, the thermodynamically stable unbranched $HS_{n+1}H$ formed in the reaction of S_n with H_2S on the singlet PES are generated via curve crossing (except for the reaction of S_4 with H_2S) in exergonic processes. The products of reaction on the triplet PES are found to be weakly attracted species and are always formed in an endergonic process. The reverse of the triplet PES is found to be exergonic while that of the singlet PES is endergonic. The instability of the triplet PES is found to provide a mechanism for the persistence of H_2S in sulfur recovered in the thermal Claus process. A manuscript describing the results in **Chapter 5** and **6** is in preparation. **Chapter 7** describes the systematic re-determination of the fitting parameters in the Colle and Salvetti (CS) correlation

formula[26] using accurately computed Laguerre-based HF wavefunction for He and H^-. The determined new fitting parameters are employed in a form of the Lee-Yang-Parr (LYP) density correlation functional[27] to compute the correlation energies of several atomic systems in an in-house code. This is an attempt to explicitly capture the long-range correlation behaviour in H^- via the new fitting parameters in order to improve the accuracy of the functional in computing the electron correlation energies of systems. Analysis of the results in this chapter suggests that accurate fitting of the CS formula to the data obtained using the computed Laguerre-based He wavefunction over a fairly large radial extent does not give good fitting parameters for the accurate computation of correlation energies of systems other than He. Nevertheless, it is found that a relaxed fitting to the data obtained using the computed Laguerre-based He wavefunction over a short radial extent gives reasonably accurate correlation energies for all atomic systems investigated even though the accuracy of the CS results is not improved in general. Furthermore, it was found that fitting to the data obtained using the computed Laguerre-based H^- wavefunction only lead to accurate electron correlation energy for H^- and does not improve the accuracy of the CS formula or the LYP functional. A manuscript describing the results in **Chapter 7** has been submitted.

Appendices

Appendix A.1

Additional structural data for PdSCN (1) and S_5

Table A.1.1. Some experimental[29] and optimised (calculated) dihedral angles of **PdSCN**.

Dihedral Angle	Value / Å		
	Expt.	**PBE**	***ω*B97XD**
C3-C2-C1-Pd28	173(2)	-177.3	176.8
C20-C2-C1-Pd28	-9(4)	5.1	-5.2
C5-C6-C1-C2	1(4)	-1.4	0.2
C10-C6-C1-C2	-176(3)	177.8	179.7
C5-C6-C1-Pd28	-177(2)	178.2	-177.2
C10-C6-C1-Pd28	6(3)	-2.5	2.4
C1-C2-C20-S23	20(4)	-19.3	9.2
C3-C2-C20-S23	-162(2)	163.2	-172.9
C16-C15-N12-Pd28	178(3)	178.3	-178.9
C11-C10-N12-Pd28	-179.1(19)	-178.4	179.0
C6-C10-N12-Pd28	0(4)	2.0	-0.9
C2-C20-S23-C24	85(3)	133.2	96.0
C2-C20-S23-Pd28	-20(3)	21.9	-8.2

The dihedral angles involving the -SMe group in the Pd-L environment together with the bond lengths and angles in **Table 3.3** (Section **3.3.1**) suggest that both approaches give values of the key structural parameters comparable to their experimentally[29] determined values.

Table A.1.2. Calculated bond angles (θ) and dihedral angles (τ) of the structures of S_5 (**5b** and **5c**) compared to literature values at the HF/3-21G*[37] level of theory. Also included in this table are the calculated θ and τ of the remaining structures of S_5 (**5d**-**5g**, **Figure 5.5** in Section **5.3.1.4**).

Structure	Parameter	Value/°	
		This work	Ref. [37]
5b	θ(1S-2S-3S)	109.9	107.7
	θ(2S-3S-4S)	103.4	104.6
	τ(1S-2S-3S-4S)	75.2	81.6
5c	θ(1S-2S-3S)	107.8	108.0
	θ(2S-3S-4S)	102.0	104.7
	θ(3S-4S-5S)	108.0	107.8
	τ(1S-2S-3S-4S)	0.0	
	τ(2S-3S-4S-5S)	180.0	
5d	θ(1S-2S-3S)	113.9	
	θ(2S-3S-4S)	68.1	
	τ(1S-2S-3S-4S)	106.5	
5e	θ(1S-2S-3S)	82.3	
	θ(2S-1S-4S)	82.7	
	θ(2S-1S-5S)	112.3	
	θ(2S-3S-4S)	88.4	
	τ(1S-2S-3S-4S)	-37.0	
	τ(2S-1S-4S-3S)	-35.1	
	τ(5S-1S-2S-3S)	146.2	
5f	θ(1S-3S-4S)	111.5	
	θ(3S-4S-5S)	111.1	
	τ(4S-2S-3S-1S)	103.3	
	τ(2S-3S-4S-5S)	32.9	
5g	θ(1S-3S-4S)	104.7	
	θ(3S-4S-5S)	104.4	
	τ(4S-2S-3S-1S)	104.6	
	τ(2S-3S-4S-5S)	45.7	

The additional structural data (the bond and dihedral angles of **5b**-**5g**) in **Table A.1.2** is presented to support the discussion in Section **5.3.1.4**.

Appendix A.2

Singlet state reaction mechanisms for $S_n + H_2S$ ($n \leq 5$ and 8) reactions

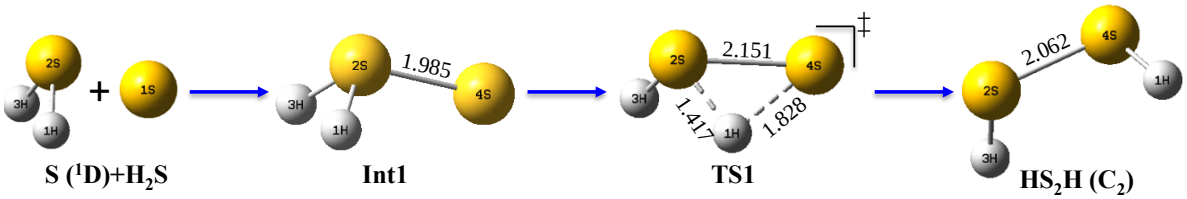

S (^{1}D)+H_2S **Int1** **TS1** **HS_2H (C_2)**

Scheme A.2.1. Reaction mechanism for the singlet $S + H_2S$ reaction.

All the given bond distances in Appendix I are in angstrom (Å) and are greater than 2.060 Å for the *r*(S-S) a 1.342 Å for the *r*(S-H). The same is true for all the given bond distances in **Appendix A.3**.

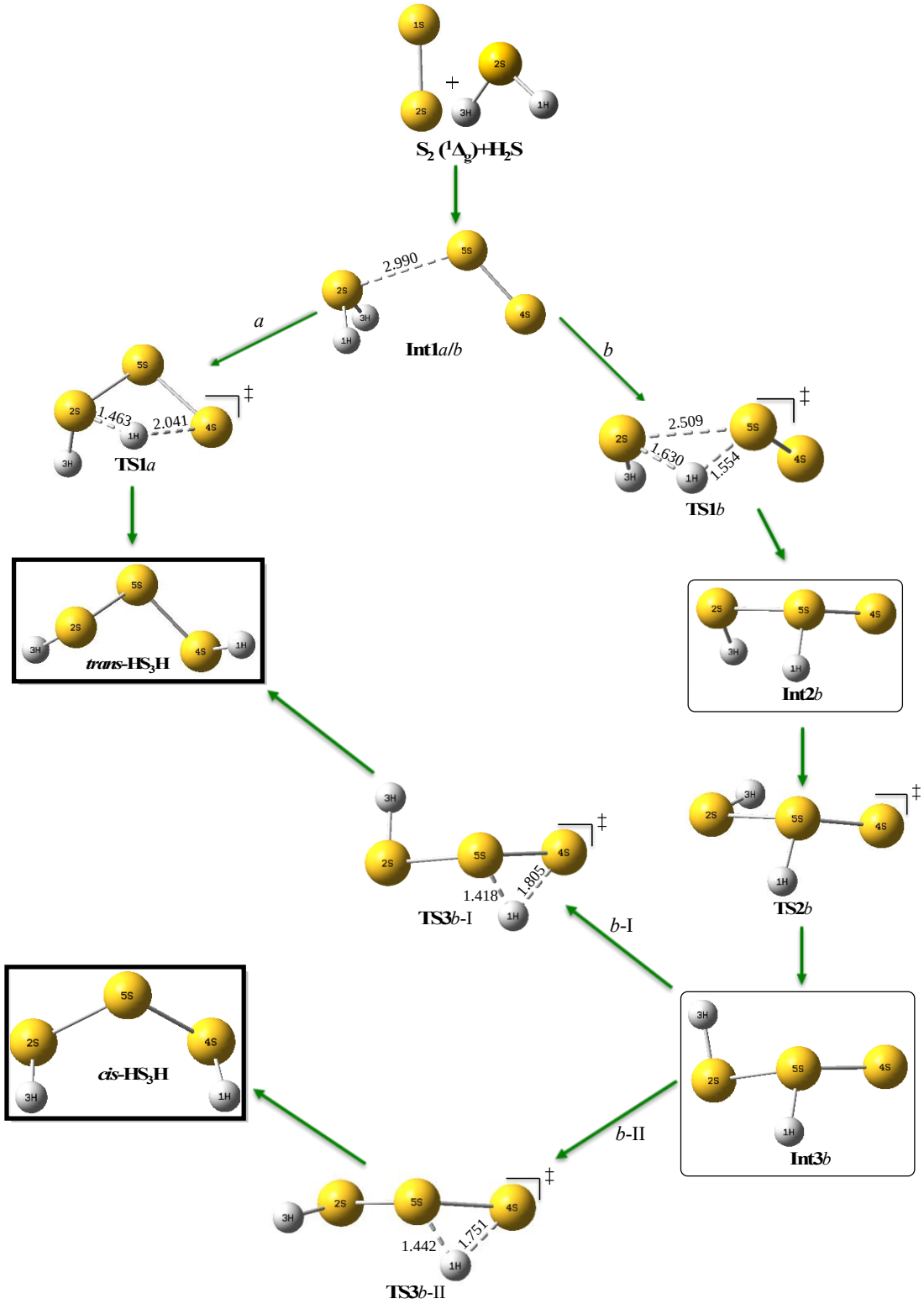

Scheme A.2.2. Reaction mechanism for the singlet $S_2 + H_2S$ reaction. **Int2*b*** and **Int3*b*** are labelled as **Int2′** and **Int2″** in the text for this reaction. Also, **TS2*b*** is labelled as **TS2** while **TS3*b*-I** and **TS3*b*-II** are collectively labelled as TS**1′** in the text for this reaction.

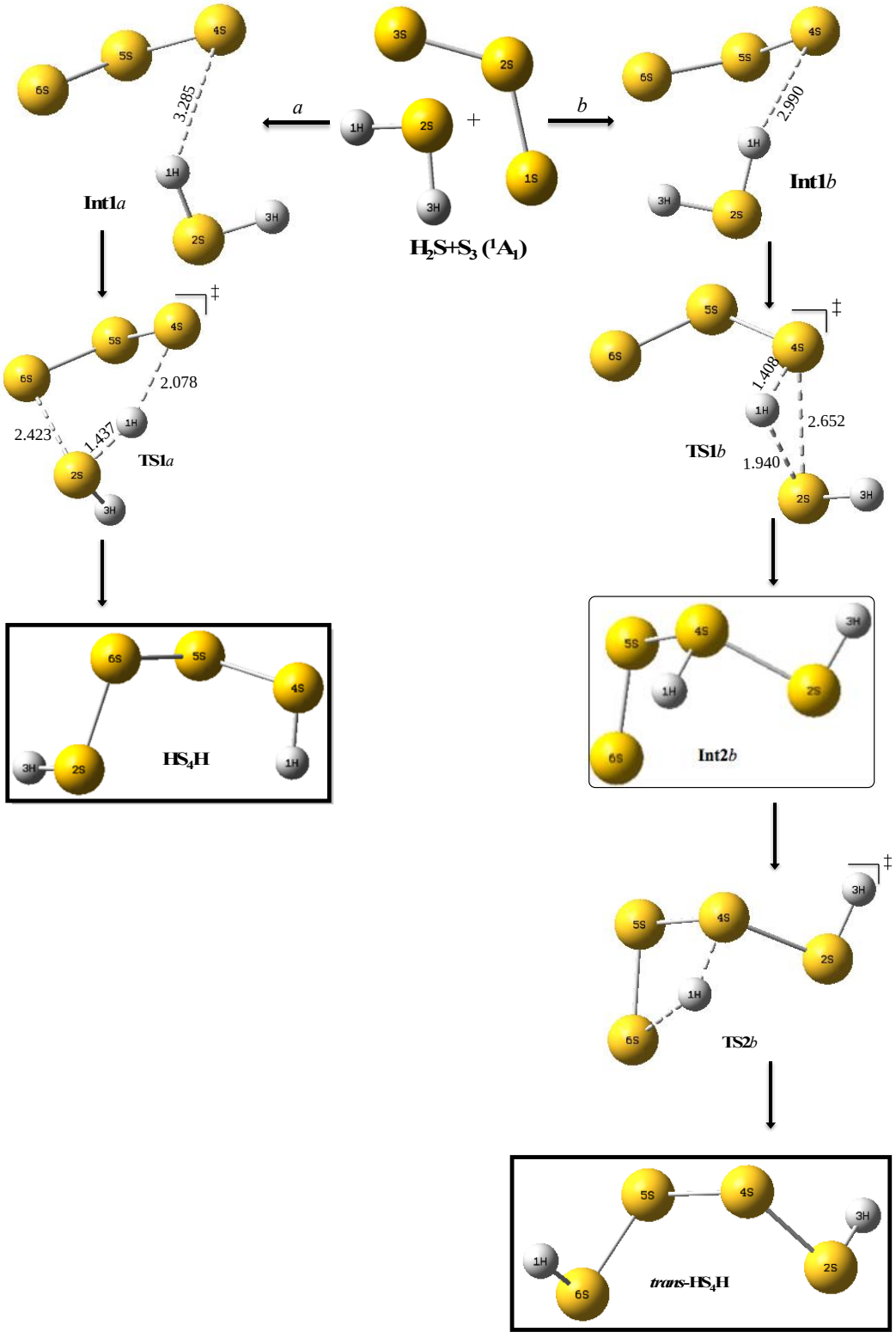

Scheme A.2.3. Reaction mechanism for the singlet $S_3 + H_2S$ reaction. **Int1*a*** and **Int1*b*** are collectively labelled as **Int1** while **Int2*b*** is labelled as **Int2′′** in the text for the S_3-H_2S reaction. Also, **TS2*b*** is labelled as **TS1′** in the text for this reaction.

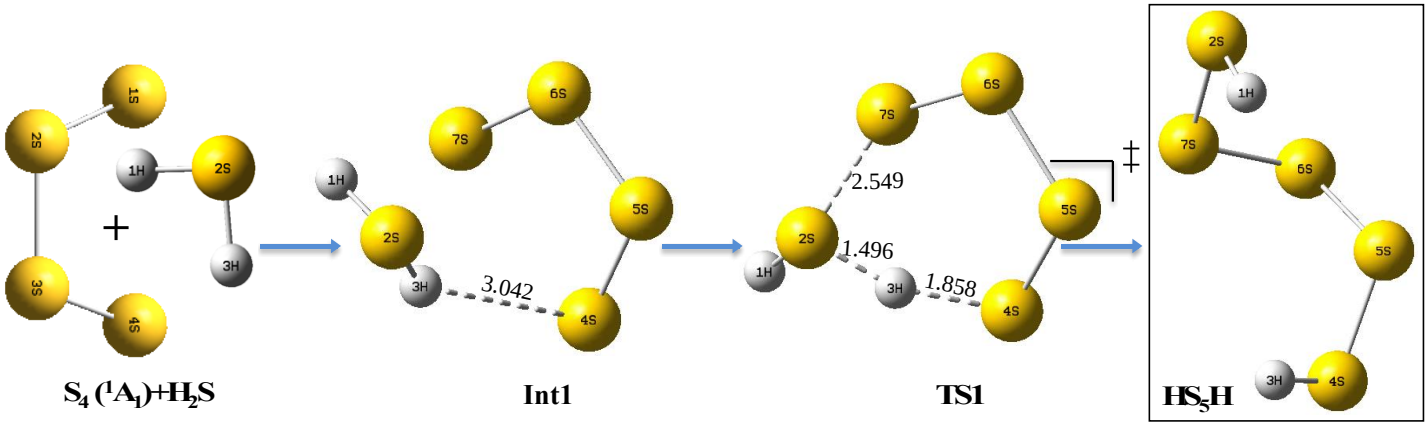

Scheme A.2.4. Reaction mechanism for the singlet $S_4 + H_2S$ reaction.

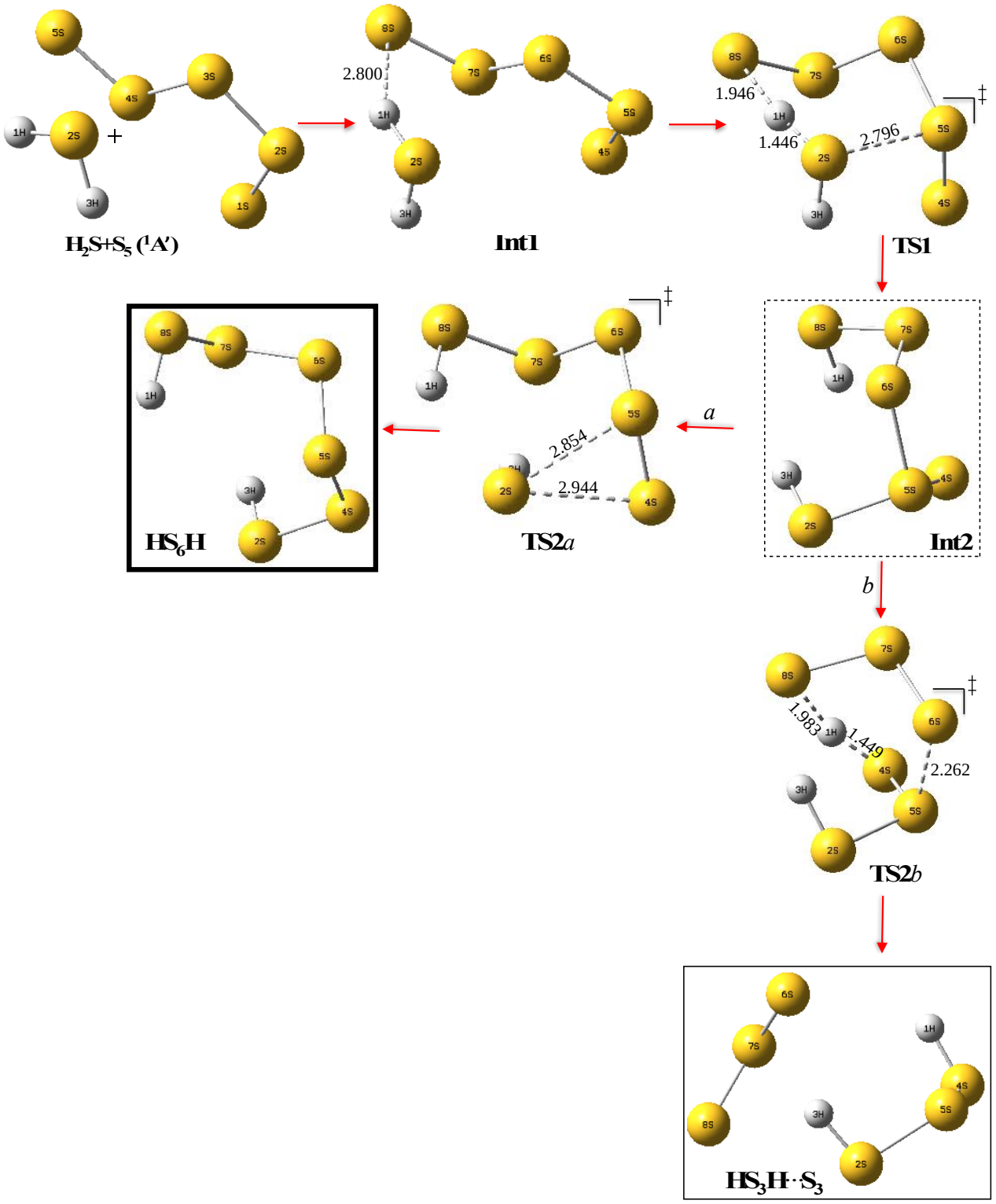

Scheme A.2.5. Reaction mechanism for the singlet $S_5 + H_2S$ reaction. **TS2*a*** and **TS2*b*** are collectively labelled as **TS2** while **Int2** is labelled as **Branched $HS_{n+1}H$** in the text for this reaction.

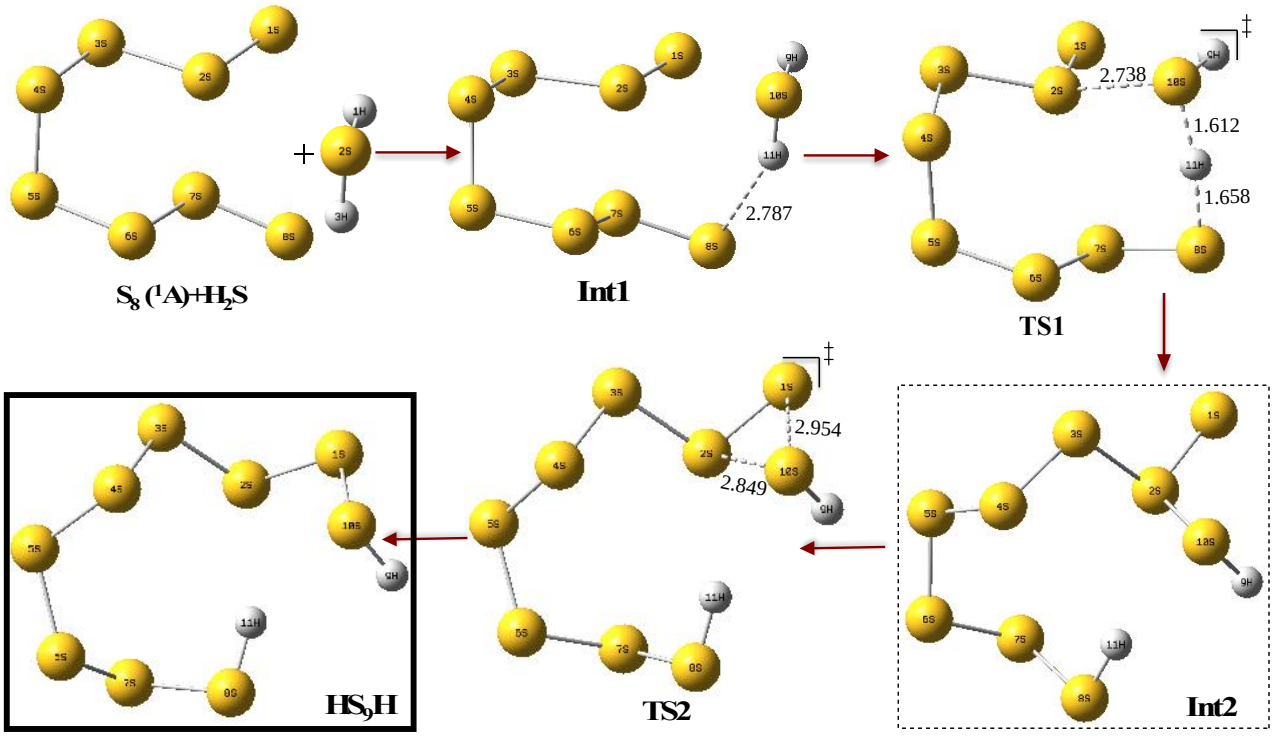

Scheme A.2.6. Reaction mechanism for the singlet $S_8 + H_2S$ reaction. **Int2** is labelled as **Branched $HS_{n+1}H$** in the text for this reaction.

Appendix A.3

Triplet state reaction mechanisms for $S_n + H_2S$ ($n \leq 5$ and 8) reactions

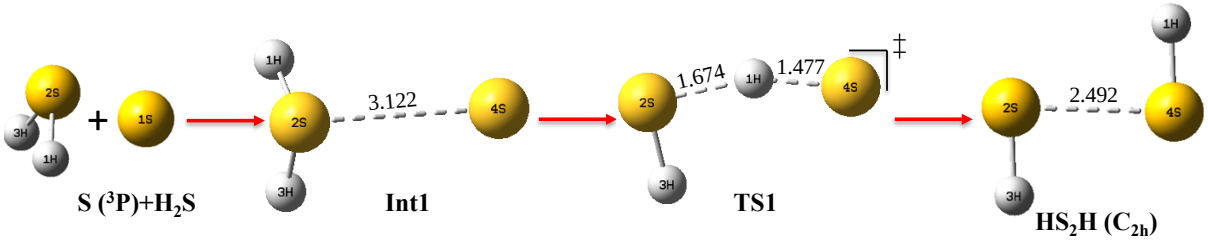

Scheme A.3.1. Reaction mechanism for the triplet $S + H_2S$ reaction.

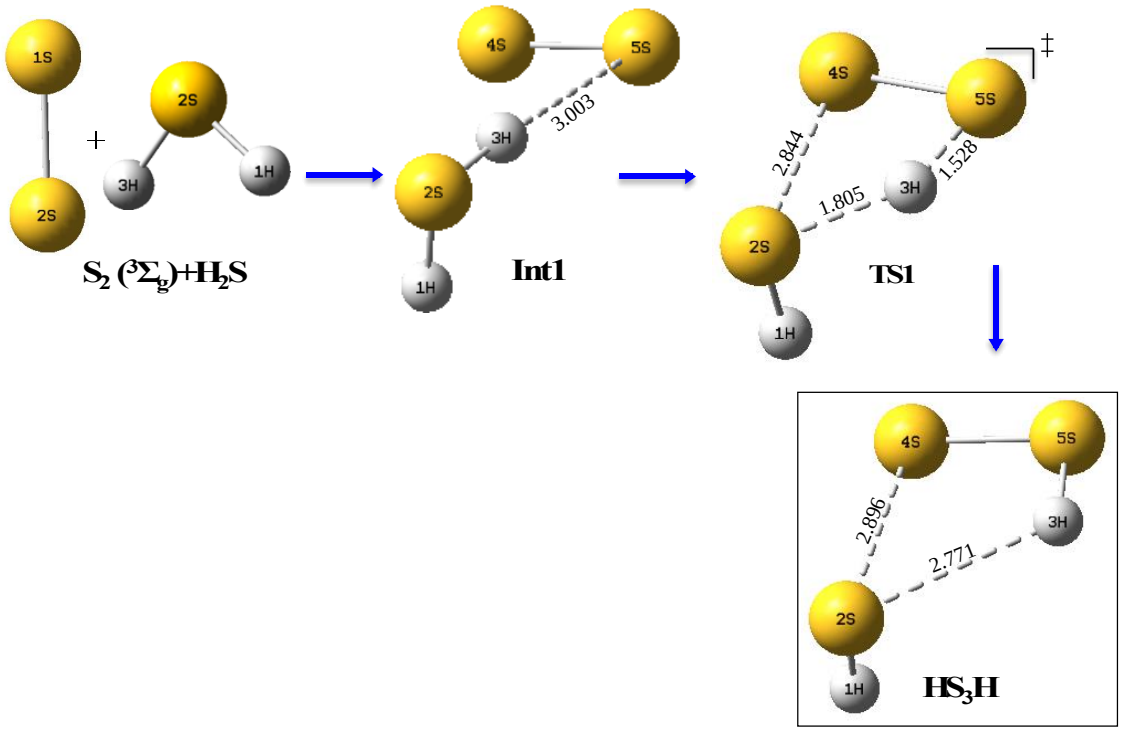

Scheme A.3.2. Reaction mechanism for the triplet $S_2 + H_2S$ reaction.

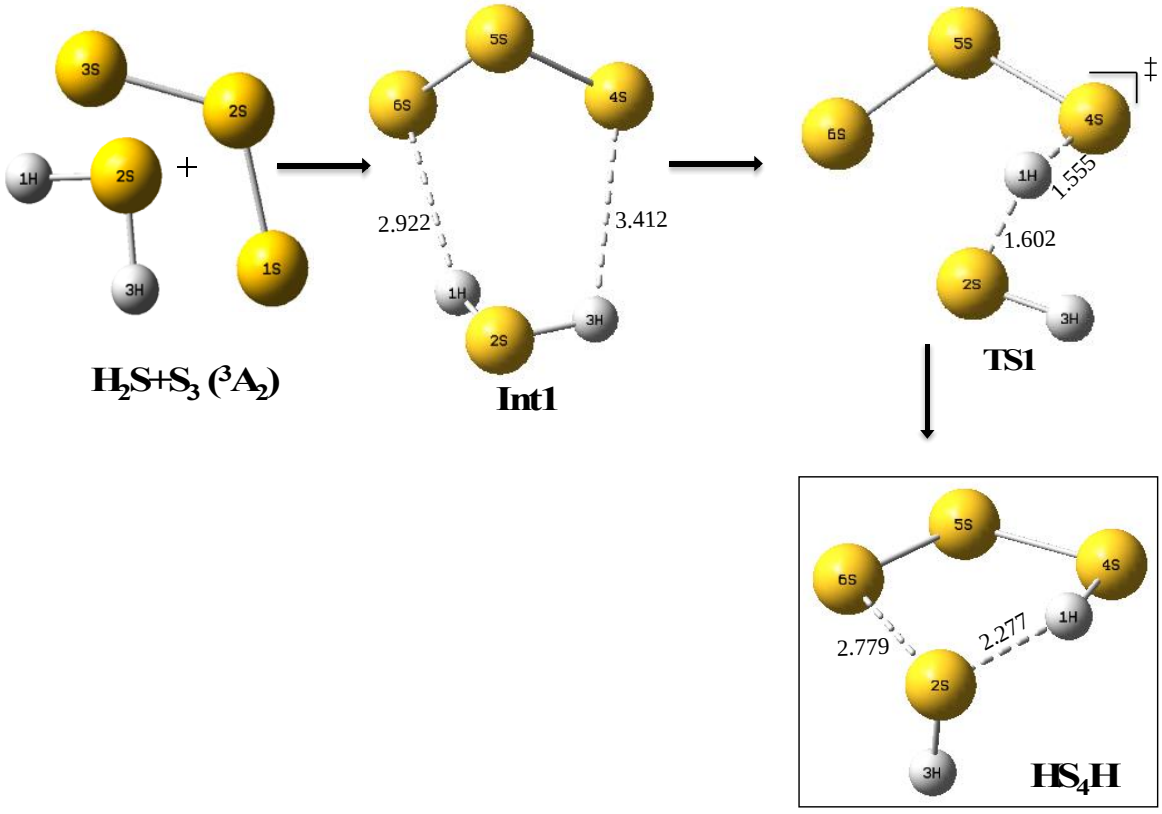

Scheme A.3.3. Reaction mechanism for the triplet $S_3 + H_2S$ reaction.

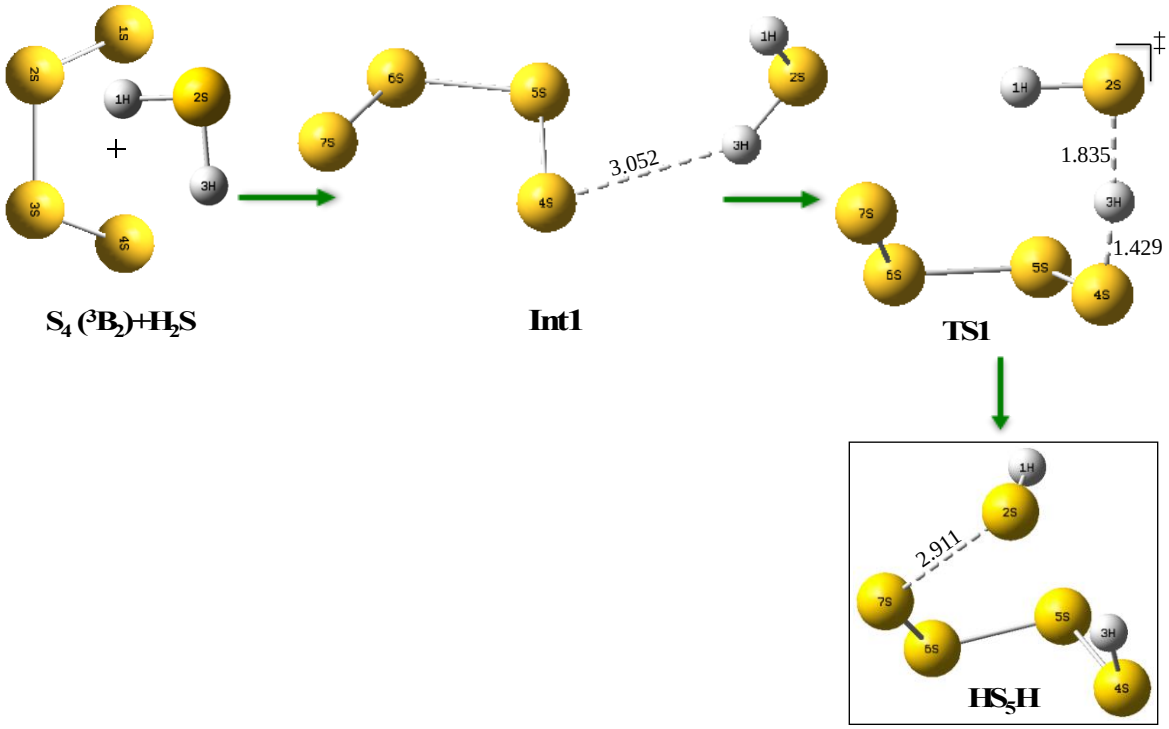

Scheme A.3.4. Reaction mechanism for the triplet $S_4 + H_2S$ reaction.

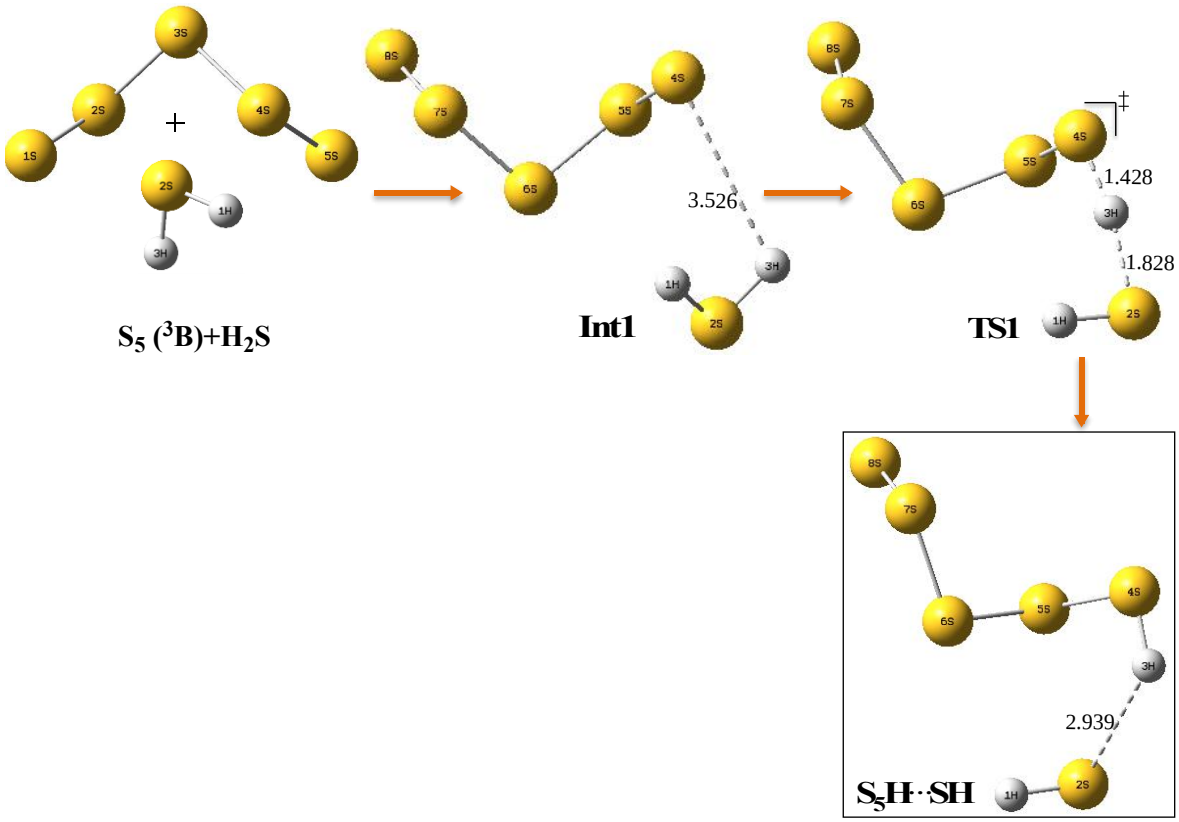

Scheme A.3.5. Reaction mechanism for the triplet $S_5 + H_2S$ reaction.

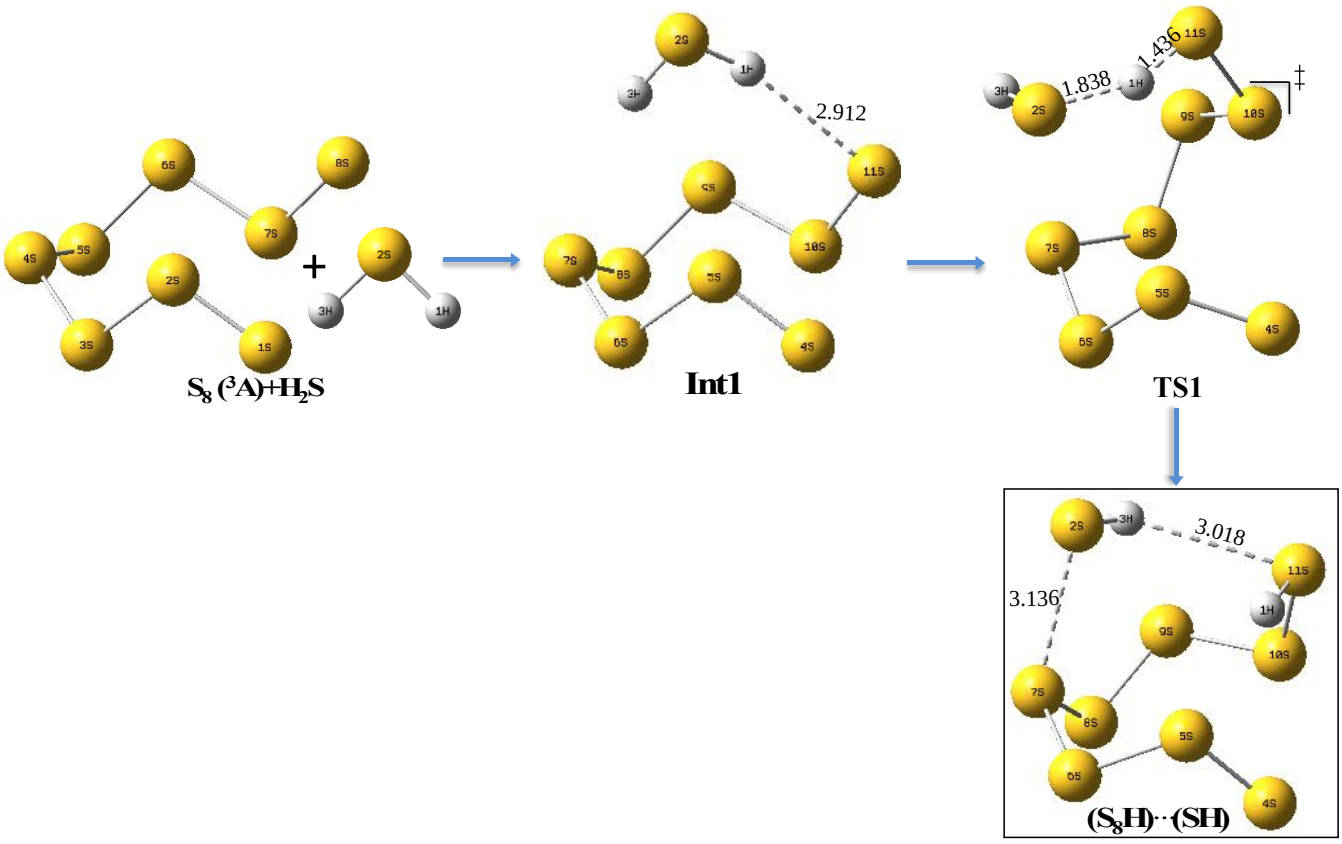

Scheme A.3.6. Reaction mechanism for the triplet $S_8 + H_2S$ reaction.

Appendix A.4

Optimised constants for fitting to helium atom and hydride ion with corresponding correlation energies for some closed-shell systems

This Appendix summarises further details of the results of fitting constants/parameters optimisation for the helium atom and the hydride ion to support the discussion in **7.3.6** and **7.3.5**. In each case, the corresponding correlation energies computed for each set of optimised constants using the implemented form of LYP correlation energy functional and the Koga et al.,[401] HF wavefunctions are tabulated. In addition, the calculated exact[16] and fixed nucleus non-relativistic experimentally estimated[423,424] correlation energies of the respective system are compared with the computed values to determine the accuracy of the computed values..

The constants optimised with the scipy.optimise least_squares method while varying R_i and R_f simultaneously using a total of 80 points, $q = 2.29$, a tolerance of 10^{-6}, the computed Laguerre-based HF wavefunction for the helium atom and boundary constraints are summarised in **Table A.4.1**.

On the overall, the results summarised in **Table A.4.1** suggests that extending the range of R does not improve the accuracy of the optimised fitting constants as the accuracy of the correlation energies corresponding to the constants are not improved.

Table A.4.1. Effect of increasing the range of R by varying both ends of R on fitting constants (a, b, c, d) optimised for the helium atom using the scipy.optimise least_squares method without boundary restrictions. Correlation energies in green are exact values[16] while those in blue are experimentally estimated.[423,424]

R_i	R_f	A	b	c	d	E_c / a.u.					
		0.08	0.16	0.58	0.8	H^-	He	Li^+	Be	B^+	Ne
						-0.039821	-0.042044	-0.043498	-0.09434	-0.11134	-0.39047
0.3	2	0.01628	0.18438	0.57594	0.80562	-0.031406	-0.041937	-0.043850	-0.094865	-0.108785	-0.390922
0.25	3	0.01556	0.17545	0.57680	0.80377	-0.030354	-0.040969	-0.043185	-0.091634	-0.104922	-0.372963
0.2	4	0.01500	0.17116	0.57700	0.80363	-0.029403	-0.039893	-0.042211	-0.088760	-0.101562	-0.359186
0.15	5	0.01510	0.17200	0.57759	0.80303	-0.029595	-0.040108	-0.042404	-0.089313	-0.102205	-0.361780
0.1	6	0.01520	0.17197	0.57767	0.80293	-0.029788	-0.040370	-0.042682	-0.089892	-0.102866	-0.364101
0.05	7	0.01534	0.17215	0.57771	0.80287	-0.030068	-0.040740	-0.043066	-0.090735	-0.103833	-0.367600
0.0	8	0.01552	0.17244	0.57772	0.80285	-0.030398	-0.041173	-0.043512	-0.091730	-0.104976	-0.371769
-0.05	9	0.01550	0.17204	0.57772	0.80286	-0.030374	-0.041160	-0.043513	-0.091657	-0.104887	-0.371279
-0.1	10	0.01123	0.01572	0.58673	0.80156	-0.025772	-0.040592	-0.047283	-0.077864	-0.087267	-0.259290
CS[26]		0.01565	0.173	0.58	0.8		-0.0416	-0.0438	-0.0926	-0.106	-0.374

A summary of the fitting constants for fitting to the hydride ion density computed with the scipy.optimise least_squares method without boundary constraints by varying R_f to increase the range of R while keeping $R_i = 0.3$ a.u., using a total of 80 points, a tolerance of 10^{-6} and the computed 25-term Laguerre-based HF wavefunction for H^- is presented in **Table A.4.2**.

The results in this table suggest that extending the range of R improves the accuracy of the attendant optimised constants as can be seen in the corresponding correlation energy for the hydride ion. Here, the best range of R is found to be $0.3 \leq R \leq 6$ a.u.

Table A.4.2. Effect of variation of R_f on fitting constants (a, b, c, d) from fitting to the hydride ion densities optimised using the scipy.optimise least_squares method, $q = 1.93985$ a.u., tolerance of 10^{-6} and a total of 80 points. Guess constants are in **bold**. Correlation energies in green are exact values[16] while those in blue are experimentally estimated.[423,424]

R_i	R_f	**a**	**b**	**c**	**d**	E_c / a.u.					
		0.01	**0.17**	**0.58**	**0.8**	**H^-**	**He**	**Li^+**	**Be**	**B^+**	**Ne**
						-0.039821	**-0.042044**	**-0.043498**	**-0.09434**	**-0.11134**	**-0.39047**
0.3	2	0.02424	0.05184	0.57460	1.06007	-0.040209	-0.066294	-0.078578	-0.133492	-0.153613	-0.501289
0.3	3	0.02461	0.05362	0.58029	1.08324	-0.040169	-0.066383	-0.078761	-0.133924	-0.154308	-0.505756
0.3	4	0.02630	0.06123	0.59008	1.18516	-0.040034	-0.066763	-0.079528	-0.135959	-0.157502	-0.526082
0.3	5	0.02883	0.07130	0.59728	1.33458	-0.039891	-0.067275	-0.080555	-0.138818	-0.161975	-0.555062
0.3	6	0.02925	0.13114	1.28975	1.42111	-0.039803	-0.065678	-0.075961	-0.127950	-0.150048	-0.554385
0.3	7	0.03333	0.14971	1.23090	1.66994	-0.039688	-0.065941	-0.076250	-0.130047	-0.154109	-0.596372
0.3	8	0.03879	0.16459	1.15815	1.99770	-0.039579	-0.066351	-0.076951	-0.133174	-0.159603	-0.646177

The computed fitting constants for fitting to the hydride ion density employing the scipy.optimise least_squares method without boundary constraints by varying R_i to increase the range of R while keeping $R_f = 2$ a.u., a total of 80 points and a tolerance of 10^{-6} is presented in **Table A.4.3**. This optimisation employs the computed 25-term Laguerre-based HF wavefunction for the hydride ion was employed.

The results in **Table A.4.3** suggest that extending the range of R by decreasing R_i in steps of 0.05 a.u. from 0.3 a.u. does not improve the accuracy of the attendant optimised constants in general as can be seen in the corresponding correlation energy for the hydride ion.

Table A.4.3. Effect of variation of R_i on fitting constants (a, b, c, d) from fitting to the hydride ion densities optimised using the scipy.optimise least_squares method, $q = 1.93985$ a.u., tolerance of 10^{-6} and a total of 80 points. Guess constants are in **bold**. Correlation energies in green are exact values[16] while those in blue are experimentally estimated.[423,424]

R_i	R_f	a	b	c	d	E_c / a.u.					
		0.01	**0.17**	**0.58**	**0.8**	**H^-**	**He**	**Li^+**	**Be**	**B^+**	**Ne**
						-0.039821	**-0.042044**	**-0.043498**	**-0.09434**	**-0.11134**	**-0.39047**
0.3	2	0.02424	0.05184	0.57460	1.06007	-0.040209	-0.066294	-0.078578	-0.133492	-0.153613	-0.501289
0.25	2	0.02428	0.05204	0.57222	1.06221	-0.040206	-0.066298	-0.078590	-0.133567	-0.153720	-0.501903
0.2	2	0.02411	0.05104	0.57120	1.05230	-0.040219	-0.066270	-0.078536	-0.133355	-0.153383	-0.499661
0.15	2	0.02357	0.04826	0.57318	1.02097	-0.040260	-0.066151	-0.078300	-0.132602	-0.152235	-0.492584
0.1	2	0.02239	0.04274	0.58064	0.95110	-0.040368	-0.065806	-0.077617	-0.130833	-0.149587	-0.477210
0.05	2	0.01999	0.03238	0.59655	0.80192	-0.040687	-0.064821	-0.075676	-0.126876	-0.143732	-0.445531
0.0	2	0.01629	0.01408	0.60613	0.56524	-0.041394	-0.062666	-0.071652	-0.119815	-0.133318	-0.392320

The results of optimisation of constants within $0.1 \leq R \leq 6$ a.u. (the optimum range, **Table 7.18**) using a total of 80 points, $q = 1.93985$, $10^{-2} \leq \text{tolerance} \leq 10^{-10}$ and the computed Laguerre-based HF wavefunction for hydride ion without boundary constraints are summarised in **Table A.4.4**.

The result in **Table A.4.4** also indicates that increasing or decreasing the tolerance for the optimisation in the optimum range of R does not improve the accuracy of the attendant optimised fitting constants.

Table A.4.4. Effect of variation of tolerance within $0.1 \leq R \leq 6$ a.u. on fitting constants (a, b, c, d) optimised using the scipy.optimise least_squares method without boundary constraints, $q = 1.93985$ a.u. and a total of 80 points. Guess values are in **bold**. Correlation energies in green are exact values[16] while those in blue are experimentally estimated.[423,424]

Tolerance	a	b	c	d	E_c / a.u.					
					H^-	He	Li^+	Be	B^+	Ne
	0.01	**0.17**	**0.58**	**0.8**	**-0.039821**	**-0.042044**	**-0.043498**	**-0.09434**	**-0.11134**	**-0.39047**
1×10^{-2}	0.02333	0.16971	0.58007	0.79990	-0.040072	-0.052255	-0.052825	-0.120571	-0.140763	-0.543684
1×10^{-3}	0.01996	0.04307	0.59587	0.80867	-0.039924	-0.062951	-0.073012	-0.124411	-0.141269	-0.445273
1×10^{-4}	0.01938	0.02080	0.59860	0.81029	-0.039687	-0.064162	-0.075554	-0.124397	-0.140693	-0.428967
1×10^{-5}	0.02764	0.05750	0.60296	1.29472	-0.039766	-0.067794	-0.081754	-0.138033	-0.160369	-0.535711
1×10^{-6}	0.02578	0.10943	1.49357	1.22388	-0.039825	-0.065826	-0.076525	-0.125969	-0.145885	-0.511579
1×10^{-7}	0.02577	0.10959	1.49643	1.22339	-0.039824	-0.065820	-0.076510	-0.125933	-0.145837	-0.511459
1×10^{-8}	0.02577	0.10959	1.49643	1.22339	-0.039824	-0.065820	-0.076510	-0.125933	-0.145837	-0.511459
1×10^{-9}	0.02577	0.10959	1.49644	1.22339	-0.039824	-0.065820	-0.076510	-0.125933	-0.145837	-0.511459
1×10^{-10}	0.02577	0.10959	1.49644	1.22339	-0.039824	-0.065820	-0.076510	-0.125933	-0.145837	-0.511459

References

[1] A. Ferretti, *Coord. Chem. Rev.* **2003**, *238–239*, 127–141.

[2] H. C. Tai, C. Lim, *J. Phys. Chem. A* **2006**, *110*, 452–462.

[3] J. G. Hill, G. Bucher, *J. Phys. Chem. A* **2014**, *118*, 2332–2343.

[4] M. G. Ferrier, E. R. Batista, J. M. Berg, E. R. Birnbaum, J. N. Cross, J. W. Engle, H. S. La Pierre, S. A. Kozimor, J. S. Lezama Pacheco, B. W. Stein, S. C. E. Stieber, J. J. Wilson, *Nat. Commun.* **2016**, *7*, 12312.

[5] W. T. Borden, R. Hoffmann, T. Stuyver, B. Chen, *J. Am. Chem. Soc.* **2017**, *139*, 9010–9018.

[6] T. K. Bijoy, A. Palaniappan, P. Murugan, *Appl. Surf. Sci.* **2017**, *418*, 275–279.

[7] A. Fabara, S. Cuesta, F. Pilaquinga, L. Meneses, *J. Nanotechnol.* **2018**, *2018*, 1–9.

[8] T. Khan, I. Azad, R. Ahmad, S. Raza, S. Dixit, *EXCLI J.* **2018**, *17*, 331–348.

[9] Y. Aimene, R. Eychenne, S. Mallet-Ladeira, N. Saffon, J.-Y. Winum, A. Nocentini, C. T. Supuran, E. Benoist, A. Seridi, *J. Enzyme Inhib. Med. Chem.* **2019**, *34*, 773–782.

[10] Y. Minenkov, Å. Singstad, G. Occhipinti, V. R. Jensen, *Dalt. Trans.* **2012**, *41*, 5526.

[11] S. Boonseng, G. W. Roffe, M. Targema, J. Spencer, H. Cox, *J. Organomet. Chem.* **2017**, *845*, 71–81.

[12] N. Wiberg, *Holleman-Wiberg: Inorganic Chemistry*, Academic Press, New York, USA, 34 Edn., **2001**.

[13] Z. F. Ismagilova, R. R. Safin, F. R. Ismagilov, *Chem. Technol. Fuels Oils* **2004**, *40*, 279–283.

[14] R. A. Marriott, E. Fitzpatrick, K. L. Lesage, *Fluid Phase Equilib.* **2008**, *269*, 69–72.

[15] J. Baltrusaitis, C. De Graaf, R. Broer, E. V. Patterson, *ChemPhysChem* **2013**, *14*, 3960–

3970.

[16] A. W. King, A. L. Baskerville, H. Cox, *Phil. Trans. R. Soc. A* **2018**, *376*, 20170153.

[17] H. Cox, A. L. Baskerville, in *Adv. Quantum Chem.*, **2018**, pp. 201–240.

[18] A. L. Baskerville, A. W. King, H. Cox, *R. Soc. Open Sci.* **2019**, *6*, 181357.

[19] E. G. Lewars, *Computational Chemistry: Introduction to the Theory and Applications of Molecular and Quantum Mechanics*, Springer Netherlands, Dordrecht, 2nd Edn., **2011**.

[20] D. C. Young, *Computational Chemistry: A Practical Guide for Applying Techniques to Real-World Problems*, John Wiley & Sons, Inc., New York, USA, **2001**.

[21] V. Milman, K. Refson, S. J. Clark, C. J. Pickard, J. R. Yates, S.-P. Gao, P. J. Hasnip, M. I. J. Probert, A. Perlov, M. D. Segall, *J. Mol. Struct. THEOCHEM* **2010**, *954*, 22–35.

[22] C. Sridevi, G. Shanthi, G. Velraj, *Spectrochim. Acta Part A Mol. Biomol. Spectrosc.* **2012**, *89*, 46–54.

[23] K. J. Bonney, F. Schoenebeck, *Chem. Soc. Rev.* **2014**, *43*, 6609–6638.

[24] M. J. Frisch, G. W. Trucks, H. B. Schlegel, G. E. Scuseria, M. A. Robb, J. R. Cheeseman, G. Scalmani, V. Barone, B. Mennucci, G. A. Petersson, H. Nakatsuji, M. Caricato, X. Li, H. P. Hratchian, A. F. Izmaylov, J. Bloino, G. Zheng, J. L. Sonnenberg, M. Hada, M. Ehara, K. Toyota, R. Fukuda, J. Hasegawa, M. Ishida, T. Nakajima, Y. Honda, O. Kitao, H. Nakai, T. Vreven, J. A. J. Montgomery, J. E. Peralta, F. Ogliaro, M. Bearpark, J. J. Heyd, E. Brothers, K. N. Kudin, V. N. Staroverov, T. Keith, R. Kobayashi, J. Normand, K. Raghavachari, A. Rendell, J. C. Burant, S. S. Iyengar, J. Tomasi, M. Cossi, N. Rega, J. M. Millam, M. Klene, J. E. Knox, J. B. Cross, V. Bakken, C. Adamo, J. Jaramillo, R. Gomperts, R. E. Stratmann, O. Yazyev, A. J. Austin, R. Cammi, C. Pomelli, J. W. Ochterski, R. L. Martin, K. Morokuma, V. G. Zakrzewski, G. A. Voth, P. Salvador, J. J. Dannenberg, S. Dapprich, A. D. Daniels, O. Farkas, J. B. Foresman, J. V. Ortiz, J. Cioslowski, D. J. Fox, *Gaussian, Inc., Wallingford CT* **2013**.

[25] A. W. King, P. E. Herlihy, H. Cox, *J. Chem. Phys.* **2014**, *141*, 044120.

[26] R. Colle, O. Salvetti, *Theor. Chim. Acta* **1975**, *37*, 329–334.

[27] C. Lee, W. Yang, R. G. Parr, *Phys. Rev. B* **1988**, *37*, 785–789.

[28] S. Boonseng, G. W. Roffe, J. Spencer, H. Cox, *Dalt. Trans.* **2015**, *44*, 7570–7577.

[29] G. W. Roffe, *The Synthesis , Catalytic Investigation , and Theoretical Rationalisation of Unsymmetrical Pincer Palladacycles*, PhD Thesis, University Of Sussex, **2016**.

[30] R. G. Mortimer, *Physical Chemistry*, Elsevier Academic Press, Burlington, USA, **2008**.

[31] W. Koch, M. C. Holthausen, *A Chemist ' s Guide to Density Functional Theory*, Wiley-VCH Verlag GmbH, Weinheim, Germany, 2nd Edn., **2001**.

[32] P. W. Atkins, R. Friedman, *Molecular Quantum Mechanics*, Oxford University Press, Oxford, UK, 4th Edn., **2005**.

[33] P. Atkins, J. de Paula, *Atkin's Physical Chemistry*, Oxford University Press, New York, USA, 8th Edn., **2006**.

[34] N. I. Levine, *Physical Chemistry*, The McGraw-Hill Companies, Inc., New York, USA, **2009**.

[35] F. Jensen, *Introduction to Computational Chemistry*, John Wiley & Sons Ltd, Chichester, UK, 2nd Edn., England, **2007**.

[36] H. B. Schlegel, *J. Comput. Chem.* **1982**, *3*, 214–218.

[37] K. Raghavachari, C. M. Rohlfing, J. S. Binkley, *J. Chem. Phys.* **1990**, *93*, 5862.

[38] B. O. Roos, P. R. Taylor, P. E. M. Siegbahn, *Chem. Phys.* **1980**, *48*, 157–173.

[39] P. O. Löwdin, *Phys. Rev.* **1955**, *97*, 1509–1520.

[40] P.-O. Löwdin, *Int. J. Quantum Chem.* **1995**, *55*, 77–102.

[41] S. R. Langhoff, E. R. Davidson, *Int. J. Quantum Chem.* **1974**, *8*, 61–72.

[42] J. M. L. Martin, J. P. François, R. Gijbels, *Chem. Phys. Lett.* **1990**, *172*, 346–353.

[43] V. Veryazov, P. Å. Malmqvist, B. O. Roos, *Int. J. Quantum Chem.* **2011**, *111*, 3329–3338.

[44] K. Raghavachari, G. W. Trucks, J. A. Pople, M. Head-Gordon, *Chem. Phys. Lett.* **1989**, *157*, 479–483.

[45] C. Møller, M. S. Plesset, *Phys. Rev.* **1934**, *46*, 618–622.

[46] K. Raghavachari, J. A. Pople, E. S. Replogle, M. Head-Gordon, *J. Phys. Chem.* **1990**, *94*, 5579–5586.

[47] P. Atkins, J. de Paula, R. Friedman, *Physical Chemistry: Quanta, Matter, and Change*

Second Edition, **2009**.

[48] J. Čížek, *J. Chem. Phys.* **1966**, *45*, 4256–4266.

[49] J. Čížek, in *Adv. Chem. Phys.*, **1969**, pp. 35–89.

[50] J. Čížek, J. Paldus, *Int. J. Quantum Chem.* **1971**, *5*, 359–379.

[51] J. Paldus, J. Čížek, I. Shavitt, *Phys. Rev. A* **1972**, *5*, 50–67.

[52] J. Paldus, J. Čížek, B. Jeziorski, *J. Chem. Phys.* **1989**, *90*, 4356–4362.

[53] T. J. Lee, J. E. Rice, G. E. Scuseria, H. F. Schaefer, *Theor. Chim. Acta* **1989**, *75*, 81–98.

[54] T. J. Lee, P. R. Taylor, *Int. J. Quantum Chem. Quantum Chem. Symp.* **1989**, *36*, 199–207.

[55] D. Jayatilaka, T. J. Lee, *J. Chem. Phys.* **1993**, *98*, 9734–9747.

[56] L. H. Thomas, N. Kaltsoyannis, *Phys. Chem. Chem. Phys.* **2006**, *8*, 1271.

[57] J. C. Rienstra-Kiracofe, W. D. Allen, H. F. Schaefer, *J. Phys. Chem. A* **2000**, *104*, 9823–9840.

[58] S. F. Sousa, P. A. Fernandes, M. J. Ramos, *J. Phys. Chem. A* **2007**, *111*, 10439–10452.

[59] P. Hohenberg, W. Kohn, *Phys. Rev.* **1964**, *136*, B864–B871.

[60] W. Kohn, L. J. Sham, *Phys. Rev.* **1965**, *140*, A1133–A1138.

[61] W. Kohn, *Rev. Mod. Phys.* **1999**, *71*, 1253–1266.

[62] J. P. Perdew, J. Tao, V. N. Staroverov, G. E. Scuseria, *J. Chem. Phys.* **2004**, *120*, 6898–6911.

[63] J. P. Perdew, K. Schmidt, in *AIP Conf. Proc.*, AIP, **2001**, pp. 1–20.

[64] A. D. Becke, *Phys. Rev. A* **1988**, *38*, 3098–3100.

[65] W. J. Carr, *Phys. Rev.* **1961**, *122*, 1437–1446.

[66] W. J. Carr, A. A. Maradudin, *Phys. Rev.* **1964**, *133*, A371–A374.

[67] D. M. Ceperley, B. J. Alder, *Phys. Rev. Lett.* **1980**, *45*, 566–569.

[68] S. H. Vosko, L. Wilk, M. Nusair, *Can. J. Phys.* **1980**, *58*, 1200–1211.

[69] J. P. Perdew, *Phys. Rev. B* **1986**, *33*, 8822–8824.

[70] A. D. Becke, *J. Chem. Phys.* **1986**, *84*, 4524–4529.

[71] J. P. Perdew, A. Zunger, *Phys. Rev. B* **1981**, *23*, 5048–5079.

[72] J. P. Perdew, K. Burke, M. Ernzerhof, *Phys. Rev. Lett.* **1996**, *77*, 3865–3868.

[73] M. Brack, B. K. Jennings, Y. H. Chu, *Phys. Lett. B* **1976**, *65*, 1–4.

[74] S. Kurth, J. P. Perdew, P. Blaha, *Int. J. Quantum Chem.* **1999**, *75*, 889–909.

[75] J. Tao, J. P. Perdew, V. N. Staroverov, G. E. Scuseria, *Phys. Rev. Lett.* **2003**, *91*, 146401.

[76] Y. Zhao, D. G. Truhlar, *J. Chem. Phys.* **2006**, *125*, 194101.

[77] J. Chai, M. Head-Gordon, *J. Chem. Phys.* **2008**, *128*, 084106.

[78] R. Peverati, D. G. Truhlar, *J. Phys. Chem. Lett.* **2011**, *2*, 2810–2817.

[79] M. P. Waller, H. Braun, N. Hojdis, M. Bühl, *J. Chem. Theory Comput.* **2007**, *3*, 2234–2242.

[80] J. Chai, M. Head-Gordon, *Phys. Chem. Chem. Phys.* **2008**, *10*, 6615.

[81] Y.-S. Lin, G.-D. Li, S.-P. Mao, J.-D. Chai, *J. Chem. Theory Comput.* **2013**, *9*, 263–272.

[82] A. D. Becke, *J. Chem. Phys.* **1997**, *107*, 8554–8560.

[83] T. Yanai, D. P. Tew, N. C. Handy, *Chem. Phys. Lett.* **2004**, *393*, 51–57.

[84] S. Miertuš, E. Scrocco, J. Tomasi, *Chem. Phys.* **1981**, *55*, 117–129.

[85] H. Ågren, K. V. Mikkelsen, *J. Mol. Struct. THEOCHEM* **1991**, *234*, 425–467.

[86] P. E. Smith, B. M. Pettitt, *J. Phys. Chem.* **1994**, *98*, 9700–9711.

[87] G. Scalmani, M. J. Frisch, *J. Chem. Phys.* **2010**, *132*, 114110.

[88] M. Cossi, N. Rega, G. Scalmani, V. Barone, *J. Comput. Chem.* **2003**, *24*, 669–681.

[89] C. J. Cramer, D. G. Truhlar, *Chem. Rev.* **1999**, *99*, 2161–2200.

[90] J. Tomasi, B. Mennucci, R. Cammi, *Chem. Rev.* **2005**, *105*, 2999–3094.

[91] A. V. Marenich, C. J. Cramer, D. G. Truhlar, *J. Phys. Chem. B* **2009**, *113*, 6378–6396.

[92] B. Mennucci, J. Tomasi, R. Cammi, J. R. Cheeseman, M. J. Frisch, F. J. Devlin, S. Gabriel, P. J. Stephens, *J. Phys. Chem. A* **2002**, *106*, 6102–6113.

[93] E. Cancès, B. Mennucci, *J. Math. Chem.* **1998**, *23*, 309–326.

[94] E. Cancès, B. Mennucci, J. Tomasi, *J. Chem. Phys.* **1997**, *107*, 3032–3041.

[95] B. Mennucci, E. Cancès, J. Tomasi, *J. Phys. Chem. B* **1997**, *101*, 10506–10517.

[96] V. Barone, M. Cossi, *J. Phys. Chem. A* **1998**, *102*, 1995–2001.

[97] R. E. Skyner, J. L. McDonagh, C. R. Groom, T. Van Mourik, J. B. O. Mitchell, *Phys. Chem. Chem. Phys.* **2015**, *17*, 6174–6191.

[98] M. Cossi, V. Barone, R. Cammi, J. Tomasi, *Chem. Phys. Lett.* **1996**, *255*, 327–335.

[99] M. J. Frisch, J. A. Pople, J. S. Binkley, *J. Chem. Phys.* **1984**, *80*, 3265–3269.

[100] T. H. Dunning, *J. Chem. Phys.* **1989**, *90*, 1007–1023.

[101] D. E. Woon, T. H. Dunning, *J. Chem. Phys.* **1993**, *98*, 1358–1371.

[102] K. A. Peterson, A. K. Wilson, D. E. Woon, T. H. Dunning Jr., *Theor. Chem. Acc.* **1997**, *97*, 251–259.

[103] A. F. Jalbout, F. Nazari, L. Turker, *J. Mol. Struct. THEOCHEM* **2004**, *671*, 1–21.

[104] M. M. Islam, M. D. H. Bhuiyan, T. Bredow, A. C. Try, *Comput. Theor. Chem.* **2011**, *967*, 165–170.

[105] C. L. Pekeris, *Phys. Rev.* **1958**, *112*, 1649–1658.

[106] H. Cox, S. J. Smith, B. T. Sutcliffe, *Phys. Rev. A* **1994**, *49*, 4520–4532.

[107] J. C. Slater, *Phys. Rev.* **1930**, *36*, 57–64.

[108] S. F. Boys, *Proc. R. Soc. London. Ser. A. Math. Phys. Sci.* **1950**, *200*, 542–554.

[109] H. Dorsett, A. White, *Overview of Molecular Modelling and Ab Initio Molecular Orbital Methods Suitable for Use with Energetic Materials*, DSTO Aeronautical And Maritime Research Laboratory, Salisbury South, Australia, **2000**.

[110] K. I. Ramachandran, G. Deepa, K. Namboori, *Computational Chemistry and Molecular Modeling: Principles and Applications*, Springer Berlin Heidelberg, Berlin, Heidelberg, **2008**.

[111] W. J. Hehre, R. Ditchfield, L. Radom, J. A. Pople, *J. Am. Chem. Soc.* **1970**, *92*, 4796–4801.

[112] R. Ditchfield, W. J. Hehre, J. A. Pople, *J. Chem. Phys.* **1971**, *54*, 724–728.

[113] W. J. Hehre, R. Ditchfield, J. A. Pople, *J. Chem. Phys.* **1972**, *56*, 2257–2261.

[114] J. S. Binkley, J. A. Pople, W. J. Hehre, *J. Am. Chem. Soc.* **1980**, *102*, 939–947.

[115] D. E. Woon, T. H. Dunning, *J. Chem. Phys.* **1994**, *100*, 2975–2988.

[116] D. E. Woon, T. H. Dunning, *J. Chem. Phys.* **1995**, *103*, 4572–4585.

[117] J. Dunning, K. A. Peterson, A. K. Wilson, *J. Chem. Phys.* **2001**, *114*, 9244–9253.

[118] K. A. Peterson, T. H. Dunning, *J. Chem. Phys.* **2002**, *117*, 10548–10560.

[119] H. Hellmann, *J. Chem. Phys.* **1935**, *3*, 61–61.

[120] P. J. Hay, W. R. Wadt, *J. Chem. Phys.* **1985**, *82*, 270–283.

[121] P. J. Hay, W. R. Wadt, *J. Chem. Phys.* **1985**, *82*, 299–310.

[122] M. Dolg, U. Wedig, H. Stoll, H. Preuss, *J. Chem. Phys.* **1987**, *86*, 866.

[123] D. Andrae, U. Häußermann, M. Dolg, H. Stoll, H. Preuß, *Theor. Chim. Acta* **1990**, *77*, 123–141.

[124] R. F. W. Bader, P. M. Beddall, *J. Am. Chem. Soc.* **1973**, *95*, 305–315.

[125] R. F. W. Bader, *Acc. Chem. Res.* **1975**, *8*, 34–40.

[126] R. F. W. Bader, S. G. Anderson, A. J. Duke, *J. Am. Chem. Soc.* **1979**, *101*, 1389–1395.

[127] R. F. W. Bader, T. T. Nguyen-Dang, Y. Tal, *J. Chem. Phys.* **1979**, *70*, 4316–4329.

[128] R. F. W. Bader, *J. Chem. Phys.* **1980**, *73*, 2871–2883.

[129] R. F. W. Bader, T. T. Nguyen-Dang, *Adv. Quantum Chem.* **1981**, *14*, 63–124.

[130] R. F. W. Bader, *Acc. Chem. Res.* **1985**, *18*, 9–15.

[131] R. F. W. Bader, *Chem. Rev.* **1991**, *91*, 893–928.

[132] R. F. W. Bader, *Phys. Rev. B* **1994**, *49*, 13348–13356.

[133] R. F. W. Bader, *J. Phys. Chem. A* **1998**, *102*, 7314–7323.

[134] C. F. Matta, R. J. Boyd, in *Quantum Theory Atoms Mol.*, Wiley-VCH Verlag GmbH & Co. KGaA, Weinheim, Germany, **2007**, pp. 1–34.

[135] R. F. W. Bader, *J. Phys. Chem. A* **2009**, *113*, 10391–10396.

[136] E. Espinosa, I. Alkorta, J. Elguero, E. Molins, *J. Chem. Phys.* **2002**, *117*, 5529–5542.

[137] M. P. Waller, A. Robertazzi, J. A. Platts, D. E. Hibbs, P. A. Williams, *J. Comput. Chem.* **2006**, *27*, 491–504.

[138] R. F. W. Bader, in *Encycl. Comput. Chem.*, John Wiley & Sons, Ltd, Chichester, UK, **2002**, pp. 1–23.

[139] D. Cremer, E. Kraka, *Angew. Chemie Int. Ed. English* **1984**, *23*, 627–628.

[140] M. Montag, I. Efremenko, G. Leitus, Y. Ben-David, J. M. L. Martin, D. Milstein, *Organometallics* **2013**, *32*, 7163–7180.

[141] J. Dupont, C. S. Consorti, J. Spencer, *Chem. Rev.* **2005**, *105*, 2527–2572.

[142] N. Selander, K. J. Szabó, *Chem. Rev.* **2011**, *111*, 2048–2076.

[143] J. Dupont, M. Pfeffer, J. Spencer, *Eur. J. Inorg. Chem.* **2001**, *2001*, 1917–1927.

[144] N. T. S. Phan, M. Van Der Sluys, C. W. Jones, *Adv. Synth. Catal.* **2006**, *348*, 609–679.

[145] G. C. Fortman, S. P. Nolan, *Chem. Soc. Rev.* **2011**, *40*, 5151.

[146] C. S. Consorti, G. Ebeling, F. Rodembusch, V. Stefani, P. R. Livotto, F. Rominger, F. H. Quina, C. Yihwa, J. Dupont, *Inorg. Chem.* **2004**, *43*, 530–536.

[147] C. S. Consorti, G. Ebeling, F. R. Flores, F. Rominger, J. Dupont, *Adv. Synth. Catal.* **2004**, *346*, 617–624.

[148] X.-Q. Hao, Y.-N. Wang, J.-R. Liu, K.-L. Wang, J.-F. Gong, M.-P. Song, *J. Organomet. Chem.* **2010**, *695*, 82–89.

[149] V. A. Kozlov, D. V. Aleksanyan, Y. V. Nelyubina, K. A. Lyssenko, E. I. Gutsul, L. N. Puntus, A. A. Vasil'ev, P. V. Petrovskii, I. L. Odinets, *Organometallics* **2008**, *27*, 4062–4070.

[150] V. A. Kozlov, D. V Aleksanyan, A. a. Vasil'ev, I. L. Odinets, *Phosphorus. Sulfur. Silicon Relat. Elem.* **2011**, *186*, 626–637.

[151] V. A. Kozlov, D. V. Aleksanyan, Y. V. Nelyubina, K. A. Lyssenko, P. V. Petrovskii, A. A. Vasil'ev, I. L. Odinets, *Organometallics* **2011**, *30*, 2920–2932.

[152] D. V Aleksanyan, V. A. Kozlov, N. E. Shevchenko, V. G. Nenajdenko, A. A. Vasil'ev, Y. V Nelyubina, I. V Ananyev, P. V Petrovskii, I. L. Odinets, *J. Organomet. Chem.* **2012**, *711*, 52–61.

[153] W. A. Herrmann, K. Öfele, D. V. Preysing, S. K. Schneider, *J. Organomet. Chem.* **2003**, *687*, 229–248.

[154] M.-C. Lagunas, R. a Gossage, A. L. Spek, G. van Koten, *Organometallics* **1998**, *17*, 731–741.

[155] F. d'Orlyé, A. Jutand, *Tetrahedron* **2005**, *61*, 9670–9678.

[156] J. G. de Vries, *Dalt. Trans.* **2006**, 421–429.

[157] K. Muñiz, *Angew. Chemie Int. Ed.* **2009**, *48*, 9412–9423.

[158] K. Karami, M. Hosseini, H. Sadeghi-aliabadi, J. Lipkowski, *Polyhedron* **2012**, *50*, 187–192.

[159] A. R. Kapdi, I. J. S. Fairlamb, *Chem. Soc. Rev.* **2014**, *43*, 4751.

[160] S. Roy, S. Pramanik, T. Ghorui, K. Pramanik, *RSC Adv.* **2015**, *5*, 22544–22559.

[161] W. A. Herrmann, C. Brossmer, K. Öfele, C.-P. Reisinger, T. Priermeier, M. Beller, H. Fischer, *Angew. Chemie Int. Ed. English* **1995**, *34*, 1844–1848.

[162] M. Beller, H. Fischer, W. A. Herrmann, K. Öfele, C. Brossmer, *Angew. Chemie Int. Ed. English* **1995**, *34*, 1848–1849.

[163] M. Catellani, G. P. Chiusoli, M. Costa, *J. Organomet. Chem.* **1995**, *500*, 69–80.

[164] M. Ohff, A. Ohff, M. E. Van der Boom, D. Milstein, *J. Am. Chem. Soc.* **1997**, *119*, 11687–11688.

[165] B. L. Shaw, *Chem. Commun.* **1998**, 1361–1362.

[166] H. Weissman, D. Milstein, *Chem. Commun.* **1999**, 1901–1902.

[167] A. Suzuki, *J. Organomet. Chem.* **1999**, *576*, 147–168.

[168] D. Zim, A. S. Gruber, G. Ebeling, J. Dupont, A. L. Monteiro, *Org. Lett.* **2000**, *2*, 2881–2884.

[169] R. B. Bedford, C. S. J. Cazin, *Chem. Commun.* **2001**, 1540–1541.

[170] R. B. Bedford, S. L. Welch, *Chem. Commun.* **2001**, *2*, 129–130.

[171] N. J. Whitcombe, K. K. (Mimi) Hii, S. E. Gibson, *Tetrahedron* **2001**, *57*, 7449–7476.

[172] R. B. Bedford, C. S. J. Cazin, S. L. Hazelwood, *Angew. Chemie - Int. Ed.* **2002**, *41*, 4120–4122.

[173] K. Yu, W. Sommer, M. Weck, C. W. Jones, *J. Catal.* **2004**, *226*, 101–110.

[174] R. B. Bedford, C. S. J. Cazin, D. Holder, *Coord. Chem. Rev.* **2004**, *248*, 2283–2321.

[175] K. Yu, W. Sommer, J. M. Richardson, M. Weck, C. W. Jones, *Adv. Synth. Catal.* **2005**, *347*, 161–171.

[176] W. J. Sommer, K. Yu, J. S. Sears, Y. Ji, X. Zheng, R. J. Davis, C. D. Sherrill, C. W. Jones, M. Week, *Organometallics* **2005**, *24*, 4351–4361.

[177] D. J. Cárdenas, B. Martín-Matute, A. M. Echavarren, *J. Am. Chem. Soc.* **2006**, *128*, 5033–5040.

[178] M. Weck, C. W. Jones, *Inorg. Chem.* **2007**, *46*, 1865–1875.

[179] R. C. da Costa, M. Jurisch, J. A. Gladysz, *Inorganica Chim. Acta* **2008**, *361*, 3205–3214.

[180] B.-S. Zhang, C. Wang, J.-F. Gong, M.-P. Song, *J. Organomet. Chem.* **2009**, *694*, 2555–2561.

[181] L. Jin, A. Lei, *Org. Biomol. Chem.* **2012**, *10*, 6817.

[182] A. R. Kapdi, A. Karbelkar, M. Naik, S. Pednekar, C. Fischer, C. Schulzke, M. Tromp, *RSC Adv.* **2013**, *3*, 20905.

[183] R. Ratti, *Can. Chem. Trans.* **2014**, *2*, 467–488.

[184] H. Font, M. Font-Bardia, K. Gómez, G. González, J. Granell, I. Macho, M. Martínez, *Dalt. Trans.* **2014**, *43*, 13525.

[185] A. R. Kapdi, G. Dhangar, J. L. Serrano, J. Pérez, L. García, I. J. S. Fairlamb, *Chem. Commun.* **2014**, *50*, 9859.

[186] M. R. Chapman, C. M. Pask, A. Ariafard, C. E. Willans, *Chem. Commun.* **2015**, *51*, 5513–5515.

[187] D. S. Rosa, F. Antelo, T. J. Lopes, N. F. de Moura, G. R. Rosa, *Quim. Nova* **2015**, *38*, 605–608.

[188] I. Moreno, R. SanMartin, B. Ines, M. T. Herrero, E. Domínguez, *Curr. Org. Chem.* **2009**, *13*, 878–895.

[189] M. Gagliardo, N. Selander, N. C. Mehendale, G. Van Koten, R. J. M. Klein Gebbink, K. J. Szabó, *Chem. - A Eur. J.* **2008**, *14*, 4800–4809.

[190] G. W. Roffe, S. Boonseng, C. B. Baltus, S. J. Coles, I. J. Day, R. N. Jones, N. J. Press, M. Ruiz, G. J. Tizzard, H. Cox, J. Spencer, *R. Soc. Open Sci.* **2016**, *3*, 150656.

[191] H. B. Schlegel, *New Theor. Concepts Underst. Org. React.* **1989**, 33–53.

[192] L. Estévez, L. W. Tuxworth, J. Sotiropoulos, P. W. Dyer, K. Miqueu, *Dalt. Trans.* **2014**, *43*, 11165.

[193] J. P. Perdew, K. Burke, M. Ernzerhof, *Phys. Rev. Lett.* **1997**, *78*, 1396–1396.

[194] J. P. Perdew, K. Burke, M. Ernzerhof, *Phys. Rev. Lett.* **1998**, *80*, 891–891.

[195] A. W. Ehlers, M. Böhme, S. Dapprich, A. Gobbi, A. Höllwarth, V. Jonas, K. F. Köhler, R. Stegmann, A. Veldkamp, G. Frenking, *Chem. Phys. Lett.* **1993**, *208*, 111–114.

[196] P. C. Hariharan, J. A. Pople, *Theor. Chim. Acta* **1973**, *28*, 213–222.

[197] R. Krishnan, J. S. Binkley, R. Seeger, J. A. Pople, *J. Chem. Phys.* **1980**, *72*, 650–654.

[198] H. Lakmini, I. Ciofini, A. Jutand, C. Amatore, C. Adamo, *J. Phys. Chem. A* **2008**, *112*, 12896–12903.

[199] C. A. Tsipis, *Coord. Chem. Rev.* **1991**, *108*, 163–311.

[200] P. K. Sajith, C. H. Suresh, *Inorg. Chem.* **2011**, *50*, 8085–8093.

[201] C. Gonzalez, H. B. Schlegel, *J. Chem. Phys.* **1989**, *90*, 2154–2161.

[202] C. Gonzalez, H. B. Schlegel, *J. Phys. Chem.* **1990**, *94*, 5523–5527.

[203] T. Lu, F. Chen, *J. Comput. Chem.* **2012**, *33*, 580–592.

[204] C. Sosa, J. Andzelm, B. C. Elkin, E. Wimmer, K. D. Dobbs, D. A. Dixon, *J. Phys. Chem.* **1992**, *96*, 6630–6636.

[205] J. E. House, *Inorganic Chemistry*, Academic Press, London, UK, **2008**.

[206] Y. Minenkov, G. Occhipinti, V. R. Jensen, **2009**, 11833–11844.

[207] K. J. Keuseman, I. P. Smoliakova, V. V Dunina, *Organometallics* **2005**, *24*, 4159–4169.

[208] E. Arunan, G. R. Desiraju, R. a. Klein, J. Sadlej, S. Scheiner, I. Alkorta, D. C. Clary, R. H. Crabtree, J. J. Dannenberg, P. Hobza, H. G. Kjaergaard, A. C. Legon, B. Mennucci, D. J. Nesbitt, *Pure Appl. Chem.* **2011**, *83*, 1637–1641.

[209] A. A. C. Braga, N. H. Morgon, G. Ujaque, F. Maseras, *J. Am. Chem. Soc.* **2005**, *127*, 9298–9307.

[210] A. A. C. Braga, N. H. Morgon, G. Ujaque, A. Lledós, F. Maseras, *J. Organomet. Chem.* **2006**, *691*, 4459–4466.

[211] K. Matos, J. A. Soderquist, *J. Org. Chem.* **1998**, *63*, 461–470.

[212] S. Grimme, *J. Comput. Chem.* **2006**, *27*, 1787–1799.

[213] P. K. Sajith, C. H. Suresh, *Dalton Trans.* **2010**, *39*, 815–822.

[214] P. K. Sajith, C. H. Suresh, *J. Organomet. Chem.* **2011**, *696*, 2086–2092.

[215] G. W. Smith, E. A. Carter, *J. Phys. Chem.* **1991**, 2327–2339.

[216] F. Amoroso, E. Zangrando, C. Carfagna, C. Müller, D. Vogt, M. Hagar, F. Ragaini, B. Milani, *Dalt. Trans.* **2013**, *42*, 14583.

[217] C. Sicre, A. A. C. Braga, F. Maseras, M. M. Cid, *Tetrahedron* **2008**, *64*, 7437–7443.

[218] P. Steenwinkel, R. A. Gossage, G. van Koten, *Chem. - A Eur. J.* **1998**, *4*, 759–762.

[219] M. Albrecht, R. A. Gossage, A. L. Spek, G. Van Koten, *J. Am. Chem. Soc.* **1999**, *121*, 11898–11899.

[220] M. Albrecht, A. L. Spek, G. Van Koten, *J. Am. Chem. Soc.* **2001**, *123*, 7233–7246.

[221] M. Enescu, B. Cardey, *ChemPhysChem* **2006**, *7*, 912–919.

[222] S. Kazemiabnavi, P. Dutta, S. Banerjee, *J. Phys. Chem. C* **2014**, *118*, 27183–27192.

[223] S. Kazemiabnavi, P. Dutta, S. Banerjee, *Phys. Chem. Chem. Phys.* **2015**, *17*, 11740–11751.

[224] C. Adamo, C. Amatore, I. Ciofini, A. Jutand, H. Lakmini, *J. Am. Chem. Soc.* **2006**, *128*, 6829–6836.

[225] H. H. Uhlig, *J. Phys. Chem.* **1937**, *41*, 1215–1226.

[226] G. van Koten, *Organometallic Pincer Chemistry*, Springer Berlin Heidelberg, Berlin, Heidelberg, **2013**.

[227] S. Boonseng, *Computational Study of the Reactivity of Palladacycles in Catalytic Applications*, PhD Thesis, University Of Sussex, **2017**.

[228] M. Targema, N. O. Obi-Egbedi, M. D. Adeoye, *Comput. Theor. Chem.* **2013**, *1012*, 47–53.

[229] G. Mann, Q. Shelby, A. H. Roy, J. F. Hartwig, *Organometallics* **2003**, *22*, 2775–2789.

[230] D. A. Culkin, J. F. Hartwig, *Organometallics* **2004**, *23*, 3398–3416.

[231] J. F. Hartwig, *Inorg. Chem.* **2007**, *46*, 1936–1947.

[232] M. L. Clarke, M. Heydt, *Organometallics* **2005**, *24*, 6475–6478.

[233] Y. Yamamoto, S. Takada, N. Miyaura, T. Iyama, H. Tachikawa, *Organometallics* **2009**, *28*, 152–160.

[234] A. Ariafard, B. F. Yates, *J. Organomet. Chem.* **2009**, *694*, 2075–2084.

[235] N. Sieffert, M. Bühl, *Inorg. Chem.* **2009**, *48*, 4622–4624.

[236] R. O. Ramabhadran, K. Raghavachari, *J. Chem. Theory Comput.* **2013**, *9*, 3986–3994.

[237] J. A. Plumley, J. J. Dannenberg, *J. Comput. Chem.* **2011**, *32*, 1519–1527.

[238] A. Karton, E. Rabinovich, J. M. L. Martin, B. Ruscic, *J. Chem. Phys.* **2006**, *125*, 144108.

[239] A. Karton, S. Daon, J. M. L. Martin, *Chem. Phys. Lett.* **2011**, *510*, 165–178.

[240] M. Abe, *Chem. Rev.* **2013**, *113*, 7011–7088.

[241] T. H. Dunning, *J. Phys. Chem. A* **2000**, *104*, 9062–9080.

[242] K. Müller-Dethlefs, P. Hobza, *Chem. Rev.* **2000**, *100*, 143–168.

[243] R. A. Klein, M. A. Zottola, *Chem. Phys. Lett.* **2006**, *419*, 254–258.

[244] J. A. Pople, *Rev. Mod. Phys.* **1999**, *71*, 1267–1274.

[245] M. Bogojeski, L. Vogt-Maranto, M. E. Tuckerman, K.-R. Müller, K. Burke, *Nat. Commun.* **2020**, *11*, 5223.

[246] H. Li, B. Tirri, E. Brémond, J. C. Sancho-García, C. Adamo, *J. Org. Chem.* **2021**, *86*, 5538–5545.

[247] I. Rossi, D. G. Truhlar, *Chem. Phys. Lett.* **1995**, *234*, 64–70.

[248] C. W. Bauschlicher, H. Partridge, *Chem. Phys. Lett.* **1995**, *245*, 158–164.

[249] J. T. Su, X. Xu, W. A. Goddard, *J. Phys. Chem. A* **2004**, *108*, 10518–10526.

[250] P. A. Denis, *J. Chem. Theory Comput.* **2005**, *1*, 900–907.

[251] A. Ramírez-Solís, F. Jolibois, L. Maron, *J. Phys. Chem. A* **2010**, *114*, 12378–12383.

[252] D. Jacquemin, C. Adamo, *Int. J. Quantum Chem.* **2012**, *112*, 2135–2141.

[253] J. M. Martell, J. D. Goddard, L. A. Eriksson, *J. Phys. Chem. A* **1997**, *101*, 1927–1934.

[254] D. D. Gregory, W. S. Jenks, *J. Phys. Chem. A* **2003**, *107*, 3414–3423.

[255] R. A. Kendall, T. H. Dunning, R. J. Harrison, *J. Chem. Phys.* **1992**, *96*, 6796–6806.

[256] R. Steudel, *Angew. Chemie Int. Ed. English* **1975**, *14*, 655–664.

[257] M. K. Kesharwani, B. Brauer, J. M. L. Martin, *J. Phys. Chem. A* **2015**, *119*, 1701–1714.

[258] J. Hahn, P. Schmidt, K. Reinartz, J. Behrend, G. Winnewisser, K. M. T. Yamada, *Zeitschrift für Naturforsch. B* **1991**, *46*, 339–343.

[259] J. Behrend, P. Mittler, G. Winnewisser, K. M. T. Yamada, *J. Mol. Spectrosc.* **1991**, *150*, 99–119.

[260] S. W. Benson, *Chem. Rev.* **1978**, *78*, 23–35.

[261] G. Herzberg, K. P. Huber, *Molecular Spectra and Molecular Structure*, Van Nostrand Reinhold Company, New York, USA, **1979**.

[262] G. L. Miessler, P. J. Fischer, A. Tarr, Donald, *Inorganic Chemistry*, Pearson Education, Inc., New York, USA, **2014**.

[263] H. Okabe, *Photochemistry of Small Molecules*, John Wiley & Sons, Inc., New York, USA, **1978**.

[264] M. Carleer, R. Colin, *J. Phys. B At. Mol. Phys.* **1970**, *3*, 1715–1723.

[265] M. H. Matus, D. A. Dixon, K. A. Peterson, J. A. W. Harkless, J. S. Francisco, *J. Chem. Phys.* **2007**, *127*, 0–7.

[266] K. A. Peterson, J. R. Lyons, J. S. Francisco, *J. Chem. Phys.* **2006**, *125*, 084314.

[267] D. J. Grant, D. A. Dixon, J. S. Francisco, *J. Chem. Phys.* **2007**, *126*, 144308.

[268] M. Schmidt, *Angew. Chemie Int. Ed. English* **1973**, *12*, 445–455.

[269] N. N. Greenwood, A. Earnshaw, *Chemistry of the Elements*, Butterworth-Heinemann, Oxford, UK, **2001**.

[270] S. Ono, J. L. Eigenbrode, A. A. Pavlov, P. Kharecha, D. Rumble, J. F. Kasting, K. H. Freeman, *Earth Planet. Sci. Lett.* **2003**, *213*, 15–30.

[271] M. W. Wong, T. S. Chwee, R. Steudel, *J. Phys. Chem. A* **2004**, *108*, 7091–7098.

[272] S. Du, T. C. Germann, J. S. Francisco, K. A. Peterson, H.-G. Yu, J. R. Lyons, *J. Chem. Phys.* **2011**, *134*, 154508.

[273] W. Feng, S. Kwon, E. Borguet, R. Vidic, *Environ. Sci. Technol.* **2005**, *39*, 9744–9749.

[274] D. Hohl, R. O. Jones, R. Car, M. Parrinello, *J. Chem. Phys.* **1988**, *89*, 6823.

[275] B. Eckert, A. J. H. Janssen, A. de Keiser, W. E. Kleinjan, I. Krossing, R. Steudel, Y. Steudel, M. W. Wong, *Elemental Sulfur and Sulfur-Rich Compounds I*, Springer Berlin Heidelberg, Berlin, Heidelberg, **2003**.

[276] T. K. Wiewiorowski, F. J. Touro, *J. Phys. Chem.* **1966**, *70*, 234–238.

[277] R. F. Bacon, R. Fanelli, *J. Am. Chem. Soc.* **1943**, *65*, 639–648.

[278] R. Fanelli, *Ind. Eng. Chem.* **1949**, *41*, 2031–2033.

[279] R. Fanelli, *Ind. Eng. Chem.* **1946**, *38*, 39–43.

[280] F. J. Touro, T. K. Wiewiorowski, *J. Phys. Chem.* **1966**, *70*, 239–241.

[281] K. Karan, R. A. Heidemann, L. A. Behie, *Ind. Eng. Chem. Res.* **1998**, *37*, 1679–1684.

[282] J. B. Hyne, E. Muller, T. K. Wiewiorowski, *J. Phys. Chem.* **1966**, *70*, 3733–3735.

[283] T. K. Wiewiorowski, A. Parthasarathy, B. L. Slaten, *J. Phys. Chem.* **1968**, *72*, 1890–1892.

[284] R. E. Powell, H. Eyring, *J. Am. Chem. Soc.* **1943**, *65*, 648–654.

[285] P. A. Rubero, *J. Chem. Eng. Data* **1964**, *9*, 481–484.

[286] M. C. Chang, S. M. Jhon, *Bull. Korean Chem. Soc.* **1982**, *3*, 133–139.

[287] J. Berkowitz, J. R. Marquart, *J. Chem. Phys.* **1963**, *39*, 275–283.

[288] D. M. Gardner, G. K. Fraenkel, *J. Am. Chem. Soc.* **1956**, *78*, 3279–3288.

[289] M. Liedtke, A. H. Saleck, K. M. T. Yamada, G. Winnewisser, S. Dobos, D. Cremer, E. Kraka, A. Dolgner, J. Hahn, *J. Phys. Chem.* **1993**, *97*, 11204–11210.

[290] H. Wieser, P. J. Krueger, E. Muller, J. B. Hyne, *Can. J. Chem.* **1969**, *47*, 1633–1637.

[291] B. Eckert, R. Okazaki, R. Steudel, N. Takeda, N. Tokitoh, M. W. Wong, *Elemental Sulfur and Sulfur-Rich Compounds II*, Springer-Verlag, **2003**.

[292] J. Berkowitz, C. Lifshitz, *J. Chem. Phys.* **1968**, *48*, 4346–4350.

[293] B. Meyer, *Chem. Rev.* **1976**, *76*, 367–388.

[294] J. Kao, *Inorg. Chem.* **1977**, *16*, 2085–2089.

[295] J. Kao, *Inorg. Chem.* **1977**, *16*, 3347–3349.

[296] M. R. Nimlos, G. B. Ellison, *J. Phys. Chem.* **1986**, *90*, 2574–2580.

[297] J. E. Rice, R. D. Amos, N. C. Handy, T. J. Lee, H. F. Schaefer, *J. Chem. Phys.* **1986**, *85*, 963–968.

[298] S. J. Rettig, J. Trotter, *Acta Crystallogr. Sect. C Cryst. Struct. Commun.* **1987**, *43*, 2260–2262.

[299] P. Hassanzadeh, L. Andrews, *J. Phys. Chem.* **1992**, *96*, 6579–6585.

[300] S. Hunsicker, R. O. Jones, G. Ganteför, *J. Chem. Phys.* **1995**, *102*, 5917.

[301] G. Ganteför, S. Hunsicker, R. O. Jones, *Chem. Phys. Lett.* **1995**, *236*, 43–49.

[302] F. Shimojo, K. Hoshino, Y. Zempo, *J. Phys. Condens. Matter* **1998**, *10*, L117–L182.

[303] M. S. Boumedien, J. Corset, E. Picquenard, *J. Raman Spectrosc.* **1999**, *30*, 463–472.

[304] S. Munejiri, F. Shimojo, K. Hoshino, *J. Phys. Condens. Matter* **2000**, *17*, 7999–8008.

[305] M. D. Chen, M. L. Liu, H. B. Luo, Q. E. Zhang, C. T. Au, *J. Mol. Struct. THEOCHEM* **2001**, *548*, 133–141.

[306] S. Millefiori, A. Alparone, *J. Phys. Chem. A* **2001**, *105*, 9489–9497.

[307] J. Cioslowski, A. Szarecka, D. Moncrieff, *J. Phys. Chem. A* **2001**, *105*, 501–505.

[308] M. W. Wong, Y. Steudel, R. Steudel, *Chem. Phys. Lett.* **2002**, *364*, 387–392.

[309] R. O. Jones, P. Ballone, *J. Chem. Phys.* **2003**, *118*, 9257–9265.

[310] M. W. Wong, R. Steudel, *Chem. Phys. Lett.* **2003**, *379*, 162–169.

[311] M. C. McCarthy, S. Thorwirth, C. A. Gottlieb, P. Thaddeus, *J. Am. Chem. Soc.* **2004**, *126*, 4096–4097.

[312] M. W. Wong, Y. Steudel, R. Steudel, *J. Chem. Phys.* **2004**, *121*, 5899–5907.

[313] S. Thorwirth, M. C. McCarthy, C. A. Gottlieb, P. Thaddeus, H. Gupta, J. F. Stanton, *J. Chem. Phys.* **2005**, *123*, 054326.

[314] J. S. Francisco, J. R. Lyons, I. H. Williams, *J. Chem. Phys.* **2005**, *123*, 054302.

[315] A. J. Ochoa-Calle, R. Hernández-Lamoneda, A. Ramírez-Solís, *J. Chem. Phys.* **2013**, *138*, 094317.

[316] I. M. Alecu, J. Zheng, Y. Zhao, D. G. Truhlar, *J. Chem. Theory Comput.* **2010**, *6*, 2872–2887.

[317] Y. Gao, P. Marshall, *J. Chem. Phys.* **2011**, *135*, 144306.

[318] M. Wang, T. Chatterjee, C. J. Foster, T. Wu, C. L. Yi, H. Yu, K. T. Wong, B. Hu, *J. Mater. Chem. C* **2020**, *8*, 3395–3401.

[319] M. D. Martin, L. Vina, M. Potemski, K. H. Ploog, *Phys. status solidi* **1999**, *215*, 229–233.

[320] L. Descôtes, R. Bellissent, P. Pfeuty, A. J. Dianoux, *Phys. A Stat. Mech. its Appl.* **1993**, *201*, 381–385.

[321] R. Winter, T. Bodensteiner, C. Szornel, P. A. Egelstaff, *J. Non. Cryst. Solids* **1988**, *106*, 100–103.

[322] D. C. Koningsberger, *On the Polymerisation of Sulfur and Selenium in the Liquid State : An ESR Study*, Eindhoven: Technische Hogeschool Eindhoven DOI: 10.6100/IR109059, **1971**.

[323] D. Schröder, S. Shaik, H. Schwarz, *Acc. Chem. Res.* **2000**, *33*, 139–145.

[324] T. Tsuneda, H. Nakano, K. Hirao, *J. Chem. Phys.* **1995**, *103*, 6520–6528.

[325] A. . Pakiari, F. Nazari, *J. Mol. Struct. THEOCHEM* **2003**, *640*, 109–115.

[326] D. L. Cooper, F. E. Penotti, R. Ponec, *Comput. Theor. Chem.* **2017**, *1116*, 40–49.

[327] P. Borowski, M. Fülscher, P.-Å. Malmqvist, B. O. Roos, *Chem. Phys. Lett.* **1995**, *237*, 195–

203.

[328] D. W. Arnold, C. Xu, E. H. Kim, D. M. Neumark, *J. Chem. Phys.* **1994**, *101*, 912–922.

[329] E. Muller, J. B. Hyne, *Can. J. Chem.* **1968**, *46*, 3587–3590.

[330] E. F. Muller, J. B. Hyne, *J. Am. Chem. Soc.* **1969**, *91*, 1907–1912.

[331] B. P. Winnewisser, *J. Mol. Spectrosc.* **1970**, *36*, 414–432.

[332] J. Hahn, *Zeitschrift für Naturforsch. B* **1985**, *40b*, 263–272.

[333] F. Grein, *Chem. Phys. Lett.* **1985**, *116*, 323–325.

[334] D. A. Dixon, D. J. Zeroka, J. J. Wendoloski, Z. R. Wasserman, *J. Phys. Chem.* **1985**, *89*, 5334–5336.

[335] J. Hahn, K. Altenbach, *Verlag der Zeitschrift für Naturforsch.* **1986**, *41b*, 675–679.

[336] D. Mauer, G. Winnewisser, K. M. T. Yamada, J. Hahn, K. Reinartz, *Zeitschrift fur Naturforsch. - Sect. A J. Phys. Sci.* **1988**, *43a*, 617.

[337] E. Herbst, G. Winnewisser, *Chem. Phys. Lett.* **1989**, *155*, 572–575.

[338] G. Pelz, K. M. T. Yamada, G. Winnewisser, *J. Mol. Spectrosc.* **1993**, *159*, 507–520.

[339] P. Mittler, K. M. T. Yamada, G. Winnewisser, M. Birk, *J. Mol. Spectrosc.* **1994**, *164*, 390–394.

[340] Y. Drozdova, K. Miaskiewicz, R. Steudel, *Zeitschrift für Naturforsch. B* **1995**, *50*, 4–8.

[341] K. M. T. Yamada, J. Behrend, S. P. Belov, G. Winnewisser, *J. Mol. Spectrosc.* **1996**, *176*, 397–402.

[342] R. Steudel, Y. Drozdova, K. Miaskiewicz, R. H. Hertwig, W. Koch, *J. Am. Chem. Soc.* **1997**, *119*, 1990–1996.

[343] M. Liedtke, K. M. T. Yamada, G. Winnewisser, J. Hahn, *J. Mol. Struct.* **1997**, *413–414*, 265–270.

[344] I. A. Gargurevich, *Ind. Eng. Chem. Res.* **2005**, *44*, 7706–7729.

[345] C. Zhou, K. Sendt, B. S. Haynes, *J. Phys. Chem. A* **2008**, *112*, 3239–3247.

[346] C. R. Zhou, K. Sendt, B. S. Haynes, *J. Phys. Chem. A* **2009**, *113*, 8299–8306.

[347] O. Suleimenov, T.-K. Ha, *Chem. Phys. Lett.* **1998**, *290*, 451–457.

[348] A. J. Cohen, N. C. Handy, *Mol. Phys.* **2001**, *99*, 607–615.

[349] N. C. Handy, A. J. Cohen, *J. Chem. Phys.* **2002**, *116*, 5411–5418.

[350] Y. Imamura, G. E. Scuseria, R. M. Martin, *J. Chem. Phys.* **2002**, *116*, 6458–6467.

[351] N. C. Handy, *Theor. Chem. Acc.* **2009**, *123*, 165–169.

[352] P. J. Knowles, N. C. Handy, *Chem. Phys. Lett.* **1984**, *111*, 315–321.

[353] J. Olsen, B. O. Roos, P. Jørgensen, H. J. A. Jensen, *J. Chem. Phys.* **1988**, *89*, 2185–2192.

[354] J. Olsen, P. Jørgensen, J. Simons, *Chem. Phys. Lett.* **1990**, *169*, 463–472.

[355] J. Olsen, O. Christiansen, H. Koch, P. Jørgensen, *J. Chem. Phys.* **1996**, *105*, 5082–5090.

[356] E. Rossi, G. L. Bendazzoli, S. Evangelisti, D. Maynau, *Chem. Phys. Lett.* **1999**, *310*, 530–536.

[357] A. Dutta, C. D. Sherrill, *J. Chem. Phys.* **2003**, *118*, 1610–1619.

[358] Z. Gan, D. J. Grant, R. J. Harrison, D. A. Dixon, *J. Chem. Phys.* **2006**, *125*, 124311.

[359] T. S. Hofer, *Front. Chem.* **2013**, *1*, 1–11.

[360] P. M. Zimmerman, *J. Chem. Phys.* **2017**, *146*, 104102.

[361] R. Singh, L. Massa, V. Sahni, *Phys. Rev. A - At. Mol. Opt. Phys.* **1999**, *60*, 4135–4139.

[362] S. Caratzoulas, P. J. Knowles, *Mol. Phys.* **2000**, *98*, 1811–1821.

[363] T. Tsuneda, T. Suzumura, K. Hirao, *J. Chem. Phys.* **1999**, *110*, 10664–10678.

[364] T. Tsuneda, K. Hirao, *Chem. Phys. Lett.* **1997**, *268*, 510–520.

[365] E. Clementi, *IBM J. Res. Dev.* **1965**, *9*, 2–19.

[366] E. Clementi, *IBM J. Res. Dev.* **1965**, *9*, 87–89.

[367] I. N. Levine, *Quantum Chemistry*, Pearson Education Inc., New York, USA, **2014**.

[368] R. McWeeny, *Methods of Molecular Quantum Mechanics*, Academic Press, London, UK, **1992**.

[369] C. C. J. Roothaan, *Rev. Mod. Phys.* **1951**, *23*, 69–89.

[370] B. Alder, *Methods in Computational Physics: Advances in Research and Applications*, Academis Press Inc., New York, USA, **1963**.

[371] E. Clementi, C. Roetti, *At. Data Nucl. Data Tables* **1974**, *14*, 177–478.

[372] E. Wigner, F. Seitz, *Phys. Rev.* **1933**, *43*, 804–810.

[373] E. Wigner, *Phys. Rev.* **1934**, *46*, 1002–1011.

[374] R. G. Mortimer, *Mathemaics for Physical Chemistry*, Elsevier Academic Press, Burlington, USA, **2005**.

[375] R. Colle, O. Salvetti, *Theor. Chim. Acta* **1979**, *53*, 55–63.

[376] L. Cohen, P. Santhanam, C. Frishberg, *Int. J. Quantum Chem.* **1980**, *18*, 143–154.

[377] R. Colle, O. Salvetti, *J. Chem. Phys.* **1983**, *79*, 1404–1407.

[378] L. Cohen, C. Frishberg, C. Lee, L. J. Massa, *Int. J. Quantum Chem.* **1986**, *19*, 525–533.

[379] B. Miehlich, A. Savin, H. Stoll, H. Preuss, *Chem. Phys. Lett.* **1989**, *157*, 200–206.

[380] A. D. Becke, *J. Chem. Phys.* **1988**, *88*, 1053–1062.

[381] R. Colle, O. Salvetti, *J. Chem. Phys.* **1990**, *93*, 534–544.

[382] M. Flocco, X.-Q. Gao, L. Massa, *Int. J. Quantum Chem.* **1990**, *38*, 213–223.

[383] F. Moscardó, E. San-Fabián, *Int. J. Quantum Chem.* **1991**, *40*, 23–32.

[384] F. Moscardó, E. San-Fabián, *Phys. Rev. A* **1991**, *44*, 1549–1553.

[385] J. Tao, P. Gori-Giorgi, J. P. Perdew, R. McWeeny, *Phys. Rev. A* **2001**, *63*, 032513.

[386] J. C. Sancho-García, F. Moscardó, *J. Chem. Phys.* **2003**, *118*, 1054–1058.

[387] S. Ragot, P. Cortona, *J. Chem. Phys.* **2004**, *121*, 7671–7680.

[388] J. P. Perdew, Y. Wang, *Phys. Rev. B* **1992**, *45*, 13244–13249.

[389] F. Moscardó, E. San-Fabián, L. Pastor-Abia, *Theor. Chem. Acc.* **2006**, *115*, 334–342.

[390] F. Moscardó, *Theor. Chem. Acc.* **2007**, *118*, 631–635.

[391] S. Pittalis, S. Kurth, S. Sharma, E. K. U. Gross, *J. Chem. Phys.* **2007**, *127*, 124103.

[392] Y. Imamura, H. Kiryu, H. Nakai, *J. Comput. Chem.* **2008**, *29*, 735–740.

[393] S. Pittalis, E. Räsänen, M. A. L. Marques, *Phys. Rev. B* **2008**, *78*, 195322.

[394] S. Ragot, *J. Chem. Phys.* **2010**, *132*, 064104.

[395] T. Udagawa, T. Tsuneda, M. Tachikawa, *Phys. Rev. A - At. Mol. Opt. Phys.* **2014**, *89*, 1–6.

[396] Y. Yang, K. R. Brorsen, T. Culpitt, M. V. Pak, S. Hammes-Schiffer, *J. Chem. Phys.* **2017**, *147*, 114113.

[397] K. R. Brorsen, P. E. Schneider, S. Hammes-Schiffer, *J. Chem. Phys.* **2018**, *149*, 044110.

[398] A. Patra, P. Samal, *Chem. Phys. Lett.* **2019**, *720*, 70–75.

[399] D. Kraft, *A Software Package for Sequential Quadratic Programming*, DFVLR, Oberpfaffenhofen, Weßling, **1988**.

[400] J. L. Morales, J. Nocedal, Y. Wu, *IMA J. Numer. Anal.* **2012**, *32*, 553–579.

[401] T. Koga, S. Watanabe, K. Kanayama, R. Yasuda, A. J. Thakkar, *J. Chem. Phys.* **1995**, *103*, 3000–3005.

[402] Maplesoft, *Maple 19. Maplesoft Inc. A Div. Waterloo Maplesoft Inc.,* **2019**.

[403] A. L. Baskerville, A. W. King, H. Cox, *Phys. Rev. A* **2016**, *94*, 042512.

[404] A. W. King, L. C. Rhodes, C. A. Readman, H. Cox, *Phys. Rev. A - At. Mol. Opt. Phys.* **2015**, *91*, 1–6.

[405] T. Kato, *Commun. Pure Appl. Math.* **1957**, *10*, 151–177.

[406] A. M. Frolov, *J. Chem. Phys.* **2007**, *126*, 104302.

[407] R. T. Pack, W. B. Brown, *J. Chem. Phys.* **1966**, *45*, 556–559.

[408] A. M. Frolov, *J. Phys. B At. Mol. Opt. Phys.* **2013**, *46*, 125001.

[409] A. M. Frolov, *Chem. Phys. Lett.* **2015**, *626*, 49–54.

[410] A. W. King, L. C. Rhodes, H. Cox, *Phys. Rev. A* **2016**, *93*, 1–7.

[411] F. A. de Saavedra, E. Buendia, F. J. Galvez, *J. Phys. B At. Mol. Opt. Phys.* **1994**, *27*, 4433–4441.

[412] "SciPy.org," "scipy.optimise.least_squares," can be found under https://docs.scipy.org/doc/scipy/reference/generated/scipy.optimise.least_squares.html,

2021.

[413] “SciPy.org,” “Optimisation and root finding (scipy.optimise),” can be found under https://docs.scipy.org/doc/scipy/reference/optimise.html, **2021**.

[414] “SciPy.org,” “Optimisation (scipy.optimise),” can be found under https://docs.scipy.org/doc/scipy/reference/tutorial/optimise.html, **2021**.

[415] “python4mpia.github.io,” “Least-squares fitting in Python,” can be found under http://python4mpia.github.io/fitting_data/least-squares-fitting.html, **2021**.

[416] P. Virtanen, R. Gommers, T. E. Oliphant, M. Haberland, T. Reddy, D. Cournapeau, E. Burovski, P. Peterson, W. Weckesser, J. Bright, S. J. van der Walt, M. Brett, J. Wilson, K. J. Millman, N. Mayorov, A. R. J. Nelson, E. Jones, R. Kern, E. Larson, C. J. Carey, İ. Polat, Y. Feng, E. W. Moore, J. VanderPlas, D. Laxalde, J. Perktold, R. Cimrman, I. Henriksen, E. A. Quintero, C. R. Harris, A. M. Archibald, A. H. Ribeiro, F. Pedregosa, P. van Mulbregt, A. Vijaykumar, A. Pietro Bardelli, A. Rothberg, A. Hilboll, A. Kloeckner, A. Scopatz, A. Lee, A. Rokem, C. N. Woods, C. Fulton, C. Masson, C. Häggström, C. Fitzgerald, D. A. Nicholson, D. R. Hagen, D. V. Pasechnik, E. Olivetti, E. Martin, E. Wieser, F. Silva, F. Lenders, F. Wilhelm, G. Young, G. A. Price, G.-L. Ingold, G. E. Allen, G. R. Lee, H. Audren, I. Probst, J. P. Dietrich, J. Silterra, J. T. Webber, J. Slavič, J. Nothman, J. Buchner, J. Kulick, J. L. Schönberger, J. V. de Miranda Cardoso, J. Reimer, J. Harrington, J. L. C. Rodríguez, J. Nunez-Iglesias, J. Kuczynski, K. Tritz, M. Thoma, M. Newville, M. Kümmerer, M. Bolingbroke, M. Tartre, M. Pak, N. J. Smith, N. Nowaczyk, N. Shebanov, O. Pavlyk, P. A. Brodtkorb, P. Lee, R. T. McGibbon, R. Feldbauer, S. Lewis, S. Tygier, S. Sievert, S. Vigna, S. Peterson, S. More, T. Pudlik, T. Oshima, T. J. Pingel, T. P. Robitaille, T. Spura, T. R. Jones, T. Cera, T. Leslie, T. Zito, T. Krauss, U. Upadhyay, Y. O. Halchenko, Y. Vázquez-Baeza, *Nat. Methods* **2020**, *17*, 261–272.

[417] P. Virtanen, R. Gommers, T. E. Oliphant, M. Haberland, T. Reddy, D. Cournapeau, E. Burovski, P. Peterson, W. Weckesser, J. Bright, S. J. van der Walt, M. Brett, J. Wilson, K. J. Millman, N. Mayorov, A. R. J. Nelson, E. Jones, R. Kern, E. Larson, C. J. Carey, İ. Polat, Y. Feng, E. W. Moore, J. VanderPlas, D. Laxalde, J. Perktold, R. Cimrman, I. Henriksen, E. A. Quintero, C. R. Harris, A. M. Archibald, A. H. Ribeiro, F. Pedregosa, P. van Mulbregt, *Nat. Methods* **2020**, *17*, 352–352.

[418] M. J. D. Powell, *The BOBYQA Algorithm for Bound Constrained Optimisation without Derivatives*, University Of Cambridge: Cambrdge NA Report NA2009/06, England, **2009**.

[419] J. Ypma, S. G. Johnson, H. W. Borchers, D. Eddelbuettel, B. Riply, K. Hornik, J. Chiquet, A. Adler, *R Interface to NLopt* **2020**, 1–48.

[420] J. A. Nelder, R. Mead, *Comput. J.* **1965**, *7*, 308–313.

[421] J. A. Nelder, R. Mead, *Comput. J.* **1965**, *8*, 27–27.

[422] W. H. Press, S. A. Teukolsky, W. T. Vetterling, B. P. Flannery, *Numerical Recipes-The Art of Scientific Computing*, Cambridge University Press, New York, USA, **2007**.

[423] E. R. Davidson, S. A. Hagstrom, S. J. Chakravorty, V. M. Umar, C. F. Fischer, *Phys. Rev. A* **1991**, *44*, 7071–7083.

[424] S. J. Chakravorty, S. R. Gwaltney, E. R. Davidson, F. A. Parpia, C. F. Fischer, *Phys. Rev. A* **1993**, *47*, 3649–3670.

[425] J. L. Gázquez, H. J. Silverstone, *J. Chem. Phys.* **1977**, *67*, 1887–1898.

[426] C. J. C. Roothaan, G. A. Soukup, *Int. J. Quantum Chem.* **1979**, *15*, 449–462.

[427] A. Savin, H. Stoll, H. Preuss, *Theor. Chim. Acta* **1986**, *70*, 407–419.